Dissertation

Submitted to the

Combined Faculty of Mathematics, Engineering and Natural Sciences

of the Ruperto Carola University Heidelberg, Germany

for obtaining the degree of

Doctor of Natural Sciences

Presented by

Bojana Pavlović, M.Sc.

born in Belgrade, Serbia

Date of oral examination: 20.9.2023

Investigating the role of Rab GTPases in Wnt secretion in *Drosophila melanogaster*

Referees:

Prof. Dr. Michael Boutros

Prof. Dr. Walter Nickel

Contents

1 Abstract 1

1 Zusammenfassung 3

2 Introduction 5

2.1 The Wnt pathway 5

2.1.1 Wnt secretion 6

2.1.2 Wnt signaling 11

2.2 Rab GTPases 13

2.3 *Drosophila melanogaster* as a model organism 18

2.4 Genetic approaches to protein visualization and manipulation 22

2.4.1 Endogenous protein tagging 22

2.4.2 Protein trap-and-release systems 23

2.5 The aims of the thesis 26

3 Results 28

3.1 Endogenous protein tagging of Wg and Evi using CRISPR 28

3.1.1 Endogenous tagging of Wg and Evi with fluorescent proteins by CRISPR/Cas9 homology-directed repair 28

3.1.2 Functional validation of endogenously fluorescently tagged Wg and Evi 31

3.1.3 Different fluorescent proteins enable the visualization of differing fractions of Wg within the wing imaginal tissue 34

3.1.4 Analysis of endogenously tagged Wg and Evi in living tissue 38

3.2 Establishing protein trap-and-release systems for use in *Drosophila* tissues 42

3.2.1 Adaptation of the RUSH system in *Drosophila melanogaster* 42

3.2.2 Adaptation of the LAMA system in *Drosophila melanogaster* 47

3.2.3 Live imaging of the LAMA system in wing imaginal discs and salivary glands 52

3.2.4 The LAMA hook can effectively sequester endogenous GFP-tagged proteins in the ER 54

3.3 Rab GTPases and their role in Wnt secretion 59

3.3.1 Rab GTPase perturbation screens for the effects on Wnt secretion 59

3.3.2 Rab7 perturbation affects intracellular and tissue localization of Wg 64

3.3.3 LAMA system reveals the temporal dynamics of Wg distribution phenotype of Rab7 overexpression 67

3.3.4 Rab7 perturbation does not affect Wnt pathway targeting in Wg-receiving cells 68

3.3.5 Rab7 perturbation does not affect Wg secretion from Wg-secreting cells 70

3.3.6 Wg accumulates upon Rab7 perturbation in lysosomes 71

4 Discussion 77

4.1 Endogenous protein tagging of Wg and Evi 77
4.2 The LAMA system 83
4.3 The role of Rab7 in Wnt secretion 88
4.4 Conclusion and outlook 93
5 Materials and Methods 97
5.1 Methods 97
5.1.1 Cloning 97
5.1.2 *Drosophila* fly line generation 99
5.1.3 *Drosophila* husbandry and fly crossing 101
5.1.4 Immunohistochemistry and fluorescence imaging 102
5.1.5 Surface protein biotinylation assay 103
5.1.6 Computational analyses 105
5.2 Materials 105
5.2.1 Plasmids and primers for tagging and sequencing 105
5.2.2 Chemicals, kits and buffers 110
5.2.3 Fly lines 113
5.2.4 Antibodies and dyes 120
6 References 122
6.1 Literature 122
6.2 List of Figures 136
6.3 List of Tables 138
7 Appendix 139
7.1 Supplemental Figures 139
7.2 Scientific publications, presentations and supervision 148
7.3 Acknowledgements 150
7.4 Erklärung zur wissenschaflitchen Praxis 153

1 Abstract

Wnt pathway is one of the main signaling pathways required for development and homeostasis. Wnt proteins must be secreted into the extracellular space in order to trigger the signaling cascade. Regulation of Wnt protein secretion is therefore crucial for Wnt pathway activity. All intracellular membrane trafficking is regulated by Rab GTPases. Very few Rab GTPases, however, have been directly associated with Wnt secretion. I performed a systematic screen by perturbing the 26 *Drosophila melanogaster* RabGTPases and observing the effects on Wnt secretion in the wing imaginal disc through immunohistochemical analysis. I identified Rab7 as a regulator of Wnt secretion and characterized its role in this process. I found that overexpression of Rab7 induces the accumulation of *Drosophila* Wnt1 homolog Wingless (Wg) in both secreting and receiving cells, as well as moderate relocalization of Wg from predominantly apical side to the basal side of these cells. The changes in Wg protein localization did not, however, affect the level of secreted Wg in the wing discs or the downstream Wg signaling. By performing colocalization staining, I determined that upon Rab7 overexpression, Wg was localizing to LAMP1- and Arl8-positive lysosomes at the basal side of the wing disc cells. Knockdown of Arl8 in cells with Rab7 overexpression reduced the translocalization of Wg to the basal side of the disc.

In order to study the interaction between Rab GTPases and Wnt secretion in living tissue, I developed novel *Drosophila* tools, which will be of use to other studies. Firstly, I endogenously tagged the Wg carrier protein Evi/Wls with the fluorescent proteins mScarlet and EGFP. Additionally, I generated a Wg:mScarlet fly line based on the existing Wg:EGFP fly line. Using these tools, I characterized the different fluorescence localization of proteins tagged with EGFP and mScarlet. I confirmed that the fluorescent tags do not affect Wg secretion, but that the difference in signal localization is due to the intrinsic properties of the fluorescent proteins. Secondly, I adapted the LAMA (ligand-modulated antibody fragments) system, an acute protein trap-and-release system previously published in human cell culture, for use in *Drosophila*. I could show that the system was functional in wing discs and salivary gland cells and that it allowed the trapping of both overexpressed and endogenous GFP-tagged proteins on the mitochondrial membrane and the endoplasmic reticulum (ER). The addition of the release molecule triggered the relocalization of the tagged proteins from the mitochondrial membrane into the cytoplasm. Using the LAMA system, I was able to show that the Wg accumulation induced by Rab7 overexpression appeared within sixty minutes of the Rab7 release.

In summary, my data indicate a role of Rab7 in the translocalization of Wg to the basal side through the late endosomal pathway. Furthermore, the development of experimental tools, especially the adaptation of a protein trap-and-release system for use in *Drosophila melanogaster*, provide a material contribution to the field.

1 Zusammenfassung

Der Wnt Signalweg ist einer der wichtigsten Signalwege während der Entwicklung und Homöostase. Wnt Proteine werden in die extrazelluläre Matrix sekretiert um die Wnt Signalkaskade zu aktivieren. Die Regulierung der Wnt Sekretion ist daher essential für die Aktivierung des Wnt Signalweges. Der gesamte intrazelluläre vesikuläre Transport wird durch Rab GTPasen reguliert. Einige der Rab GTPasen sind direkt mit der Sekretion von Wnt Proteinen assoziiert. In meiner Arbeit habe ich einen systematischen Screen durchgeführt, in dem ich den Einfluss der 26 *Drosophila melanogaster* Rab GTPasen auf die Wnt Sekretion in der Flügel Imaginal-Scheibe durch Immunohistochemie analysiert habe. Dabei habe ich Rab7 als Kandidat identifiziert und im Folgenden dessen Funktion auf die Wnt Sekretion analysiert. Die Überexpression von Rab7 induziert eine Akkumulation des *Drosophila* Wnt1 homologen Proteins Wingless (Wg) in Sender- und Empfängerzellen. Desweitern ist eine reilweise Relokalisierung von Wg von der normalerweise apikalen Zellseite zur basalen Seite in diesen Zellen zu beobachten. Diese Veränderung hatte jedoch keinen Effekt auf die Wg Sekretion und auf den Wnt Signalweg in der Empfängerzelle. Desweitern habe ich Färbungen durchgeführt um die Lokalisation von Wg in Zellen mit Überexpression von Rab7 zu bestimmen. Ich konnte zeigen, dass Wg mit den Lysosomen-Markern LAMP1 und Arl8 an der basalen Seite der Flügel Imaginal-Scheiben kolokalisiert. Knock-down von Arl8 in Zellen mit Rab7 Überexpression reduzierte die Lokalisierung von Wg an der basalen Seite der Imaginal-Scheiben Zellen.

Um die Interaktion zwischen Rab GTPasen und der Wnt Sekretion in lebenden Geweben analysieren zu können, habe ich neuartige molekulare Werkzeuge in *Drosophila* etabliert, die auch in anderen Studien Anwendung finden können. Zuerst habe ich den Wg Rezeptor Evi-Wls mit fluoreszenten Proteinen endogen markiert. Dann habe ich eine fluoreszent markierte Fliegenlinie mit Wg:mScarlet basierend auf der bereits generierten Wg:EGFP Fliege hergestellt. Dadurch konnte ich die Lokalisierungen der fluoreszenz-markierten Fliegen charakterisieren und nachweisen, dass die Sekretion von Wg nicht beeinflusst wird. Eine leicht veränderte Lokalisierung der verschiedenen Fliegenlinien war auf die unterschiedlichen chemischen und physikalischen Eigenschaften der fluoreszenten Proteine zurückzuführen. Im Folgenden habe ich das LAMA-System für die Anwendung in *Drosophila* adaptiert. Das System wurde ursprünglich in humaner Zellkultur etabliert, wobei Proteine gezielt in Organellen festgehalten und wieder freigegeben werden. Ich konnte zeigen, dass das LAMA-System in den Flügel Imaginal-Scheiben und in den Speicheldrüsen Zellen funktioniert. Überexprimierte oder endogene GFP-markierte Proteine konnten auf der Mitochondrienmembran sowie im Endoplasmatischen Retikulum (ER) festgehalten werden. Die Zugabe des Freigabe-Moleküls führte erwartungsgemäß zu der Re-Lokalisierung der GFP-markierten Proteine von der Mitochondrienmembran in das Zytoplasma. Anhand des LAMA-Systems konnte ich zeigen, dass der durch die Rab7 Überexpression entstandene Wg Akkumulation innerhalb von sechzig Minuten nach dem Freisetzen von Rab7 hervorgerufen wurde.

Zusammenfassend zeigen meine Daten, dass Rab7 durch den späten endosomalen Signalweg an der Lokalisierung von Wg zu der basalen Zellseite beteiligt ist. Im Weiteren konnte ich neue molekulare Werkzeuge für *Drosophila melanogaster* etablieren, im Besonderen das LAMA-System, die einen wichtigen Beitrag für die weitere Forschung leisten können.

2 Introduction

Communication between individual cells in a tissue is essential for the coordination of their differentiation during embryonic development, their functioning during homeostasis, and their response to stress [Alberts et al., 2014]. Neighboring cells can communicate directly through membrane gap junctions [Goodenough & Paul, 2009] and synapses [Südhof & Malenka, 2008] in the form of juxtacrine or direct signaling. Non-neighboring cells of the same tissue or organ rely on paracrine signaling to communicate, whereby one cell secretes ligands into the direct cellular environment. These can bind to the receptors on the surface of the nearby cells to induce a multitude of signaling pathways. Wnt signaling, for example, is a form of paracrine signaling controlling the tissue patterning in the *Drosophila* wing imaginal discs [Swarup & Verheyen, 2012]. A further form of this type of signaling is endocrine signaling, in which hormones travel through the blood stream from their place of secretion to other organs in the body rather than staying in the immediate environment [Hiller-Sturmhöfel & Bartke, 1998]. Lastly, autocrine signaling allows the cells to regulate their own function by the binding of their ligands to their own receptors. T-cell lymphocytes, for instance, signal themselves through the secretion of Interleukin-2 to promote their own proliferation [Ross & Cantrell, 2018]. In all cases, however, the ligands must be synthesized and transported within the cell to the release site before they are secreted.

Once released, ligands bind to receptors and trigger signaling pathways in the receiving cells, which in turn alter cellular processes in order to coordinate development and function. One of the crucial signaling pathways for development is the Wnt signaling pathway, playing a role in cell fate determination, proliferation, cell cycling and proliferation [Logan & Nusse, 2004]. Wnt proteins must be secreted into the extracellular space where they can bind to the receptors belonging to the Frizzled protein family [Bhanot et al., 1996], activating thereby several canonical and non-canonical downstream signaling pathways [Nusse & Clevers, 2017; Yang & Mlodzik, 2015]. The process of Wnt secretion is a complex one, however, with multiple modes of release and trafficking away from the Wnt-secreting cells identified for different cell types, organs and model organisms. For this reason, I was interested in studying the secretion of Wnt proteins in the model organism *Drosophila melanogaster* in this thesis.

2.1 The Wnt pathway

The Wnt pathway is a highly conserved signaling pathway required for embryonic development as well as maintenance of tissue homeostasis [Hayat et al., 2022]. Wnt proteins are morphogens which trigger the expression of target genes through the binding to Wnt ligand receptors and the activation of the Wnt signaling cascade [Willert & Nusse, 2012]. The Wnt pathway is present in all metazoans [Holstein, 2012], with thirteen highly conserved Wnt subfamilies (Wnt 1-11, 13 and A) defined throughout the phylogenic tree of this biological kingdom [Croce & McClay, 2008]. It is essential for the formation of bilateral body symmetry in early development, specifically the anteroposterior axis [Petersen & Reddien, 2009]. During later stages of development, Wnt signaling plays an important role in tissue patterning, such

as in the *Drosophila melanogaster* wing imaginal disc, where it directs the precise expression of downstream target genes required for the formation of specific wing structures [Swarup & Verheyen, 2012]. Moreover, Wnt pathway dysregulation has been closely associated with both congenital illnesses like Robinow syndrome [White et al., 2018], as well as diseases like cancer and metabolic disorders [Ng et al., 2019].

First discovered through the study of viral-induced oncogenesis in mice [Nusse & Varmus, 1982], Wnt proteins take the form of a horse-shoe or a 'palm' with extended 'thumb' and 'index finger' domains, through which they bind to their ligand receptors [Janda et al., 2012]. The number of Wnt proteins varies in different species, with 19 Wnts described in humans, 5 in *C. elegans*, 13 in hydra, and 7 in fruit flies [Buechling & Boutros, 2011]. They share common features, such as 22 cysteine residues which form intramolecular disulfide bridges [MacDonald et al., 2014] and a signal sequence at their N-terminus for secretion which differs in length for each Wnt protein and which is cleaved upon protein maturation [Willert et al., 2003; Mikels & Nusse, 2006]. Importantly, all Wnts except WntD (the *Drosophila* ortholog of Wnt8) are lipid-modified in the process of their maturation by acylation [Chu et al., 2013].

2.1.1 Wnt secretion

Wnt synthesis and ER exit

Secreted proteins such as Wnts are initially synthesized from their mRNA in the endoplasmic reticulum (ER), a large and dynamic molecule surrounding the nucleus, by the ribosomes which attach to its membrane on the cytosolic side [Alberts et a., 2014]. The polypeptide chain of the nascent protein is translocated into the ER lumen concurrently with its synthesis [Walter & Johnson, 1994] and folded with the aid of chaperone proteins and enzymes [Ellgaard et al., 2016]. The folding is then followed by post-translational protein modification, including disulfide bond formation [Bulleid, 2012], oligomerization [Christis et al., 2008] and N-linked glycosylation [Aebi, 2013]. After several quality control checks, properly folded proteins are transported to the Golgi apparatus, a multi-structure organelle composed of a number of cisternae stacked in the cis-to-trans polar orientation [Alberts et al., 2014], while misfolded proteins are targeted to the ER-associated degradation pathway (ERAD), which functions by retro-translocating misfolded proteins back into the cytosol for proteasome degradation [Lemus & Goder, 2014].

After translation and folding, Wnt proteins are post-translationally modified through glycosylation and acylation. The N-glycosylation takes place at several conserved asparagine residues and is important for protein stability, secretion and signaling [Smolich et al., 1993; Yamamoto et al., 2013]. However, this modification is not essential for the functioning of all Wnt proteins, as the *Drosophila* WNT1 homologue Wingless (Wg) is not affected by the removal of the glycosylation sites [Tang et al., 2012]. More important than the glycosylation is the acylation of Wnt proteins. The O-palmitoleoyltransferase Porcupine (Porcn) modifies Wnts by adding a palmitoleic acid at a conserved serine residue (S239 in *Drosophila* Wg) [Takada et al., 2006]. Due to this lipid modification, Wnt proteins are very hydrophobic and must be shielded from the aqueous extracellular environment. The palmitoleic acid enables

the interaction of Wnt proteins with their dedicated transfer protein, referred to as Evenness interrupted (Evi) or Wntless (Wls) [Bartscherer et al., 2006; Bänziger et al., 2006; Nygaard et al., 2021]. Evi forms a complex with Porcn and the ATPase VCP, and its fate depends on the presence or absence of Wnts [Glaeser et al., 2018] – in the presence of Wnts, Porcn induces their palmitoylation and loads them onto Evi; in their absence, Evi is polyubiquitinated by VCP, ERLIN2, FAF2 and UBXN4, and targeted for the ERAD [Wolf et al., 2021].

Correctly folded proteins in the ER are relocated to the ER exit sites (ERES) [Kurokawa & Nakano, 2019], where the Coat Protein Complex II (COPII) accumulates on the ER membrane and forms vesicles around the cargo [Barlowe et al., 1994]. COPII vesicles bud from the ERES and travel to the Golgi, where they fuse with the cis-Golgi membrane and release their cargo. The Golgi serves as the primary location for the finalization of protein and lipid maturation, as well as polysaccharide synthesis. Secreted proteins are transported through the Golgi network into the trans-Golgi-network (TGN), a tubular-vesicular compartment extending from the trans-Golgi [Fort ed al., 2021]. Once they reach the TGN, proteins are sorted depending on their final destination (the plasma membrane, endosomes, or lytic compartments) with the help of specific sorting signals and dedicated proteins and lipids [Alberts et al., 2014]. This sorting is important especially in polarized cells (such as the *Drosophila* wing imaginal disc epithelial cells), as it contributes to the targeting and delivery of apical and basolateral proteins to the correct section of the plasma membrane, which in these cells has distinct domains [Mellman & Nelson, 2008]. The vesicles are delivered to the plasma membrane along the cytoskeleton by motor-mediated transport on microtubules [Bi et al., 1997]. The exocyst complex mediates the fusion of the two membranes in question [Heider & Munson, 2012], releasing the proteins into the extracellular space by exocytosis.

Wnt proteins are similarly transported through this secretion route. Once the Wnt proteins are loaded onto Evi, they are concentrated at the ERES sites through the interaction with the proteins belonging to the p24 family [Port et al., 2011; Buechling et al., 2011]. p24 proteins recruit COPII subunits to the ER membrane in order to induce vesicle budding [D'Arcangelo et al., 2015]. At least one member of the family, Baiser, has been linked to both Evi and Sec22, which plays a role in ER-to-Golgi vesicle tethering [Li et al., 2015]. Sec22 is a vesicle Soluble *N*-ethylmaleimide-sensitive factor adaptor protein receptor (v-SNARE), a protein anchored in the vesicular membrane which builds helix bundles with its target membrane t-SNARE partners in order to force the two membranes into close contact, facilitating membrane fusion [Söllner et al., 1993; Han et al., 2017]. In addition, Evi has been shown to interact with the guanosine nucleotide exchange factor Sec12 and its effector Sar1 [Sun et al., 2017]. Sar1 initiates the formation of COPII coat and facilitates vesicle budding [Sato & Nakano, 2005], thus providing an additional method of loading the Wnt-Evi complex for exit from the ER. The Wnt-Evi complex passes through the Golgi apparatus and is transported to the cell surface, where it is secreted in an exocyst-dependent manner [Chaudhary & Boutros, 2019].

Modes of Wnt trafficking

Several modes of Wnt protein trafficking have been described in the last years [Routledge & Scholpp, 2019]: on Wnt carrier proteins, on extracellular matrix components, on cytonemes, and on exosomes. Whether they are mutually exclusive or exist concurrently in one cell type is still debated. So far, these studies indicate that the mode of trafficking largely depends the cell identity, tissue specificity and the model organism. This makes it likely that context specificity plays a significant role in how Wnts reach the neighboring cells.

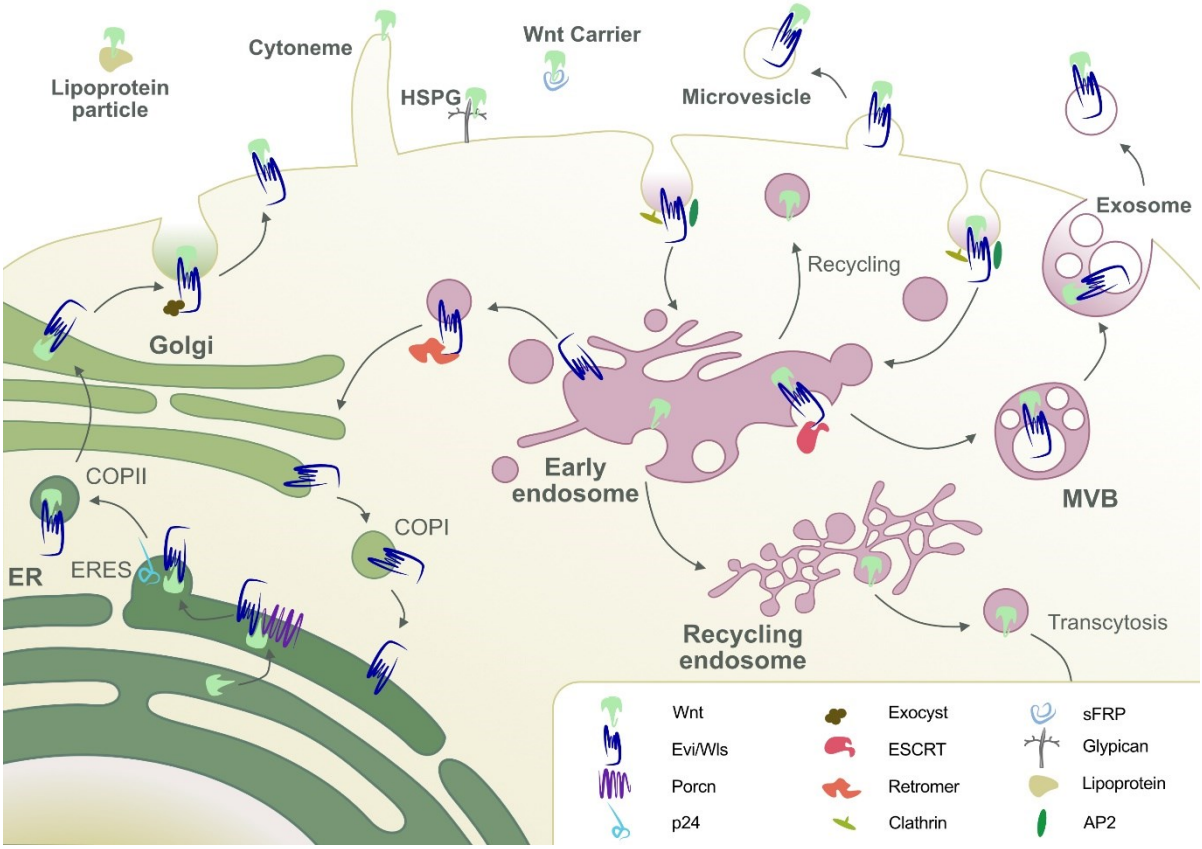

Figure 1: Wnt secretion and trafficking

Wnts are synthesized and palmitoylated by Porcn in the ER, after which they're loaded onto Evi and transported to the Golgi on COPII vesicles. After secretion from the Golgi to the surface by the Exocyst complex, Wnts can be trafficked on cytonemes, lipoprotein particles, HSPGs, Wnt carriers or microvesicles; they can be internalized by endocytosis into the endosomal pathway and secreted on exosomes. They can also be recycled to the surface or transcytosed through the cell to the opposite membrane. Once unloaded, Evi is returned to the endosomal pathway and trafficked back to the Golgi by the Retromer complex, to be returned to the ER on COPI vesicles for further use.

One trafficking mode relies on Wnt carrier proteins found on the surface of the secreting cells. Several potential Wnt carrier proteins have been identified in different model organisms. In *Drosophila*, the lipocalin protein Secreted Wg-interacting Molecule (Swim) may play a role in the maintenance of Wg diffusion range in the extracellular space [Mulligan et al., 2012]. However, no vertebrate homologue has been described yet. Afamin, a glycoprotein from the serum albumin family, can solubilize Wnts and enable Wnt signaling in vertebrates [Mihara et al., 2016; Naschberger et al., 2017]; however, Afamin has no homologues in invertebrates. In addition, lipoproteins have been described as Wnt carrier proteins, for example for Wnt3a in mouse fibroblasts [Neumann et al., 2009] and for Wnt5a in the central nervous system [Kaiser et al., 2019]. Moreover, secreted frizzled-related proteins (sFRPs) can serve in low

concentrations as Wnt carrier proteins [Xavier et al., 2014]. They are non-membrane-bound glycoproteins with frizzled-like cysteine-rich domain [Rattner et al., 1997], which in high concentrations can also inhibit Wnt signaling, potentially by competing with Wnt receptors [Üren et al., 2000].

The extracellular matrix components may also assist in the transport of Wnts through the extracellular space. Among these, heparan sulfate proteoglycans (HSPGs) – proteins carrying glycosaminoglycan chains – have been studied the most, and have been referred to as co-receptors, given that they promote ligand-receptor binding [Kirkpatrick & Selleck, 2007; Mii & Takada, 2020]. Glypicans are one of the three main HSPG families, and the *Drosophila* glypican Dally-like protein (Dlp) has been implicated in Wnt secretion [Baeg et al., 2001]. Its upregulation resulted in the accumulation of extracellular Wg, whereas expression of sugar-deficient HSPGs caused a removal of Wg from the cell surface. A further study has demonstrated how Dlp can shield the palmitoleic acid of Wg to facilitate its movement on the cell surface [McGough et al., 2020]. Additionally, HSPGs have been shown to function as endocytosis receptors [Christianson & Belting, 2014] and may have a role in the uptake of exosomes [Christianson et al., 2013]. Therefore, they may assist in the delivery of larger Wnt-carrying complexes as well.

Cytonemes have been suggested as an alternative mode of Wnt transport [Stanganello & Scholpp, 2016]. These are signaling filopodia which facilitate morphogen signaling by enabling the intracellular transport of ligands or their receptors across a distance before presentation at the point of contact between the cytoneme and the neighboring cell [Zhang & Scholpp, 2019]. Wnts have been found on cytonemes in vertebrates, a process which is important for neural plate formation in zebrafish [Stanganello et al., 2015]. Interestingly, the formation of cytonemes which activate paracrine Wnt/β-catenin pathway through the delivery of Wnt8a in vertebrates is regulated by the autocrine Wnt/PCP pathway [Mattes et al., 2018], with the Wnt/PCP protein Vangl2 playing a central role in this process [Brunt et al., 2021]. Cytonemes also exist in *Drosophila* and are a kay delivery mechanism for Hedgehog signaling [Callejo et al,. 2011]. However, instead of carrying Wnt ligands away from the secreting cells, in *Drosophila* they have been found to carry Frizzled receptors to them from the neighboring receiving cells [Huang & Kornberg, 2015].

Wnts and Evi have both been detected on exosomes [Koles et al., 2012], indicating that both Wnts and Evi can be secreted through the endosomal pathway. The endosomal pathway is composed of a network of organelles with common properties, and whose function is sorting and transportation of internalized cargo throughout the cell [Alberts et al., 2014]. Proteins enter it from the cell surface through endocytosis, which can be facilitated by several different mechanisms, the primary of which is mediated by Clathrins [Kaksonen & Roux, 2018]. During clathrin-mediated endocytosis, Clathrins cluster at the plasma membrane, forming a mesh which is attached to the plasma membrane by Adaptor protein 2 (AP2) and which induces invagination [Kirchhausen et al., 2014]. After maturation, GTPase Dynamin located at the neck of the invagination induces the fission of the vesicle from the plasma membrane [Schmid &

Frolov, 2011]. The Clathrin coat is then disassembled, allowing the vesicle to travel to and fuse with the endosome [Rothman & Schmid, 1986]. Wg is endocytosed in a Dynamin-dependent manner which is required for Wg secretion in *Drosophila* wing discs [Strigini & Cohen, 2000], and Evi possesses a conserved amino acid motif YEGL required for its internalization by AP2, Clathrin and Dynamin [Gasnereau et al, 2011].

The identity of the endosomes in the endosomal pathway is fluid rather than rigidly defined, dependent on the cargos it carries and the markers found in its membrane, and which are exchanged in the maturation process [Behnia & Munro, 2005]. One of the aspects of endosome identity is their acidity. Early endosomes are weakly acidic, with the average pH value being 6.5 [Paroutis et al., 2004]. As part of the maturation process, the pH value of the organelles declines due to the activity of the vacuolar H^+ ATPase [Jeffries at al., 2008], so that the average pH value of late endosomes is 5.5 and that of lysosomes is 4.5.

Early endosomes are the main sorting station of the endocytic pathway [Jovic et al., 2010]. They are a morphologically diverse and dynamic organelle, displaying both cisternal, tubular and tubulovesicular structures [Gruenberg, 2001]. The markers for early endosomes are primarily the Rab5 GTPase and the Early endosomal antigen 1 (EEA1) [Simonsen et al., 1998]. Endocytosed cargo is sorted in the early endosomes either for degradation or for recycling [Jovic et al., 2010]. Two recycling routes exist: the rapid recycling route, regulated by Rab4 found on the peripheral early endosomes and transporting the proteins directly back to the plasma membrane [Scheff et al., 1999]; and the indirect recycling route, passing through the Rab11-positive recycling endosomes first [Li & DiFiglia, 2012], which are in addition responsible for transcytosis in polarized cells [Ducharme et al., 2007]. In *Drosophila*, Wg passes through the Rab4-mediated rapid recycling route during recycling and apical secretion [Witte et al., 2020], while Rab11 is required for the secretion of Evi-carrying exosomes in *Drosophila melanogaster* [Koles et al., 2012].

Early endosomes undergo maturation into late endosomes; this process is driven by the Rab5-to-Rab7 switch [Langemeyer er al., 2020], where the early endosome marker Rab5 is gradually replaced by the late endosome marker Rab7. Part of this process is in addition the acidification of the organelle through the activity of the V-ATPase protein [Lafourcade et al., 2008]. Before and during maturation, early endosomes experience inward membrane budding, resulting in the formation of intraluminal vesicles (ILVs) within multivesicular bodies (MVBs) which contain cargo primarily sorted for degradation [Woodman & Futter, 2008]. The process can be facilitated by the Endosomal Sorting Complexes Required for Transport (ESCRT) machinery [Paper & Katzmann, 2010; Babst, 2011] or though the ceramide-dependent ILV formation route which is responsible for the formation of exosomes, small extracellular vesicles which are released from MVBs targeted to the plasma membrane [Trajkovic et al., 2008].

Wnt secretion is impeded in vertebrates by the lack of endosomal acidification during MVB formation, through which exosomes are formed [Coombs et al., 2010]. This process was

shown to be regulated by the SNARE protein Ykt6 in fruit flies [Gross et al., 2012], though other publications raise into question exosomes as Wnt delivery methods in *Drosophila* wing imaginal discs [McGough et al., 2020]. In other tissues such as the *Drosophila* neuromuscular junction, however, Wg and Evi have both been detected on exosomes [Korkut et al., 2009], potentially showing that in some contexts, the Wnt-Evi complex remains bound after secretion as well. Wnt-carrying exosomes have been found in vertebrates as well [Tassew et al., 2017], and their presence may play a role in cancer chemotherapy resistance [Hu et al., 2019].

In polarized cells such as the epithelial cells of the wing imaginal disc in fruit flies, Wnts are distributed between the apical and basal membrane by transcytosis, as secretion occurs at both sides [Yamamoto et al., 2013]. In cases where Wnts are initially brought to the apical membrane, such as in the fruit fly wing imaginal disc, endocytosis and transport through the endosomal pathway is necessary for transcytosis. The ESCRT complex serves in the sorting of Wnts in the endosomal pathway [Pradhan-Sundd & Verheyen, 2014], with other proteins such as the E3-ligase Godzilla [Yamazaki et al., 2016], SNARE protein Synaptobrevin [Linnemannstöns et al., 2020] and motor protein Klp98A [Witte et al., 2020] also mediating this process.

Wnt-Evi complex must be released at some point during Wnt secretion, as the palmitoleic acid shielded by Evi is equally required for the binding of Wnt proteins to their Frizzled receptors [Janda et al., 2012; Nygaard et al., 2021]. This is believed in most cases to happen at the plasma membrane, leaving Evi to be recycled for further use while Wnts are secreted. The cargo recycling route from early endosomes back to the TGN is mediated by the retromer complex [Seaman, 2012]. The retromer complex is composed of two subcomplexes: the cargo selection subcomplex, composed of Vps26, Vps29 and Vps35 proteins, and the membrane recognition and deformation subcomplex, composed of Snx-BAR sorting nexins (Snx1/2 and Snx5/6). Once Wnt is secreted, the unloaded Evi is returned by endocytosis to the early endosomes from the plasma membrane [Yu et al., 2014]. From there, Evi is targeted for recycling back into the TGN by the retromer complex [Port et al., 2008], with the aid of a dedicated Snx3 protein [Harterink et al., 2011]. Once it reaches the Golgi, Evi is returned to the ER via COPI-mediated retrograde transport [Beck et al., 2009; Yu et al., 2014], where it can once again interact with newly synthesized Wnts.

2.1.2 Wnt signaling

Wnt signaling pathways are activated by the binding of the Wnt ligand to the corresponding receptors on the surface of receiving cells [Nusse & Clevers, 2017]. Three different Wnt signaling pathways have been identified, defined as one canonical or β-catenin dependent signaling pathway and two non-canonical pathways, namely the planar cell polarity (PCP) and the Calcium (Ca^{2+}) pathway [Yang & Mlodzik, 2015].

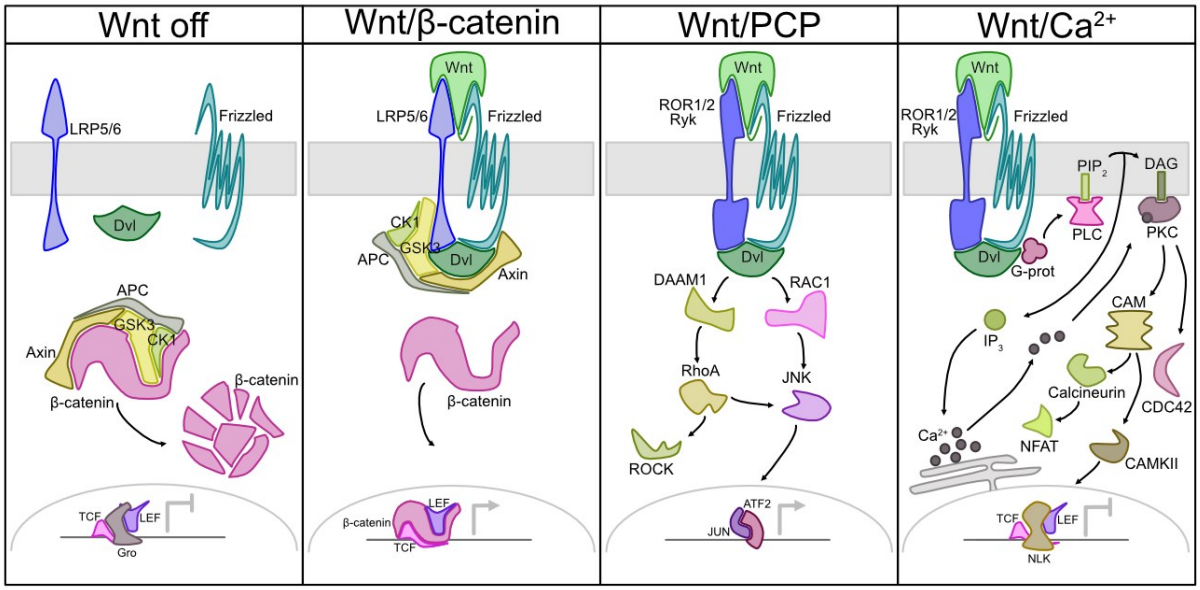

Figure 2: Wnt signaling pathways
Wnt off: When Wnts aren't bound to Frizzled and LRP5/6, β-catenin is bound to the destruction complex composed of Axin, APC, GSK3*β*, CK1α and targeted for degradation; Groucho binds to TCF/LEF and prevents transcriptional activation.
Wnt/β-catenin pathway: After Wnts bind to Frizzled and LRP5/6, Dvl is recruited to the ligand-receptor complex, and in turn recruits the destruction complex. β-catenin is stabilized and translocates to the nucleus, where it binds to TCF/LEF and activates transcription.
Wnt/PCP pathway: Binding of Wnts to Frizzled and ROR1/2 or Ryk receptors recruits Dvl, which in turn activates DAAM1 and Rac1. DAAM1 activates RhoA, which in turn activates ROCK. Rac1 activates JNK, which activates JUN and drives transcription.
Wnt/Ca^{2+} pathway: Binding of Wnts to Frizzled and ROR1/2 or Ryk receptors recruits Dvl, which in turn activates G-protein. G-protein induces PLC to break down PIP_2 into IP_3 and DAG. IP_3 triggers Ca^{2+} release from the ER, and the binding of Ca^{2+} leads to binding of PKC to DAG, which activates CDC42, as well as CAM. CAM activates Calcineurin, which activates NFAT, as well as CAMKII, which dephosphorylates NLK. NLK binds to TCF/LEF and prevents transcriptional activation.

The canonical Wnt/β-catenin signaling pathway [Nusse & Clevers, 2017] depends on the activity of the 'destruction complex', a protein complex composed of the scaffold protein Axin, Adenomatous polyposis coli (APC), and two serine/threonine kinases, Glycogen synthase kinase 3 beta (GSK3β) and Casein kinase 1 alpha (CK1α) [Ikeda et al., 1998; Stamos & Weis, 2013]. In the absence of Wnt ligands, the destruction complex binds β-catenin and induces its degradation. β-catenin is a member of the Cadherin protein complex [Valenta et al., 2012], through which it is involved in cell adhesion at the plasma membrane [Ozawa et al., 1989], but it also possesses a secondary function in gene transcription regulation in the nucleus [Behrens et al., 1996]. The destruction complex mediates the N-terminal phosphorylation of β-catenin, which targets it for ubiquitination and subsequent degradation by the proteasome [Aberle et al., 1997]. In the absence of β-catenin, transcription factors T cell factor (TCF) and Lymphoid enhancer factor (LEF) are repressed by the repressor Groucho (Gro), which prevents transcription of Wnt target genes [Cavallo et al., 1998].

Wnt ligands bind to the transmembrane receptors Frizzled (Fzd in mammals, Fz in *Drosophila*) [Bhanot et al., 1996] and Low-density lipoprotein-receptor-related proteins 5/6 (LRP5/6) on the cell surface [Tamai et al., 2000], which are normally not complexed in the absence of Wnts. The binding induces the recruitment of Dishevelled (Dvl in mammals, Dsh in *Drosophila*) to the complex in the cytoplasm [Tauriello et al., 2012]. In the canonical Wnt pathway, this triggers the recruitment of Axin and GSK3β from the destruction complex to Dvl and the

phosphorylation of LRP5/6 [Davidson et al., 2005]. Once the destruction complex has been dismantled, β-catenin is no longer targeted for degradation, but rather accumulates and translocates to the nucleus. There, β-catenin binds to the TCF/LEF transcription factors and initiates the expression of Wnt target genes [Behrens et al., 1996; Daniels & Weis, 2006].

The binding of Wnts to Fzds can also trigger the two non-canonical pathways, though different co-receptors are engaged – Receptor tyrosine kinase-like orphan receptors 1/2 (Ror1/2), Related to tyrosine kinase (Ryk) and Collagen triple helix repeat containing 1 (CTHRC1) for the Wnt/PCP and the Wnt/Ca2+ pathways respectively [Yang & Mlodzik, 2015]. The binding of Wnts to the receptors recruits Dvl in this case as well, however, the non-canonical pathways do not depend on β-catenin. In the Wnt/PCP pathway, Dvl recruits two different proteins that trigger signaling cascades for actin rearrangement: recruited Dishevelled-associated activator of morphogenesis 1 (DAAM1) activates Profilin and the G-protein Rho, which in turn activates Rho-associated kinase (ROCK) [Fanto et al., 2000; Liu et al., 2008]; recruited Rac1 activates JUN N-terminal kinase (Jnk) leading to transcriptional regulation [Boutros et al., 1998].

The Wnt/Ca^{2+} pathway regulates the Ca^{2+} levels in the cell by controlling of Ca^{2+} release from the ER, which in turn regulates processes like ventral patterning and cell adhesion/migration. This signaling cascade requires not only the recruitment of Dvl to the ligand-receptor complex, but also the heterotrimeric G-protein, which directly interacts with Fzd [Katanaev et al., 2005]. The interaction between Dvl and G-protein activates Phospholipase C (PLC), which breaks down phosphatidylinositol-phospholipid $PI(4,5)P_2$ into inositol-triphosphate (IP_3) and diacylglycerol (DAG) [Sheldahl et al., 2003; Slusarski et al., 1997]. The binding of IP_3 to its receptor in the ER membrane results in Ca^{2+} release. High Ca^{2+} concentrations in the cytoplasm trigger several downstream events: the activation of Protein kinase C (PKC) through the binding with DAG, followed by CDC42 activation, which induces ventral patterning [Sheldahl et al., 1999; Carvalho et al., 2019]; the activation of Calmodulin (CAM), which in turn activates the phosphatase Calcineurin and the Ca^{2+}/CAM-dependent kinase II (CAMKII) [Kühl et al., 2000]. Calcineurin dephosphorylates Nuclear factor of activated T cells (NFAT), which regulates cell adhesion and migration; CAMKII activates Nemo-like kinase (NLK), which interferes with the canonical Wnt signaling through the inhibition of TCF/LEF [Ishitani et al., 1999].

2.2 Rab GTPases

Rab GTPases are small proteins of the Ras superfamily which function as master regulators of membrane trafficking in eukaryotic cells [Pfeffer, 2017]. They can serve as organelle markers, and their interactions with other proteins enable them to control all stages of cellular trafficking. The first Rab to be identified was Ypt1 in yeast [Schmitt et al., 1986]; since then, the Rab protein family has been subdivided into six supergroups, with high degree of conservation in all eukaryotes [Klöpper et al., 2012] and a large number of identified Rab proteins – 66 in humans [Li & Marlin, 2015], 11 in yeast and 26 in fruit flies [Stenmark & Olkkonen, 2001].

The Rab cycle

After their synthesis, Rab GTPases bind to Rab escort proteins (REPs), which allow the Rab geranylgeranyl-transferase to prenylate their C-terminus cysteine residues [Homma et al., 2021]. The prenylation is required for the insertion of Rab GTPases into the lipophilic membrane. A guanosine diphosphate (GDP) is attached to the Switch region of Rabs, and the GDP dissociation inhibitor (GDI) protein forms a complex with GDP-bound Rabs, masking the prenyl groups and keeping the Rab protein soluble and cytoplasmic.

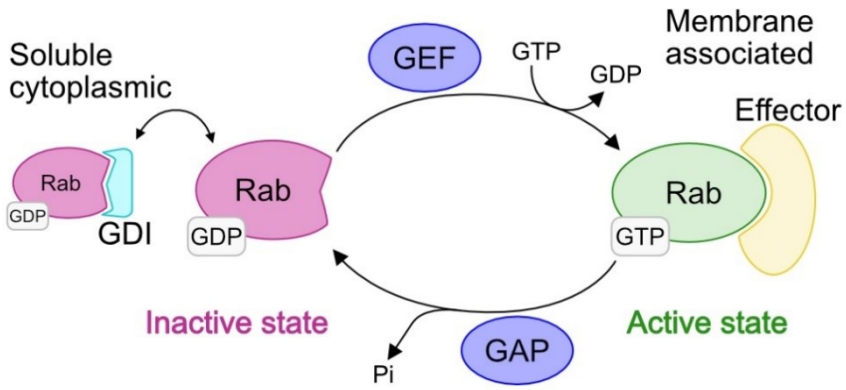

Figure 3: The Rab cycle

Rabs are inactivated by the binding of GDP, and in the inactive state, they are associated with GDP dissociation inhibitors (GDIs), which make them soluble in the cytoplasm. Guanine nucleotide exchange factors (GEFs) activate Rabs by exchanging the GDP for GDP. In their active GTP-bound state, Rabs are membrane-associated and interact with effectors to fulfill their function. Their activity is assisted by their enzymes GTPase-activating proteins (GAPs), which induce the hydrolysis of GTP into GDP and a phosphate group, as a result inactivating the Rabs.

Rab are GTPases; this means that they hydrolyze the guanosine triphosphate (GTP) as an energy source to fulfill their function. As a consequence, they have two distinct states that they cycle through: the inactive, GDP-bound state and the active, GTP-bound state [Homma et al., 2021]. In their inactive state, GDP-bound Rabs interact with the guanine nucleotide exchange factors (GEFs), which exchange the GDP for GTP. Active forms of Rabs are not associated with GDIs; rather, their unmasked prenyl groups allow them to be inserted into specific organelle membranes. Once active forms of Rabs are in their correct position, they recruit their binding partner proteins, the Rab effectors, who in turn regulate the various membrane trafficking steps. Finally, in order to deactivate them, the GTPase-activating proteins (GAPs) catalyze the hydrolytic activity of Rabs, turning GTP into GDP and inactivating the Rab protein. This allows the GDIs to remove the inactive forms of Rabs from the membranes and relocate them into the cytoplasm.

Single amino-acid mutations in the G motifs of Rab GTPases are enough to prevent their binding to either GTP or GDP [Lee et al., 2009]: A mutation of threonine or serine into asparagine (TN or SN mutations) results in a GTP binding defective Rab GTPase referred to as the dominant negative (DN) form, while a mutation of a glutamine into leucine (QL mutation) results in a GDP binding defective Rab GTPase called the constitutively active (CA) form. In *Drosophila melanogaster*, all 26 confirmed Rab GTPases also have known DN and CA forms [Zhang et al., 2007].

Rabs in cellular trafficking

Rab GTPases are involved in cargo selection and vesicle budding, the transport of vesicles and their targeting to specific membranes, and finally vesicle fusion and cargo release [Stenmark, 2009]. They regulate cellular trafficking through their binding partners, the Rab effectors. The effector proteins can be recruited or activated by GTP-bound Rabs, and include coat proteins (e.g. COPI, COPII, clathrin), sorting adaptors, motor proteins (dynein and kinesin), tethering complexes (e.g. exocyst and HOPS complexes), SNAREs, kinases and phosphatases [Cai et al., 2007].

Cargo selection can be facilitated by specific Rabs whose effectors are sorting proteins. For example, TIP47 is a sorting protein for the mannose-6-phosphate receptors (M6PRs) and is required for their recycling from late endosomes to the TGN. Active Rab9 on late endosomes recruits TIP47 to the membrane and increases its affinity for the M6PRs, thereby facilitating cargo selection for the recycling pathway [Carroll et al., 2001].

Rab5 is a conserved and ubiquitously-expressed marker for early endosomes [Simonsen et al., 1998]. It is involved in both the assembly and disassembly of clathrin-coated vesicles during their budding process: The GDI-bound form of Rab5 is required for adaptor-dependent sequestration of transferrin into clathrin-coated vesicles [McLauchlan et al., 1998]. It is also required for the disassembly of AP2 from the clathrin-coated vesicles via its GEF protein GAPVD1 [Semerdjieva et al., 2008].

Motor proteins are both direct and indirect effectors of various Rab GTPases in the cell. The Rab11 effector RAB11-FIP2 interacts with myosin Vb and facilitates the movement of recycling endosomes to the plasma membrane [Hales et al., 2002]. Rab7 recruits the dynein-dynactin complex to the late endosomes through its effector RILP, which transports late endosomes and lysosomes away from the cell periphery [Jordens et al., 2001]. Rab6, found on the Golgi, directly recruits the kinesin KIF20A [Echard et al., 1998], and indirectly the dynein-dynactin complex through its effector bicaudal D1 [Matanis et al., 2002], facilitating retrograde transport from the Golgi to the ER. These examples demonstrate the role of Rab GTPases in the mechanics of vesicular transport through the cell.

Vesicle fusion is primarily facilitated by the interaction of SNAREs, specifically the vesicle v-SNAREs and target t-SNAREs, which build a complex forcing the vesicle and the target membrane into close proximity. Rab5 is required for this process as well – its effector EEA1 directly interacts with the early endosomal t-SNAREs Syntaxin6 [Simonsen et al., 1999] and Syntaxin13 [McBride et al., 1999]. Another example for Rab regulation of vesicle fusion is Rab7, which enables the endosome-lysosome fusion through the recruitment of the HOPS complex to the late endosomal membrane by its effector RILP [Lin et al., 2014].

The variety of trafficking steps that Rabs are involved with makes them one of the two most important molecular groups for determining the identity of the organelles in the endosomal pathway [Elkin et al., 2016]. They are recruited to the correct organelle membrane by Rab

GTPase regulators, which are in turn recruited by phosphatidylinositol phospholipids (PIPs), the other most important organelle identity determining molecular group [Jean & Kiger, 2012]. PIPs are derivatives of phosphatidylinositol which can be phosphorylated at positions 3, 4 and 5 of the inositol ring, and which can be converted between one another through the functioning of lipid phosphatases and kinases [Di Paolo & De Camilli, 2006]. The lipid phosphatases and kinases are often Rab effectors, thereby enabling the two groups to coordinate membrane identity changes in the endosomal pathway.

Rabs in Drosophila melanogaster

31 Rab GTPase genes have been discovered in *Drosophila melanogaster* based on sequence homology [Zhang et al., 2007], and their expression patterns and subcellular localization have been demonstrated by several studies [Chan et al., 2011; Jin et al., 2012; Dunst et al., 2015]. Of those, 26 genes have been shown to actually be expressed. Half of them are either exclusively expressed or strongly enriched in neurons – not surprising, given their role in cellular trafficking and its importance in synaptic signaling, which is the primary mode of neuronal cell interaction [Kiral et al., 2018]. Of the remaining half, eight Rab GTPases (Rabs 1, 2, 5, 6, 7, 8, 11, 35) are essential for cell survival, and their null mutations result in lethality in early embryonic to larval stages [Kohrs et al., 2021]. Accordingly, these Rabs are all ubiquitously expressed in *Drosophila*, and have been shown to regulate crucial steps in cellular trafficking.

Rab1 regulates ER-to-Golgi trafficking, as well as trafficking in the Golgi itself [Satoh et al., 1997]. Rab2, which in human cells has been associated with retrograde Golgi-to-ER trafficking [Tisdale & Jackson, 1998], has in *Drosophila* been associated with lysosomal degradation of both autophagosomal and endosomal cargo as well [Lőrincz et al., 2017]. Rab5 is the key regulator of early endosomal membrane trafficking [Yuan & Song, 2020]. Rab6 is found on the Golgi membrane and is involved in intra-Golgi transport [Dickson et al., 2020], as well as retrograde transport to the TGN [Satoh et al., 2016]. Rab7 is crucial for the functioning of late endosomes, lysosomes and autolysosomes [Guerra & Bucci, 2016]. Rab8 localizes to the TGN, post-Golgi vesicles and plasma membrane, playing a role in anterograde transport of cargo at this final stage [Bellec et al., 2018]. Rab11 localizes to the recycling endosomes and controls vesicle exocytosis [Takahashi et al., 2012]. Lastly, Rab35 has also been implicated in a Rab11-independent endocytic recycling pathway [Kouranti et al., 2006].

The role of Rabs in Wnt secretion

Since Wnt proteins are secreted into the extracellular space, they must pass through the secretory and endosomal pathways, where their trafficking would fall under the control of various Rab GTPases. Nevertheless, only a select small number of Rabs have been directly implicated in this process.

Overexpression of Rab1-DN resulted in the accumulation of overexpressed WntD, a Wnt ligand unique to *Drosophila melanogaster* which does not require palmitoylation for functioning [Ching et al., 2008]. Wg is recycled from early endosomes to the plasma

membrane by the Ykt6 SNARE protein via Rab4-positive endosomes in a transcytosis-independent route [Linnemannstöns et al., 2020; Witte et al., 2020]. While no direct involvement of Rab5 in Wg trafficking has been shown, Rab5 has been implicated in the process of recycling Evi from the cell surface. The knockdown of Rab5 (and thus disruption of endocytosis and the early endosomes) resulted in the accumulation of Evi on the plasma membrane in these cells [Belenkaya et al., 2008].

In mice, the Evi homologue Gpr177 interacted directly with Rab8a through its C-terminal tail, and Rab8a was required for the anterograde transport of Gpr177 [Das et al., 2015]. The study found that knockout of Rab8a in Paneth cells caused a significant reduction of Wnt3a secretion. Rab9 was also associated with Gpr177 as indicated by immunoprecipitation in the same study, though further studies to address this topic are missing. Lastly, the release of Evi-carrying exosomes at the neuromuscular junction of *Drosophila melanogaster* was facilitated by Rab11 in conjunction with Syntaxin1A, and this process was necessary for the secretion of Wg into the synaptic junctional region from the synaptic boutons [Koles et al., 2012].

Rab GTPases have also been shown to have roles in the downstream Wnt signaling pathway. For example, Rab5-mediated endocytosis of Wg in the receiving cells limited the spread of Wg secreted from the dorsoventral boundary [Marois et al., 2006]. The study found that Wg in these cells colocalized with both Rab5 in early endosomes and Rab7 in late endosomes. Furthermore, overexpression of the Rab5-DN resulted in the increase of extracellular Wg levels. By contrast, overexpression of the Rab7-DN resulted in the accumulation of Wg in the receiving cells, likely due to the disrupted degradation pathway.

Rab7 GTPase

Rab7 is a member of the Rab GTPase protein family, ubiquitously expressed and crucial for proper cellular function [Guerra & Bucci, 2016]. It is found on the membranes of the late endosomal pathway organelles, serving as the primary late endosomal marker. Its recruitment to the early endosomes facilitates endosomal maturation through the 'Rab5-to-Rab7 switch' [Langemeyer et al., 2020]. On early endosomes, Rab5 binds the heterodimeric complex Mon1-Ccz1, which serves as a guanine nucleotide exchange factor (GEF) for Rab7. Once Mon1-Ccz1 is recruited to the early endosomal membrane, it in turn recruits GDP-bound Rab7 and activates it by the exchange of GDP to GTP. Mon1 then induces the removal of Rab5 from the membrane by displacing the Rab5 GEF Rebex-5, thereby completing the switch [Poteryaev et al., 2010].

Rab7 has been implicated in selective sorting of endosomal cargo – for example, it is required for the sorting of mannose-6-phosphate receptor and interferon alpha-receptor, but not for EGF or recycling of transferrin [Girard et al., 2014]. It recruits the cargo-recognition subcomplex of the Retromer complex through direct interaction with the Vps26 retromer subunit [Rojas et al., 2008]. Additionally, it facilitates the movement of late endosomes through indirect interactions with the motor proteins Dynein and Kinesin [Jordens et al., 2001; Pankiv et al., 2010].

At the late endosome, Rab7 facilitates their tethering and fusion to lysosomes, the organelles which serve as reservoirs for the cell's hydrolases and where proteolytic degradation occurs [Yang & Wang, 2021]. Lysosomes are highly acidic, with a pH of 4.5, and are positive for Lysosome-associated membrane protein 1 (LAMP1). The fusion of late endosome and lysosome is facilitated by the Homotypic Fusion and Vacuole Protein Sorting (HOPS) complex [Vanlandingham & Ceresa, 2009]. The HOPS complex is initially assembled on the lysosome through the recruitment of its subunit Vps41 by the GTPase Arl8 [Khatter et al., 2015]. The HOPS complex is in parallel recruited to the late endosome by interacting with the Rab7 effector RILP, which brings the two compartments together and facilitates their fusion [Lin et al., 2014]. Beyond that, RILP has been shown to interact with the subunits of the Vacuolar ATPase, a protein complex regulating the lysosomal pH, to control its assembly and function [De Luca & Bucci, 2014]. Therefore, Rab7 is not only involved with the endosome-lysosome fusion, but also the acidification of lysosomes themselves.

Additionally, Rab7 has also been implicated in autophagosome maturation into autolysosomes by their fusion with the lysosome [Lőrincz et al., 2017], a process also facilitated by the HOPS complex through its interaction with Syntaxin 17 (Syx17) [Van der Beek et al., 2019]. Autophagosomes are a specialized double-membraned organelle whose primary function is autophagy, the sequestration of cytosolic content destined for degradation [Glick et al., 2010]. The Atg8 protein family is a marker family for autophagosomes and is required for autophagosome formation as well as autophagosome fusion to lysosome [Lee & Lee, 2016].

Rab7 has therefore emerged as a crucial player for the regulation of various steps of the endocytic pathway, from early endosomal maturation into late endosomes, to the lysosome fusion with both endosomes on the one end of the pathway and autophagosomes on the other. It is thus one of the extremely well researched Rab GTPases in the field.

2.3 *Drosophila melanogaster* as a model organism

The small fruit fly, *Drosophila melanogaster*, belongs to the family Drosophilidae in the order Diptera and has served as one of the most commonly used model organisms for over a hundred years [Hales et al., 2015]. Research using *Drosophila melanogaster* has led to significant discoveries in the fields of genetics, evolution, development and disease, which has resulted in Nobel Prizes for the general contributions to biology, chemistry and medicine [Reider & Larschan, 2014]. The first study was performed by Thomas Hunt Morgan, who demonstrated the X-chromosome-linked inheritance of the *white* gene, whose mutation changed the fruit fly eyes from red to white [Morgan, 1910]. Morgan's work with *Drosophila* led to the further interest in the model organism in the nascent fields of inheritance, and allowed him and colleagues to define many of the basic principles of genetics.

The advantage of *Drosophila melanogaster* as a model organism lies in the fast individual development and generational turnover time, combined with the ease and low costs of handling and maintenance. In addition, *Drosophila* shares 60% genome homology with

humans and many of its organ systems are also functionally analogous [Ugur et al., 2016]. This makes is suitable for the study of human diseases, including cancer [Mirzoyan et al., 2019]. Lastly, due to the large and sustained interest in it as a model organism for the study of genetics especially, many powerful genetic tools have been invented and perfected for use in *Drosophila*, chief among them the Gal4/UAS system [Dahmann, 2008].

Drosophila life cycle

The life cycle of the *Drosophila melanogaster* is holometabolic, consisting of four life stages: embryo, larva, pupa, and adult. As with most ectothermic organisms, development time varies depending on the environmental temperature. While the ideal temperature for fly development is 25°C, requiring 10 days from egg-laying to eclosion, flies can also be reared at 18°C (21 days life cycle) and 29°C (7 days life cycle) depending on the experimental setup.

Fertilized female fruit flies reared at 25°C lay on average 100 eggs per day, with their egg production capacity declining with their age [Rogina et al., 2007]. The embryonic development lasts 24 hours and the next generation hatch as larvae that begin feeding immediately. The larvae undergo two moltings, thus developing through three larval instar stages lasting 24h (first instar), 24h (second instar) and 48h (third instar), and which result in a significant increase in their size [Tennessen & Thummel, 2011]. Third instar larvae depart from the medium near the end of their developmental stage to crawl on the vial walls as 'wandering larvae' in search of an ideal pupariation location. The pupal stage of development lasts for roughly 5 days at this temperature, and during this stage, the fruit fly undergoes complete metamorphosis [Bainbridge & Bownes, 1981]. Most of the fruit fly appendages develop during this stage from specialized larval organs called 'imaginal discs', which consist of undifferentiated epithelial cells [Beira & Paro, 2016]. At the end of the pupal stage, the adult flies eclose from the pupae as fully developed adult individuals, with the females ready for mating within 8 to 12 hours post-eclosion at 25°C.

Wing imaginal disc and salivary gland

The imaginal discs found in the *Drosophila* larval stage of development are specialized organs functioning as precursor structures to adult fly appendages [Beira & Paro, 2016]. *Drosophila melanogaster* larva has 9 bilateral sets of imaginal discs located cranially (one each of labial, clypeolabral, eye-antennal, humeral, wing and haltere discs, as well as three sets of leg discs), and one additional genital disc located caudally in the larval body [Aldaz & Escudero, 2010]. Imaginal discs are composed of a single layer of polarized columnar epithelial cells, with third instar discs having between 10.000 and 50.000 cells.

The wing imaginal disc is one of the largest imaginal discs found in the *Drosophila* larva, and during metamorphosis, it gives rise to not only the wing, but also the wing joint and one half of the thorax [Diaz de la Loza & Thompson, 2017]. Morphologically, it is divided into three segments – the pouch, the hinge and the notum, corresponding respectively to the adult structures. Wing disc cells undergo mitosis during the three larval instar stages until reaching the full size of the organ, forming in the process the anteroposterior (AP) and the dorsoventral

(DV) compartment boundaries [Diaz de la Loza & Thompson, 2017]. The formation of compartment boundaries is regulated by the Wnt [Neumann & Cohen, 1997] and Dpp (Decapentaplegic, a BMP morphogen) [Zecca et al., 1996] pathways respectively. The crosstalk between the two pathways, together with the Hedgehog and Hippo pathways as well as the activity of the *Drosophila* hormone ecdysone, coordinate the wing disc growth [Gou et al., 2020; Parker & Struhl, 2020]. During the pupal stage, the wing disc epithelium undergoes eversion by invagination along the dorsoventral boundary until the dorsal and ventral compartments are aligned on their basal sides. This is followed by tissue elongation and shaping, which results in the characteristic adult fruit fly wing.

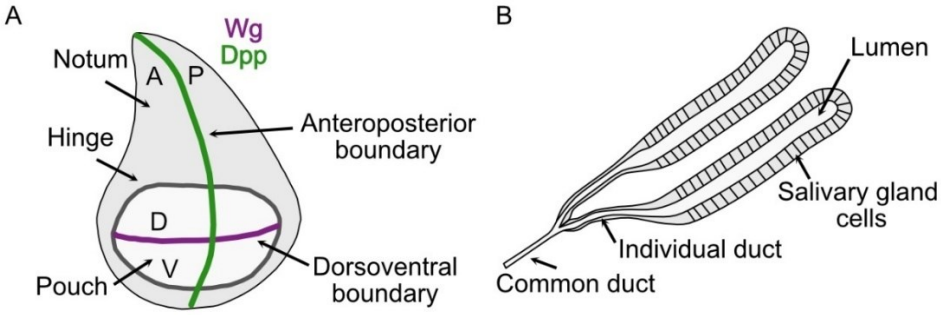

Figure 4: **Drosophila melanogaster *wing imaginal disc and salivary glands***
A Larval wing imaginal disc; consists of a notum (forms the adult thorax), hinge (forms the wing joint) and pouch (forms the wing blade), and is divided into the dorsal and ventral compartment by the expression of Wg at the dorsoventral boundary, as well as the anterior and posterior compartment by the expression of Dpp at the anteroposterior boundary.
B Larval salivary glands; consist of two lateral glands with single layer epithelium enclosing the duct lumen. The individual ducts fuse into the common duct.

Fruit fly larvae possess a pair of specialized secretory organs called the salivary glands, whose main function is to produce glycosylated mucins, the 'glue' which the larva uses during the initial pupariation stages to attach itself to the pupariation surface [Andrew et al., 2000]. The organ system consists of two lateral glands built from columnar epithelial cells with a duct at its center, which fuse into the central common duct. The salivary gland cells are one of the largest in the fruit fly larva due to their polytene chromosomes needed for their metabolic requirements. Brief high levels of the hormone 20-hydroxyecdysone (20E) in the early third instar larval stage initiate the glue synthesis and packaging into granules within the cells [Farkaš et al., 2015]. A second strong pulse of 20E shortly before pupariation triggers the wandering larval stage and also stimulates the secretion of the granules by exocytosis into the ducts, resulting in the expansion of the duct and the shrinking of the cells themselves. Finally, about 16h after pupariation, the salivary glands undergo histolysis as part of the metamorphosis process and are fully lost by the adult fly stage [Farkas & Mechler, 2000].

The Gal4/UAS system

Protein overexpression in *Drosophila melanogaster* by the Gal4/UAS system [Brand & Perrimon, 1993] is one of the bedrocks of experimental methods in the *Drosophila* field. The Gal4/UAS is a system with two components: the Gal4 transcription factor, which is expressed under the control of a chosen promoter sequence (the flies carrying these constructs are referred to as 'driver lines'), and a transgenically inserted sequence encoding for a protein or an RNA with a Gal4-binding upstream activation sequence (UAS) enhancer placed in front of

it (the flies carrying this transgenic insertion are referred to as 'reporter lines'). On its own, Gal4 is non-toxic and does not affect cellular function. Upon the crossing of the driver line flies to the reporter line flies, Gal4 binds to the UAS and activates transcription of the downstream sequence, thereby inducing transgenic overexpression of the protein or RNA of interest.

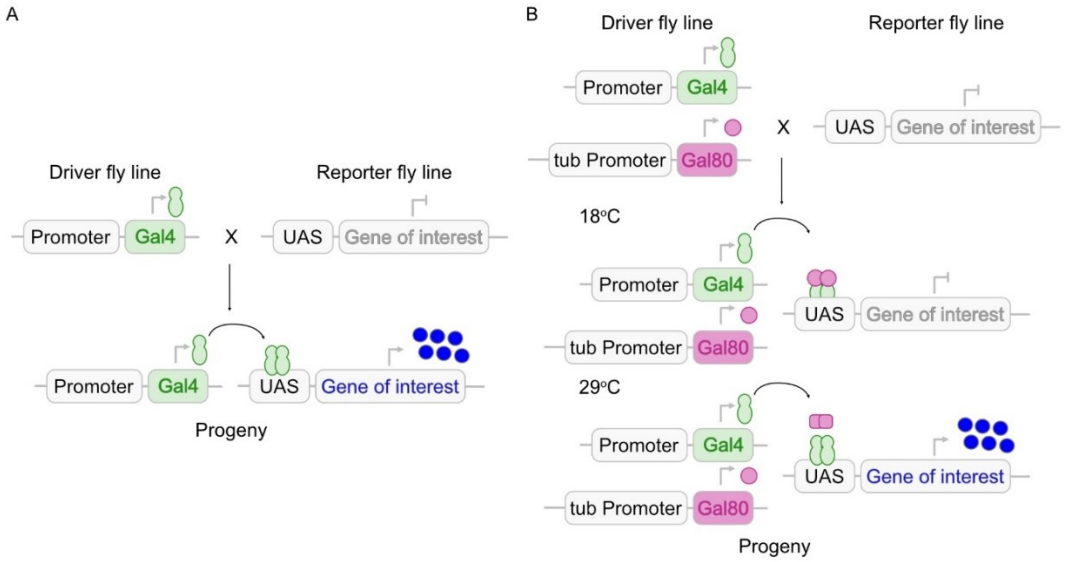

Figure 5: The Gal4/UAS and Gal80^{ts}/UAS systems
A The Gal4/UAS system works by driving the expression of Gal4 under a spatially-controlled promoter. Gal4 binds to the UAS and activates the overexpression of the gene of interest downstream of it.
B The Gal80^{ts}/UAS system works by driving the expression of Gal4 under a spatially-controlled promoter, and the expression of Gal80^{ts} under the tubulin promoter. At 18°C, Gal80 binds to Gal4 and suppresses its activity, blocking the overexpression of the gene of interest. At 29°C, Gal80^{ts} cannot bind to Gal4, and Gal4 can drive the overexpression of the gene of interest.

One of the largest benefits of the Gal4/UAS system lies in the variety of driver lines which provide spatial control of overexpression, so that the UAS construct is only expressed in a chosen subset of cells which show activity of the chosen driver line promoter. However, since the Gal4/UAS system results in strong overexpression of the UAS construct, it can be toxic depending on what that UAS construct is or when it is expressed during development. For this reason, a common variation of the system has been developed – the Gal80^{ts}/UAS system – which allows temporally as well as spatially controlled expression [McGuire et al., 2003]. Gal80^{ts} is a repressor of Gal4 and binds to it at 18°C, preventing the activation of the UAS construct transcription. At 29°C, however, Gal80^{ts} is unable to bind to Gal4, thus releasing Gal4 to activate the expression of the UAS construct. This system allows the controlled duration as well as initiation of expression, as the process is reversible. If flies are returned from 29°C to 18°C, Gal80^{ts} will bind to Gal4 again. It should be kept in mind that this is not a quick process, and that though expression speed will depend on the chosen driver line, the transcription and translation of the protein will still require several hours.

2.4 Genetic approaches to protein visualization and manipulation

2.4.1 Endogenous protein tagging

Protein visualization is one of the main methods of studying the localization of proteins within organelles, colocalization with potential protein interaction partners, protein movement dynamics and protein abundance. One of the most common ways in which proteins can be visualized in fixed and live imaging studies, as well as *in vitro* studies, is by fusing a visualization tag to them. These visualization tags can be short sequences designed for detection by antibodies (such as a His [Hochuli et al., 1988] or V5 tag [Hanke et al., 1992]), or separate proteins that facilitate visualization through their own intrinsic properties (i.e. fluorescent proteins) or the binding of chemical labelling dyes (e.g. HaloTag [Los et al., 2008] or SnapTag [Keppler et al., 2003]). This is done by adding their genomic sequence to the gene sequence of the protein of interest so that the cells express the resulting protein fusion. CRISPR/Cas9 homology-directed repair (HDR) system has proven an extremely efficient method for endogenous protein tagging [Gratz et al., 2014; Port et al., 2014].

CRISPR/Cas9 system [Jinek et al., 2012; Cong et al., 2013] is a method allowing for the precise cutting of the DNA sequence, derived from the bacterial immune system [Mojica et al., 2005]. In order for the Cas9 endonuclease (derived from *Streptococcus pyogenes*) to induce a double-stranded break (DSB) at a precise location in the genome, it requires a single guide RNA (sgRNA). sgRNA is a complementary 20 nucleotide DNA sequence directly upstream of the protospacer adjacent motif (PAM) sequence (NGG for Cas9). When both are present in the cell, Cas9 will cut the cellular DNA three nucleotides upstream of PAM. The HDR system relies on the cellular DSB repair system. The cell is provided with an exogenous DNA sequence containing the insert of choice flanked on either end by homology arms complementary to the DNA sequence directly adjacent to the insertion site. This complementarity allows the cell to repair the DSB by using the exogenous DNA as a template, thereby incorporating the insert into its DNA.

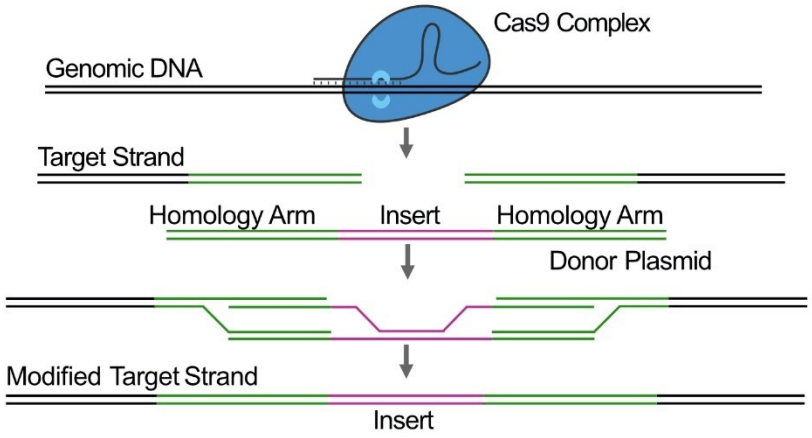

Figure 6: CRISPR HDR tagging system
Cas9 is guided to the cut site by sgRNA, where it induces the double-stranded break. The cell repairs the break using HDR based on the exogenous DNA containing homology arms extending on either side of the double-stranded break with the insert between them, thereby incorporating the insert into the genomic DNA at the chosen site.

The use of fluorescent proteins as visualization tags stems from the discovery of the green fluorescent protein (GFP) in the *Aequorea victoria* jellyfish [Shimomura et al., 1962; Chalfie et al., 1994]. The physical properties of fluorescent proteins – their excitation and emission spectra, maturation time, fluorescence lifetime, brightness, and their pKa value – can be significantly affected by the changes in their amino acid sequence and their environment. The

former has resulted in the use of genome engineering for the purposes of developing fluorescent protein variants and derivatives with improved properties [Shaner et al., 2007]. The latter has imposed limitations on the selection of suitable fluorescent proteins for specific experimental and cellular contexts [Constantini et al., 2015].

The pKa value is the pH value at which protein's fluorescence intensity drops by half, and is thus the measure of the protein's acid sensitivity [Haupts et al., 1998]. Because of this, the sub-cellular environment that the fluorescent protein is in can have a significant impact on its functionality [Constantini & Snapp, 2013]. In eukaryotic cells, the pH value of various organelles can differ significantly – e.g., the ER has a neutral pH value of 7.2 while the lysosome possesses a much more acidic pH of 4.5 [Paroutis et al., 2004]. Thus, fluorescent proteins passing through the secretory and endocytic pathways of eukaryotic cells will encounter a range of pH values between these two. This is especially relevant for the visualization of secreted proteins which pass through numerous different organelles depending on their mode of secretion. Therefore, it may be necessary to consider the pKa value of the fluorescent protein tag in the context of endogenous tagging of proteins targeted for secretion.

Fluorescent proteins can be fused to the proteins of interest by inserting their genetic sequence into the genomic locus of the protein of interest. Insertion of the fluorescent protein sequence right before the start codon (for N-terminal tagging) or right before the stop codon (for C-terminal tagging) is the simplest positioning solution for endogenous protein tagging. The success of this method, however, is predicated on the protein folding and no disruption of the protein activity. For proteins targeted to specific organelles through N-terminal targeting sequences or proteins with C-terminal sequences for retention or retrieval of the protein, insertion of the fluorescent protein tags at the protein termini can easily disrupt protein function. In such cases, the alternative is the insertion of the fluorescent protein sequence somewhere within the sequence of the protein of interest to prevent such problems. Overall, the insertion of the fluorescent tag within the endogenous locus requires strategic planning, followed by experimental testing to circumvent interfering with the protein's function.

2.4.2 Protein trap-and-release systems

Manipulation of protein activity through the change in protein structure, interaction partners or protein localization is an important way to study the role of proteins in different cellular contexts. Protein dynamics are tightly bound with protein localization, as proteins must be targeted to their sites of activity after synthesis in order to exert their function. Protein secretion equally requires the transport of proteins through the secretory pathway, and manipulating the localization of secreted protein through their blocking or redirection at a specific secretion step can reveal much about the overall secretion process. Methods which allow for the sequestration of the protein of interest at a specific organelle, followed by a trigger that would release the sequestered protein synchronously, can be of great benefit for such studies. Two separate but similar experimental systems of this sort have been developed

in the last decade – the RUSH system [Boncompain et al., 2012] and the LAMAs [Farrants et al., 2020].

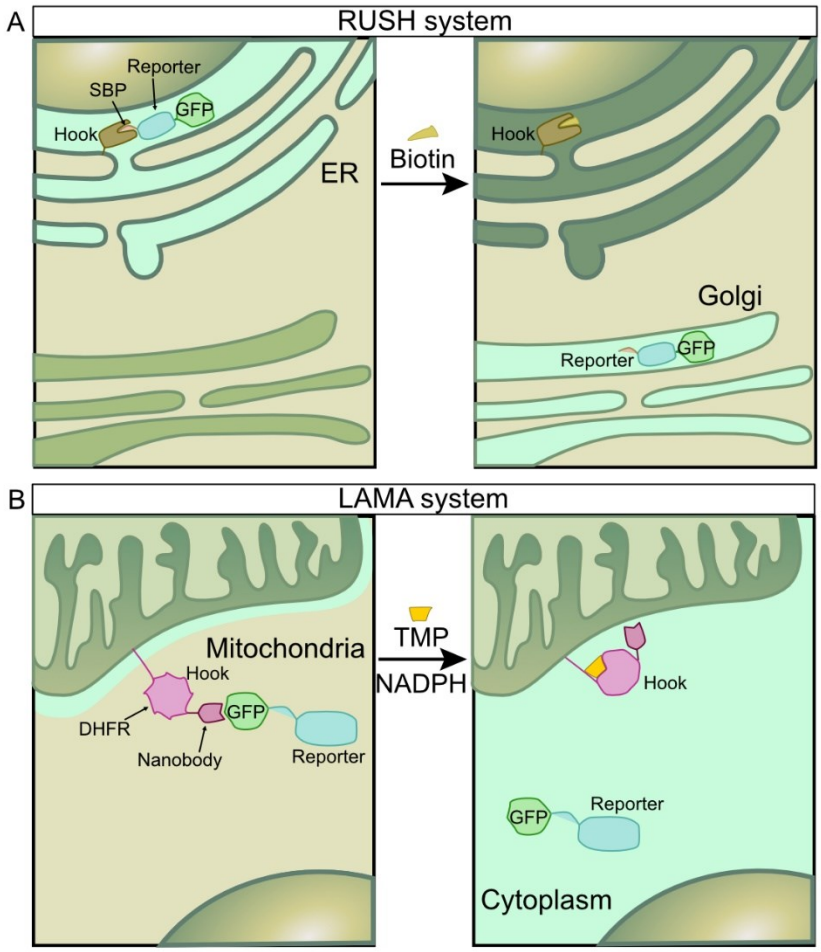

Figure 7: The RUSH and LAMA systems
A The Streptavidin-based RUSH hook traps the reporter, which is fused to the SBP. After addition of biotin, the reporter is freed from the hook by the stronger affinity of the Streptavidin for the biotin. If the hook is in the ER, the reporter will continue to travel through the secretory pathway.
B The LAMA hook composed of DHFR and a GFP-specific nanobody traps the reporter-GFP fusion. Upon addition of TMP in the presence of NADPH, the hook changes conformation and frees the reporter. If the hook is on the cytoplasmic side of the outer mitochondrial membrane, the reporter will be released into the cytoplasm.

The RUSH system

The RUSH (retention using selective hooks) system [Boncompain et al., 2012] is a two-state assay which allows for a rapid, synchronous switch from the bound to the released state. The RUSH system requires expression of two proteins. The first protein is the 'hook', a membrane protein stably anchored to an organelle of choice and tagged with streptavidin. The second is the reporter protein tagged with the streptavidin-binding peptide (SBP). Due to the high binding efficiency of streptavidin and SBP, upon expression, the reporter is trapped by the hook at the selected organelle and away from its place of activity. This binding can be disrupted by the addition of vitamin biotin, which is non-toxic and readily passes the cell membranes to enter subcellular compartments. As biotin has a higher binding affinity for streptavidin than SBP, its addition to the cells induces the synchronous release of the reporter from the hook. Subsequently, the reporter is free to travel to its cellular compartment and there perform its activity. The visualization of the hook and the reporter is achieved through the fusion of fluorescent proteins or chemical tags to the constructs.

The RUSH system has so far been used almost exclusively in mammalian cell culture, for example in neuronal [Watson et al., 2023] and HeLa cells [Graab et al., 2019]. It has been employed primarily for the study of protein transport in the ER and Golgi, with one study

using it to analyze Wnt trafficking through the cell [Moti et al., 2019]. The authors tracked RUSH-Wnt3a and RUSH-Wnt8a transport from the ER through the Golgi to the plasma membrane of HeLa cells. For this, they performed live imaging of fluorescently labeled proteins after release from the KDEL ER-RUSH-hook by the addition of biotin to the culture medium. The study showed that Wnt3a vesicles paused for several minutes underneath the plasma membrane prior to disappearing, as well as that Wnt3a does not remain for long on the plasma membrane. It also demonstrated the presence of Wnt3a vesicles in HeLa cell protrusions.

Only one publication so far exists employing the RUSH system in *Drosophila melanogaster* [Glashauser et al., 2023]. The authors primarily tested the RUSH system in the *Drosophila* embryos, with the biotin delivery by injection, though they also showed the functional expression of the system in larval wing imaginal discs and adult ovarian follicles. The only hook they used was a KDEL ER-RUSH-hook, expressed in combination with the streptavidin-tagged overexpressed Serpentine (Serp), a chitin deacylase endogenously expressed in embryonic tracheal cells; endogenously expressed Fasciclin II (Fas2), a GPI-anchored membrane protein; and endogenously expressed Notch receptor. Upon the addition of biotin, they were able to demonstrate the change in the localization of RUSH-Serp and RUSH-Fas2 in *Drosophila* embryonic tissue and egg chambers from the ER to the tracheal lumen and the plasma membrane respectively. No incubation with biotin was performed on wing imaginal discs. In addition, they were able to show that without the addition of biotin, the RUSH system can trap the endogenous Notch receptor in the ER, causing the phenocopying of the Notch loss-of-function phenotype.

The LAMA system

The LAMAs (ligand-modulated antibody fragments) [Farrants et al., 2020] are a system which shares the functional setup with the RUSH, though it uses different components. The two components of the LAMA system are a reporter protein tagged with GFP and a membrane-anchored hook protein fused with the circularly permutated *Staphilococcus aureus* dihydrofolatereductase (cpDHFR) coupled to a GFP-specific nanobody. When co-expressed, the nanobody of the hook binds the GFP of the reporter, trapping it at the specific organelle membrane where the hook is anchored. Addition of a small antibacterial molecule trimethoprim (TMP) together with the nicotinamide adenine dinucleotide phosphate (NADPH) found naturally in cells induces a conformational change to the cpDHFR, which results in the decoupling of the nanobody from the GFP. Once released, the GFP-tagged reporter can localize to its correct compartment in the cell.

So far, the LAMA system has only been used in one study [Francis et al., 2022], to observe the change in localization of Rab35 from the mitochondria, where the Mito-LAMA-hook was expressed, to the sites of actin polymerization in HUVEC cells. There are no publications where the LAMA system was employed in the *Drosophila melanogaster* tissues or organs.

Applications in the Drosophila melanogaster *system*

While the use of the RUSH and LAMA systems in cell culture by necessity focuses on intracellular processes, their adaptation for *Drosophila melanogaster* would allow for the study of trafficking processes and protein sequestration on the organ rather than the cellular level. Two general experimental applications arise from their implementation in the fruit fly. The first experimental application is the use of the systems for the general study of cytoplasmic protein localization, as well as the direct study of secretory traffic dynamics by the trapping and release of secreted proteins. The second experimental application is their use for protein manipulation on the supracellular level. The primary system used for spatial and temporal control of protein expression in *Drosophila* is the Gal80^{ts}/UAS overexpression system, which cannot be used for the direct manipulation of endogenously expressed proteins. Additionally, Gal80^{ts}/UAS system is not synchronous across the tissue and is not acute, requiring several hours between system induction and protein expression. It therefore allows for the observation of intermediate-term or long-term effect of protein overexpression only. The RUSH or LAMA systems in combination with the Gal4/UAS system could be used for both endogenously tagged and overexpressed proteins. Furthermore, it would permit a synchronous, acute activation of the protein through its release from the hook and relocation to the site of activity and therefore allow for the study of immediate or short-term changes in the tissue, potentially in live imaging studies.

2.5 The aims of the thesis

Wnt proteins must be secreted from the producing cells in order to coordinate tissue growth, development and homeostasis. Although the process of Wnt synthesis and secretion is well described, not all steps of this process have been fully elucidated. One of the protein families which have only marginally been implicated in the different stages of the Wnt secretion process are Rab GTPases. Given that Rab GTPases are master regulators of membrane trafficking, it can be assumed that they are also required for Wnt secretion in the cells. Until now, however, only the two general secretion Rabs – Rab8a in murine Paneth cells [Das et al., 2015] and Rab11 in *Drosophila* neuromuscular junctions [Koles et al., 2012] – have been directly connected, respectively, to anterograde trafficking of Wnt3a from the Golgi to the cell surface and the exosome secretion of Wg. The question remains, therefore, whether any Rab GTPases have dedicated roles in the different modes of Wnt secretion, or if only the Rabs responsible for the general secretion and endocytosis steps are involved with Wnt trafficking within the secreting cells.

Answering this question was the main biological goal of my thesis. As no systematic analysis of the potential roles of Rab GTPases in Wnt secretion has been published in *Drosophila melanogaster* until now, I performed a screen on all 26 *Drosophila* Rab GTPases by perturbing them in wing imaginal discs and observing the changes in Wnt distribution in the tissue. After identifying positive candidates, I then characterized the effects of their perturbation on Wg secretion specifically by studying the changes in Wg intracellular localization in Wg-secreting cells, the secreted Wg, and the effect on downstream Wnt pathway target gene expression.

The secondary goal of my thesis was the development of novel *Drosophila* tools which I could use in the characterization of Rab GTPase perturbation effect on Wnt secretion. One of the ways I intended to do this was by observing the process in living wing imaginal discs imaged *ex vivo*, for which the visualization of endogenous Wg and Evi was a prerequisite. Wg was endogenously tagged by Fillip Port and his colleagues with EGFP [Port et al., 2014]; prior attempts by my colleagues in the laboratory to endogenously tag Evi, however, resulted in hypomorphic alleles and were deemed unsuccessful. I therefore undertook to generate a fly line expressing a functional endogenously tagged Evi protein, as well as to generate a novel fly line expressing the Wg protein tagged with the red fluorescent protein mScarlet [Bindels et al., 2017] as a complement to the previously existing Wg:EGFP fly line. After generating the fly lines, I functionally validated them, comparing Wg:mScarlet to Wg:EGFP, as well as tested their functionality in live imaging studies.

Another way I chose to study Rab GTPase perturbation effects on Wnt secretion was by acute manipulation of the Rab proteins and their localization within the cells. This could be achieved by a method which would sequester the Rab proteins away from their organelle of activity and subsequently acutely release them from sequestration in live imaging studies. I identified two protein trap-and-release systems, the RUSH and the LAMA systems, which were developed and implemented in cell culture, though neither were adapted for use in other biological models at the time. The RUSH system is the better-established system of the two, but the LAMA system's use of GFP nanobodies carries the advantage of the compatibility with pre-existing GFP-tagged protein fly lines. I therefore tested both systems in the wing imaginal discs and salivary glands in order to identify the one better suited for use in *Drosophila* research. Subsequently, I tested the more advantageous system in the context of the two *Drosophila* experimental applications listed in the previous section. My intent was to interrogate the general system function through the trapping and release of the Rab GTPases with an effect on Wg secretion, which would allow me to observe the dynamics of the phenotype on the tissue level. Secondly, I wished to determine whether the selected system could be implemented as an alternative to the Gal80^{ts}/UAS system.

The three main aims, as presented in the remainder of the thesis, can be summarized as following:

Aim 1: Endogenously tag Wg and Evi proteins with fluorescent tags using the CRISPR/Cas9 system
Aim 2: Adapt and optimize a protein trap-and-release system for use in Drosophila *tissues*
Aim 3: Screen for novel roles of Rab GTPases in Wnt secretion

Finally, I hoped that the novel tools I generated and the method I adapted for use in fruit fly organs would be a material contribution to the *Drosophila* field, while the characterization of Rab GTPases in Wnt secretion would provide a greater insight into the Wnt secretion pathway and the varied Wnt trafficking modes identified so far.

3 Results

3.1 Endogenous protein tagging of Wg and Evi using CRISPR

Protein visualization is important for the study of protein dynamics, especially in live imaging studies where immunohistochemistry cannot be used, as it requires cell fixation. Overexpression of a fluorescently tagged protein of interest requires simple and well-established delivery methods such as the use of the Gal4/UAS system in *Drosophila*, but can create an artificial environment in the cell. Tagging of endogenous proteins, on the other hand, reveals direct information about the native state of the protein, but requires careful selection of insertion sites and advanced gene editing methods such as the CRISPR/Cas9 homology directed repair (HDR) system.

I chose to endogenously fluorescently tag the *Drosophila* Wnt1 homolog Wingless (Wg) and its cargo carrier protein Evi/Wls in order to study the behavior of these proteins and their interaction with Rab GTPases using live imaging without resorting to their overexpression. I first used the CRISPR/Cas9 HDR system to insert the gene sequences of fluorescent proteins into the endogenous locus of Wnt and Evi proteins. After this, I functionally validated the resulting fusion proteins and analyzed their suitability for live and fixed imaging studies.

3.1.1 Endogenous tagging of Wg and Evi with fluorescent proteins by CRISPR/Cas9 homology-directed repair

As I was interested in studying Wnt secretion in *ex vivo* imaged living *Drosophila melanogaster* organs, I decided to endogenously tag Wg and Evi proteins with fluorescent protein tags, namely EGFP (green, 26.9kDa) and mScarlet (red, 26.4kDa). Selection of suitable insertion sites is the first step to endogenous protein tagging. Wg was previously successfully tagged with EGFP in *Drosophila* [Port et al., 2014]. Hence, I chose to use the same locus to tag Wg with mScarlet. In addition, I used the Wg:EGFP fly line generated by Port and colleagues for all my experiments requiring this construct. In the case of Evi, I decided against the protein termini for tag insertion. The N-terminus of Evi may contain a potential signaling sequence [Bänziger et al., 2006], while the C-terminus has been shown to carry an ER-targeting recycling sequence [Yu et al., 2014].

In order to identify suitable insertion sites within the *evi* locus, I aligned the *D. melanogaster* Evi amino acid sequence with those of three other organisms, two phylogenetically related (the insect species *A. gambiae* and *T. madens*) and one phylogenetically diverse (*H. sapiens*), and identified the degree of conservation for all of the amino acids of the *Drosophila* Evi protein (Figure 8A). In addition, I referenced the putative Evi structure available at the time, which was before the crystal structure of human Evi was published [Nygaard et al., 2021].

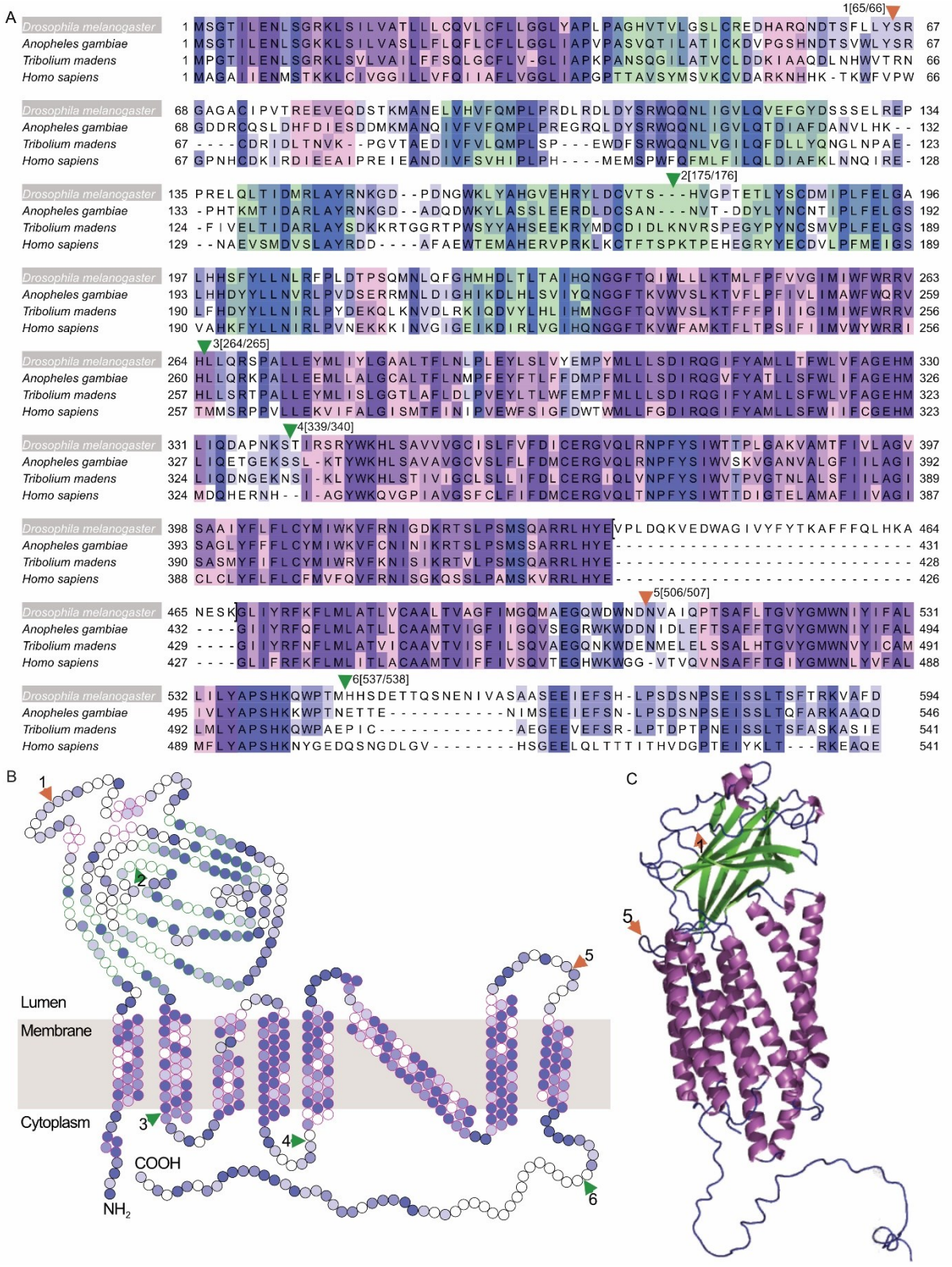

Figure 8: Potential endogenous tag insertion sites identified in Evi based on protein sequence conservation

A Alignment of Evi sequences for three closely related insect species and the distantly related human protein.

B Schematic representation of the putative structure of *Drosophila* Evi, based on human Evi structure published by Nygaard et al., 2021 and *Drosophila* Evi structure predicted by the Alphafold program.

C *Drosophila* Evi structure predicted by the Alphafold program (UniProt code B4QPR1).

Light-to-mid blue are residues with weak-to-strong sequence similarity. Dark blue are residues with sequence conservation within the four aligned species' Evi sequences. Magenta highlights indicate α-helices; green highlights indicate β-sheet lattices. Orange arrows indicate successful insertion sites; green arrows indicate unsuccessful insertion sites.

Evi is a transmembrane protein. I therefore chose three potential insertion sites on its cytoplasmic/intracellular side (between amino acids 65/66, 175/176 and 506/507) and three on its luminal/extracellular side (between amino acids 264/265, 339/340 and 537/538), such that the insertion sites were located in the unconserved regions of the protein, with flexibility regarding the phylogenic sequence similarity of these regions.

The precise location of the chosen insertion sites within the Evi sequence is shown with arrowheads in Figure 8A. Figure 8B shows these insertion sites placed within the updated two-dimensional structure of Evi, which incorporates the newly published crystallography information, including the β-sheet lattices found in the first luminal/extracellular loop. In both, conserved residues are marked in dark blue, with the α-sheets colored in magenta and β-sheet latices colored in green for orientation purposes.

I used the genome editing CRISPR/Cas9 HDR system to test for the endogenous tag insertion at each of the six chosen sites. I succeeded in generating stable fly line stocks carrying Evi:Tag insertions in two of these six sites, which I confirmed by locus genotyping. These are site 1, between 65Y and 66S, located in the first luminal/extracellular loop; and site 5, between 506D and 507N, located in the fourth luminal/extracellular loop (orange arrowheads, Figure 8). The predicted three-dimensional structure of the *Drosophila* Evi protein, generated by the IA program Alphafold, is shown in Figure 8B, with the insertion sites marked with orange arrowheads in order to show where the tags would be physically located within Evi.

The insertion of the fluorescent protein into Wg and Evi was confirmed by Sanger sequencing and confocal microscopy. The sequencing was performed using a PCR fragment ranging from about 100 nucleotides before the 5' homology arm to about 100 nucleotides after the 3' homology arm, in order to determine that there were no additional mutations occurring in the process of genome editing. For Wg:mScarlet, as well as Evi:EGFP-5, Evi:mScarlet-1 and Evi:mScarlet-5, no mutations within the homology regions of either protein were found.

Additionally, confocal microscopy was used to confirm the functionality of the inserted fluorescent proteins. Wing imaginal discs of larvae expressing the tagged proteins were dissected, fixed and imaged. Immunohistochemistry for Wg and Evi proteins was performed on wildtype wing imaginal discs as control. Lastly, Wg:EGFP fly line was used as an additional control of the insertion of mScarlet into Wg.

As expected from Sanger sequencing, Wg:Tag and Evi:Tag were both expressed in the tissue. Wg:mScarlet was present at the dorsoventral boundary in the pouch of the wing discs, as well as in the hinge ring and the notum patch. The pattern of Wg:mScarlet was similar to Wg:EGFP pattern and the immunofluorescent staining of wildtype Wg (Figure 9A-C). Similarly, Evi:EGFP-5, Evi:mScarlet-1 and Evi:mScarlet-5 were detectable by confocal imaging; they were expressed ubiquitously in the wing imaginal discs, with higher protein levels found at the dorsoventral boundary and the pouch ring. The pattern of all three Evi:Tag proteins matched that of the immunofluorescent staining of wildtype Evi (Figure 9D-G). Thus, I concluded that

my endogenous tagging of both Wg and Evi with mScarlet as well as EGFP (in the case of Evi) in *Drosophila melanogaster* was successful.

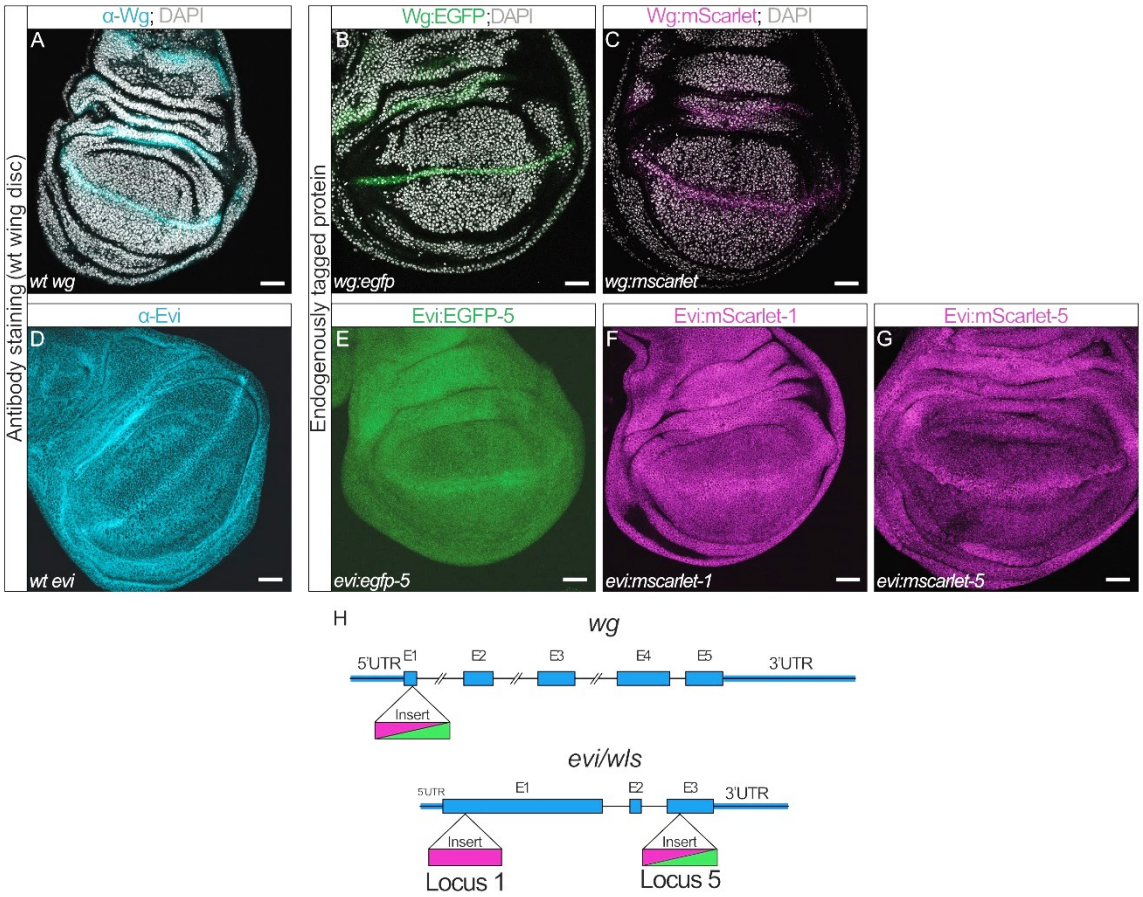

Figure 9: Wg and Evi endogenously tagged with mScarlet and EGFP show the same expression pattern in the wing imaginal disc as wildtype proteins

A-C Representative images of wing imaginal discs of Wg protein visualized by antibody staining (A) to endogenously tagged Wg with EGFP (B) or mScarlet (C).

D-G Representative images of wing imaginal discs of Evi protein visualized by antibody staining (D) to endogenously tagged Evi with EGFP in position 5 (E), as well as with mScarlet in position 1 (F) and position 5 (G).

H Schematic showing the locations of tag insertions within the *wg* and *evi* loci.

Scale bar = 50µm.

3.1.2 Functional validation of endogenously fluorescently tagged Wg and Evi

Despite the validation of the correct tag localization within the *wg* and *evi* locus in *Drosophila*, this does not exclude the possibility that protein functionality itself is affected. Many incorrectly tagged proteins display hypomorphic rather than lethality phenotypes. Therefore, I next tested the established fly lines carrying the endogenously tagged Wg:mScarlet, Evi:EGFP-5, Evi:mScarlet-1 and Evi:mScarlet-5 in order to confirm that the insertion of the tags did not affect the functionality of the proteins.

Wg and Evi are highly conserved, essential genes, and loss of their function results in embryonic lethality in *Drosophila*. The successful establishment of viable homozygous stocks for all four fly lines indicated that the fluorescent proteins did not significantly disrupt the gene function. However, the hypomorphs of both Wg and Evi are viable, though they display

characteristic wing notches in adult flies. In order to determine whether any of the generated fly lines had reduced protein functionality, I studied the wings of adult flies belonging to these fly lines. As negative control, I used wildtype flies; for positive controls, I knocked out Wg and Evi independently using the CRISPR/Cas9 system driven by the hedgehog-Gal4 (hh-Gal4) driver, which affects the posterior half of the wing disc and thus the bottom half of the adult wings. I also studied the wings of Wg:EGFP flies as an additional control for Wg:mScarlet.

Flies expressing Wg:mScarlet had wings identical to the wings of both Wg:EGFP expressing flies and wildtype flies, in direct contrast to the flies with Wg knockout under the hh-Gal4 driver, which showed obvious wing notches (Figure 10A-D). Similarly, all Evi:Tag expressing flies had wings identical to wildtype flies, in contrast to flies with Evi knockout under the hh-Gal4 driver, whose notches were even more pronounced than those of Wg RNAi (Figure 10A, E-H). This result confirmed that the Wg:Tag and Evi:Tag constructs did not show reduced function compared to wildtype Wg and Evi during fly development.

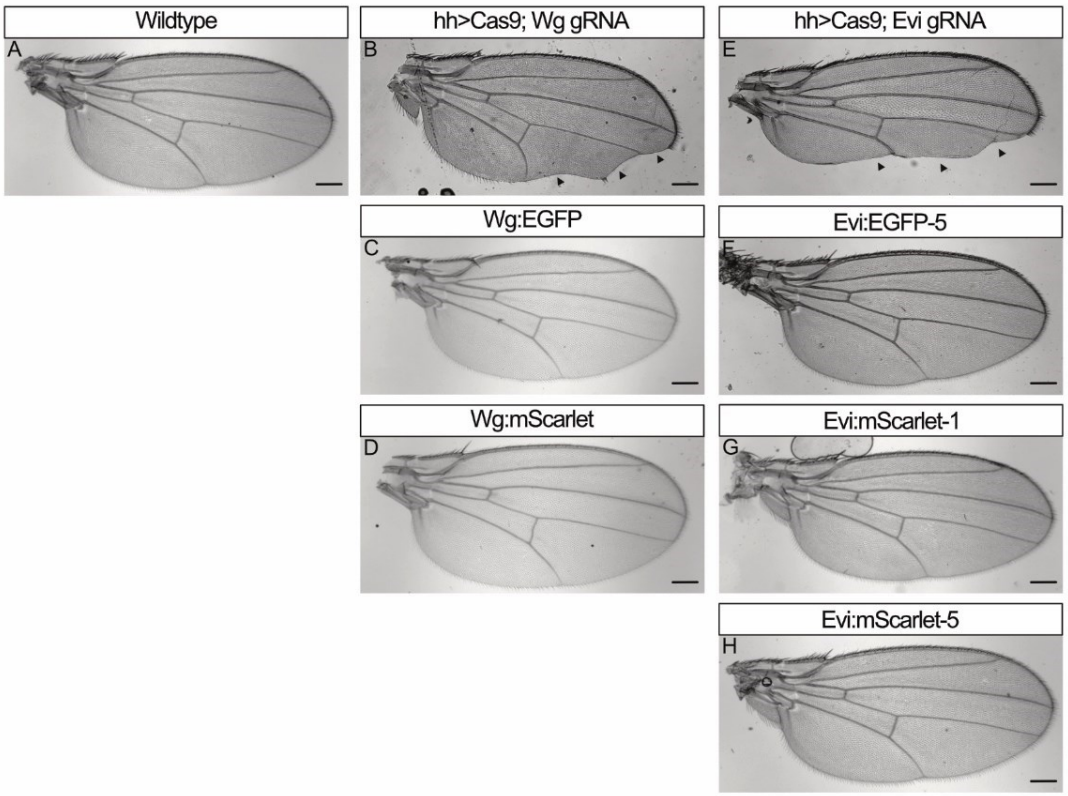

Figure 10: Endogenously tagged Wg and Evi do not cause any aberrant adult fly wing phenotypes

A Representative images of adult fly wings of wildtype flies.

B-D Representative images of adult fly wings of Wg knockout flies (B), as well as flies expressing Wg:EGFP (C) and Wg:mScarlet (D).

E-H Representative images of adult fly wings of Evi knockout flies (E), as well as flies expressing Evi:EGFP-5 (F), Evi:mScarlet-1 (G) and Evi:mScarlet-5 (H).

Arrowheads indicate wing notches. Scale bar = 0.2mm.

Though wing shape is a strong indicator of Wg and Evi protein functionality in *Drosophila*, I wished to confirm the functionality molecularly as well as developmentally. Wg requires Evi for secretion, and absence of Evi in Wg-expressing cells results in the accumulation of Wg in

their secretory pathway [Bänziger et al., 2006]. In turn, Evi is stabilized by Wg binding, and in the absence of Wg, Evi is rapidly degraded by the ERAD pathway [Glaeser et al., 2018]. Therefore, I wanted to use this knowledge to determine how Wg:mScarlet and Evi:mScarlet would behave in the absence of Evi and Wg respectively in the Wg-secreting cells.

In order to assess the functionality of Wg:mScarlet, I used the Flp/FRT system, a widely-used site-directed recombination system [Golic et al., 1997], to induce the formation of mutant clones carrying the Evi null mutation in wing discs of Wg:mScarlet expressing flies. The Flp/FRT system uses the Flippase protein (Flp) whose synthesis is activated by short-term heatshock at 37°C to induce mitotic recombination between two FRT sites on two sister chromosomes. One chromosome carries the null mutation that is homozygous lethal, while the other carries a transgenically inserted ubiquitously expressed GFP (ubi-GFP) for clone marking. Upon heatshock and Flp expression, recombination takes place at the FRT site, and subsequent to cell mitosis, one daughter cell inherits the homozygous null mutation, while the other inherits two ubi-GFP transgenes, allowing for easy identification of null mutant clones. As the wing disc grows significantly during development, the earlier the Flp/FRT system is induced, the larger the clones will be in the third instar larval stage of the disc.

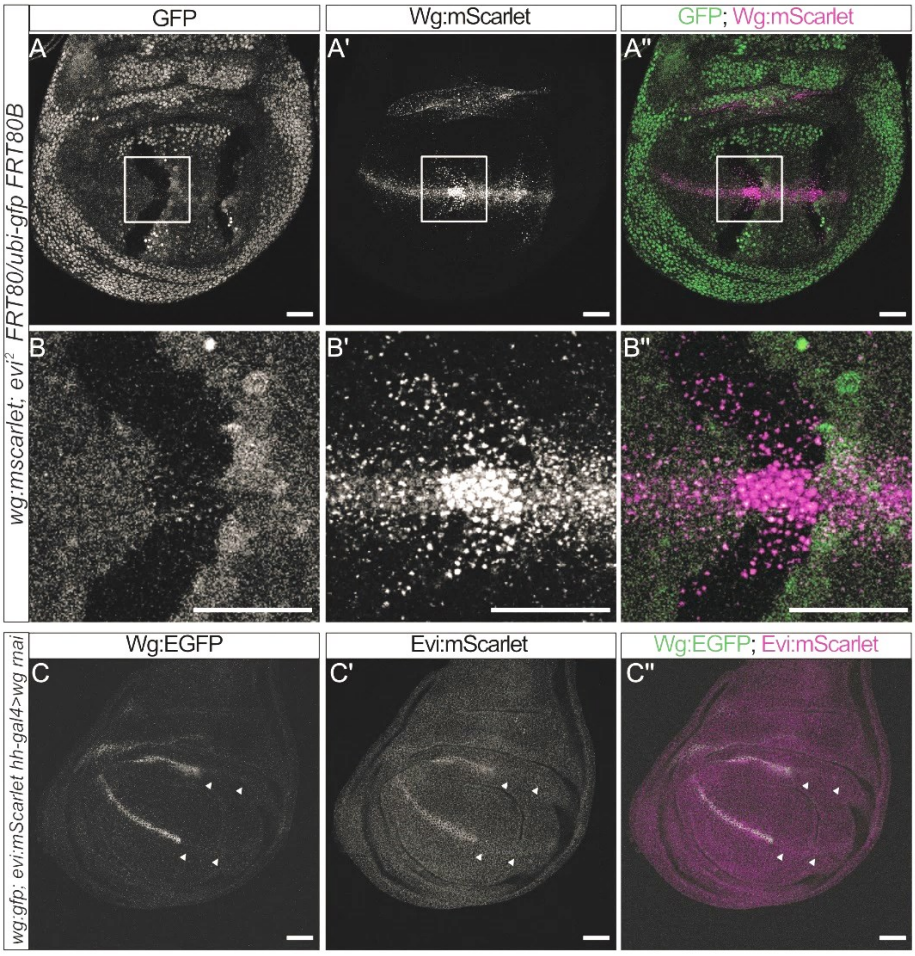

Figure 11: Wg:mScarlet accumulates in secreting cells upon induction of Evi clones and Evi:mScarlet-5 is no longer stabilized in cells with Wg knockdown

A-B Representative images of Evi null mutant clones (Evi^2) induced in Wg:mScarlet expressing wing discs. Wg:mScarlet accumulates in secreting cells within the Evi null mutant clones.

C Representative images of Wg knockdown under the hh-Gal4 driver in Wg:EGFP, Evi:mScarlet-5 expressing wing discs. Evi:mScarlet-5 no longer accumulates in secreting cells once Wg is knocked down.

Scale bar = 50µm.

I induced the Flp/FRT system 48 hours after egg laying by shifting the flies carrying the Flp/FRT system with a heterozygous Evi null mutation (Evi^2) and a heterozygous Wg:mScarlet to 37°C

for 30 to 90 minutes. I identified Evi null mutant clones by the absence of GFP expression which extended dorsoventrally through the wing imaginal disc (Figure 11A-B). In the secreting cells within the clone boundaries, Wg:mScarlet accumulated at a significantly higher level than in the secreting cells outside of the Evi null mutant clones. This indicates that Evi is required for the secretion of Wg:mScarlet, and that the fluorescent tag does not affect the ability of Wg:mScarlet to bind to Evi.

In order to test the functionality of Evi:mScarlet, I used the hh-Gal4 driver to induce the knockdown of Wg using Wg RNAi in the posterior half of the wing discs expressing Wg:EGFP and Evi:mScarlet-5. Upon the knockdown of Wg, Evi:mScarlet was no longer present in the perturbed Wg-secreting cells in the levels detectable in the unperturbed half of the wing imaginal disc (Figure 11C). The loss of Evi:mScarlet upon Wg knockdown therefore indicates that the tagging by mScarlet does not affect the functional stabilization of Evi:mScarlet by Wg.

Taken together, these results demonstrate that both tagged Wg and tagged Evi retain their full functionality, and that therefore the insertion of the tags does not cause any negative effects for either the folding or the function of these proteins.

3.1.3 Different fluorescent proteins enable the visualization of differing fractions of Wg within the wing imaginal tissue

In the course of characterizing the endogenously tagged Wg fly lines, I noticed that while the expression pattern of Wg:EGFP and Wg:mScarlet in the wing imaginal disc corresponds to that of wildtype Wg, the cellular localization appears to differ. In wing imaginal discs heterozygous for both Wg:EGFP and Wg:mScarlet, both are expressed at the dorsoventral boundary and hinge ring in the expected Wg pattern (Figure 12A). However, the magnification in Figure 12B clearly shows that Wg:EGFP localizes mainly intracellularly within the Wg-secreting cells, with few puncta in or on Wg-receiving cells, similar to the Wg antibody staining (comparison in Figure 9). In contrast, Wg:mScarlet largely localizes in puncta and is present in higher amounts in or on the neighboring receiving cells. As this difference in expression was unexpected, I decided to investigate whether it is an indication of the fluorescent proteins affecting Wg secretion and potentially also signaling.

The first question I asked was whether one tagged version of Wg confers fitness advantage or disadvantage to the fly line compared to the other. Fitness-reducing genetic manipulations are removed from a population under evolutionary pressure, while fitness-increasing ones are favored. This can be detected through unequal distribution of chromosomes carrying the manipulation as compared to chromosomes carrying the wildtype form of the protein. Therefore, chromosomal distribution analysis can be used to establish whether a genetic manipulation is harmful when present in a fly line.

In order to compare the second chromosome distribution between wildtype and tagged fly lines, I crossed the homozygous stock of Wg:EGFP and Wg:mScarlet to a fly line carrying the wg^{sp} gene, a mutation in the *wg* gene that dominantly expresses a hair phenotype on the fly

thorax above the leg joints (Sp phenotype), and which is homozygous lethal. I then crossed these heterozygous F1 generation flies to each other and quantified the number of flies in the F2 generation with and without the Sp phenotype to determine the percentage of homozygous non-Sp-expressing flies and the heterozygous Sp-expressing flies. *wg^{sp}* and *wg:tag* cannot recombine onto the same chromosome, therefore the presence or absence of the Sp phenotype correlates to the chromosomal distribution of the second chromosome. The distribution of homozygous-to-heterozygous flies was similar between the wildtype and the two Wg:Tag fly lines (around 45%, Supplemental Figure S1). This indicates that the chromosomal distribution is not affected by the tagging of Wg.

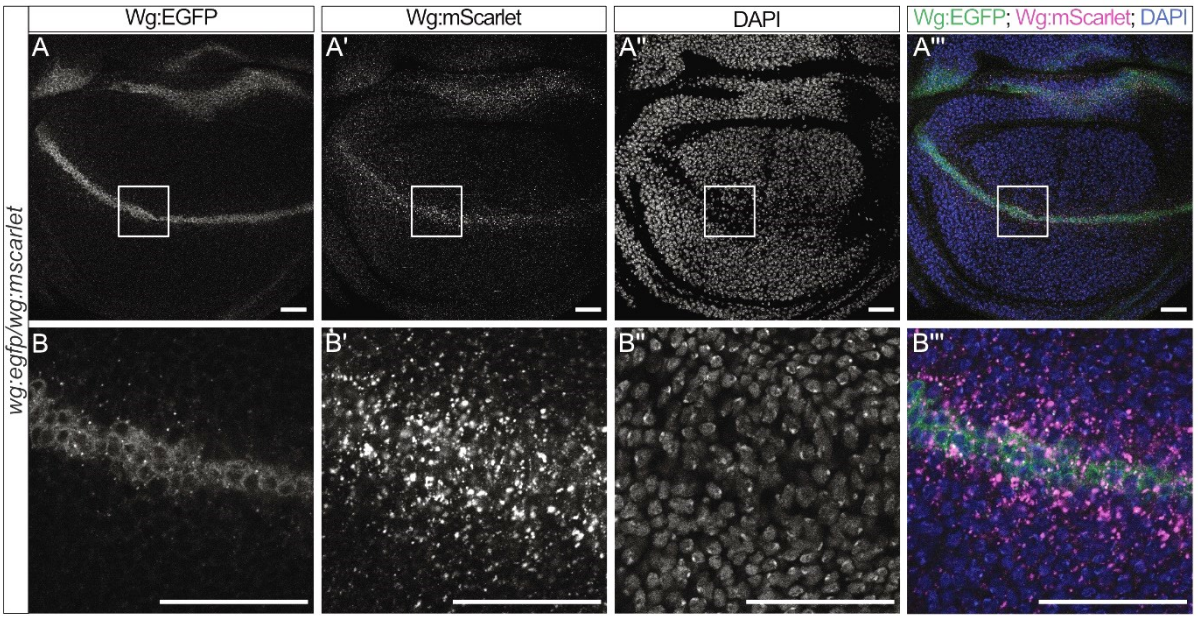

Figure 12: Wg:EGFP and Wg:mScarlet are expressed in the same pattern in the wing imaginal disc, but intracellular localization differs

A Representative images of a wing imaginal disc of the fly heterozygous for Wg:EGFP and Wg:mScarlet. Wg was detected at the dorsoventral boundary and in the hinge rings in both cases.

B Magnification of the dorsoventral boundary showing the difference in localization between Wg:EGFP and Wg:mScarlet fluorescence.

Scale bar = 50µm.

Wg:mScarlet fluorescence was strongly punctate and present in the Wg-receiving cells adjacent to the Wg-secreting cells. I performed antibody surface staining for Wg of Wg:EGFP and Wg:mScarlet wing discs in order to determine whether the Wg:mScarlet localization matches that of secreted Wg. Surface staining is a variation of the established immunofluorescence method in which the antibody incubation is performed prior to fixation on living tissue on ice. Since cells are not yet permeabilized, the antibody can only bind to the protein that is found on the cell surface or in the extracellular space. Incubation on ice prevents any endocytosis of the bound antibody-protein complex.

Stronger colocalization of surface α-Wg staining was present with Wg:mScarlet than with Wg:EGFP, and this colocalization extended beyond Wg-secreting cells into the neighboring receiving cells (Figure 13A-B). In contrast, Wg:EGFP fluorescence colocalized less with the

surface Wg and almost exclusively on Wg-secreting cells. In addition, immunofluorescent staining of Wg:mScarlet with a Wg antibody showed less colocalization within Wg-secreting cells than was the case for Wg:EGFP (Supplemental Figure S2). These results may indicate that more Wg:mScarlet is secreted than Wg:EGFP.

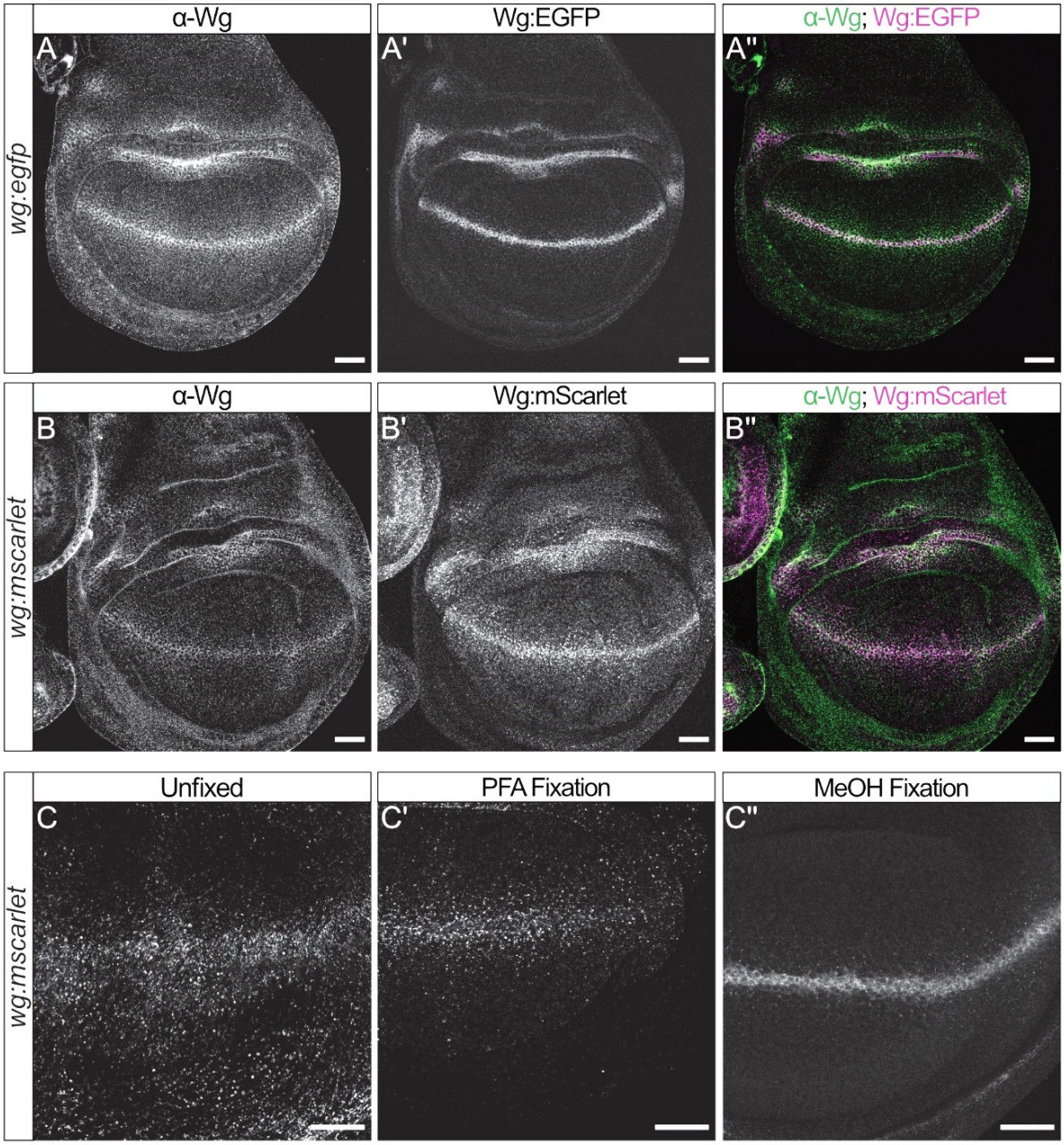

Figure 13: Wg:mScarlet resembles the surface staining of Wg, but methanol fixation reveals a previously weakly detectable intracellular Wg:mScarlet fraction in secreting cells

A Representative image of surface staining with anti-Wg antibody of Wg:EGFP expressing wing disc.

B Representative image of surface staining with anti-Wg antibody of Wg:mScarlet expressing wing disc.

C Representative images of Wg:mScarlet wing disc after fixation with 4% PFA (C') and 100% MeOH (C'') in comparison to living tissue (C).

Scale bar = 50µm.

To determine whether the lower levels of Wg:mScarlet fluorescence accumulation within secreting cells is due to less Wg in these cells, I tested, in addition to the standard formaldehyde fixation method, also fixation with methanol. Formaldehyde fixation crosslinks proteins and preserves the lipid membranes. In contrast, methanol fixation dehydrates the cells and leads not just to the precipitation of the protein, but also results in the loss of lipids and extracellular proteins.

Wg:mScarlet fluorescence upon formaldehyde fixation closely resembled the fluorescence pattern in living, unfixed tissue (Figure 13C). After methanol fixation, on the other hand, Wg:mScarlet fluorescence was similar to the Wg:EGFP fluorescence (for comparison see Figure 12). This indicates that Wg:mScarlet is in fact present in Wg-secreting cells, but cannot be visualized due to the much stronger intensity of the extracellular punctate fluorescence. Once the extracellular fluorescence is lost through methanol fixation, the intracellular fluorescence becomes visible.

Together, these experiments suggest two scenarios: either Wg is more secreted when tagged with mScarlet than with EGFP, or Wg secretion is unaffected and the problem lies in the detection of the fluorophores instead.

In order to answer this question, I decided to analyze the amount of secreted Wg protein in wing discs expressing wildtype Wg, Wg:EGFP and Wg:mScarlet by surface protein biotinylation. Since cell-impermeable biotin is used for this assay, only surface proteins before cell lysis are labeled. These are pulled down with streptavidin agarose beads and then analyzed by Western blot. Tubulin served as the control for an intracellular protein, whereas Fasciclin-II served as the control for a cell-surface protein.

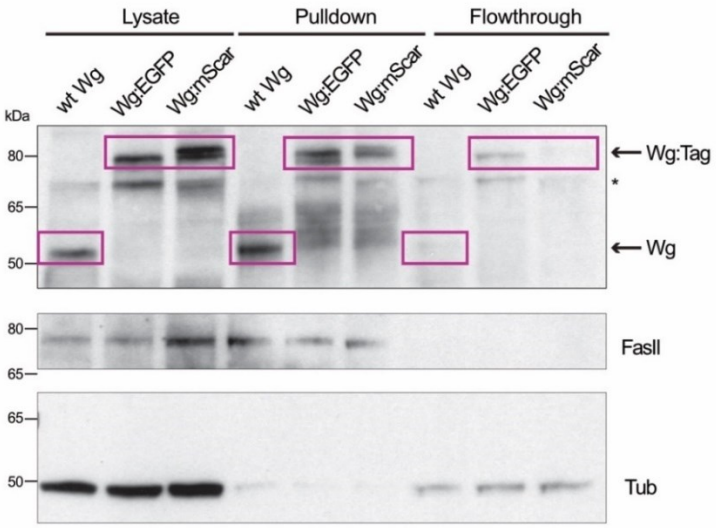

Figure 14: Surface protein biotinylation shows that Wg:mScarlet is secreted in similar amounts as Wg:EGFP and wildtype Wg

Western blot analysis with indicated antibodies after surface protein biotinylation of 50-70 wing imaginal discs and streptavidin pulldown; lysate= total cell lysate of wing discs; pulldown = protein pulled down on streptavidin-agarose beads; flowthrough = remaining supernatant after pulldown. One of two independent experiments, representative for both, is shown. FasII is used as control for a cell surface proteins. Tub is used as control for a protein within the cell.

Wg was present in all fractions of the Western blot, with the tags adding roughly 25kDa to Wg:Tag compared to its wildtype form (Figure 14). The Wg:EGFP band in the pulldown fraction was slightly stronger than the one in the Wg:mScarlet fraction, indicating that there is more Wg:EGFP on the cell surface than Wg:mScarlet. This argues against the hypothesis that Wg:mScarlet is secreted in higher amounts than Wg:EGFP.

Taken together, these results indicate that Wg:mScarlet fluorescence is more detectable on the surface of the wing imaginal disc cells, while the Wg:EGFP fluorescence is more detectable intracellularly within Wg-secreting cells. However, this effect is not caused by a change in Wg secretion levels and is thus a matter of fluorescence detection due the two different FPs used.

In essence, each fluorescent protein allows for the detection of a specific Wg fraction that is not fully detectable by the other fluorescent protein. This hypothesis is further strengthened by a similar effect occurring in wing discs heterozygously expressing Evi:EGFP-5 and Evi:mScarlet-5, whose fluorophores are located within the lumen of the secretory pathway, similar to the tagged Wg. Evi:mScarlet is much more detectable in the dorsoventral boundary cells than Evi:EGFP, though Evi:EGFP fluorescence is overall more even throughout the tissue as well (Supplemental Figure S3).

3.1.4 Analysis of endogenously tagged Wg and Evi in living tissue

One of the advantages of endogenously tagged proteins over immunohistochemistry is that the tissue can be imaged live. I thus wanted to test whether the endogenously tagged Wg would be suitable for this purpose. In order to track Wg in real-time, I established a method for culturing wing imaginal discs *ex vivo* by dissecting and mounting them on polylysin-coated multi-well cell culture slides in culture medium at room temperature. The culture medium was based on previously published work [Tsao et al., 2016; Strassburger et al., 2017].

I imaged Wg:EGFP for up to 1hr using both laser-scanning and spinning-disc confocal microscopes immediately after wing disc mounting. Due to the small size of wing disc epithelial cells and the curvature of the wing pouch, better results could be achieved by imaging the hinge ring, rather than the dorsoventral boundary. This permitted for more volume of each individual columnar polar epithelial cell of the wing imaginal disc to be visible in a single imaging plane, and thus allowed for more precise imaging of the intracellular movement of the Wg:EGFP.

Live imaging of Wg:EGFP revealed active movement of Wg, as indicated by EGFP-positive puncta travelling through the cells bidirectionally between the apical and basal side of the cells. Figure 15A shows a snapshot of a live imaging series with individual puncta annotated in circles. Their movement path until this point was tracked using particle tracking analysis, shown as red lines in the image. Paths of select individual Wg:EGFP puncta are shown in Figure 15B, with the puncta detectable for 2 to 3 minutes on average within the imaging plane. Imaging with the spinning-disc confocal microscope resulted in less photobleaching than imaging with the laser-scanning confocal microscope.

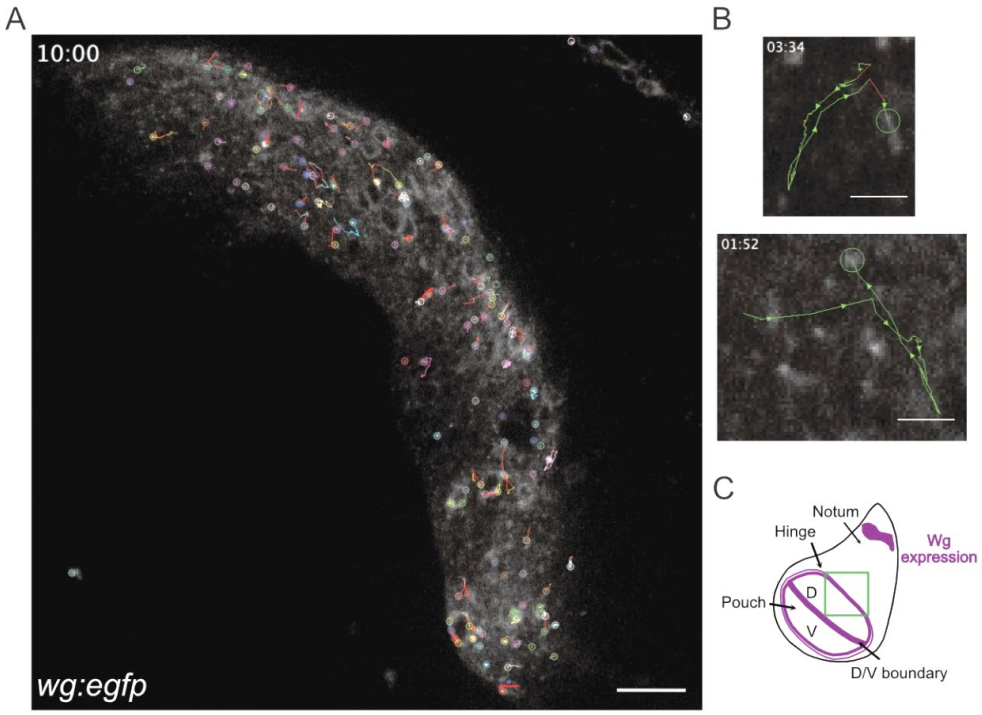

Figure 15: Live imaging of wing imaginal discs facilitates tracking of Wg:EGFP through the wing disc cells and enables particle tracking analysis

A Representative image of a live imaging series at 10 min continual imaging of Wg:EGFP expressing hinge region of wing imaginal disc. Circled are individual tracked fluorescence puncta; red lines are tracking lines belonging to the attached puncta (imaging does not provide single-molecule resolution).

B Selected images showing the tracks of individual fluorescence puncta after particle tracking analysis. The showed time marks the elapsed time of tracking.

C Schematic of a wing imaginal disc with the Wg expression pattern, showing the imaged section for orientation purposes. Scale bar = 5µm.

I imaged the wing imaginal discs of flies expressing Wg:mScarlet in the same way as those of flies expressing Wg:EGFP. Imaging at the dorsoventral boundary in the z-plane in addition to the time course allowed for the identification of two distinct types of fluorescence puncta. Fluorescence puncta located in close proximity to the dorsoventral boundary were mostly static, with small bidirectional apical-to-basal movement during imaging of up to 15 minutes (Figure 16A). Individual puncta are shown tracked within three z-planes over a period of two minutes, with each color denominating the same fluorescence puncta within all images (Figure 16B).

During live imaging, fluorescence puncta could be detected not just around the Wg-secreting cells of Wg:mScarlet expressing wing imaginal discs, but also more distantly within the region of the wing pouch. Unlike the mostly static puncta at the dorsoventral boundary, these more distant fluorescent ones were dynamic when imaged at the apical surface of the wing disc (Figure 16C-E). Example kymographs in Figure 16E were calculated from the trajectories of two puncta (marked in Figure 16D) to demonstrate their movement. The observed speed of these fluorescent puncta was up to 1 µm/sec and they moved away from the dorsoventral boundary towards the edges of the wing pouch. They remained within the imaging plane for up to 3 minutes.

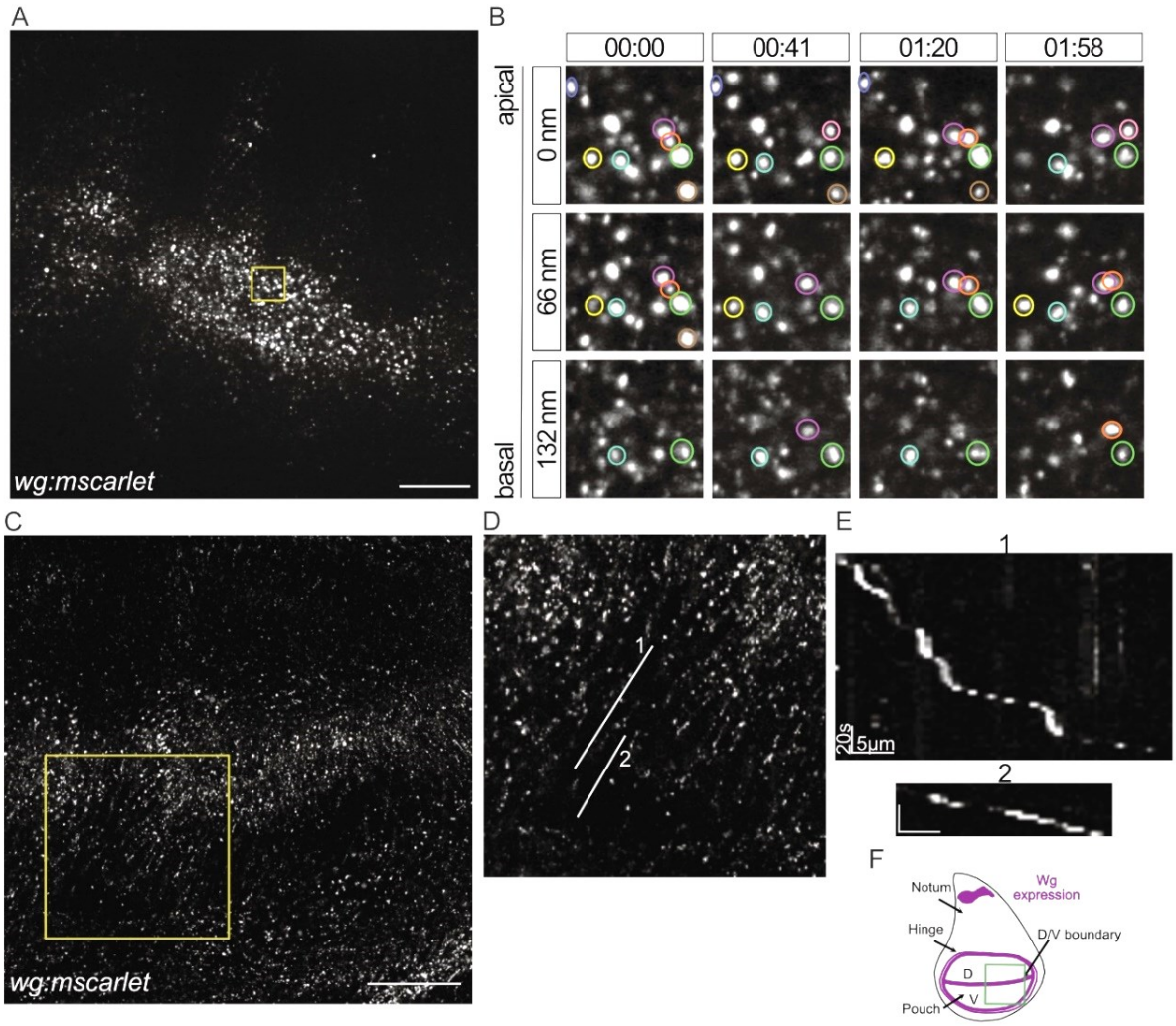

Figure 16: Live imaging of Wg:mScarlet reveals diverse dynamics of puncta depending on the fluorescence localization within the wing imaginal disc

A-B Live imaging snapshot of Wg:mScarlet at the dorsoventral boundary of wing imaginal disc (A); scale bar = 10µm. (B) Montage of the selected area with three imaging planes. Circle colors identify individual puncta.

C-E Live imaging snapshot of Wg:mScarlet at the dorsoventral boundary of the wing imaginal disc at the apical side of the disc (C); scale bar = 50 µm. Dynamic puncta found in the selected area (D), with example kymographs of dynamic puncta showing their movement distance over time (E). Kymograph scale bar indicated on image.

F Schematic of a wing imaginal disc with the Wg expression pattern, showing the imaged section for orientation purposes.

Evi is the cargo carrier protein of Wnts, and is thus required for the secretion of Wg [Bartscherer et al., 2006]. For this reason, I wanted to analyze the colocalization of the endogenously tagged Wg:EGFP and Evi:mScarlet in *ex vivo* cultured wing imaginal discs. As Wg and Evi are on different chromosomes, combining the two constructs in one fly required only regular fly crossing.

Many, but not all, Wg:EGFP puncta colocalized with Evi:mScarlet puncta (Figure 17A; examples denoted by white arrows; green and magenta arrows indicate non-colocalizing Wg and Evi puncta respectively). The puncta were visible in the imaging plane for not longer than 1 min and the colocalization remained consistent over a longer imaging time period for up to 20 minutes.

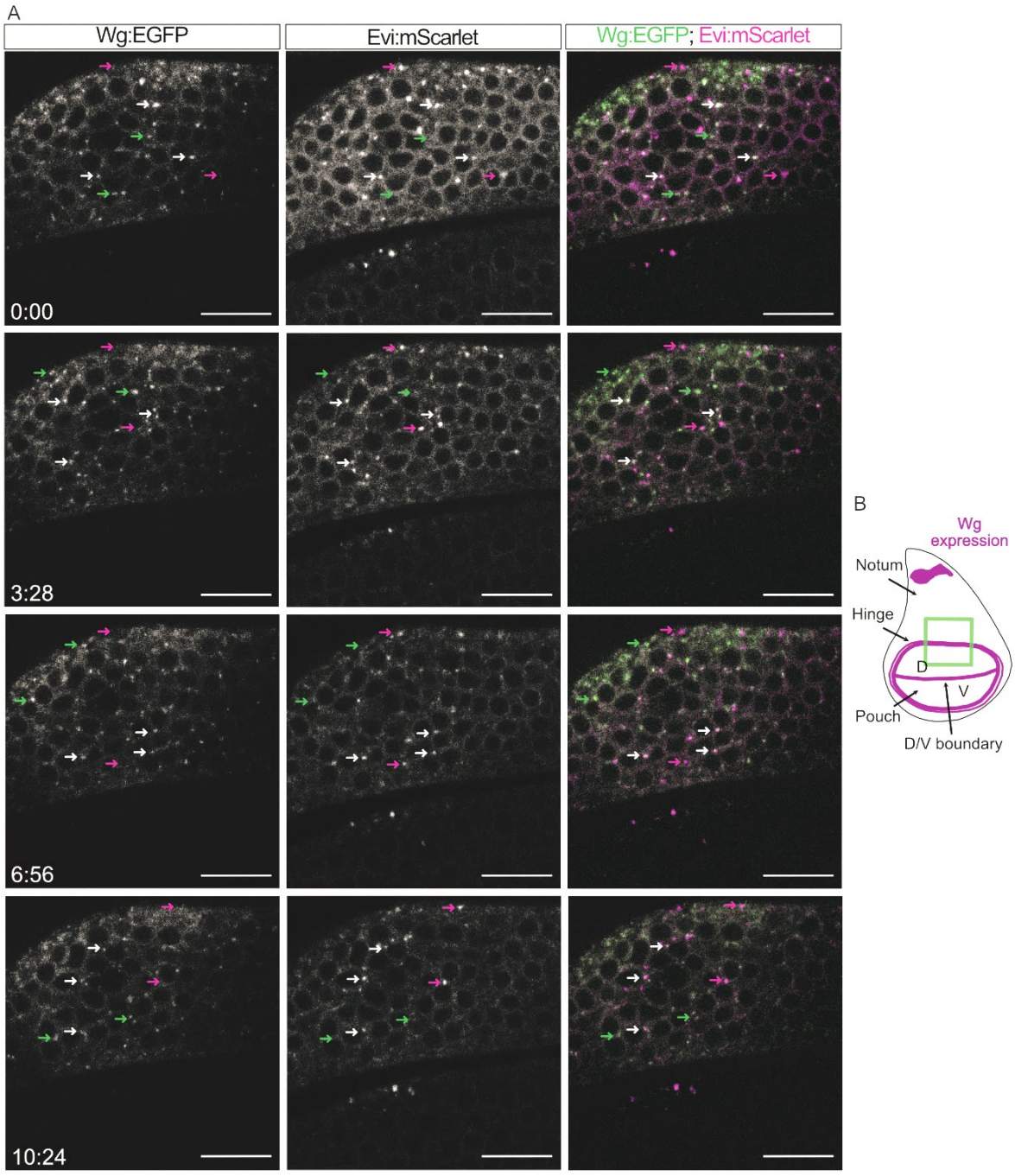

Figure 17: Live imaging and tracking of Wg:EGFP and Evi:mScarlet over time reveals that Wg and Evi colocalize most of the time, but not always

A Montage of the Wg:EGFP and Evi:mScarlet fluorescence captured over 10 minutes at 20sec intervals in one wing disc. White arrows indicate colocalization events; green arrows indicate Wg:EGFP-only puncta; magenta arrows indicate Evi:mScarlet-only puncta. Individual panels have not been adjusted for brightness or contrast in order to show the degree of photobleaching occurring over the time period imaged.

B Wing imaginal disc schematic with the Wg expression pattern showing the location of the imaged cells within the wing disc for orientation purposes.

Scale bar = 10µm.

I was able to endogenously tag Wg and Evi proteins, as well as show that these constructs can be used in live imaging to track their movement over time or to determine colocalization with other proteins or different organelles. My work therefore provided a valuable toolset to the *Drosophila* field of research as well as my own research.

3.2 Establishing protein trap-and-release systems for use in *Drosophila* tissues

Tracking protein movement through the cell or tissue can provide answers about protein activity and its interaction partners. I was interested in studying the process of Wg protein secretion, as well as Rab GTPases as potential players in this process. For this reason, I decided to establish a protein trap-and-release system in *Drosophila melanogaster* wing imaginal discs and salivary glands. My plan was to use the system to help answer the main biological question of my thesis, which was to identify the Rabs important for Wnt secretion in *Drosophila* wing imaginal disc and to characterize their roles in this process. More precisely, I wanted to study the effects of the trapping and acute release the Rab GTPases on Wg secretion in these cells.

I identified two published systems which shared this experimental setup – the RUSH and the LAMA systems (Introduction Section 2.5.2). Both systems require two components, a hook and a reporter protein. They function by inducing the binding of the reporter to the hook through protein tags, which can be disrupted by the addition of a specific small molecule trigger. The first step I performed was to express both systems in the fruit fly and determine which of them would be more advantageous for further study. Following this, I analyzed the chosen system to determine its experimental use and any limitations it may have in *Drosophila* tissues and cells.

3.2.1 Adaptation of the RUSH system in *Drosophila melanogaster*

The RUSH system [Boncompain et al, 2012] relies on the affinity between Streptavidin and the Streptavidin binding peptide (SBP) for reporter sequestration to the organelle of choice; the small molecule which triggers the separation of the hook and reporter is biotin. Adaptation of the RUSH system for *Drosophila* studies required the generation of fly lines containing the RUSH components. The RUSH toolbox was generated by WellGenetics Inc. (Taipei, Taiwan) in collaboration with the Hiesinger laboratory of Free University of Berlin. The generated fly lines carrying RUSH hooks included the overexpression constructs for three ER-RUSH-hooks (UAS-Streptavidin-Ii, UAS-Streptavidin-KDEL, and UAS-Streptavidin-STIM1-NN) and one Golgi-RUSH-hook (UAS-Streptavidin-Golgin84).

The generated RUSH reporter lines included overexpression constructs for all *Drosophila* Rab GTPases (UAS-SBP-YFP-Rab, referred to as RUSH-Rab). Since I planned to implement the protein trap-and-release method for the study of the effects of Rab sequestration and acute release on Wnt secretion, generating the required tools and using them for the analysis of the RUSH system from the beginning was advantageous for the project, which was why I chose the Rab GTPases as reporter proteins from the start.

The first step to adapting the RUSH system for use in *Drosophila* wing imaginal disc was to determine if its components can be successfully overexpressed in the tissue. I began with the Golgi-RUSH-hook and RUSH-Rab7 reporter, with the intention of testing the ER-RUSH-hooks and additional RUSH-Rab reporters in subsequent experiments. Golgi-RUSH-hook uses the

Golgin84 protein, which is anchored to the Golgi apparatus membrane by its C-terminus. The Streptavidin is fused to its N-terminus in the hook [Boncompain et al., 2012].

I overexpressed the Golgi-RUSH-hook alone, the RUSH-Rab7 reporter alone, and co-expressed both constructs together under the control of the nubbin-Gal4 driver (nub-Gal4), which is active in the pouch region of the wing imaginal disc. As RUSH-Rab7 already carries the YFP, it could be directly visualized by fluorescence microscopy. For the visualization of the Golgi-RUSH-hook, I stained the expressing wing discs with an α-Streptavidin antibody after fixation.

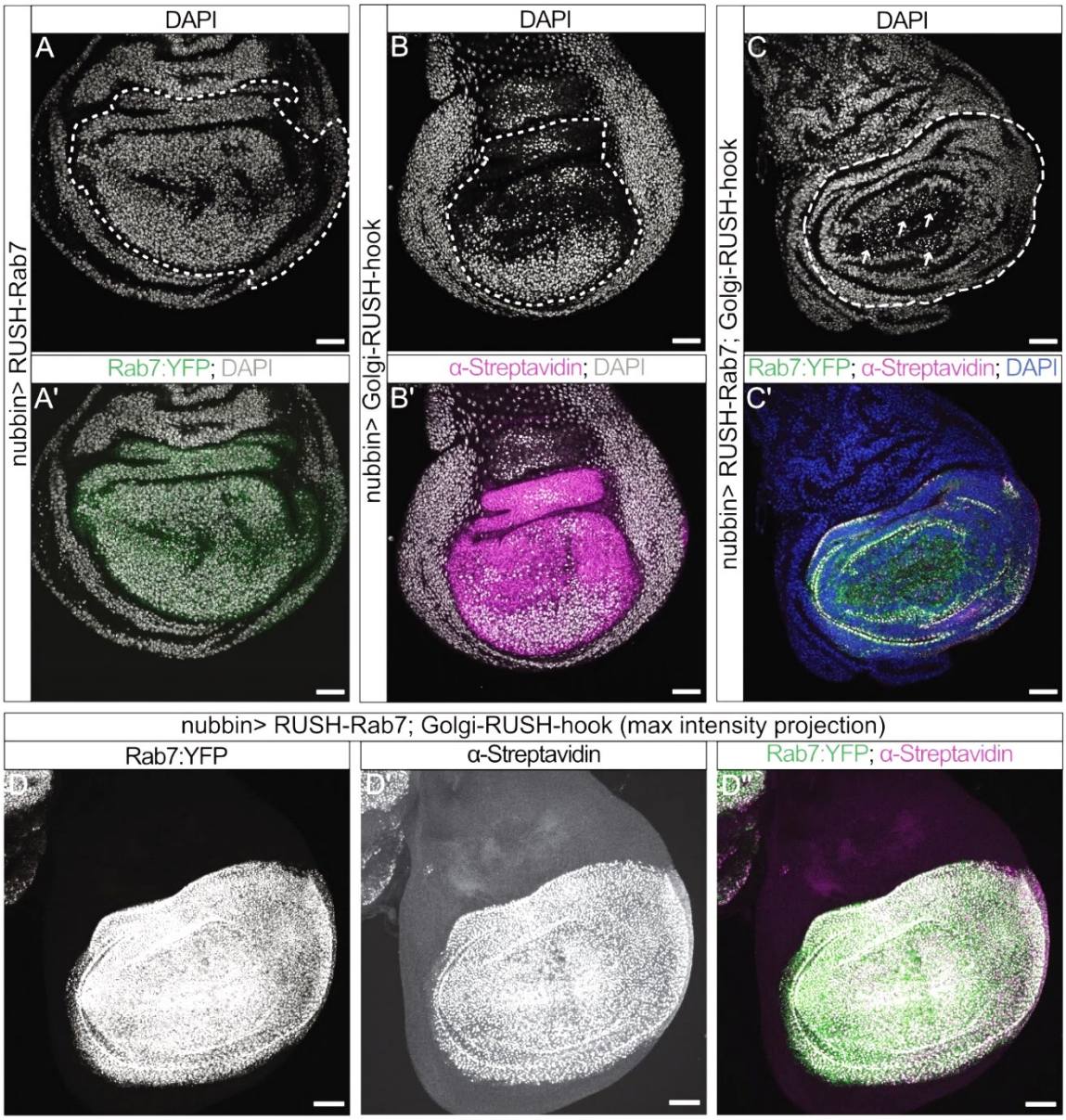

Figure 18: The RUSH system components Golgi-RUSH-hook and RUSH-Rab7 induce mild apoptosis when co-expressed in wing imaginal discs

A-B Representative images of wing discs expressing RUSH-Rab7 (A) and Golgi-RUSH-hook (B) under the nub-Gal4 driver.
C-D Representative images of wing discs expressing RUSH-Rab7 and Golgi-RUSH-hook under the nub-Gal4 driver. (C) Individual slice through the disc; white arrows indicate apoptotic cell extrusion and debris. (D) Maximum intensity projection of RUSH components showing their colocalization. Significant amount of Rab7 fluorescence does not colocalize with hook staining.
Scale bar = 50µm; dotted line marks area of expression.

Individually, both the Golgi-RUSH-hook and the RUSH-Rab7 reporter could be expressed with no adverse effects in the wing imaginal discs (Figure 18A-B), indicating that they are well tolerated by the tissue in question. However, co-expression of both RUSH system components caused moderate cell lethality and minor wing disc deformities, indicated in Figure 18C with white arrows. In addition, though both Golgi-RUSH-hook and RUSH-Rab7 are strongly expressed in these wing disc pouch, colocalization analysis showed that a significant amount of Rab7 fluorescence does not colocalize with the hook staining (Figure 18D), indicating that not all RUSH-Rab7 was bound to Golgi-RUSH-hook and that the system is leaky.

Flies are reared on standard fly food containing yeast, which in turn contains biotin (vitamin B7), the small molecule serving as the trigger for the RUSH system by displacing the SBP-tagged reporter from the Streptavidin-tagged hook and allowing the reporter to travel away, thus no longer colocalizing with the hook. I hypothesized that the most likely cause of the system leakage is therefore the ingestion of normal, biotin-containing fly food by the larvae prior to dissection and analysis. Previous studies used biotin-deficient fly food in fly husbandry [Landenberger et al., 2004; Smith et al., 2008] by adding avidin to the recipe, which binds the biotin and prevents it from being active upon ingestion by the flies. For this reason, I repeated the previous experiment with flies fed on biotin-deficient fly food (BDF), rather than normal fly food.

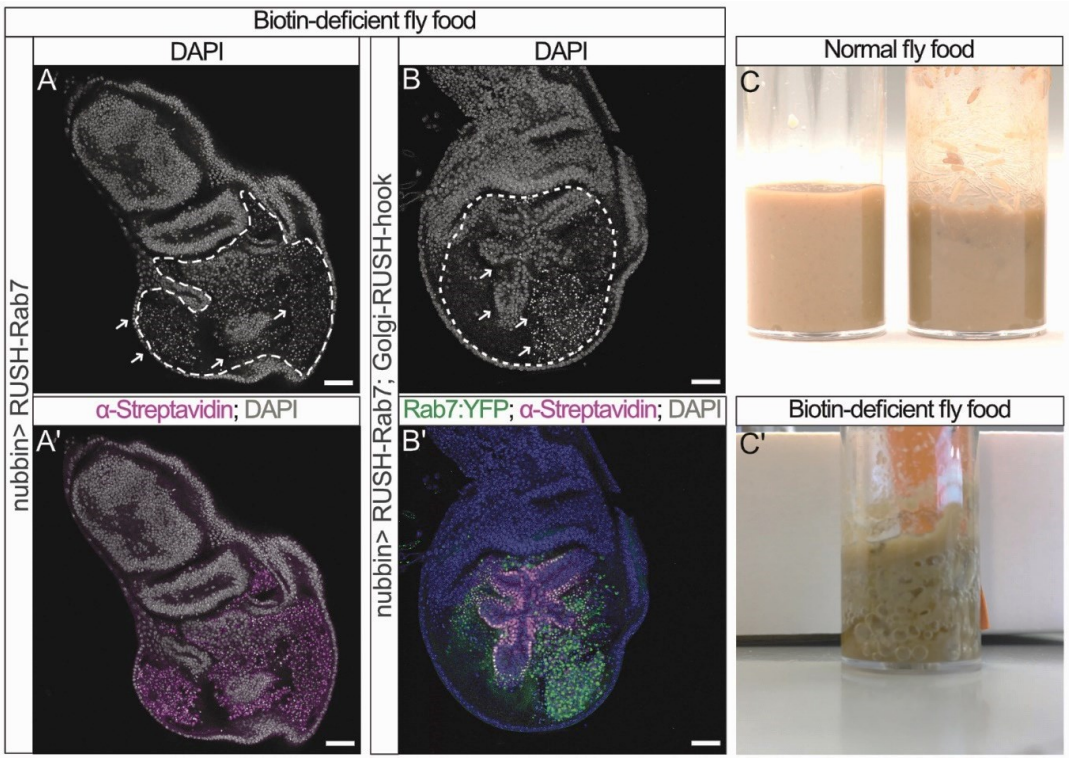

Figure 19: Overexpression of Golgi-RUSH-hook alone or together with RUSH-Rab7 in flies fed on biotin-deficient fly food (BDF) causes massive morphological deformities and apoptosis in the tissue

A Wing disc expressing Golgi-RUSH-hook under the nub-Gal4 driver in flies fed on BDF.

B Wing discs expressing RUSH-Rab7 and Golgi-RUSH-hook under the nub-Gal4 driver in flies fed on BDF.

C Fly vials filled with normal fly food (C) and BDF (C'). BDF easily spoils and becomes toxic for the flies.

Scale bar = 50µm; dotted line marks area of expression; white arrows indicate apoptotic cell debris and morphological deformities.

The wing discs of flies fed on BDF which overexpressed either the Golgi-RUSH-hook by itself or in combination with RUSH-Rab7 showed extreme apoptosis of the tissue, resulting in significant morphological deformities (Figure 19A-B). Co-expression of Golgi-RUSH-hook and RUSH-Rab7 in larvae fed on BDF was lethal in pupal stage, while only a small number of escaper flies expressing only Golgi-RUSH-hook eclosed. The wings of these flies were severely deformed, in comparison to the wings of wildtype flies fed on BDF food, which did not show any morphological deformities.

Mated wildtype as well as RUSH flies fed on BDF laid significantly more unfertilized eggs, as well as fertilized eggs that showed an increased embryonic and larval lethality. In addition, I noticed that BDF spoiled very easily, often developing gas bubbles that in some cases managed to displace the food within the vial upwards (Figure 19C).

In addition to the Golgi-RUSH-hook and RUSH-Rab7, I tested the Ii ER-RUSH-hook. This hook has the Streptavidin fused to the N-terminus of the human invariant chain of the class II major histocompatibility complex (MHC-II) [Boncompain et al., 2012], ensuring that the Streptavidin is located on the cytoplasmic side of the ER membrane and can bind to the RUSH reporters found in the cytoplasm. I co-expressed the ER-RUSH-hook with the RUSH-RabX1 reporter in flies fed on both normal food and BDF. Unlike Golgi-RUSH-hook, the ER-RUSH-hook co-expression with the RUSH-RabX1 reporter did not induce apoptosis in wing discs of flies reared on normal food, but it did in flies reared on BDF (Supplemental Figure S4). Similar to the co-expression of the Golgi-RUSH-hook and RUSH-Rab7, the RUSH system in this case was also leaky in flies fed on normal fly food.

Due to the toxicity of the RUSH system in wing imaginal discs when flies were fed BDF, I was unable to test whether the incubation of the discs with biotin would induce the release of the reporter from the hook.

In addition to the wing imaginal discs, I also tested the RUSH system in the *Drosophila* salivary glands. I chose to do this because unlike the small columnar cells of the wing disc, the salivary gland cells are much larger and allow for better imaging with intracellular resolution. I again used the Golgi-RUSH-hook and RUSH-Rab7 reporter and drove the co-expression in the salivary glands using the Salivary gland secretion 3-Gal4 (sgs3-Gal4) driver in flies fed on normal fly food and BDF.

The larvae expressing the RUSH system in their salivary glands and which fed on both normal food and BDF were able to develop into adults and were able to successfully attach to the walls of the vials they were kept in, indicating that the salivary glands in these larvae were functional. As previously seen in wing imaginal discs, colocalization of the Golgi-RUSH-hook and RUSH-Rab7 reporter was low in flies fed on normal fly food (Figure 20A). The colocalization was much higher when flies were fed on BDF (Figure 20B).

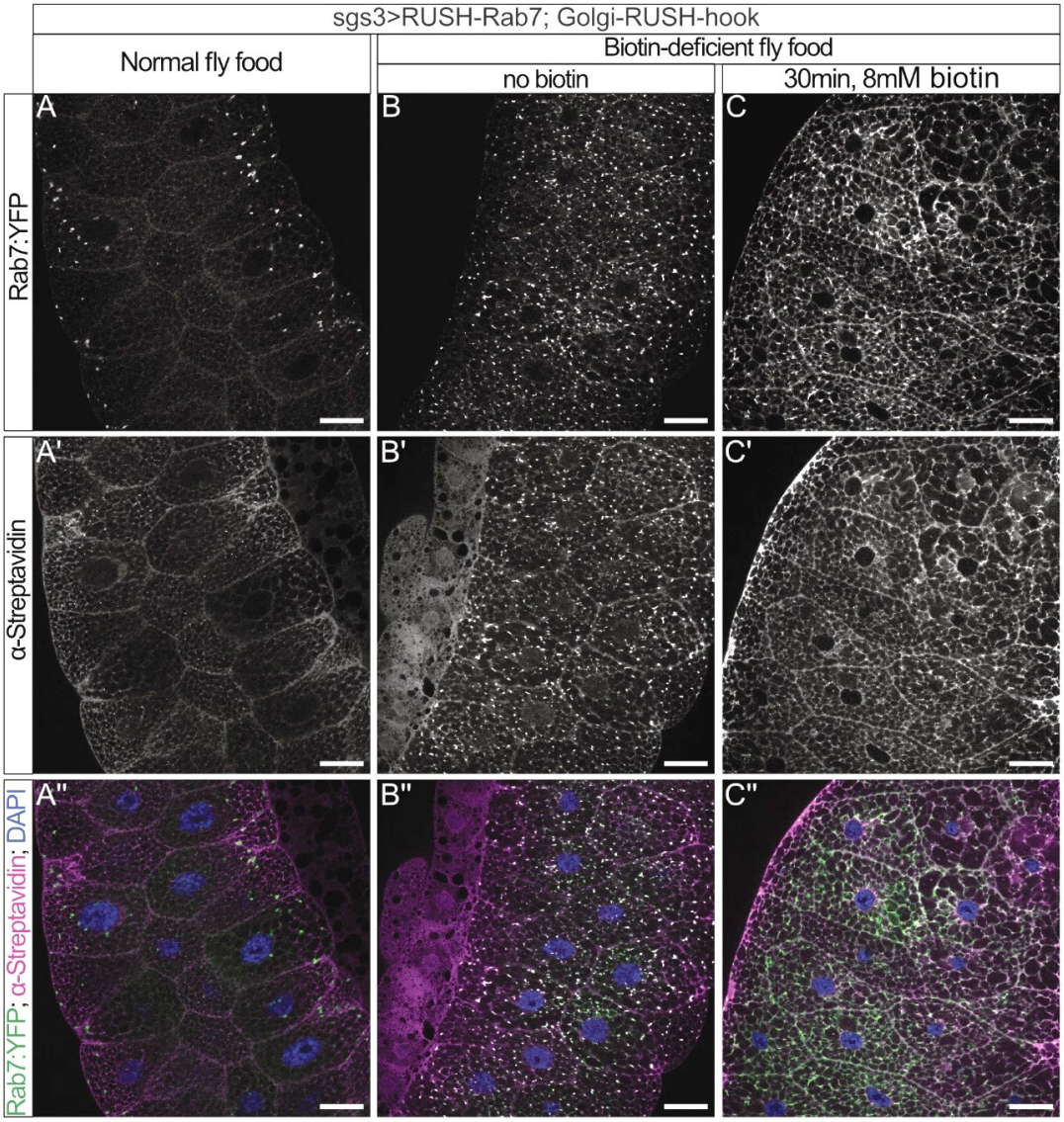

Figure 20: RUSH system expressed in the salivary glands using Golgi-hook and RUSH-Rab7 causes morphological changes to the Golgi, but functions well when reared on biotin-deficient fly food and can be released with biotin incubation
A Co-expression of the Golgi-hook and RUSH-Rab7 in salivary glands of larvae reared on normal food.
B-C Co-expression of the same components in larvae reared on biotin-deficient fly food prior to release (B), showing the morphological changes to the Golgi, and after 30 min of biotin release (C), showing the relocalization of RUSH-Rab7 and the return of Golgi to its normal morphology.

To test the functionality of the RUSH system in this organ context, I incubated the salivary glands for 30 min in culture medium containing 8 mM biotin (2mg/mL) *ex vivo*, after which I fixed and stained them with α-Streptavidin antibody to visualize the Golgi-RUSH-hook. The high colocalization of RUSH-Rab7 and the Golgi-RUSH-hook present before addition of biotin to the culture medium was significantly reduced after biotin incubation (Figure 20B-C). This indicates that the addition of biotin can successfully displace the RUSH reporter from the RUSH hook in larval salivary gland cells of *Drosophila melanogaster.*

Altogether, my data show that the RUSH system can be expressed in *Drosophila melanogaster*. However, the system is leaky when used in larval tissues due to the presence of its release molecule biotin in the standard food that flies are fed. Thus, it requires instead

the use of biotin-deficient fly food in order to ensure the high trapping of the reporter to the hook. Its expression using the Golgi and ER hooks is tolerated by certain tissues (salivary glands) but not others (wing discs) and can lead to significant toxicity and lethality in the larval and pupal stages. However, in the salivary glands, the addition of biotin induced the release of the reporter from the hook, visualized through the reduction in fluorescence colocalization.

3.2.2 Adaptation of the LAMA system in *Drosophila melanogaster*

The LAMA system [Farrants et al., 2020] requires the expression of two components: The reporter protein must be tagged with GFP, while the hook protein must be fused with a construct consisting of a circularly permutated dihydrofolate reductase (DHFR) and a GFP-specific nanobody. The addition of the small molecule trimethoprim (TMP) in the presence of NADPH induces a change in the conformation of the DHFR and breaks the binding of the nanobody to the GFP, thereby releasing the reporter from the hook.

In order to ensure comparable expression of the RUSH and LAMA systems, the Golgi-LAMA-hook construct was designed based on the Golgi-RUSH-hook. The fly line carrying the Golgi-LAMA-hook was generated by WellGenetics Inc. (Taipei, Taiwan) in collaboration with the Hiesinger laboratory of Free University of Berlin. The construct uses the Golgin84 together with the DHFR-nanobody sequence and the SNAP tag for visualization [Farrants et al., 2020]. The LAMA nanobody can bind both GFP and YFP equally well due to sequence and structure similarity between GFP and its derivative YFP. This allowed me to use the previously generated RUSH-Rab7 reporter, which is N-terminally tagged with the 36aa-long SBP and YFP, in the assessment of the LAMA system as well as the RUSH system. I used the experimental setup as previously, and overexpressed the LAMA system components under the control of the nub-Gal4 driver. I fed the flies on normal fly food only, as the LAMA system does not use biotin as its trigger molecule and thus does not require the biotin-deficient fly food. The Golgi-LAMA-hook carries the SNAP tag as part of its construct, which I could visualize by incubation with the cell permeable SNAP-Cell 647-SiR substrate.

Co-expression of both the Golgi-LAMA-hook and RUSH-Rab7 under the control of the nub-Gal4 driver caused significant apoptosis in the wing imaginal discs, as well as severe morphological deformities. These discs also displayed significant colocalization of the two LAMA system components (Figure 21A). This indicated strong toxicity of the hook and reporter combination. The flies were unable to reach adulthood, and died in pupal stage. Nevertheless, enough larvae reached the third larval instar stage to allow for the incubation with TMP. After dissection but before fixation, I incubated the wing imaginal discs in culture medium with 100µM TMP for 40 minutes. In spite of the toxicity of the system, addition of TMP resulted in the reduced colocalization of the RUSH-Rab7 fluorescence with the Golgi-LAMA-hook staining (Figure 21B).

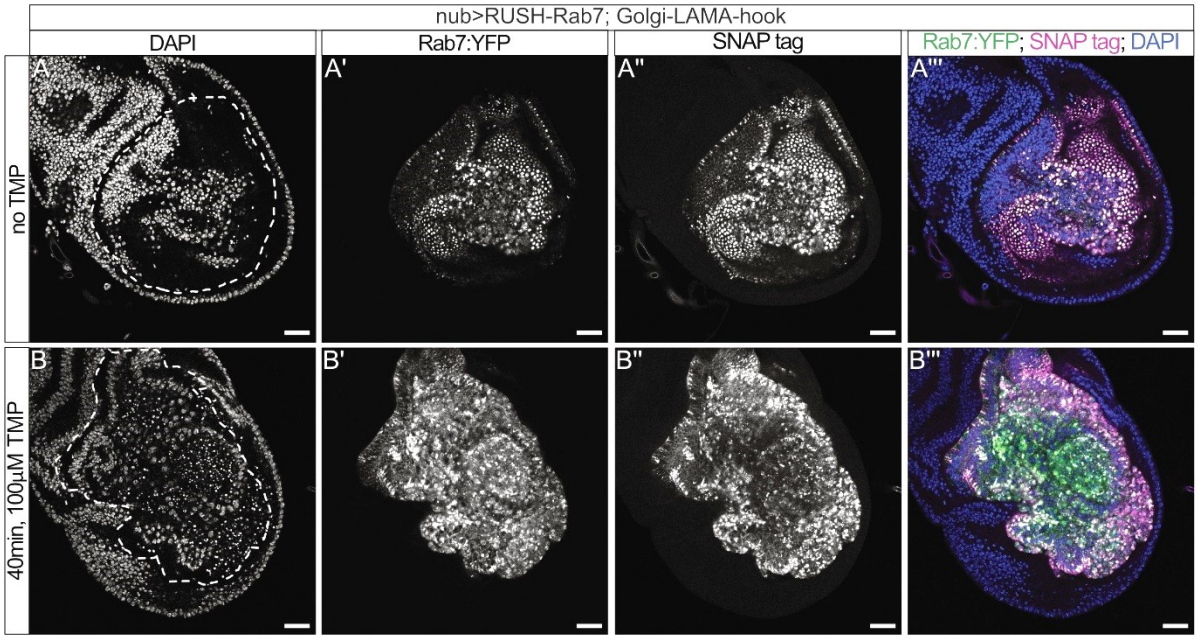

Figure 21: Co-expression of the RUSH-Rab7 together with the Golgi-LAMA-hook in wing imaginal discs causes severe apoptosis and morphological defects

A Representative image of the wing imaginal disc with co-expressed RUSH-Rab7 and Golgi-LAMA-hook under the nub-Gal4 driver, without TMP incubation.

B Representative image of the wing imaginal disc with co-expressed RUSH-Rab7 and Golgi-LAMA-hook under the nub-Gal4 driver, after 40min incubation with 10µM TMP in culture medium.

Scale bar=50µm.

The Gal4/UAS system which I used for the overexpression of the LAMA system components limits the overexpression spatially but not temporally. In order to determine how quickly after overexpression the tissue begins deteriorating, I switched from the nub-Gal4 to the patched-Gal4; tubulin-Gal80^{ts} (ptc-Gal80^{ts}) driver, which allowed me to temporally control the expression by inducing it through temperature regulation. ptc-Gal4 in third larval instar wing imaginal discs expresses in a narrow stripe at the anteroposterior axis, which would additionally limit the tissue degeneration. I induced the overexpression of the Golgi-LAMA-hook and RUSH-Rab7 for 12h and 36h by shifting the larvae from 18^{o}C to 29^{o}C.

12 hours after the temperature shift, both components of the LAMA system were expressed and the tissue appeared unaffected, as indicated by the lack of basal extrusion of apoptotic cells in the ptc-Gal80^{ts} expression region (white arrows; Figure 22A). By contrast, 36h after the temperature shift, the basal extrusion of apoptotic cells was present in the region of Golgi-LAMA-hook and RUSH-Rab7 overexpression (white arrows; Figure 22B), though these wing discs showed no morphological deformities. Therefore, the LAMA system using the Golgi-LAMA-hook could induce tissue toxicity within 36 hours expression, even with a narrowly spatially controlled promoter.

In order to determine whether the Golgi-LAMA-hook is inducing the toxicity of the wing imaginal disc, I generated a fly line carrying a mitochondrial LAMA-hook in order to avoid the sequestration of the reporter on the organelles of the secretory system. In order to anchor the hook to the outer mitochondrial membrane, I used the transmembrane region of the

TOM20 protein in accordance with the original LAMAs publication [Farrants et al., 2020]. This ensured that the hook faces the cytoplasmic, rather than the luminal side of the membrane.

In order to test the Mito-LAMA-hook, I co-expressed it with the RUSH-Rab7 under the control of engrailed-Gal4 (en-Gal4) driver, which induces the expression of UAS constructs in the posterior segment of the third larval instar wing imaginal disc. I chose this driver for ease of the experimental setup and its similarity to the hh-Gal4 driver, which induces the expression in the same location. As previously, I visualized the Mito-LAMA-hook using its SNAP tag.

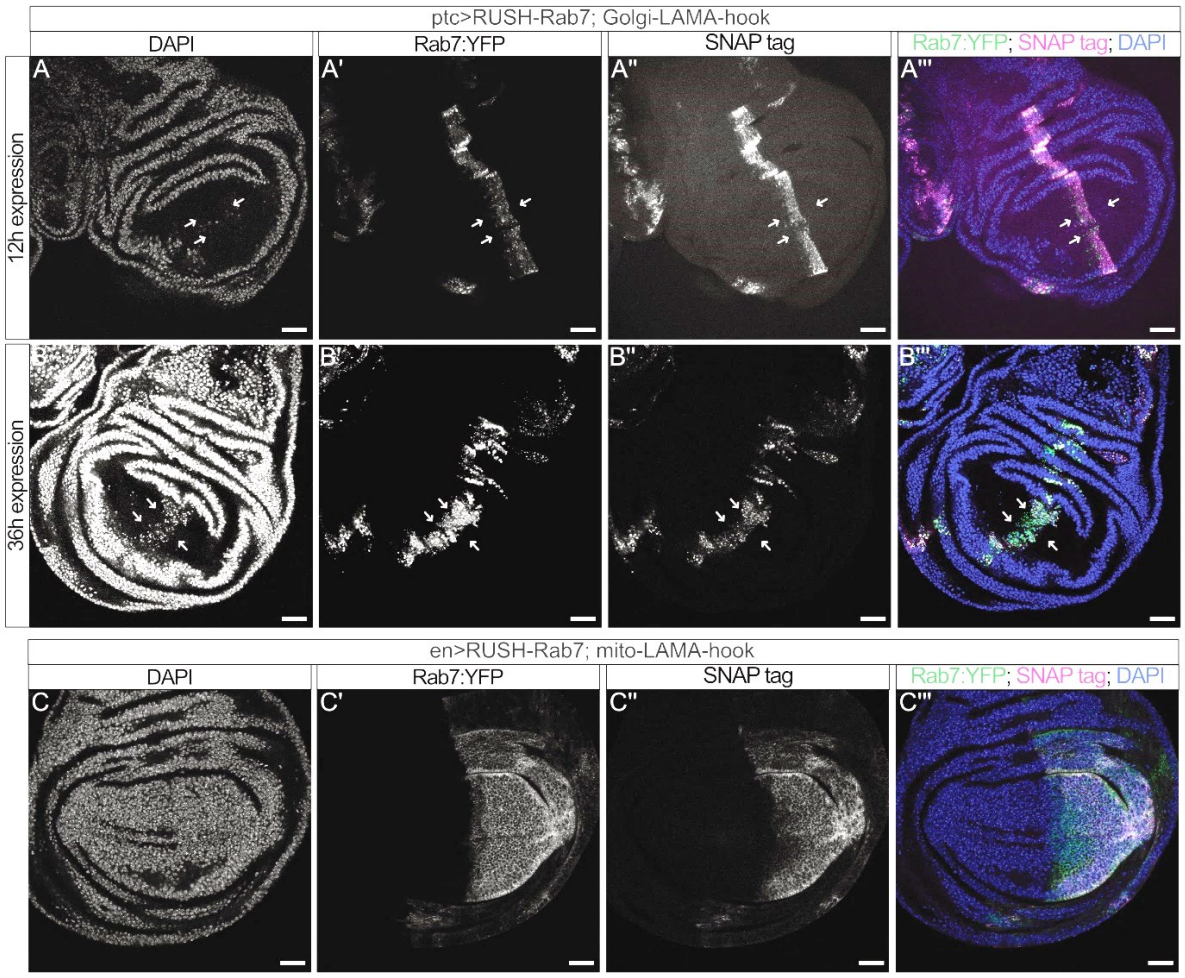

Figure 22: Golgi-LAMA-hook causes toxicity within 36h of expression, whereas the Mito-LAMA-hook is well tolerated by the wing imaginal disc cells

A-B Representative images of the wing imaginal disc after 12h (A) and 36 (B) hours of expression of the Golgi-LAMA-hook and RUSH-Rab7 under the ptc-Gal80^{ts} driver; toxicity is absent after 12h, but present after 36h of expression; white arrows indicate apoptotic cells and cell debris.

C Representative image of the wing imaginal disc with co-expressed Mito-LAMA-Hook and RUSH-Rab7 under the en-Gal4 driver; no tissue toxicity is present in the wing discs.

Scale bar=50µm.

Upon overexpression of the Mito-LAMA-hook and RUSH-Rab7 under the en-Gal4 driver, the flies reached adulthood with no deformities of their wings, no morphological changes of the wing imaginal discs, and no signs of excessive cell apoptosis (Figure 22C). This demonstrated that, unlike the Golgi-LAMA-hook, the Mito-LAMA-hook does not induce toxicity in the wing imaginal discs when co-expressed with the RUSH-Rab7 reporter.

Similarly to the RUSH system, I tested the LAMA system not only in the wing imaginal discs, but also the salivary glands of *Drosophila* larvae. I again used the sgs3-Gal4 driver to overexpress the Golgi-LAMA-hook and RUSH-Rab7 in the third larval instar salivary glands, and visualized the hook through its SNAP tag. In addition, I incubated the salivary glands for 30 min with 100µM TMP in order to test whether the release of the reporter from the hook can be achieved in this tissue.

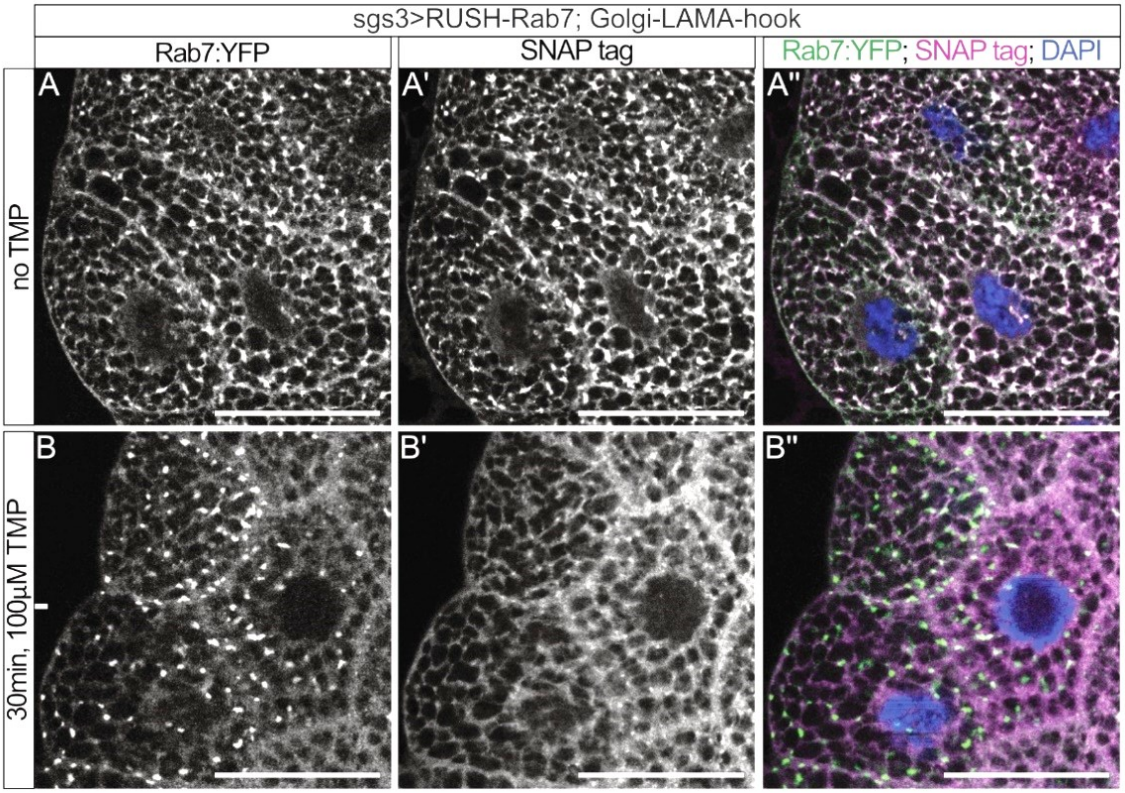

Figure 23: The LAMA system using the Golgi-LAMA-hook is not toxic to salivary gland cells and the addition of TMP can reduce the localization of RUSH-Rab7 to the hook
A-B Representative images of salivary gland cells co-expressing the Golgi-LAMA-hook and RUSH-Rab7 under the sgs3-Gal4 driver without TMP (A) and after 30min of incubation with 100µM TMP (B). Scale bar=50µm.

Unlike the wing imaginal discs, salivary gland cells tolerated the co-expression of the Golgi-LAMA-hook and RUSH-Rab7 well. The larvae were able to successfully attach to the walls of the vials during pupariation and develop into adult forms. Upon dissection, I observed very strong colocalization between the hook and the reporter in the salivary gland cells. The RUSH-Rab7 fluorescence and the hook staining were both diffusely distributed around the 'glue' vacuoles, with moderate punctate accumulation present as well (Figure 23A). After 30 minutes of incubation in the TMP-containing culture medium, the colocalization was significantly reduced, and the Golgi-LAMA-hook became almost completely diffuse, while the RUSH-Rab7 became more punctate (Figure 23B). This indicates that the addition of TMP to the culture medium is able to induce the release of the reporter from the Golgi-LAMA-hook in the cytoplasm of salivary glands.

I also tested the Mito-LAMA-hook in the same context as the Golgi-LAMA-hook by overexpressing it in salivary gland cells together with the RUSH-Rab7 under the sgs3-Gal4

driver. In addition to the visualization of the hook through its SNAP tag, I also visualized mitochondria using the MitoTracker dye in order to confirm that the Mito-LAMA-hook is correctly localizing to the mitochondria. Finally, I incubated these salivary glands for 60min in culture medium containing 100µM TMP and studied the colocalization of the hook, the reporter and the MitoTracker staining afterwards.

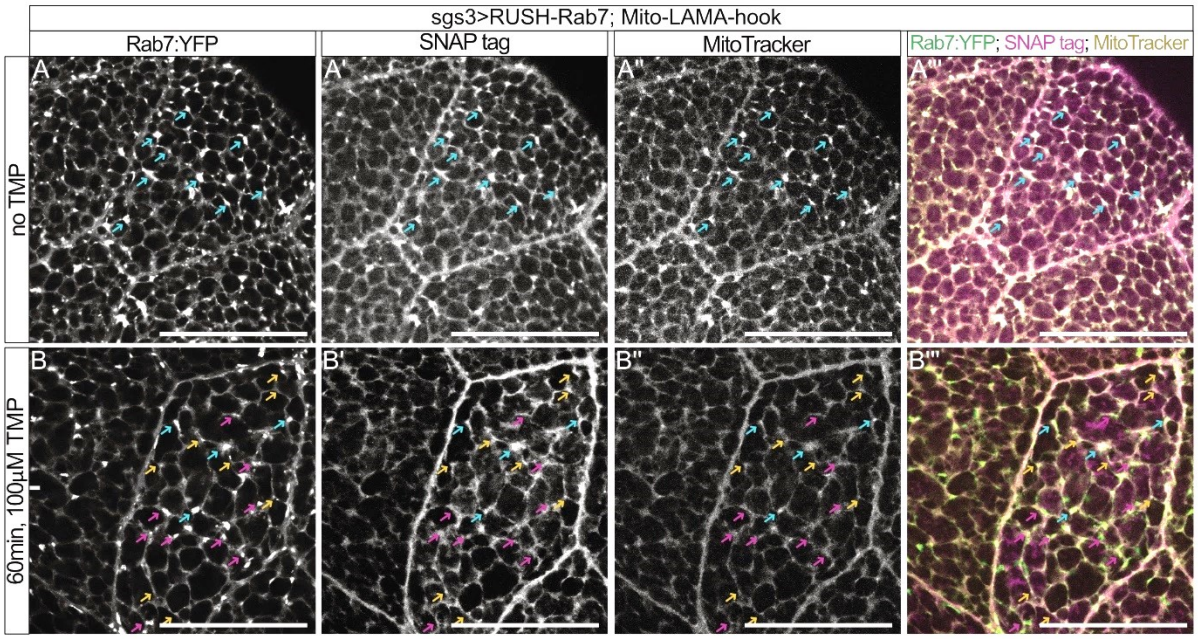

Figure 24: The Mito-LAMA-hook correctly localizes to the mitochondria in salivary gland cells and the addition of TMP can reduce the localization of RUSH-Rab7 to the hook and the mitochondria

A-B Representative images of salivary gland cells co-expressing the Golgi-LAMA-hook and RUSH-Rab7 under the sgs3-Gal4 driver without TMP (A) and after 60min of incubation with 100µM TMP (B). The discs were stained with MitoTracker to mark the mitochondria. Blue arrows indicate the colocalization of RUSH-Rab7, Mito-LAMA-hook and mitochondria; magenta arrows indicate RUSH-Rab7 not colocalizing with the Mito-LAMA-hook and mitochondria; yellow arrows indicate the Mito-LAMA-hook and mitochondria not localizing with RUSH-Rab7. Scale bar=50µm.

The SNAP tag staining for the visualization of the Mito-LAMA-hook strongly colocalized with the MitoTracker staining, indicating that the hook is correctly localizing to the expected organelle. Moreover, the bright fluorescence puncta of RUSH-Rab7 colocalized with the bright puncta of both the hook and the MitoTracker stainings, indicating that the hook can successfully sequester the RUSH-Rab7 reporter to the surface of the mitochondria (blue arrows; Figure 24A). After 60 min of incubation in TMP-containing medium, the colocalization of the Mito-LAMA-hook and MitoTracker staining remained high. However, RUSH-Rab7 fluorescence colocalization was reduced and there was an increased number of bright fluorescence puncta which did not colocalize with any similar hook or mitochondrial staining puncta (magenta arrows, Figure 24B). In addition, I also observed Mito-LAMA-hook staining puncta which did not colocalize with RUSH-Rab7. This indicates that upon TMP addition, RUSH-Rab7 is released from the Mito-LAMA-hook and moves away from the mitochondria, confirming the functionality of the LAMA system in these cells.

Together, my data show that the LAMA system can be expressed in the *Drosophila* wing imaginal discs and salivary glands. Similar to the RUSH system, the use of the Golgi-LAMA-

hook facing the cytoplasm in wing imaginal discs, but not in salivary glands, induced cell toxicity and significant morphological deformities. This problem could be circumvented through the limitation of the LAMA system expression to 12 hours, or by the use of the Mito-LAMA-hook instead for the trapping of cytoplasmic reporter proteins. Finally, the addition of TMP induced the release of the RUSH-Rab7 reporter from both hooks in salivary gland cells. The MitoTracker staining showed that the RUSH-Rab7 released from the Mito-LAMA-hook was able to travel away from the mitochondria where it was previously sequestered.

In direct comparison between the RUSH and the LAMA system, their limitations were similar, but the requirement of the biotin-deficient fly food for the RUSH system made it strongly disadvantageous compared to the LAMA system. I therefore judged that the LAMA system is better suited for use in *Drosophila melanogaster* and continued using it for further experiments.

3.2.3 Live imaging of the LAMA system in wing imaginal discs and salivary glands

The main advantage of the LAMA system is the synchronous release of the reporter protein from the hook upon addition of TMP. This allows for the direct observation of the system's dynamics in real time by live fluorescence imaging. Wing imaginal disc cells are too small to easily allow for the observation of intracellular dynamics of the LAMA system. However, establishing a protocol for the live imaging of the LAMA system in wing imaginal discs still allows for the observation of the system in a supracellular context. This could be beneficial for the study of any organ-wide changes that the acute release of sequestered reporter may induce within a short amount of time.

In order to test if the LAMA system is usable in live imaging studies, I used the previously established protocol for *ex vivo* culturing of living wing imaginal discs. However, in this case, I incubated the wing discs with the SNAP tag fluorescent substrate prior to mounting in order to visualize the Mito-LAMA-hook. Once mounted, I imaged individual discs. In the case of wing discs cultured without addition of TMP to the culture medium, I imaged for 10 to 60 minutes. In the case of wing discs in which I imaged the changes upon the release of the LAMA system reporter from the hook, I imaged for 5 to 10 minutes before the addition of TMP to the culture medium (timepoint 0). I subsequently imaged the same wing discs for 45 to 60 min after TMP addition in order to capture the system's dynamics. In both cases, I expressed the RUSH-Rab7 and Mito-LAMA-hook under the control of the en-Gal4 driver.

RUSH-Rab7 fluorescence and the Mito-LAMA-hook staining colocalized in punctate structures in the wing imaginal discs cultured without the addition of TMP (white arrows; Figure 25A-B). The colocalization was persistent and the structures were largely static over the course of the imaging. The expression of the RUSH-Rab7 reporter and the Mito-LAMA-hook was not even throughout the posterior compartment of the wing discs, where the en-Gal4 driver is active. The hook was strongly expressed towards the edges of the wing disc pouch, while the reporter was more expressed towards the center of the pouch.

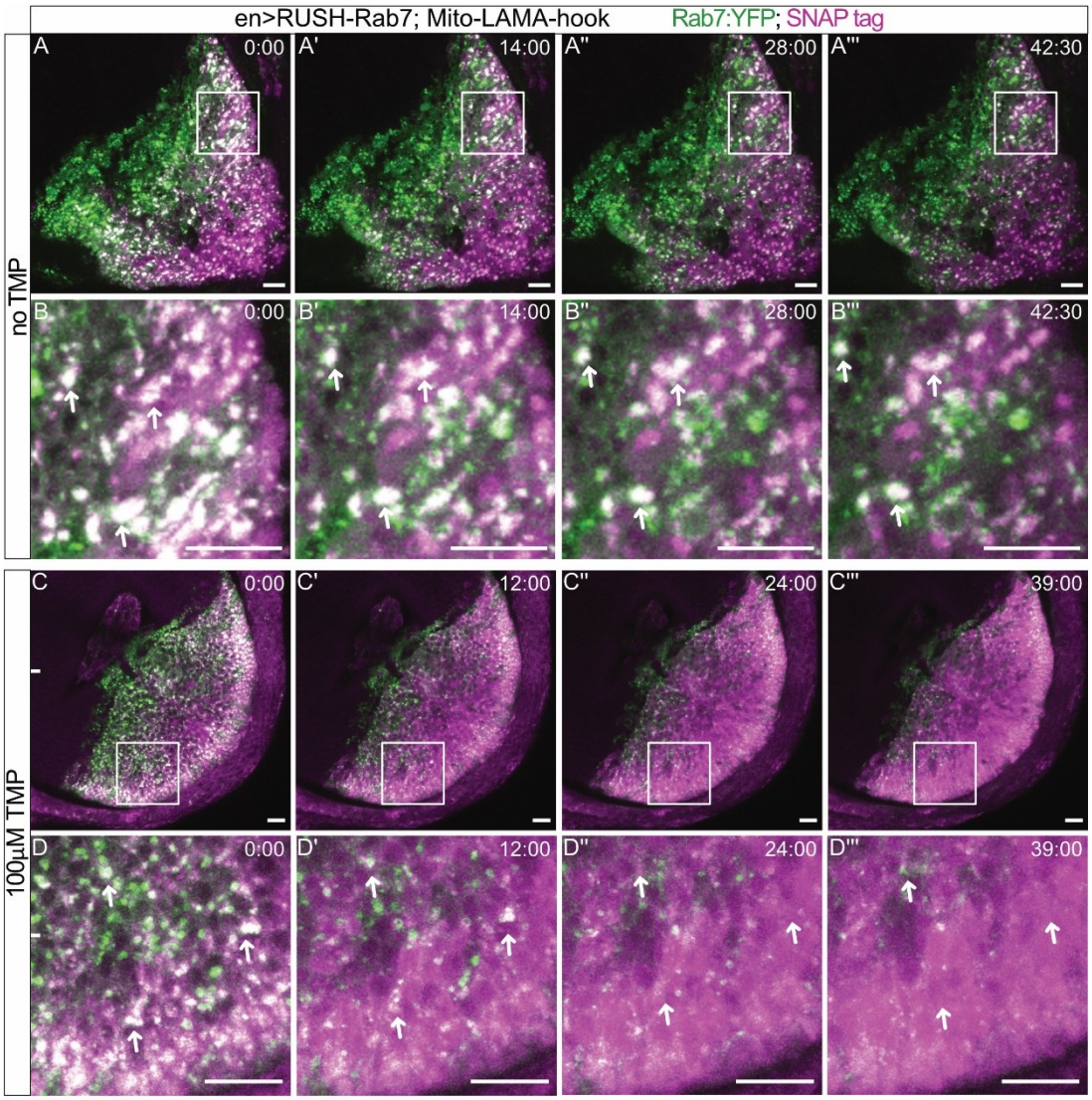

Figure 25: Live imaging of the LAMA system using RUSH-Rab7 and Mito-LAMA-hook demonstrates the changes in the distribution of the LAMA system components within the wing imaginal disc tissue after addition of TMP

A-B Individual images of a 45min live imaging series at selected time points of wing discs expressing RUSH-Rab7 and the Mito-LAMA-hook under the en-Gal4 driver in TMP-free culture medium. Posterior wing disc compartment (A) and its magnification (B).

C-D Individual images of a 45min live imaging series at selected time points of wing discs expressing RUSH-Rab7 and the Mito-LAMA-hook under the en-Gal4 driver after 100uM TMP addition to the culture medium. Posterior wing disc compartment (C) and its magnification (D).

Scale bar=10µm; Images are maximum intensity projections of five 1µm slices through the wing disc; white arrows indicate RUSH-Rab7 and Mito-LAMA-hook colocalization events.

Upon the addition of TMP, the colocalization of the RUSH-Rab7 fluorescence with the Mito-LAMA-hook staining gradually reduced (white arrows; Figure 25C-D). The RUSH-Rab7 fluorescence remained partially punctate throughout the posterior compartment of the wing discs, but the signal intensity was gradually reduced over time. The hook staining shifted from strongly punctate into more diffuse throughout the expressing wing disc compartment and its signal intensity gradually increased as well.

My live imaging data of the LAMA system show that in the case where the Mito-LAMA-hook was used to sequester the RUSH-Rab7 reporter, the release of the reporter could be observed

throughout the tissue within the first ten minutes, as indicated by the reduced colocalization of the reporter and the hook, and that these changes affected the distribution of both components in the expressing compartment of the wing discs.

3.2.4 The LAMA hook can effectively sequester endogenous GFP-tagged proteins in the ER

My previous experiments showed that the LAMA system can be successfully used to sequester cytoplasmically located overexpressed reporter proteins in *Drosophila* tissues to the LAMA hook facing the cytoplasm. I next wanted to test whether the LAMA system can also be used to sequester endogenous proteins, as well as proteins destined for secretion, such as the Wnt proteins, which are translocated into the ER lumen after synthesis. Sequestration of endogenous proteins would potentially allow for a way to study the loss-of-function effects in a spatially controlled manner, as well as the short-term response of the tissue to the phenotype rescue through the addition of TMP and the release of endogenous proteins from the LAMA hook.

As I previously endogenously tagged Wnt secretion components, I chose to use Wg:EGFP and Evi:EGFP to test the sequestration of endogenous proteins by the LAMA hook. Wg is synthesized and processed in the ER lumen, after which it is transported by its carrier Evi, a transmembrane protein, through the secretory pathway until it is secreted from the cell [Bartscherer et al., 2006]. Therefore, Wg:EGFP could only be trapped in the lumen of the secretory pathway organelles. The EGFP of my tagged Evi variant is located within the last intraluminal loop, meaning that after synthesis, it is found in the ER lumen rather than the cytoplasm, and thus the trapping of Evi:EGFP by the LAMA hook could also only be achieved if the hook was facing the organelle lumen.

For this reason, I generated an intraluminal ER-LAMA-hook by fusing the KDEL C-terminal sequence together with an ER-targeting N-terminal sequence to the LAMA hook construct. The KDEL motif is found in higher eukaryotes including *Drosophila melanogaster* [Abrams et al., 2013] and serves to prevent ER proteins from entering the secretory route through the binding to the KDEL receptor facing the ER lumen, as well as target these proteins to the retrograde transport from the Golgi to the ER when necessary [Denecke et al., 1992]. I overexpressed the ER-LAMA-hook under the control of en-Gal4 driver in flies carrying the endogenously tagged Wg:EGFP and dissected the third larval instar wing imaginal discs of these flies. Additionally, I performed a similar experiment with endogenously tagged Evi:EGFP, using the hh-Gal4 driver instead of the en-Gal4 driver for ease of fly crossing, as hh-Gal4 and en-Gal4 drivers both express in the posterior compartment of the wing disc. In both cases, I visualized the ER-LAMA-hook using its SNAP tag.

The endogenously tagged Wg:EGFP strongly accumulated in the posterior wing disc compartment, where the ER-LAMA-hook was overexpressed under the en-Gal4 driver (Figure 26A). This indicates that the endogenous protein was successfully bound by the ER-LAMA-hook. By comparison, endogenously tagged Evi:EGFP showed only mild accumulation in wing

discs overexpressing the ER-LAMA-hook under the hh-Gal4 driver. The results point towards the likelihood of variation in how effectively the ER-LAMA-hook can bind different reporter proteins (Figure 26B).

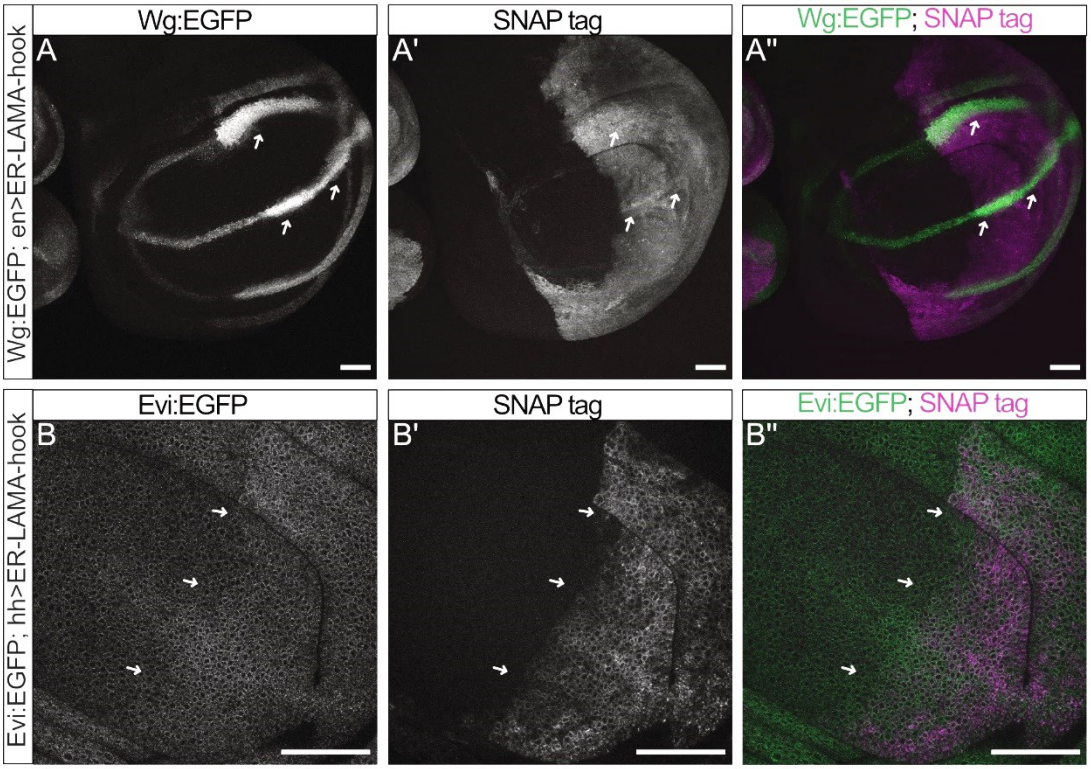

Figure 26: Expression of the ER-LAMA-hook in wing discs endogenously tagged for Wg:EGFP or Evi:EGFP caused a strong accumulation of Wg:EGFP and a mild accumulation of Evi:EGFP in the cells

A Representative image of Wg:EGFP wing discs overexpressing the ER-LAMA-hook under the en-Gal4 driver. Maximum intensity projection of the full disc.

B Representative image of Evi:EGFP wing discs overexpressing the ER-LAMA-hook under the hh-Gal4 driver. Individual slice in the middle region of the wing disc.

Scale bar=50µm; white arrows indicate stronger fluorescence area.

The next question I wanted to answer was whether the LAMA system can be used to induce a loss-of-function phenotype if it binds GFP-tagged *Drosophila* endogenous proteins. To do this with the flies carrying endogenously tagged Wg:EGFP, I repeated the previous experiment and performed surface staining with the α-GFP antibody to visualize the secreted Wg:EGFP protein. As these flies were heterozygous for untagged Wg and Wg:EGFP, I expected half of the total Wg amount produced by these cells to be untagged and therefore secreted rather than trapped by the LAMA hook, which was why I did not use the Wg antibody. In addition, I used a fly line previously established by Michaela Holzem in the laboratory carrying Wg:EGFP, Distalless:Tomato (Dll:Tom) and hh-Gal4 to express the ER-LAMA-hook. Dll is a Wnt pathway target gene active a moderate distance from the dorsoventral boundary Wg-secreting cells [Neumann & Cohen, 1997]. Reduction in Wg secretion would thus affect the expression of the Dll protein, making Dll:Tom a viable tool for the assessment of Wnt signaling.

As expected, the antibody surface staining using the α-EGFP antibody of the wing discs carrying the endogenously tagged Wg:EGFP and overexpressing the ER-LAMA-hook under the

en-Gal4 driver showed an almost complete loss of Wg:EGFP secretion in the posterior wing disc compartment (white arrows, Figure 27A). The results further confirm that ER-LAMA-hook is able to strongly bind Wg:EGFP and sequester it, such that it cannot travel through the secretory pathway and be secreted, as would be expected of the Wg protein.

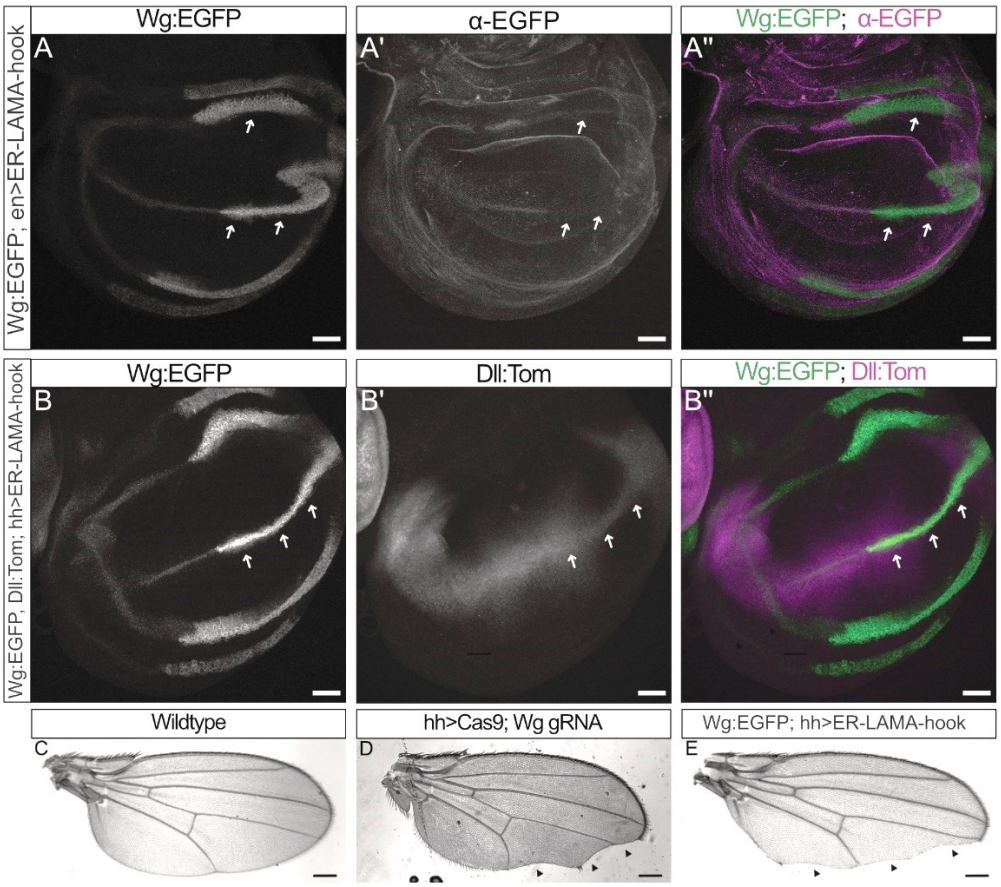

Figure 27: Sequestration of the Wg:EGFP in ER-LAMA-hook expressing cells causes a significant reduction in Wg:EGFP secretion as well as reduction in Wnt pathway target gene expression

A Representative image of Wg:EGFP wing discs overexpressing the ER-LAMA-hook under the en-Gal4 driver and antibody surface stained for EGFP.

B Representative image of Evi:EGFP, Dll:Tom wing discs overexpressing the ER-LAMA-hook under the hh-Gal4 driver.

Scale bar=50µm; maximum intensity projections of the discs; white arrows indicate the area of Wg:EGFP accumulation due to the expression of the ER-LAMA-hook.

C-E Representative images of adult fly wings of flies homozygous for Wg:EGFP expressing ER-LAMA hook under the hh-Gal4 driver (E), as well as wildtype flies (C) and Wg knockout flies (D). Scale bar=0.2mm.

In wing discs expressing the endogenously tagged Wg:EGFP and Dll:Tom as well as the ER-LAMA-hook under the hh-Gal4 driver, clear reduction in Dll:Tom signal was observed in the posterior wing disc compartment (white arrows, Figure 27B). This demonstrates that downstream Wnt signaling was also affected by the loss of Wg:EGFP secretion induced through the binding with ER-LAMA-hook. The reduction of the signal was gradual rather than abrupt along the dorsoventral boundary, likely because Wg secreted from the anterior compartment was able to bind to the receptors on the Wg-receiving cells nearest the anteroposterior boundary due to diffusion and activate Dll expression in these cells. Additionally, wings of adult flies of this cross carrying homozygous Wg:EGFP showed the typical notch phenotype associated with loss of Wg signaling (Figure 27C-E).

I next wanted to answer the question of whether the addition of TMP can induce the release of the Wg:EGFP from the LAMA hook in the ER lumen. I expressed the ER-LAMA-hook under the hh-Gal4 driver in flies carrying the endogenously tagged Wg:EGFP and Dll:Tom, and incubated the wing discs in culture medium containing 1mM TMP for up to 2 hours.

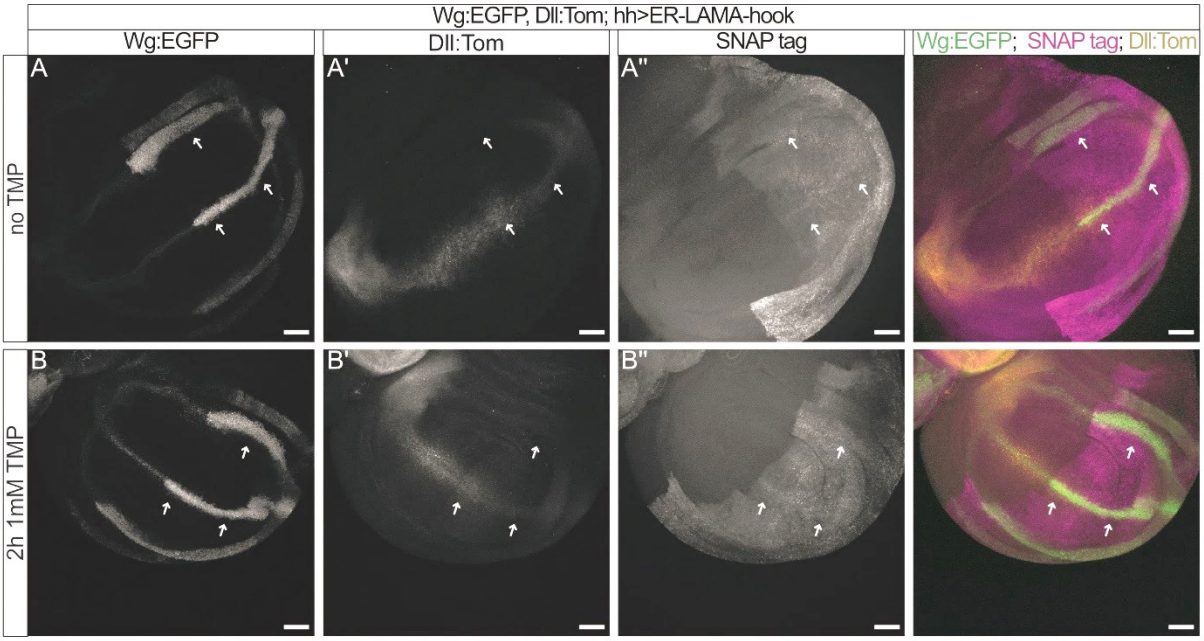

Figure 28: TMP incubation for 2 hours does not induce the secretion of Wg:EGFP from the ER-LAMA-hook expressing cells
A Representative image of Wg:EGFP, Dll:Tom wing discs overexpressing the ER-LAMA-hook under the hh-Gal4 driver without incubation with TMP.
B Representative image of Wg:EGFP, Dll:Tom wing discs overexpressing the ER-LAMA-hook under the hh-Gal4 driver after 2h incubation with 1mM TMP.
Scale bar=50µm; maximum intensity projections of the discs; white arrows indicate the area of Wg:EGFP accumulation due to the expression of the ER-LAMA-hook.

I found that the Wg:EGFP was still highly accumulated in Wg-secreting cells overexpressing the ER-LAMA-hook after 2 hours of TMP incubation, and that the reduction of Dll:Tom expression in this wing disc compartment was also unchanged from the levels prior to TMP incubation (Figure 28). I further tested this by adding 1mM TMP to the normal fly food on which flies were fed, as well as by limiting the expression of the hook to 24 hours prior to 1 hour incubation with 1mM TMP using the hh-Gal80^{ts} driver. In both of these cases as well, the accumulation of Wg:EGFP was unchanged in these cells (Supplemental Figure S5). This indicates that the ER-LAMA-hook is capable of binding Wg:EGFP in the Wg-secreting cells and through this sequestration inducing the Wnt loss-of-function phenotype, but that the addition of TMP does not induce the release of Wg:EGFP from the cells.

As TMP was unable to trigger the release of Wg:EGFP from the ER-LAMA-hook, I decided to test whether the GFP-tagged endogenous protein found in the cytoplasm can be sequestered to the Mito-LAMA-hook and released from it upon TMP incubation. For this, I used the fly line carrying endogenously tagged Shaggy:EGFP (Sgg:EGFP) commercially available from the Bloomington Drosophila Stock Center (BDSC) to overexpress the Mito-LAMA-hook using en-

Gal4 driver. Sgg is the *Drosophila* homolog of GSK3, one of the members of the destruction complex which targets β-catenin for degradation if Wnt ligands are not bound to their receptors, and is thus found in the cytoplasm. I tested the release of Sgg:EGFP from the hook by incubating the wing discs in culture medium containing 1mM TMP for 1 hour.

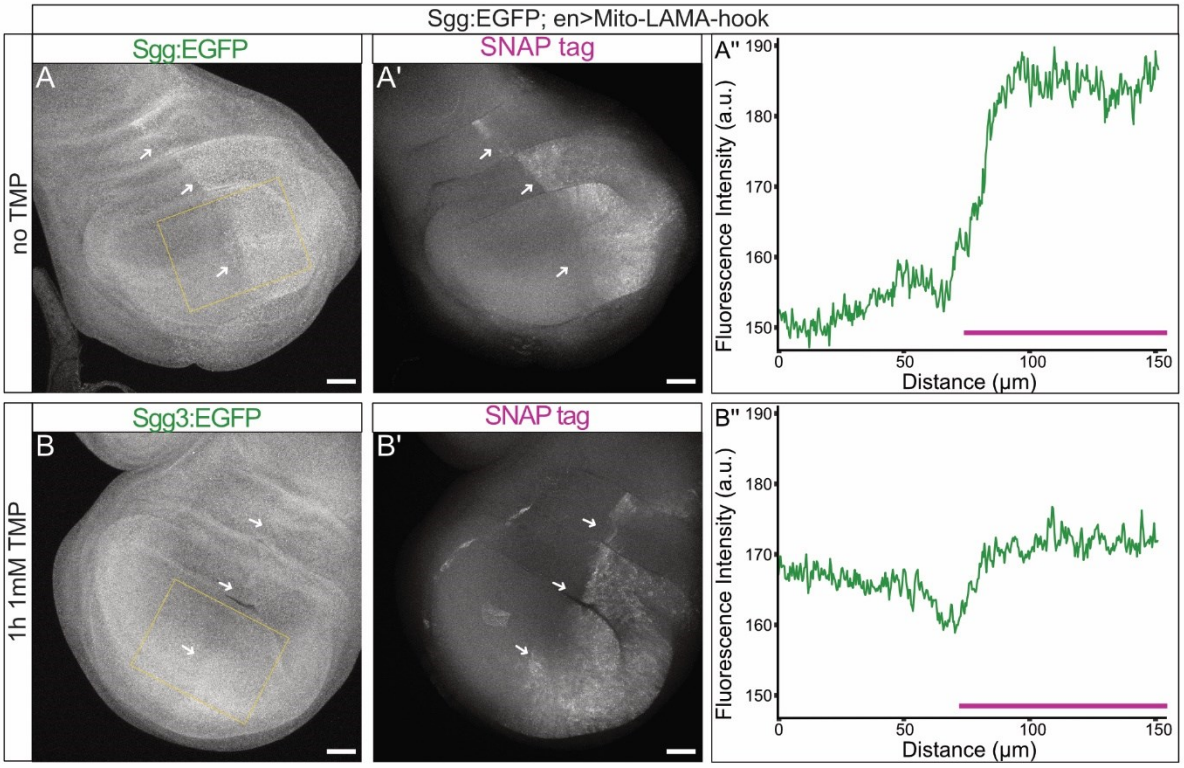

Figure 29: Mito-LAMA-hook can successfully sequester endogenous Sgg:EGFP present in the cytoplasm, which is released upon addition of TMP

A-B Representative image of Sgg:EGFP wing discs overexpressing the ER-LAMA-hook under the hh-Gal4 driver without incubation with TMP (A) or after 1h incubation with 1mM TMP (B). Maximum intensity projections of the discs; Sgg:EGFP signal intensity was quantified by calculating the plot profiles within the yellow rectangles; white arrows indicate the area of Sgg:EGFP accumulation due to the expression of the Mito-LAMA-hook; scale bar=50µm.

Sgg is ubiquitously expressed in all cells of the wing imaginal disc. Upon overexpression of the Mito-LAMA-hook in the posterior wing disc compartment, Sgg:EGFP accumulates in the cells (white arrows, Figure 29A). This accumulation is almost fully lost after 1 hour of incubation with TMP and the Sgg:EGFP fluorescence in the posterior wing disc compartment returns to similar levels as the fluorescence in the anterior compartment (fluorescence intensity profile plot; Figure 29B).

Together, these data indicate that the LAMA system can be used to sequester GFP-tagged endogenously expressed proteins in both cytoplasm and the ER, and that this sequestration can induce loss-of-function phenotypes expected if the protein is not available to perform its function in the tissue in question. While TMP was unable to trigger the release of Wg:EGFP from the hook in the ER lumen, this was not the case in the cytoplasm, where Sgg:EGFP could be released from the Mit-LAMA-hook, in line with the results of the LAMA system using an overexpressed transgenic reporter protein.

3.3 Rab GTPases and their role in Wnt secretion

For secretion, Wnt proteins must travel through various intracellular compartments: from ER to Golgi, from Golgi to the cell surface, and then further into early endosome and late endosomes/MVBs if secreted on exosomes (Introduction Section 2.1). These trafficking processes are regulated by Rab GTPases, small proteins in the Ras superfamily (Introduction Section 2.2). Therefore, it can be assumed that Rab GTPases are involved in Wnt secretion in some manner, though not much is known about this (prior publications are summarized in Introduction Section 2.2 'The role of Rab GTPases in Wnt secretion').

While some Rabs (such as Rab1, Rab5 or Rab7) have a broad role in the general secretion and endosomal trafficking, others have more specific roles in individual cellular processes. I wanted to determine if any Rab GTPases exist which have dedicated roles in Wnt secretion, with the alternative being that Wnt proteins are trafficked through the cell for secretion under the direction of the general, ubiquitous Rabs. I therefore decided to systematically analyze which Rab GTPases are important for Wnt secretion by performing two screens in *Drosophila* larval wing imaginal discs and adult wings. After identifying suitable screen candidates, I afterwards wanted to study their precise role in Wnt secretion.

3.3.1 Rab GTPase perturbation screens for the effects on Wnt secretion

To identify which members of the Rab protein family play roles in Wnt secretion, I performed two screens of all *Drosophila* Rabs GTPases. The first screen I performed was the study of adult wings of all viable *Drosophila* Rab GTPase homozygous null mutant fly lines. I studied the adult wings because defects in Wnt secretion and signaling induce a characteristic wing notches phenotype (for reference, see Figure 10B and 10E). Additionally, Wnt pathway is involved in the regulation of wing size through crosstalk with Dpp signaling [Parker & Struhl, 2020].

The Rab GTPase null mutant fly line collection was generated by the Hiesinger laboratory of Free University of Berlin. Eighteen out of twenty-six *Drosophila* Rab GTPases are considered non-ubiquitous and their null mutants are viable. The remaining eight Rab GTPases (Rab 1, 2, 5, 6, 7, 8, 11 and 35) are ubiquitously expressed and their null mutants are lethal early in larval development. Due to this, characterization of their loss-of-function effects on an organismal level was impossible and they were excluded from further analysis. I therefore focused on the non-ubiquitous Rabs in my wing characterization screen, the results of which were published in Kohrs et al., 2021.

I performed the screen by studying the wings of Rab null mutant flies kept under optimal or stress conditions. Flies kept under optimal conditions were reared at 18°C on standard fly food. Flies kept under stress conditions were either reared at 29°C on standard fly food or at 18°C on 20% diluted fly food. I scored the wings for unusual wing shapes, as well as measured the wing surface area to observe the wing size of all fly lines. As control, I used w^{1118} fly line, which carries only the *white* null mutant gene and is otherwise genetically wildtype.

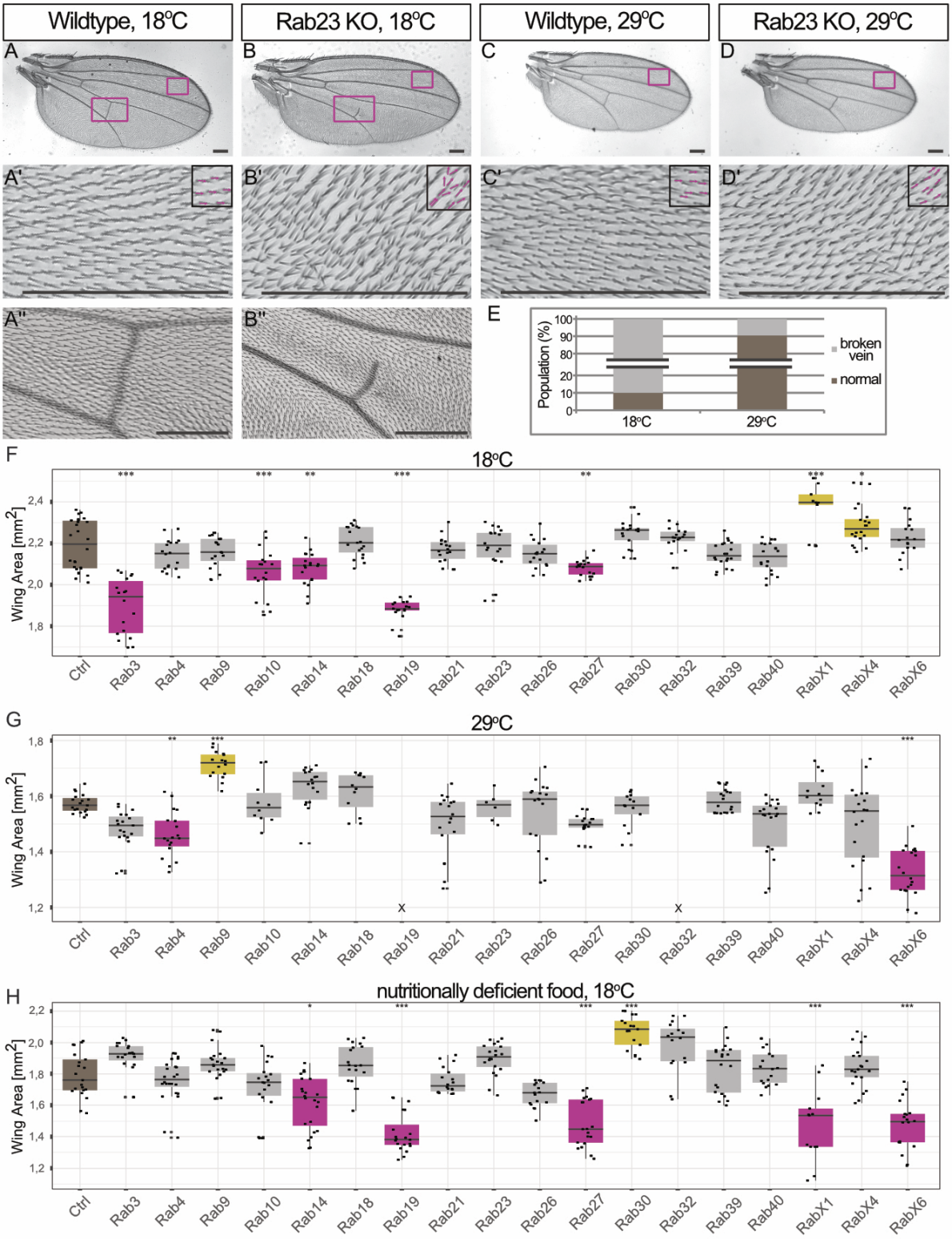

Figure 30: Characterization of adult wings of 18 non-ubiquitous homozygous viable Rab null mutants

A-E Representative images of adult control (A, C) or Rab23 null mutant fly wings (B, D). Magenta arrows indicate hair growth direction; scale bar = 0.2mm (E). Graph showing percentage of Rab23 KO flies with normal or broken posterior crossvein in homozygous population reared at 18°C or 29°C; n^{18}=105, n^{29}=68.

F-H Wing surface area measurement for homozygous viable Rab mutants reared at 18°C (F), 29°C (G) and under nutritional stress (H). Brown bars are wildtype controls; magenta are mutants with significant size reduction; yellow are mutants with significant size increase. Horizontal line of boxplot is the median. n=15 to 22 wings; * = p<0.05; ordinary one-way ANOVA with pair-wise comparison. Data previously published in Kohrs et al., 2021.

None of the eighteen Rab null mutant lines showed any notch phenotype in adult wings. However, Rab23 KO wings displayed a doubling and misalignment of wing surface hairs (Figure 30B and 30D), a planar cell polarity (PCP) phenotype. In addition, 89,5% of the wings displayed the broken posterior crossvein phenotype at 18°C (Figure 30B''), which was mostly lost at 29°C, where only 11,8% of the flies showed the phenotype (Figure 30E).

I measured the wing surface area for 15 to 22 wings of adult flies homozygous for Rab null mutation of all non-ubiquitous Rabs, reared under optimal conditions (18°C, Figure 30F), as well as during temperature stress (29°C; Figure 30G) and under nutritional stress (20% diluted food; Figure 30H). Rab null mutant fly lines with statistically significant deviations in wing size from wildtype were present in all three conditions, with more similarity between optimal and nutritional stress conditions than optimal and temperature stress conditions. There were no Rabs whose null mutation induced wing size differences in all three conditions, however.

Under optimal conditions, null mutants of Rab 3, 10, 14, 19 and 27 had smaller wings, while Rab X1 and X4 null mutants had larger wings compared to wildtype (Figure 30F). Temperature stress rescued these phenotypes, as at 29°C all of these fly lines displayed wing sizes which were similar to the wildtype flies. Instead, Rab4 and RabX6 null mutants had smaller, while Rab9 null mutant had larger wings than wildtype in this condition. Additionally, the knockout of Rab19 and Rab32 caused pupal lethality at 29°C (Figure 30G). Lastly, under conditions of nutritional stress, null mutants of Rab 14, 19 and 27 had smaller wings than wildtype, similarly to being reared under optimal conditions. In addition, Rab X1 and X6 also had smaller wings, while Rab30 had larger wings than wildtype (Figure 30H). RabX6 is the only null mutant fly line whose wings were smaller in both stress conditions.

Altogether, the data I obtained from the first screen showed no typical Wnt phenotypes in adult flies carrying Rab null mutations. Rab23 null mutation induced a PCP phenotype in the wings which may be due to disrupted Wnt/PCP signaling; however, this was unlikely to be the case based on prior published literature, and I did not further pursue the phenotype. Altogether, I observed 11 out of 18 Rabs whose knockout affected wing size under either optimal or stress conditions, of which two (Rab 19 and 32) caused lethality at 29°C, showing the importance of Rab GTPases in the developmental process of *Drosophila melanogaster*.

The second of the two screens I performed was an immunohistochemical screen in wing imaginal discs of third instar larvae to investigate the direct effects of Rab GTPase perturbation upon Wnt secretion, focusing on Wg protein (*Drosophila* homolog of Wnt1). Several forms of Rab GTPases exist, including wildtype (WT), constitutively active (CA) and dominant negative (DN). The CA Rab GTPase form can only bind GTP and is thus continually active even when low or no activity is preferred by the cell; by contrast, the DN Rab GTPase form can only bind GDP therefore competes with the WT Rab for the binding to interaction partners without performing its function. Rab-CA overexpression often phenocopies Rab-WT overexpression, whereas Rab-DN overexpression phenocopies Rab knockdown or knockout.

A

	Expression Pattern	Wing Disc	-/- Lethality	WT	DN	CA	RNAi	KO
Rab1	Ubiquitous	Yes	Lethal					
Rab2	Ubiquitous	Yes	Lethal					
Rab3	Neuron-specific	No	Viable					
Rab4	Neuron-enriched	Yes	Viable					
Rab5	Ubiquitous	Yes	Lethal					
Rab6	Ubiquitous	Yes	Lethal					
Rab7	Ubiquitous	Yes	Lethal					
Rab8	Ubiquitous	Yes	Lethal					
Rab9	Neuron-enriched	Maybe	Viable					
Rab10	Widespread	Yes	Viable					
Rab11	Ubiquitous	Yes	Lethal					
Rab14	Widespread	Maybe	Viable					
Rab18	Widespread	Yes	Viable					
Rab19	Neuron-specific	Maybe	Viable					
Rab21	Neuron-enriched	Yes	Viable					
Rab23	Neuron-enriched	Yes	Viable					
Rab26	Neuron-specific	No	Viable					
Rab27	Neuron-specific	No	Viable					
Rab30	Widespread	Yes	Viable					
Rab32	Neuron-specific	No	Viable					
Rab35	Ubiquitous	Yes	Lethal					
Rab39	Widespread	Yes	Viable					
Rab40	Neuron-specific	Maybe	Viable					
RabX1	Neuron-specific	Maybe	Viable					
RabX4	Neuron-specific	No	Viable					
RabX6	Neuron-specific	Maybe	Viable					

Figure 31: Genetic screening of Rab GTPase perturbation revealed Rab7 overexpression caused changes in Wg secretion

A Table summarizing the results of the perturbation screen performed in wing imaginal discs by overexpressing WT, CA and DN Rab as well as KD by RNAi using hh-Gal4 or ptc-Gal80^{ts} drivers, as well as stable KO lines. Wg and Sens distribution visualized by antibody staining was used as readout. Green field indicates unperturbed Wg expression; yellow field indicates Wg phenotype present; magenta field indicates cell apoptosis present; black field indicates lines lethal before third instar stage. n=5 to 15 wing discs. Table includes cell type specificity of each Rab [acc. Chan et al., 2011; Jin et al., 2012] and its expression in the wing disc [acc. Chan et al., 2011; Dunst et al., 2015].

B-D Example wing discs of Rab1-DN (B), Rab5-DN (C) and Rab7-WT (D) overexpression. Wing disc segment with Rab overexpression is outlined with dashed line. Scale bar = 50 µm.

I used the Gal4/UAS system to induce either the overexpression of WT, CA and DN forms of both ubiquitous and non-ubiquitous *Drosophila* Rab GTPases, or knockdown (KD) of these Rabs through RNA interference (RNAi). I additionally analyzed the wing imaginal discs of non-ubiquitous Rab knockout (KO) lines I used in the first screen. In all perturbation cases, I performed immunofluorescence antibody staining to visualize Wg and its target gene Senseless (Sens). Further, I used driver lines hh-Gal4, hh-Gal80^{ts} and ptc-Gal80^{ts}, which are only expressed in a segment of the wing discs, so that the unperturbed sections of the discs could serve as internal control (Figure 31A).

Overexpression of the DN form and knockdown of both Rab1 and Rab5 induced extremely severe apoptosis responses in the wing discs and I was forced to use the Gal80^{ts}/UAS system to limit expression to 24 hours. Wg secretion was disturbed in both of these cases. Rab1 perturbation resulted in the accumulation of large Wg patches in the disrupted segment of the tissue (Figure 31B), similar to WntD accumulation upon Rab1-DN overexpression [Ching et al., 2008]. Rab5 perturbation resulted in the accumulation of Wg in Wg secreting cells on the apical side and complete loss of Wg on the basal side (Figure 31C). I chose not to further pursue either of the phenotypes, as it is likely that the severity of the effects on Wg secretion were a direct consequence of cell apoptosis and the lethality phenotypes accompanying these perturbations made it impossible to determine any downstream effects on adult flies.

The overexpression of wildtype Rab7 as well as Rab7 knockdown gave a Wnt accumulation phenotype without causing lethal effects to the cells (Figure 31D). Knockdown of Rab11 was lethal when driven by hh-Gal4, but the wing discs did not display any toxicity upon 24h knockdown using the hh-Gal80^{ts} driver, nor was any Wg phenotype observed in this case. Additionally, overexpression of Rab14-WT and Rab21-WT showed significant cell death, though Wg expression was unperturbed, thus I excluded these three candidates from further analysis (Supplemental Figure S6A-B). Overexpression of Rab26-CA also caused strong cell lethality and morphological deformity, accompanied by detectable Wg staining in the morphologically damaged section of the wing disc (Supplemental Figure S6C). Rab26 is not endogenously expressed in the wing disc cells, and neither wildtype Rab26 overexpression, nor any of the three forms of activity suppression perturbations (knockout, knockdown, or DN overexpression) induced a similar phenotype. I therefore concluded that the Wg presence in the posterior compartment was likely a side-effect of the severity of cellular apoptosis and excluded Rab26 from further analysis.

After obtaining all of the results of the screen for the Rab perturbation effects on Wnt distribution, Rab7 was the only candidate which gave a consistent and noticeable Wg phenotype without significant cell toxicity. Thus, I decided to analyze its role in Wnt secretion.

3.3.2 Rab7 perturbation affects intracellular and tissue localization of Wg

Based on the results of the Rab perturbation screen on Wg secretion in wing imaginal disc, I identified Rab7 as a suitable candidate for further studies. As I wanted to determine the precise role Rab7 plays in Wnt secretion, I began by characterizing the Rab7 phenotype. I overexpressed on the one hand the WT, DN and CA forms of Rab7 tagged with YFP, and on the other, I induced the knockdown of Rab7 by using RNAi under the control of the hh-Gal4 driver, which is active in the posterior but not the anterior half of the wing imaginal disc. I performed immunohistochemistry staining on these wing discs using a Wg antibody to visualize the Wg pattern.

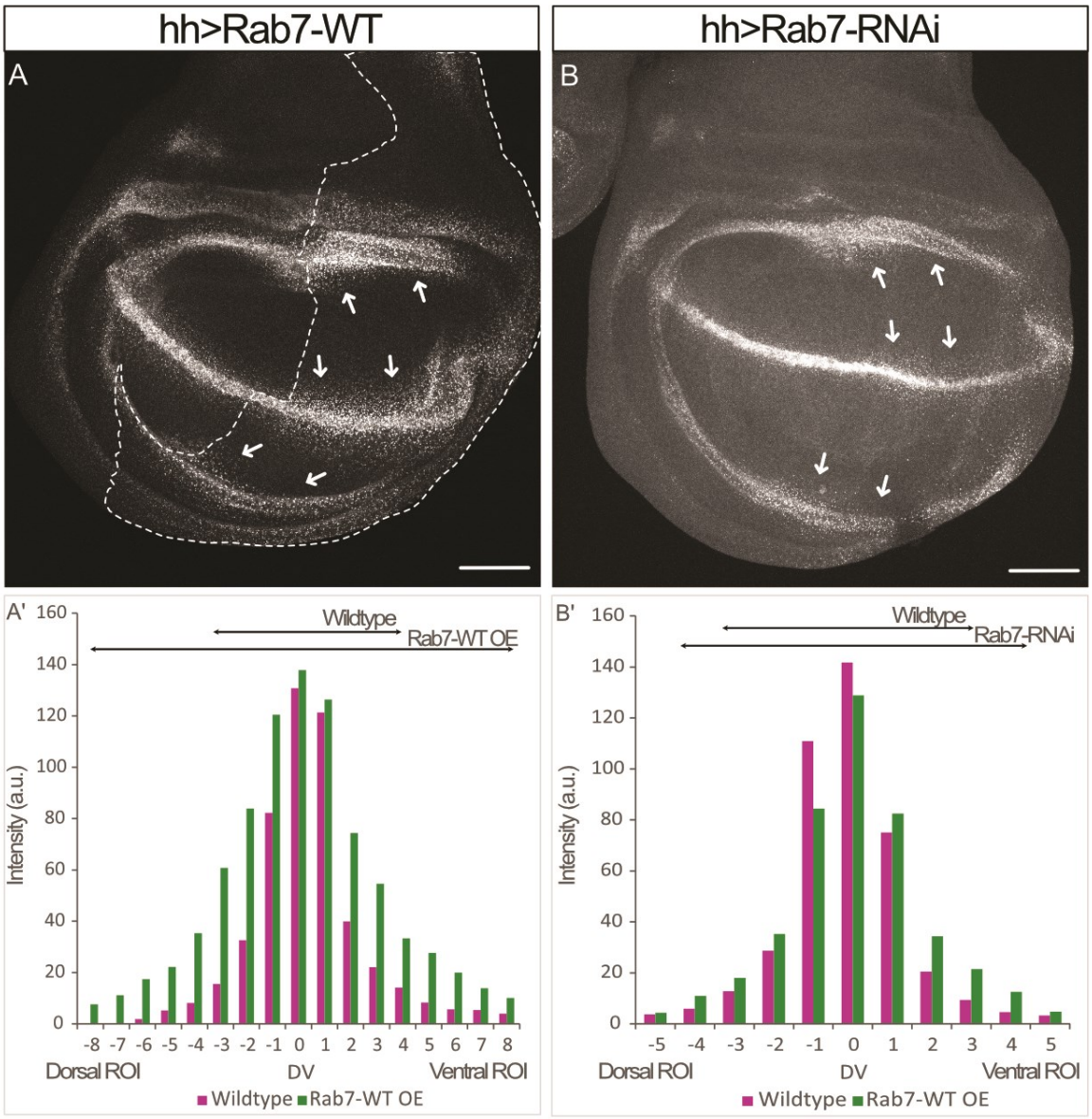

Figure 32: Rab7-WT overexpression and Rab7 knockdown by RNAi cause more Wg accumulation in the cells close to the dorsoventral boundary

Upper panel: Representative images of wing discs with Rab7-WT overexpression (A) or Rab7 KD by RNAi (B) under the control of hh-Gal4 driver, with Wg visualization using immunofluorescence staining. Maximum intensity projection; scale bar = 50μm.

Lower panel: Wing discs were quantified (A', B') by marking adjacent one-cell-wide regions of interest (ROI) dorsally and ventrally from the DV boundary and plotting the signal intensity mean after background subtraction.

Rab7-WT overexpression in the posterior wing disc compartment induced a higher number of Wg-positive puncta at a further distance from the Wg-secreting cells than in the wildtype anterior wing disc compartment (Figure 32A). Rab7 knockdown was phenotypically similar, though weaker, compared to the Rab7-WT overexpression (Figure 32B). However, overexpression of Rab7-DN and Rab7-CA did not phenocopy the phenotypes of Rab7 RNAi and Rab7-WT respectively (Supplemental Figure S7).

In order to determine the distance of the Wg spread away from the dorsoventral boundary, I quantified the phenotype of Rab7-WT overexpression and Rab7 knockdown (Figure 32A'-B'). I marked adjacent one-cell-wide regions of interest (ROI) dorsally and ventrally of the dorsoventral boundary (position 0) in either the perturbed posterior half of the wing discs or the unperturbed anterior half of the wing disc serving as 'wildtype' control. After measuring the signal intensity mean in each ROI, I subtracted the background value measured in the pouch region of the wing disc away from the dorsoventral boundary and plotted the results (Figure 32A' and 32B'). The secreting cells, with high signal intensity due to their synthesized but not yet secreted Wg, extend one cell-width away from the central dorsoventral boundary area of interest (positions 1 dorsally and ventrally). Beyond this region, the Wg staining represents secreted Wg or Wg internalized by the receiving cells, and the signal intensity drops to significantly lower levels. Upon Rab7-WT overexpression, high Wg signal intensity extended on average eight cell widths away from the dorsoventral boundary in each direction, whereas upon Rab7 knockdown, the spread was smaller but still between two and four cell widths away in either direction. Additionally, in both cases, the intensity of the Wg staining was higher in the posterior half of the disc than the anterior, control one, confirming that Rab7 perturbation induces the accumulation of Wg.

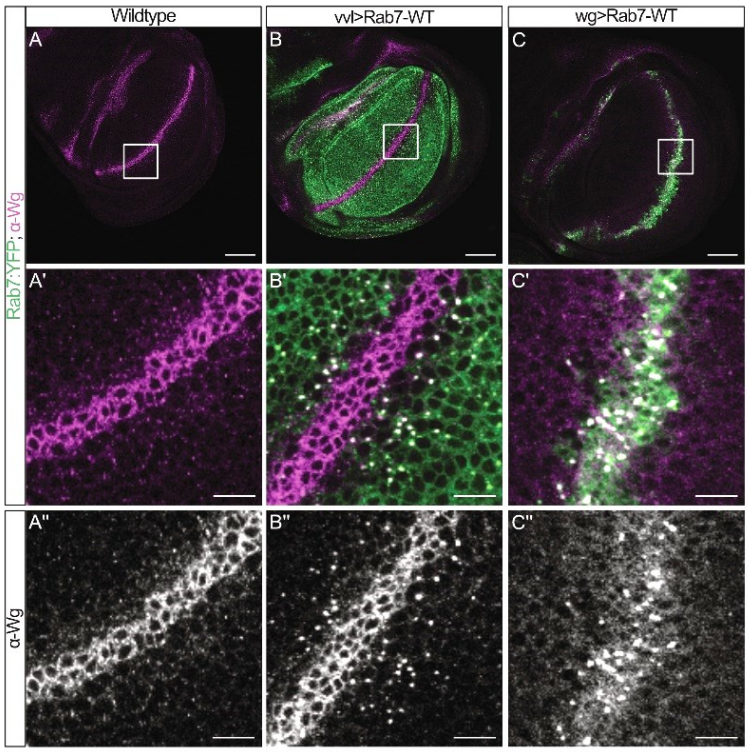

Figure 33: Rab7-WT expression in both secreting and receiving cells induces Wg accumulation in large Rab7-positive puncta

A-C Representative image of Wg antibody staining of wing discs expressing Rab7-WT under the control of vvl-Gal4 (receiving cells, B) and wg-Gal4 (secreting cells, C). Wg accumulates in larger puncta (B'', C'') than in wildtype wing discs (A). Scale bar (A, B, C) = 50 µm; Scale bar (A'',B', B'',C', C'') = 10 µm

The cause of this could be either an increase in Wg secretion or the retention of Wg within receiving cells upon ligand-receptor complex internalization. In order to determine which of these two possibilities causes the phenotype, I overexpressed Rab7-WT using Gal4 drivers that are specific for either Wg-secreting (wg-Gal4) or Wg-receiving (vvl-Gal4) cells. I found that in both cases Wg accumulated in punctate structures in the cells expressing Rab7-WT, accompanied by extremely strong colocalization of Wg and Rab7 (Figure 33A-C). This indicates that Rab7 plays a role in both the secretion of Wg and in downstream Wg signaling and ligand degradation.

The next question I asked was whether Rab7 overexpression changes the intracellular localization of Wg. To answer this, I observed the apical and basal sides of wing discs overexpressing Rab7-WT under the control of the hh-Gal4 driver for Wg staining. As can be seen from the maximum intensity projections of five 1um thickness slices from the apical and the basal side of the disc (Figure 34D-E), while the accumulation of Wg-positive puncta is increased on the apical side primarily in the Wg receiving cells, there is a significant accumulation of Wg-positive puncta in the secreting cells on the basal side of the disc. This indicates that Rab7-WT overexpression causes translocation of Wg within the secreting cells from apical to the basal side of the polarized wing disc epithelial cells.

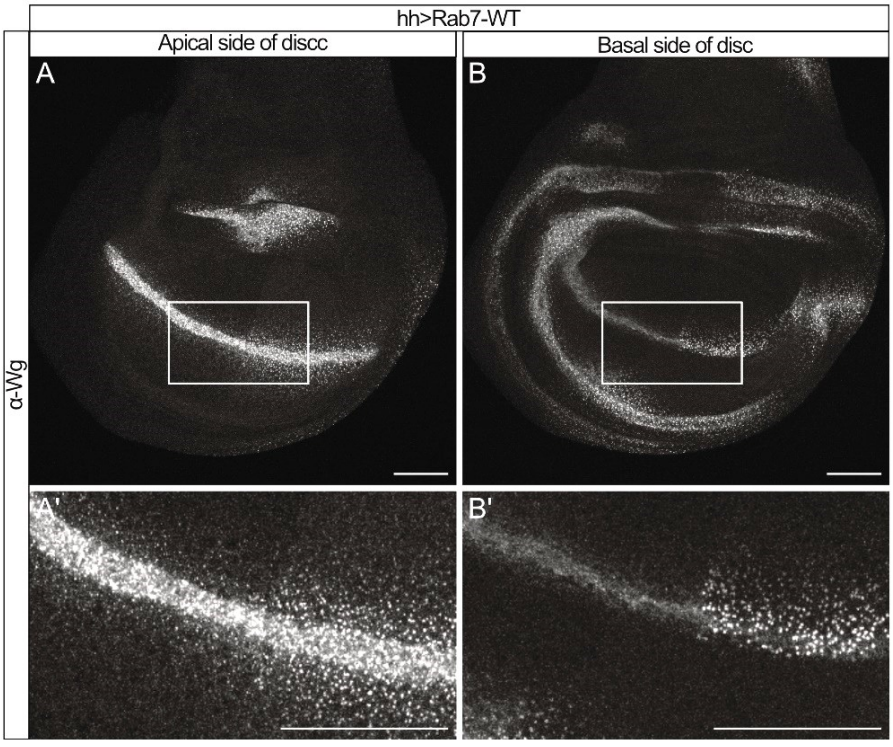

Figure 34: Rab7-WT over-expression caused a strong accumulation in Wg puncta on the basal side of the discs

A-B Representative image of Wg antibody staining of wing disc expressing Rab7-WT under the control of hh-Gal4; more Wg puncta accumulate on the basal side (E) than on the apical side (D) of the disc. Maximum intensity projections of five 1um thickness slices. Scale bar = 50 µm.

My data showed that overexpression of wildtype Rab7 or its knockdown by RNAi affects the intracellular localization of Wg within secreting as well as receiving cells by accumulating Wg in Rab7-positive puncta on the basal side of the wing disc. In addition, these perturbations result in more Wg-positive puncta at a further distance from the dorsoventral boundary than in wildtype cells, likely by retention in Wg-receiving cells upon internalization of the ligand.

3.3.3 LAMA system reveals the temporal dynamics of Wg distribution phenotype of Rab7 overexpression

One of the questions that emerged during the characterization of the effect of Rab7 perturbation on Wnt secretion was how quickly Wg phenotype is induced. This presented an excellent opportunity to implement the LAMA system I previously optimized. Thus, I co-expressed the Mito-LAMA-hook together with the RUSH-Rab7, which is the wildtype form of Rab7 and thus induces the same phenotype as the YFP-Rab7 construct. I immunostained for Wg before incubation (no release), as well as 15, 30 and 60 min after incubation with the molecule TMP (release), as well as visualized the Mito-hook using its SNAP tag.

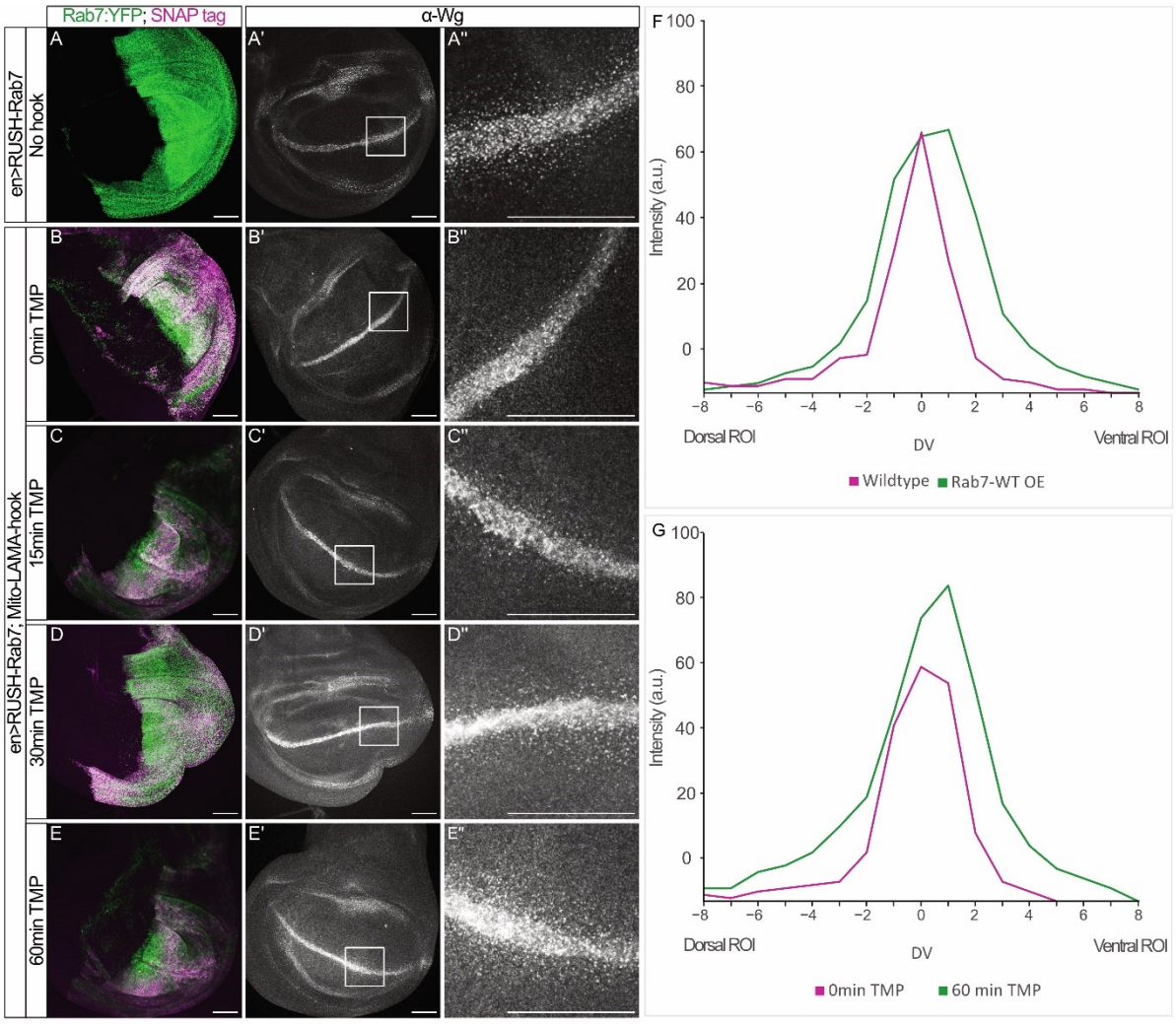

Figure 35: Trapping RUSH-Rab7 with the Mito-LAMA-hook almost fully rescues the Wg phenotype, which begins reconstituting within 30 minutes of TMP incubation

A-E Representative images of α-Wg staining of wing discs expressing RUSH-Rab7 under the control of the en-Gal4 driver, either alone (A) as positive phenotype control, or with co-expression of the Mito-LAMA-hook without release (B) or after 15 (C), 30 (D) or 60 min (E) of release with 100mM TMP. Scale bar = 50µm.

F-G Quantification of the Wg signal for unperturbed (wildtype) and Rab7-WT expressing wing disc compartments in the wing disc not expressing the Mito-LAMA-hook as positive phenotype control (F) and for LAMA expressing wing disc compartments of discs before (0min release) and 60 min after TMP incubation (G). Wing discs were quantified by marking adjacent one-cell-wide regions of interest (ROI) dorsally and ventrally from the DV boundary and plotting the signal intensity mean after background subtraction.

As positive control, I used the wing discs expressing only RUSH-Rab7 under the en-Gal4 driver (Figure 35A). In wing discs expressing the LAMA system with RUSH-Rab7 and the Mito-LAMA-hook which were not incubated with TMP, Wg staining showed almost no accumulation of puncta in either Wg-secreting or Wg-receiving cells neighboring the dorsoventral boundary (0 min TMP; Figure 35B). After 15 minutes of TMP incubation, the Mito-hook showed signs of release similar to those observed in live imaging experiments of the LAMA system (Figure 25B), with only mild accumulation of Wg puncta in the Wg-receiving cells closest to the DV boundary (Figure 35C). By 30 minutes of TMP incubation, Wg was noticeably accumulating in Wg-secreting cells further away from the DV boundary (Figure 35D). After 60 min of TMP incubation, Wg puncta were present in Wg-receiving cells at a distance of several cells away from the DV boundary and in amounts similar to those of Rab7-WT overexpression (Figure 35E). I quantified the phenotype in the same way as previously for the Rab7 phenotype characterization, using the unperturbed anterior compartment of the wing disc overexpressing Rab7 without the Mito-hook as the 'wildtype' (Figure 35F, Supplemental Figure S8). I additionally observed some variability with respect to the strength of the Wg accumulation phenotype between biological replicates, though the appearance of Wg accumulation was always present by 60 minutes of TMP incubation.

The results showed that the changes which Rab7 perturbation induces on Wg localization are fast-acting, as Wg accumulation occurred within 30 to 60 minutes of TMP addition. The experiment thus demonstrated that the LAMA system can be used to study the effects of short-term, rapid induction of overexpression by trapping the overexpressed Rab7 on the Mito-LAMA-hook and acutely releasing it using TMP. Lastly, it revealed that the LAMA system can be used to study the speed of phenotype induction of such a perturbation.

3.3.4 Rab7 perturbation does not affect Wnt pathway targeting in Wg-receiving cells

In previous experiments, I showed that the overexpression of wildtype Rab7 induced the accumulation of Wg within both secreting and receiving cells, as well as translocation of Wg from apical to the basal side of the wing imaginal disc. The next question I asked was how this change affects Wg localization and distribution, and the downstream signaling pathway of Wg.

In order to answer this question, I performed immunofluorescent staining on wing discs expressing Rab7-WT under the hh-Gal4 promoter for the protein Senseless (Sens), which is a high-threshold downstream target gene of Wnt signaling. Sens is responsible for the formation of hair bristles on the edges of the wings [Jafar-Nejad et al., 2006]. I additionally crossed into these flies the endogenously tagged Distalless:Tomato (Dll:Tomato) and Frizzled3-RFP (Fz3-RFP), a fly line expressing RFP under the regulatory sequence of the *fz3* gene, in order to observe potential pattern changes for these proteins. Fz3 and Dll are both downstream target genes of Wnt signaling, though requiring lower thresholds of Wg than Senseless [Neumann & Cohen, 1997; Sivasankaran et al., 2000].

Overexpression of Rab7-WT in the posterior wing disc compartment did not affect the expression of Sens, Fz3-RFP or Dll:Tom (Figure 36A-C). This result indicated that downstream Wnt signaling pathway was not affected by the changes in Wg localization and distribution in the wing imaginal disc cells.

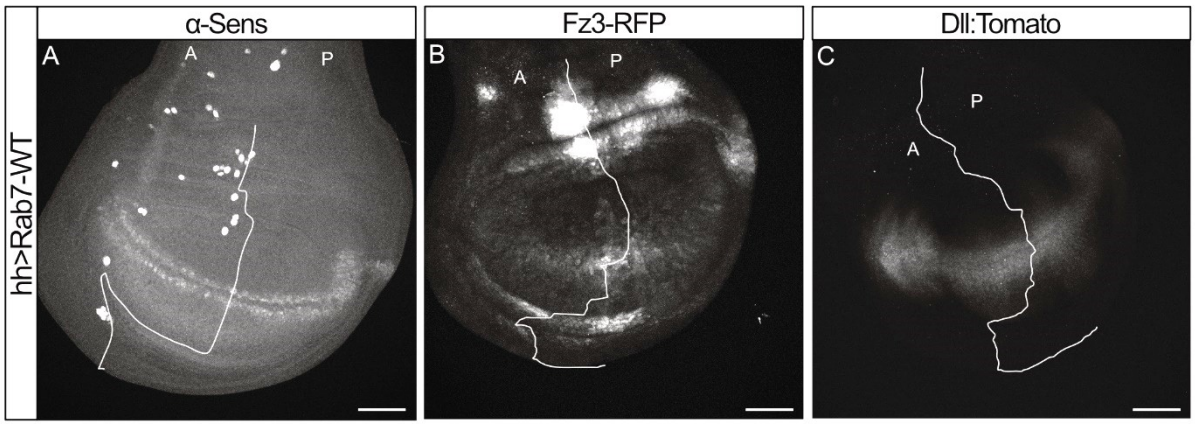

Figure 36: Overexpression of Rab7-WT does not affect the expression of downstream Wnt signaling targets Sens, Fz3 and Dll

A-C *Representative images showing expression of Wnt pathway target genes Senseless (Sens, A), Frizzled3 (Fz3, B) and Distalless (Dll, C) in wing discs expressing Rab7-WT in the P compartment under control of the hh-Gal4 driver.*
Scale bar=50 µm.

Wing imaginal discs in fly larvae give rise to adult fly wings and thorax in the process of metamorphosis during pupal stage. I studied the wings of flies overexpressing Rab7-WT in wing imaginal discs to determine if Wg accumulation affected this process. I overexpressed Rab7-WT or RUSH-Rab7 under the control of nubbin-Gal4 (nub-Gal4) driver, as well as the RNAi for Rab7 to induce Rab7 knockdown. nub-Gal4 driver expresses in the wing pouch section of the wing imaginal disc, which gives rise to the adult wings during the metamorphosis in the pupal stage.

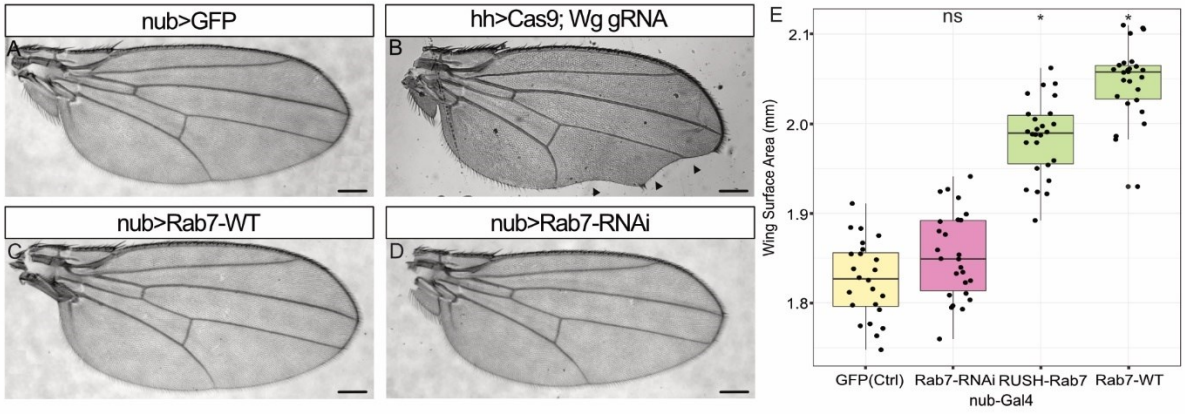

Figure 37: Overexpression of Rab7-WT does not affect the shape of adult wings, though it does have an effect on wing size

A-D *Representative images showing wings of adult flies expressing GFP as negative control (A), Rab7-WT (C) and Rab7-RNAi (D) under the nub-Gal4 driver. Positive control by Wg knockdown using CRISPR/Cas9 under control of hh-Gal4 driver (B) shown for comparison. Scale bar = 0.2mm.*

E *Surface area measurement of the wings of adult flies expressing either GFP as control, Rab7-RNAi or two different Rab7-WT constructs under the nub-Gal4 promoter. Horizontal line of boxplot is the median. n=24 to 28 wings; ns=not significant; * = p<0.05; ordinary one-way ANOVA with pair-wise comparison.*

I could not observe any aberrant wing shape or wing bristle phenotypes in the wings of flies, neither by overexpressing Rab7-WT nor by RNAi-mediated knockdown of Rab7 (Figure 37C-D) in comparison to the control flies overexpressing GFP (Figure 37A). Wg knockout using CRISPR/Cas9 under the control of hh-Gal4 is shown as positive control. As expected, these wings have notches, a typical phenotype of Wnt signaling disruption (Figure 37B).

Further, I compared the surface area of the wings, as the Wnt pathway has been shown to regulate wing size in addition to the proper formation of the wing margin [Parker & Struhl, 2020]. While the Rab7 knockdown did not affect the wing size, overexpression of both the Rab7-WT and the RUSH-Rab7 resulted in statistically significant enlargement of wings compared to the wings expressing GFP, which I used as wildtype control (Figure 37E). This enlargement may be caused by Wg accumulation in the cells; however, as Rab7 plays a central role in the endosomal pathway, the effect its overexpression has on wing size is also likely to be caused by the disruption of other processes in the tissue.

It is therefore not possible to directly connect the wing size phenotype to Wg accumulation caused by Rab7 overexpression. This, combined with the lack of downstream signaling phenotypes including both any changes in target gene expression and wing notch or bristle phenotypes, strongly indicated that the perturbation-induced change in Wg localization and distribution did not affect downstream Wnt signaling in Wg-receiving cells.

3.3.5 Rab7 perturbation does not affect Wg secretion from Wg-secreting cells

As Rab7 perturbation did not affect Wnt pathway target gene expression, my next question was whether Wg secretion itself was undisturbed upon Rab7 overexpression. I therefore performed surface antibody staining for Wg on wing discs overexpressing Rab7-WT under the hh-Gal4 driver in order to determine if the changes in Wg localization within secreting cells impacted how much and on which side of the wing disc Wg is being secreted.

The pattern of secreted Wg on the surface of wing disc cells did not change upon Rab7-WT overexpression, neither with regards to the total amounts of Wg (Figure 38A) nor to the localization on the apical and basal sides of the wing discs (Figure 38B-C). To confirm, I quantified the wing discs by plotting the profiles of the Wg staining in the central pouch region over the dorsoventral boundary equidistant from the anteroposterior boundary (yellow rectangles in Figure 38A-C; plot profiles 38A'-C') and normalizing the obtained intensity measurements to the plot average.

The surface staining data of the wing discs show that the Rab7-perturbed cells still secreted the correct amount of Wg protein from both apical and basal side of the disc in spite of the basal accumulation of Wg within the cells. This indicates that while Rab7 plays a role in the Wnt pathway by affecting the accumulation and localization of Wg within secreting cells, the effect does not disrupt their ability to secrete Wg protein.

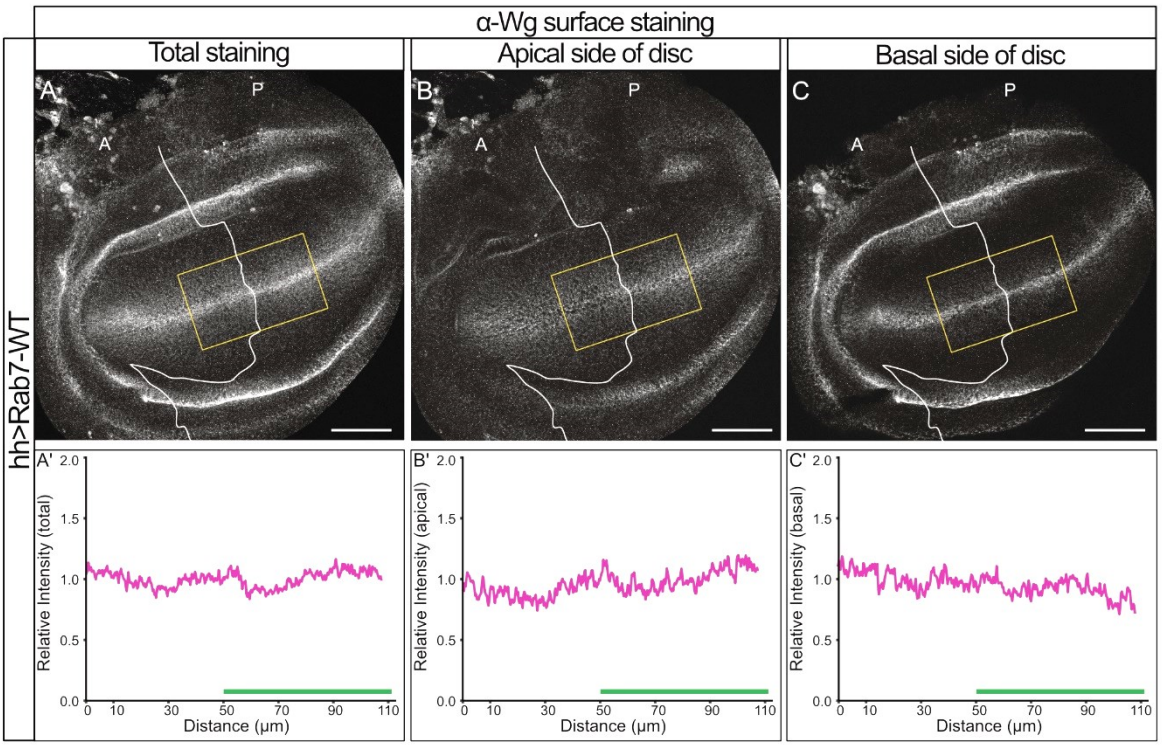

Figure 38: Overexpression of Rab7-WT does not affect Wg secretion at the dorsoventral boundary

Upper panels: Representative images showing surface staining with Wg antibody of a wing disc expressing Rab7-WT under hh-Gal4 promoter. Maximum intensity projections of the whole disc (A), ten 1µm thickness slices on the apical (B) and basal side (C) of the disc. Scale bar=50µm.

Lower panels: Wg staining was quantified by calculating the plot profiles for total (A'), apical (B') and basal (C') images within the yellow rectangles and normalizing to the average value of each profile.

3.3.6 Wg accumulates upon Rab7 perturbation in lysosomes

Wg strongly colocalizes with Rab7 upon overexpression of Rab7-WT (Figure 33B' and 33C'). Rab7 was detected on a variety of vesicles and organelles, including maturing endosomes, where it is required for early-to-late endosome transition; late endosomes/multivesicular bodies; lysosomes; and autolysosomes [Chavrier et al., 1990; Bucci et al., 2000; Lőrincz et al., 2017]. This points towards the accumulation of Wg in the downstream part of the endocytic pathway upon Rab7 overexpression; however, it left the question of which Rab7-positive organelle precisely is the place where Wg accumulates. I therefore performed colocalization studies of Wg and overexpressed Rab7-WT with markers for the endosomal pathway organelles to determine at which stage of the endocytic pathway does Wg accumulate.

Rab7 is required for the maturation of endosomes from their early to late stages [Langemeyer et al., 2020]. To determine if Wg is accumulating in early and maturing endosomes upon Rab7 overexpression, I stained the wing discs overexpressing Rab7-WT in the posterior wing disc compartment under the hh-Gal4 driver, in addition to the Wg antibody, also with the Rab5 antibody, as this is the primary early endosomal marker [Bucci et al., 1992]. I found no change in colocalization between Wg and Rab5 in these wing discs (Supplemental Figure S9) and concluded that Wg trafficking through the endosomal pathway of either Wg-secreting or Wg-receiving cells is not affected at the stage of early endosomes.

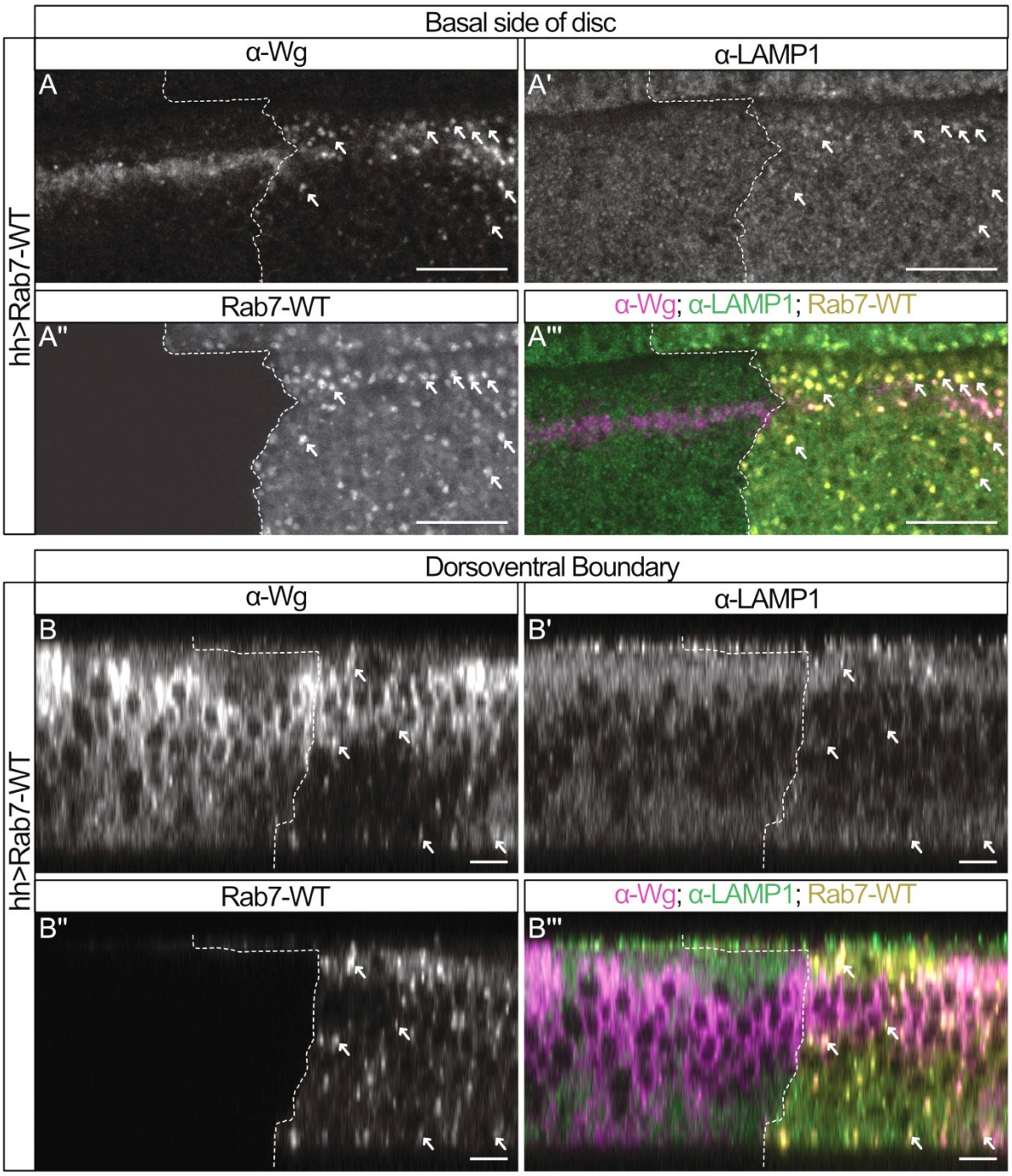

Figure 39: Colocalization of Wg and LAMP1 with Rab7 overexpressed in wing imaginal disc cells

A Representative image of the basal side of the dorsoventral boundary of wing discs expressing Rab7-WT under control of hh-Gal4 driver, stained with Wg and LAMP1 antibodies.

B Representative image of the lateral view through the Wg-secreting dorsoventral boundary cells of wing discs expressing Rab7-WT under control of hh-Gal4 driver, stained with Wg and LAMP1 antibodies.

White arrows indicate the colocalization of Rab7, LAMP1 and Wg; individual slices shown; scale bar=10 µm.

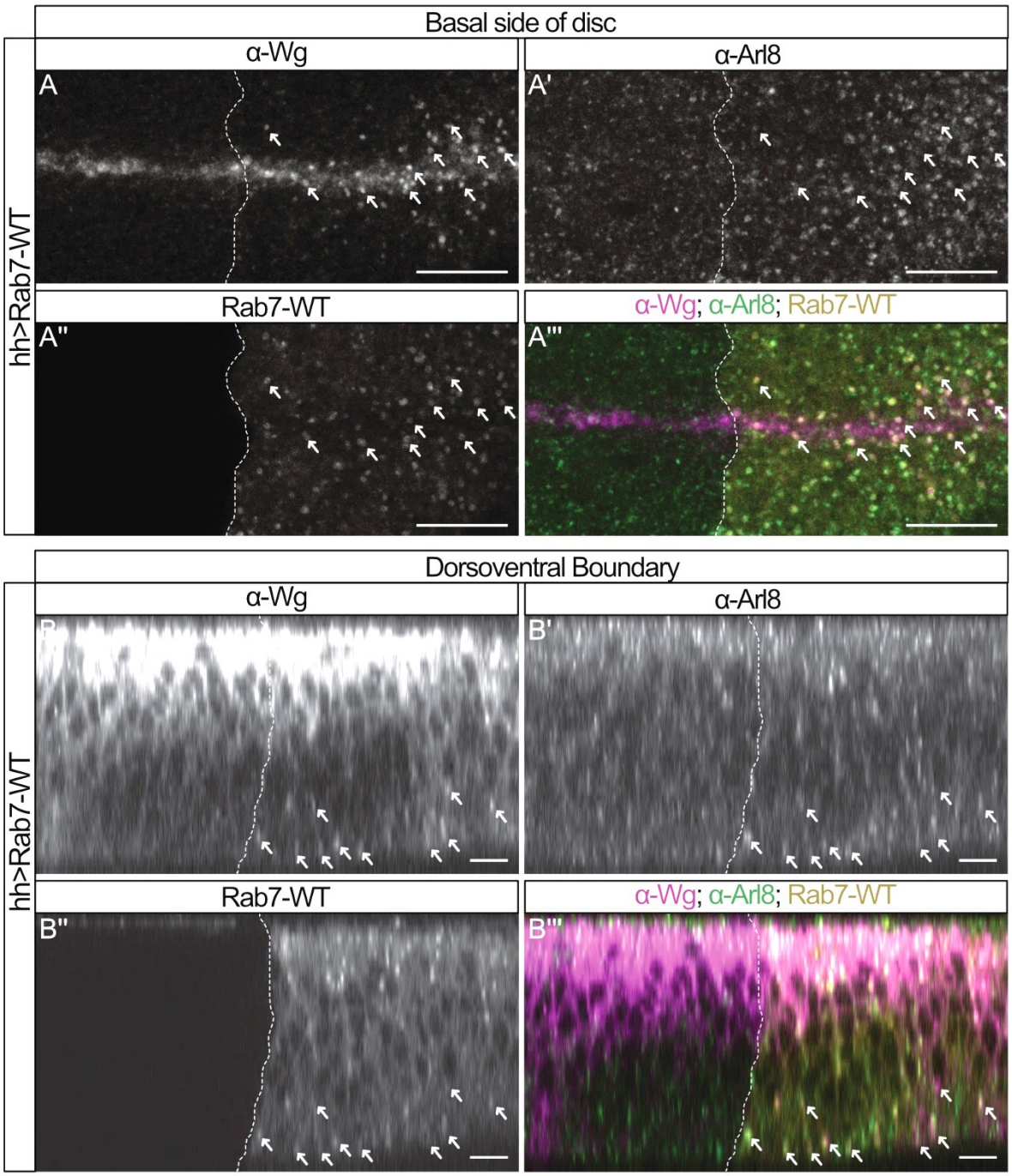

Figure 40: Colocalization of Wg and Arl8 with Rab7 overexpressed in wing imaginal disc cells

A Representative image of the basal side of the dorsoventral boundary of wing discs expressing Rab7-WT under control of hh-Gal4 driver, stained with Wg and Arl8 antibodies.

B Representative image of the lateral view through the Wg-secreting dorsoventral boundary cells of wing discs expressing Rab7-WT under control of hh-Gal4 driver, stained with Wg and Arl8 antibodies.

White arrows indicate the colocalization of Rab7, Arl8 and Wg; individual slices shown; scale bar=10 µm.

Lysosomes are the primary organelles of the cellular degradative pathway and Rab7 facilitates the fusion of late endosomes, which carry the cargo designated for degradation, with the lysosomes [Vanlandingham & Ceresa, 2009]. Thus, to determine if Wg is directed to the lysosomes upon Rab7 overexpression, I stained the wing discs overexpressing Rab7-WT under the hh-Gal4 driver with the Wg antibody and either the LAMP1 antibody or the Arl8 antibody. LAMP1 (lysosomal-associated membrane protein 1) is the primary marker for late endosomes and lysosomes in the cell [Eskelinen et al., 2003], while Arl8 is found on the lysosomes and through the recruitment of the HOPS complex plays a role in their fusion with late endosomes and autophagosomes [Khatter et al., 2015].

Many Wg staining puncta found on the basal side of the Wg-receiving cells colocalized with both overexpressed Rab7 and LAMP1 staining in the affected wing disc compartment (Figure 39A), though some colocalization was also present within the Wg-secreting cells (Figure 39B) as well. Furthermore, I observed mild LAMP1 upregulation in the posterior wing disc compartment where Rab7-WT was overexpressed (Figure 39A' and 39B'). However, not all of the Rab7 fluorescence colocalized with the LAMP1 staining.

The results of Arl8 staining were similar to those of LAMP1 upon Rab7 overexpression. Wg puncta colocalized together with the overexpressed Rab7 and Arl8 staining primarily on the basal side of both Wg-secreting and Wg-receiving cells (Figure 40A-B). This colocalization was more pronounced than the colocalization between Wg, Rab7 and LAMP1. Moreover, Arl8 was noticeably upregulated upon Rab7-WT overexpression (Figure 40A') in the posterior wing disc compartment.

These colocalization studies therefore indicate that overexpression of Rab7 induces the upregulation of lysosome-associated proteins, and that Wg previously found to strongly colocalize with Rab7 (Figure 33) and accumulate on the basal side of the wing disc (Figure 34) also colocalizes with LAMP1 and Arl8 in both Wg-secreting and Wg-receiving cells.

Rab7 has been connected to the formation of autolysosomes through the fusion of lysosomes and autophagosomes [Lőrincz et al., 2017]. I therefore also studied the colocalization of Wg and Rab7 with the autophagosome marker Atg8 [Lee & Lee, 2016] in wing discs overexpressing Rab7-WT under the hh-Gal4 driver. I observed no colocalization of Wg, Rab7 and Atg8 in either the Rab7-overexpressing posterior wing disc compartment, or the unperturbed anterior compartment (Supplemental Figure S10). This indicates that Wg is not found in autophagosomes upon Rab7 overexpression.

As Wg colocalized with Arl8, has been shown to be a general positive regulator of lysosomal fusion events in *Drosophila* [Boda et al., 2019], I wondered what would happen to Wg accumulation if I downregulated Arl8, thereby preventing lysosomal fusion. I knocked down Arl8 by using RNAi in combination with Rab7-WT overexpression in order to determine whether it facilitates the translocation of Wg to the basal side of the disc. I used the wg-Gal4 driver to limit the overexpression to Wg-secreting cells only, as I wanted to exclude any effects

on Wg-receiving cells, and visualized Wg using immunofluorescence staining. In addition, I also knocked down EEA1, the primary early endosomal marker, in combination with Rab7-WT. Since Rab7-positive late endosomes mature from EEA-positive early endosomes, blocking the formation of early endosomes should therefore block the transfer of Wg to the late endosomes and lysosomes regardless of Rab7 overexpression and serve as a positive control.

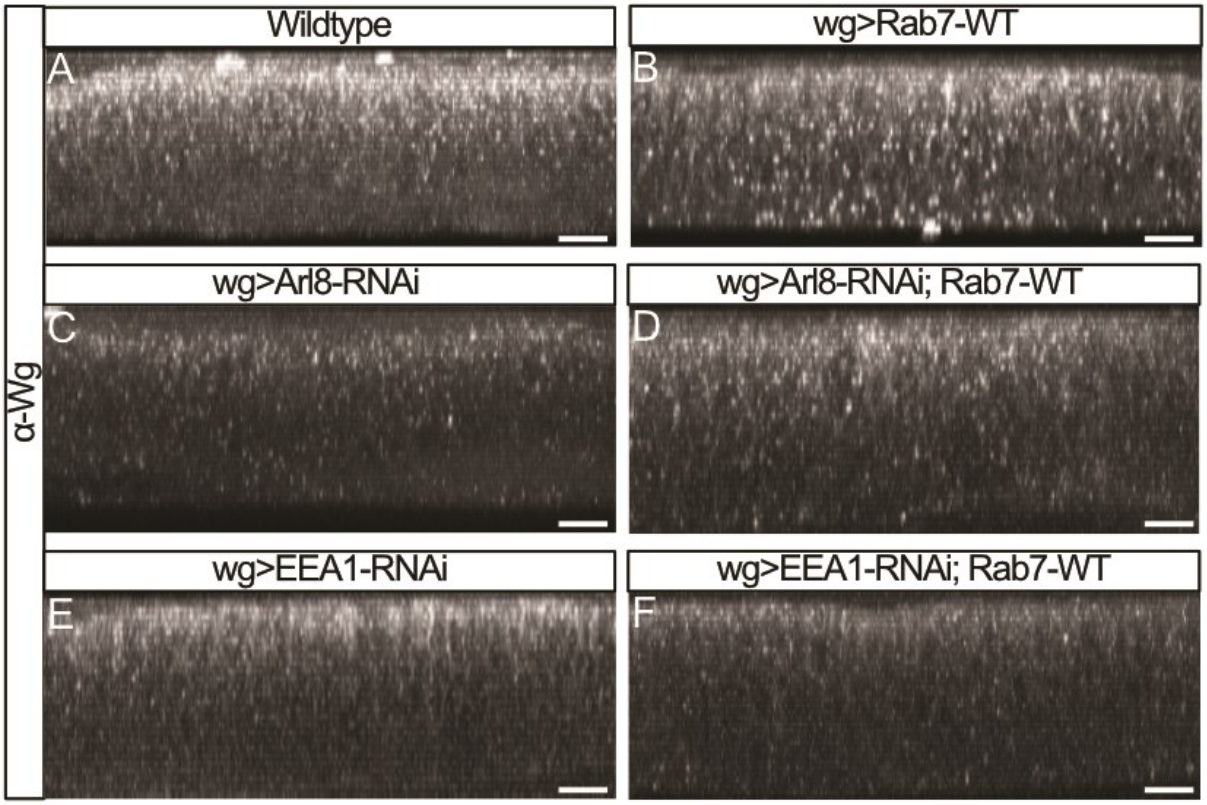

Figure 41: Knockdown of Arl8 in wing discs expressing Rab7-WT in Wg-secreting cells ameliorates the Wg basal translocation phenotype
A-B Lateral maximum intensity projections of Wg antibody staining through the Wg-secreting cells of wing imaginal discs with protein perturbations. (A) Wildtype control. (B) Rab7-WT overexpression.
C-D Knockdown of EEA1, alone (C) or with concurrent overexpression of Rab7-WT (D).
E-F Knockdown of Arl8, alone (E) or with concurrent overexpression of Rab7-WT (F).
Scale bar=10µm.

Overexpression of Rab7-WT in Wg-secreting cells resulted in the accumulation of Wg at the basal side of the wing disc, in contrast to wildtype wing discs (Figure 41A-B). In addition, as expected, knocking down EEA1 inhibited the Rab7-WT induced translocation of Wg to the basal side of the wing disc cells (Figure 41E-F). The knockdown of Arl8 together with Rab7-WT overexpression partially rescued Wg translocation by reducing the accumulation of Wg at the basal side of the wing disc, though not to the extent of EEA1 knockdown (Figure 41C-D). This indicates that Arl8 plays a role in the accumulation of Wg in lysosomes on the basal wing disc side. In addition, LAMP1 was upregulated in these wing discs, especially on the apical side of the discs, and LAMP1 staining strongly colocalized with YFP-Rab7-WT fluorescence (Supplemental Figure S11).

The results therefore show that upon Rab7-WT overexpression, Wg is translocated in significant amounts to the basally located Rab7-positive compartments, and that a significant fraction of these compartments are Arl8- and LAMP1-positive lysosomes. Furthermore, knockdown of Arl8 partially rescues the phenotype by reducing the size and number of accumulating Wg puncta.

Altogether, my data show that non-ubiquitous Rab GTPases aren't required for Wg secretion in the wing imaginal disc, and that overexpression of Rab7 induces the accumulation of Wg in the lysosomes of secreting and receiving cells and the translocation to the basal side of the cells. The accumulation nonetheless does not affect Wg secretion or downstream signaling. The accumulation is in Wg-secreting cells partially rescued by the blocking of late endosome/lysosome fusion through the knockdown of Arl8.

4 Discussion

4.1 Endogenous protein tagging of Wg and Evi

Visualization of proteins within cells is a crucial method of studying protein localization, dynamics and interactions. However, not all ways of protein visualization are suitable for live imaging and tracking of protein movement within cells and tissue. Methods such as immunohistochemistry require not just an available antibody against the protein of interest, but also fixation of the tissue. Fluorescent proteins emit light upon excitation with a specific wavelength. Their use as tags for visualization purposes has therefore been part of scientific practice for a number of decades. These proteins, however, are not small, and if placed incorrectly, their positioning within the protein sequence can disturb the functionality of the protein of interest.

The easiest positions to tag proteins are at the termini. However, these positions also commonly contain other important protein segments such as signaling sequences required for protein export to a specific compartment or for recycling back to the compartment of origin. Insertion of fluorescent proteins in these locations can thus lead to cleavage of the tag or impaired function of the protein of interest and hypomorphic phenotypes. The alternative to termini is the insertion within the protein coding sequence, which requires structural understanding of the protein of interest when choosing the insertion site. Disruption of any tertiary structures required for interaction with other protein partners or insertion of the tag within regions that are in some way shielded from the environment (such as transmembrane regions) can equally disrupt the protein function or may lead to protein degradation.

Since tagging Wg within the protein coding sequence was already previously done by Port et al. in 2014, replacing one tag with another appeared to be the logical consequence. However, as Evi had not been endogenously tagged in *Drosophila* before and the protein structure of Evi was not yet published at this timepoint, identification of suitable insertion sites required studying the sequence conservation and the putative structure available. I identified six potential sites spread evenly throughout the protein sequence, with half of them being on either side of the transmembrane protein. Out of the six sites, insertion was successful at two.

Since then, the crystal structure of human Evi was resolved by Nygaard at al. in 2021 and the Alphafold program was developed, significantly improving the protein structure prediction capability in the field. With this new information available, I reanalyzed the chosen insertion sites, the result of which are shown in Figure 8. My repeat analysis revealed that site 2 is located within the β-sheet lattice of the first luminal/extracellular loop, while sites 3 and 4 were located at the very beginning of α-helices 2 and 5. This is the most likely reason why tagging of these three sites was unsuccessful. The other possible reason could be that the chosen sgRNA sequences for the CRISPR/Cas9 system were not effective. This remains as a likely reason for why the insertion at site 6 failed. While neither of the successful sites are

found on the cytoplasmic side of the protein, the overall tagging strategy was successful, resulting in functional endogenously fluorescently tagged Evi and Wg in *Drosophila*.

Genetic manipulation and transgenic constructs are initially done heterozygously in *Drosophila* using balancer chromosomes to preserve the induced change. These are standardized chromosomes whose sequence has been rearranged in various ways with the goal of preventing recombination events during meiosis [Miller et al., 2019]. One way to experimentally achieve homozygosity for the genetic manipulation in a fly line is to exclusively cross homozygous individuals to each other. This is only possible when homozygous individuals can reach adulthood and are fertile. I successfully established a stable homozygous fly line for Wg:mScarlet and Evi:EGFP, however, this was not the case for either of the two Evi:mScarlet lines.

One of the potential problems of the CRISPR/Cas9 system are off-target mutations. In order to determine if the homozygosity issue of Evi:mScarlet fly lines was due to problems with the functionality of Evi:mScarlet or due to the use of CRISPR/Cas9 for endogenous tagging, I back-crossed both fly lines for five generations to w^{1118} flies, one of the standard control fly lines carrying only a *white* allele on the X chromosome. This allowed for homologous recombination of other parts of the third chromosome, which carries the *evi* gene, while allowing for the tracking of Evi:mScarlet by genotyping. After this back-crossing and rebalancing, I was able to establish homozygous stocks for fly lines carrying both Evi:mScarlet-1 and Evi:mScarlet-5, indicating that the problem was presumably due to off-target mutations that were lost through back-crossing, rather than the function of the tagged construct itself.

Surprisingly, endogenous tagging of Wg revealed different localization of Wg:EGFP and Wg:mScarlet fluorescence, with Wg:EGFP primarily localizing within the secreting cells with some puncta in or on the neighboring receiving cells, whereas Wg:mScarlet appeared significantly more punctate and much more present on or in the neighboring receiving cells (Figure 12). The general pattern of expression within the wing imaginal disc was as expected and similar in both fly lines. Moreover, both fly lines are homozygous and viable, indicating that whatever caused this difference, it did not interfere with the Wg signaling pathway itself. This difference in localization should be taken into account for future experiments. Two large potential sources of this observed difference can be due to Wg itself or the fluorophores – namely, Wg function could be affected by different fluorophores through, for example, changes in protein conformation or blocking of important binding sites, or fluorophore detectability might be different between these constructs.

Of the two hypotheses, the latter proved to be more likely – namely, that the detectability of fluorescent proteins differed, allowing for the visualization of Wg protein fractions that are not detectable with the other fluorophore. I came to this conclusion by examining whether mScarlet in some way affects the Wg secretion process, given that the Wg:EGFP fluorescence

localization closely matches that of immunohistochemical Wg protein visualization (Supplemental Figure S2A).

One of the validation experiments I performed on Wg:mScarlet was to test whether it correctly interacts with Evi, its cargo carrier protein required for Wg secretion [Bartscherer et al., 2006]. I did this by inducing Evi null mutant clones and observing that Wg:mScarlet accumulates in the Wg-secreting cells within the clones (Figure 11A-B). Loss of Evi blocks Wg secretion, with the natural consequence of Wg accumulation in the cells. I could therefore show that the interaction between Wg:mScarlet and Evi is not affected by the fluorophore insertion.

Unlike Wg:EGFP, Wg:mScarlet fluorescence resembled the results of antibody surface staining with the Wg antibody (Figure 13B), an immunofluorescence method used for the visualization of the secreted protein fraction [Witte et al., 2021]. This and the localization of the Wg:mScarlet fluorescence in the region of Wg-receiving cells neighboring the dorsoventral boundary indicated that the fluorescence was likely to be the secreted Wg protein. Given that not all of the Wg:mScarlet fluorescence in this region colocalized with the Wg surface staining, it is also likely that at least some of this Wg:mScarlet fluorescence is in fact internalized but not yet degraded Wnt signal-receptor complex.

For comparison purposes, I performed Wg surface staining on wing discs of flies homozygously expressing Wg:EGFP in parallel with the staining of Wg:mScarlet expressing wing discs. Interestingly, Wg:EGFP fluorescence mostly does not colocalize with the antibody Wg staining in the region of Wg-receiving cells neighboring the dorsoventral boundary (Figure 13A). Given that no wildtype Wg is present within the tissue, there is a strong possibility that Wg:EGFP is present but not detectable on the Wg-receiving cells, which also argues against the hypothesis that Wg:EGFP is far less secreted than Wg:mScarlet.

This assumption is strengthened by the results obtained by methanol fixation of Wg:mScarlet. Methanol, unlike formaldehyde, does not crosslink proteins, but rather leads to the precipitation of proteins by dehydrating the cells. As this causes degradation and loss of membrane lipids, it also results in the loss of extracellular proteins which would otherwise be crosslinked to the lipids and preserved with formaldehyde fixation. When the extracellular Wg:mScarlet fluorescence was removed through methanol fixation, the intracellular Wg:mScarlet fluorescence became more prominent. Indeed, when I oversaturated the fluorescence intensity during confocal imaging of Wg:mScarlet expressing tissue, I could see previously undetected mScarlet fluorescence within secreting cells (data not shown). All of this points towards the hypothesis that Wg:mScarlet fluorescence is more easily detected outside of the cells than inside, causing the false impression of more protein being secreted from the cells.

To verify that EGFP and mScarlet do not affect Wg secretion, I analyzed the Wg protein levels found on the surface of the wing imaginal disc cells. For this purpose, I performed the surface

protein biotinylation assay, which allowed me to biotinylate only the Wg protein population exposed to the extracellular space. I could then perform a pulldown and separate this population in order to analyze it by Western blotting. In two independent experiments comparing wildtype Wg, Wg:EGFP and Wg:mScarlet, the amount of extracellular Wg:EGFP that was pulled down was similar to the amount of extracellular Wg:mScarlet (Figure 14). This further confirmed the conclusion that the fluorescent proteins do not change Wg secretion levels.

Excluding the hypothesis that mScarlet affects Wg secretion left the other possible reason for the difference in localization, which was that the two fluorescent proteins are not equally detectable by confocal imaging at all stages of the Wg secretory process. This suggests that different fluorescent proteins could be used for the visualization of particular fractions of the protein of interest that may otherwise be overlooked if the protein visualization is performed using only one fluorophore. However, it also suggests that caution must be taken during fluorophore selection, as well.

Though this is beyond the scope of the thesis, the logical follow-up question is which properties of the fluorescent proteins lead to this visualization difference. Fluorescent proteins require time for chromophore maturation, as well as a specific acidity of their environment for fluorescence (denoted by their pKa value). They have unique brightness, fluorescence lifetime and protein stability, as well as higher or lower tendency towards oligomerization. Red fluorescent proteins have also been noted to be quite stable against lysosomal proteases and low pH values of their environment, resulting in puncta accumulation in the cells [Katayama et al., 2008].

mScarlet is a protein whose sequence was developed synthetically rather than from an existing fluorophore [Bindels et al., 2017], with the intention to avoid oligomerization common for other red fluorophores such as Cherry or DsRed. It has several advantages over EGFP in most statistics, like longer fluorescence lifetime (3.9ns vs 2.6ns of EGFP), stronger brightness (70 vs 33.54 of EGFP) and higher quantum yield (0.7 vs 0.6 of EGFP) [Patterson et al., 1997]. However, it requires significantly longer time for maturation (174min vs 25min for EGFP).

It is also more stable at lower pH values than EGFP, having a pKa value – the pH value at which a fluorophore's brightness is decreased by half – of 5.4, compared to the 6 pKa value of EGFP. Different organelles within eukaryotic cells have different pH environments. Within the secretory pathway, the pH value ranges from 7.2 in the endoplasmic reticulum to 5.7 in the secretory vesicles [Paroutis et al., 2004]. Wg passes through this pathway and, if secreted on exosomes, also gets internalized into multivesicular bodies after reaching the cell membrane, where the pH value is 5.5. This might be one of the reasons for the observed difference of fluorescence between Wg:EGFP and Wg:mScarlet. In addition, it might also explain any visible

Wg:mScarlet that has been internalized by the receiving cells for degradation, since the lysosome pH value is 4.5.

Although Evi is a transmembrane protein, both successful tagging locations were located within the ER lumen. Indeed, Evi:EGFP-5 and Evi:mScarlet-5 show a similar visualization discrepancy as could be observed with the tagged Wg. Evi:EGFP signal is significantly less detectable at the very center of the dorsoventral boundary than Evi:mScarlet (Supplemental Figure S3B). The additional observed difference in fluorescence levels between the Wg-secreting and Wg-receiving cells in Evi:mScarlet expressing tissue (Supplemental Figure S3A) is explainable by the very slow maturation time of mScarlet and the relatively fast degradation rate of Evi when not stabilized by the presence of Wnts, with the much faster maturing EGFP providing a contrast to this visualization effect.

As the endogenous tagging with EGFP and mScarlet did not negatively affect the function of either Wg or Evi protein, I was confident in proceeding to test them in a live imaging setup and to optimize the experimental procedure for their use. Wing imaginal discs are one of the most studied larval organs, and thus several attempts have already been made to culture them *ex vivo*. In optimal conditions, they can survive up to 12 hours post-dissection, but this requires medium agitation for oxidation in addition to a more complex medium recipe [Strassburger et al. 2017]. If cultured in simple Schneider's or M3 medium, their function deteriorates roughly 3 hours post-dissection. As I was interested in short-term live imaging of up to 90min, I did not expect any problems with culturing wing discs for my purposes.

Sample photobleaching was a larger problem – both EGFP and mScarlet bleached within ten to fifteen minutes, especially on higher magnifications when imaged by a laser scanning confocal microscope. Switching to spinning disc confocal microscope mitigated the issue, as well as allowed for overall faster imaging. mScarlet was photobleached faster than EGFP throughout my live imaging experiments, the fluorescence becoming significantly weaker within 15 minutes of constant laser exposure (this effect can be observed in Figure 17A). Given this fact, it might be worth exchanging mScarlet for either another red fluorescent protein or a chemical tag in the future.

Though photobleaching is in general a problematic effect, it can also be beneficial in specific instances, such as for FRAP (fluorescence recovery after bleaching) analysis [reviewed in Lippincott-Schwartz et al., 2018]. Tagged Wg and Evi would therefore likely be very useful in FRAP experiments, where the goal is to study the kinetics of protein translocation into the photobleached area of the tissue from the surrounding cells, or the *de novo* protein synthesis rate within the photobleached cells.

One limitation that I encountered during the live imaging of wing imaginal discs is the very small size of epithelial cells of this organ. Wing imaginal discs contain roughly 50.000 polarized columnar cells that are extremely densely packed. Therefore, images obtained in the xy-plane, especially of Wg:EGFP that is mostly intracellular, were not very useful. Imaging

orthogonally through the tissue provides more useful data, as it would allow for imaging transcytosis of Wg within the secreting cells. Additionally, imaging the Wg expressing rings on the edges on the wing hinge, which are often angled with respect to the dorsoventral boundary cells due to the natural curvature of the tissue, was of more benefit (Figure 15A). The following particle tracking analysis indicated that the vast majority of the puncta were detected at a single z- imaging plane not longer than 3 minutes.

Imaging of Wg:mScarlet revealed that most fluorescent puncta located at the dorsoventral boundary are quite static over short periods of time (up to 5 min), and tend to move very little apically or basally (Figure 16A). In contrast, Wg:mScarlet fluorescence puncta found farther away from the dorsoventral boundary cells moved much faster in the direction away from the Wg-secreting cells, reaching the speed of up to 1 µm/sec. These are likely to be extracellular vesicles carrying secreted Wg:mScarlet proteins towards Wg-receiving cells located more distantly from the Wg-secreting cells. The experiment demonstrates the benefit of endogenously tagged Wg:mScarlet, as the extracellular Wg:EGFP fluorescence could not be detected in the levels required for the visualization of this movement.

Finally, these constructs are useful tools for colocalization analyses. For this purpose, I generated a fly line carrying both Wg:EGFP and Evi:mScarlet. As expected, the two proteins colocalize to a significant extent (Figure 17). A fraction of Wg:EGFP and Evi:mScarlet does not colocalize, which can have several explanations: Evi is internalized back into ER once Wg is secreted, thus a fraction of Evi present in the cell is not associated with any Wg protein (Evi-positive and Wg-negative puncta); a part of Wg-positive and Evi-negative puncta may be newly synthesized Wg that has not yet been loaded onto Evi in the ER; finally, the differing brightness of EGFP and mScarlet in combination with different protein concentrations may result in some puncta being detectable in one channel but not in the other.

Importantly, colocalization of Wg:EGFP and Evi:mScarlet could be detected over a period of 20 minutes in live imaging, and though individual colocalizing puncta were not detectable for longer than 1 min within one imaging plane, the overall ratio of the colocalizing puncta to non-colocalizing puncta remained the same, demonstrating a steady rate of Wg and Evi interaction. The ability to detect the colocalization of Wg:EGFP and Evi:mScarlet thus also indicates that these proteins can likely be used with other tagged proteins or organelle markers, making them beneficial for the study of both Wnt secretion and signaling.

In conclusion, Evi and Wg were successfully endogenously tagged in *Drosophila melanogaster*. My results indicate that these tagged constructs can be used for various purposes, such as live imaging and colocalization studies, which can materially contribute to the *Drosophila* scientific community. In addition, these results demonstrate the benefits of endogenously tagging proteins of interest – especially proteins targeted to the secretory or endocytic pathways – with multiple fluorophores, as this can reveal protein fractions that may be undetectable with only a single fluorescent protein.

4.2 The LAMA system

As part of this thesis, I adapted a protein trap-and-release system for use in *Drosophila* tissues. I identified two published systems working on the similar principle, the RUSH system [Boncompain et al., 2012] and the LAMA system [Farrants et al., 2020]. The RUSH system is based on the binding affinity between streptavidin and the streptavidin binding peptide (SBP), which are fused to the hook protein stably anchored into an organelle membrane and the reporter protein respectively. This binding can be disrupted by the presence of biotin, which binds with stronger affinity to streptavidin than SBP. The LAMA system functions on the similar principle; however, it uses a circularly permutated version of the bacterial protein dihydrofolate reductase (cpDHFR) fused to a GFP-specific nanobody for the hook protein, and a GFP-tag for the reporter protein. Binding of trimethoprim (TMP) and NADPH to cpDHFR induces conformational changes and release of the GFP-tag from the nanobody.

My first step was to determine which of the two systems is more applicable for use in *Drosophila* tissues. For this purpose, I expressed the systems using the same reporter protein (Rab7) with system-specific hooks in wing imaginal discs and salivary glands. While both tissues are composed of polarized epithelial cells, wing disc cells are very small and columnar, while the salivary gland cells are large, square cells with polytene chromosomes. This makes salivary gland cells much more suitable for the observation of intracellular protein dynamics than wing discs. However, wing discs are one of the most widely used organs of the *Drosophila* larval stage due to the complexity of intercellular communication and coordination required for its development and metamorphosis. Thus, establishment of one of the systems in wing discs would be of great benefit even if intracellular protein localization changes are hard to resolve in them.

My conclusion was that the LAMA system was better suited than the RUSH system for use in the fruit fly model organism. This conclusion was largely based on the leakiness of the RUSH system caused by the fly food on which the larvae were fed. The yeast component of normal fly food naturally contains biotin, which is required for optimal fly development during its earlier developmental stages [Landenberger et al., 2004]. Biotin-deficient fly food (BDF) can be made through the addition of avidin to the food, which binds to biotin and prevents it being active after ingestion. However, in addition to problems of BDF production which I encountered, such as fast spoiling and formation of air bubbles capable of displacing the food in the vial (Figure 19C), flies fed on this food lay large quantities of unfertilized or embryonically lethal eggs. Moreover, the larvae that do hatch from the eggs also suffer difficulties in further development and often die before reaching pupariation.

Glashauser and colleagues used the RUSH system in *Drosophila* as well, and also noted similar issues with system leakiness [Glashauser et al., 2023]. As they studied the release of reporters from their RUSH-hook in embryos and ovaries of adults, one of the ways they addressed the problem was by minimizing the ingestion of biotin beforehand through the use of apple juice agar plates supplanted with yeast paste made with fresh baker's yeast. This is not a viable

solution for experiments using *Drosophila* larvae, as this developmental stage requires sufficient nutrition. Indeed, the authors showed no effects of biotin incubation on wing discs, though they did express the RUSH system in this tissue as well.

The other approach to the system leakiness they employed was to increase the overexpression of the hook through the insertion of multiple copies of the hook transgene into the fly genome. They were able to demonstrate that a high ratio of hook to reporter could mitigate the problem. I observed a similar effect in flies heterozygous or homozygous for the hook transgene with both RUSH and LAMA systems in the case when the reporter protein was also an overexpression construct rather than endogenous protein. This, however, was not a feasible solution in my case due to the toxicity of the Golgi-hook.

The matter of the BDF made the LAMA system more appealing than the RUSH system in my estimation, as the LAMA system uses the antibacterial component TMP for release rather than biotin and requires no changes to the fly food on which the larvae are fed. The second large advantage that the LAMA system has over the RUSH system is the tag used for binding the reporter to the hook. GFP and its derivatives such as the YFP are the most widely used fluorescent proteins for the tagging of both transgenes and endogenous loci in *Drosophila* research. This makes the use of the LAMA system more advantageous, as the RUSH system would likely require generation of novel reporter fly lines tagged with SBP, while the LAMA system reporters would be largely already available from commercial sources or individual laboratories. Taken together, the two considerations were enough for me to decide to proceed with the LAMA system for further experiments.

One notable fact is that the two systems showed surprising similarities in one of their limitations. The use of a cytoplasm-facing Golgi-hook in both systems induced strong toxicity of wing disc cells, which resulted in severe morphological deformities of the tissue (Figures 19 and 21). This makes it likely that the problem lies with the hook overexpression, rather than the trapping protein used (streptavidin or cpDHFR-nanobody). The Gal4/UAS system induces strong overexpression overall, even though the individual driver promoter induction levels differ. This makes it plausible that the Golgi apparatus of wing disc cells is not able to tolerate such a large amount of the hook being added to its membrane.

As the salivary glands were not affected when the Golgi-hook was overexpressed in this tissue in either system (Figures 20 and 23), it is possible that the wing disc cells are less tolerant of this effect than salivary gland cells. This could be due to their small size or because of their function. Wing disc cells must accommodate for several different signaling pathways, including the Hedgehog, Dpp, Notch and Wnt pathways [Dye et al., 2017], which requires them to precisely regulate the synthesis and secretion of diverse signaling pathway protein ligands. This could make their secretory pathway organelles, including the Golgi, more sensitive to stress such as the hook overexpression. This supposition is strengthened by the

fact that short-term hook overexpression of up to 12 hours did not cause the toxicity, but longer-term expression of 36 hours did (Figure 22A-B).

By comparison, the primary function of the salivary gland cells is the production of the 'glue' in significant quantities, which accounts for their polytene chromosomes and large size. The mucoproteins of the 'glue' are synthesized in the ER and transported to the Golgi, from which they are secreted into the cytoplasm in granules [Farkaš et al., 2015]. The salivary glands therefore likely require larger Golgi than the wing disc cells, which can potentially tolerate the addition of the Golgi-hook where the wing disc Golgi cannot.

Sequestration of the cytoplasmically located reporter on the outer membrane of the mitochondria through the Mito-LAMA-hook proved a viable alternative to the cytoplasmically oriented Golgi-hook in wing discs (Figure 22C). The LAMA system using the Mito-hook together with an overexpressed reporter protein was well tolerated by the wing disc cells and did not induce any morphological changes or negative effects on later wing development. Salivary gland cells were similarly unaffected, and by visualizing the mitochondria in these cells using the MitoTracker dye, I was able to show that the RUSH-Rab7 reporter, initially highly localized to the mitochondria, was released from the Mito-hook and departed the mitochondria to a large extent within 60 minutes of TMP incubation (Figure 24).

Live imaging of the immediate effects of the TMP addition to the wing discs in culture medium revealed that the localization pattern of the Mito-LAMA-hook significantly changed after the RUSH-Rab7 was released from it, from strongly punctate to largely diffuse (Figure 25). I observed similar, though significantly milder, effects to both the Mito-hook and Golgi-hook in salivary gland cells. This may overall point towards the binding of the RUSH-Rab7 reporter and LAMA-hooks inducing changes in organelle morphology or localization within the cells, though in wing disc cells the intracellular resolution is too low to positively confirm whether this is the case. As I did not observe similar effects after trapping an endogenously expressed cytoplasmic protein (Sgg:GFP) with the Mito-LAMA-hook in wing discs (Figure 29), it is likely that this effect is reporter-specific with regards to either which reporter protein is chosen, or how high the amounts of the protein are in the cells. Nevertheless, the effect is something that should not be overlooked in spite of the functionality of the system. Any unexpected and unusual phenotypes in other experimental contexts may potentially be a system artefact consequence of potential organelle rearrangement, rather than a true phenotype.

I additionally experienced some initial issues with the live imaging of the TMP-induced release, where the imaged wing disc did not show any hook and reporter localization changes for up to one hour after addition of TMP to the medium while other wing discs in the same well did. The problem was overcome by the adjustment of laser intensities to lower settings; thus, I hypothesized that the cause may be that the TMP molecule is photosensitive and is degraded by strong laser intensities before it can bind to the hook in the cells. This may have

to be taken into account if weakly expressed tagged proteins are part of the experimental setup, for which stronger laser intensities are required for visualization.

An open question remaining regarding the Golgi-LAMA-hook is whether a hook facing the lumen of the Golgi would have similar effects to the hook facing the cytoplasm. This would be an important consideration in the biological context of secreted proteins such as Wnts, whose trapping would have to take place in either the Golgi or the ER. Rather than generating another Golgi-LAMA-hook, however, I decided instead on the lumen-oriented ER-LAMA-hook, as this allowed me to test the tolerance of the ER of wing disc cells to the LAMA system expression. Trapping endogenous secreted proteins also provided the opportunity to combine my endogenously tagged Wg and Evi with the LAMA system. Wg is fully localized to the ER lumen after synthesis, including the EGFP tag, while my Evi:EGFP construct was tagged on the luminal side of transmembrane protein in question. Therefore, the KDEL ER-LAMA-hook was capable of trapping both of these proteins, and its expression in the wing discs resulted in strong accumulation of Wg:EGFP and mild accumulation of Evi:EGFP in the cells (Figure 26).

Importantly, the trapping of Wg:EGFP in these cells practically fully prevented its secretion into the extracellular space in the posterior wing disc compartment where the hook was expressed, and as a direct consequence affected the Wnt signaling pathway, for which I used the expression of the Wnt target gene Dll as a readout (Figure 27). This demonstrates that the LAMA system can be used to induce loss-of-function resembling phenotypes in the tissue by trapping Wg in the ER. Glashauser and colleagues showed a similar result with the RUSH system using Notch as the reporter protein [Glashauser et al, 2023]. The choice of reporter protein is likely important in this context, as may be concluded from the differences in the level of trapping between Wg:EGFP and Evi:EGFP. Positioning of the GFP tag is likely important, as the conformation of the reporter and the hook would dictate how efficient the binding between the two is.

I was unable to induce the release of Wg:EGFP from the cells by incubation with TMP in spite of attempting to increase the concentration (from 100µM I used for the Mito-hook to 1mM), to extend the incubation period (up to 2 hours) and even adding TMP to the fly food or limiting the expression of the hook to 24 hours prior to incubation (Figure 28, Supplemental Figure S5). Wg interacts with several proteins in the ER during its synthesis and maturation, including being palmitoylated by Porcupine and loaded onto its cargo carrier Evi. It is possible that the binding to the ER-hook disrupts this process and results in its misfolding, which would cause it to remain in the ER instead of entering the secretory pathway.

Another potential cause is that the TMP is unable to enter the ER from the cytoplasm. Published literature, however, indicates that the ER membrane is more porous than the cellular membrane [Le Gall et al., 2004], which argues against this possibility. A third reason may be NADPH levels in the ER. NADP+ and NADPH are required in the ER for several

metabolic pathways, among them the disulfide bond formation during post-translational protein processing [Gansemer & Rutkowski, 2022]. ER has a native NADPH/NADP+ ratio which is independently established within the organelle, as the ER membrane is impermeable to pyridine nucleotides [Piccirella et al., 2006]. The LAMA hook requires the cooperative binding of NADPH and TMP for the release of the GFP-tagged reporter; if the amount of NADPH in the ER is too low, TMP addition is likely insufficient to induce the reporter release. This additionally raises the question of using the LAMA system in the Golgi lumen as well.

One of my reasons for the establishing the LAMA system in *Drosophila* was because I believe it could serve as an alternative to the Gal80^{ts}/UAS system for the temporal control of protein manipulation (see Introduction Section 2.3). The Gal80^{ts}/UAS system allows for the induction of protein overexpression at specific stages of fruit fly development. Sequestration of the protein away from its place of activity with the LAMA system can function similarly to the blocking of overexpression through temperature regulation, as the protein is unable to exert its function. The release of the binding between the reporter and the LAMA hook would thus phenotypically mimic the induction of expression by the Gal80^{ts}/UAS system once shifted to 29^{o}C.

The Gal80^{ts}/UAS system only allows for the study of protein overexpression effects several hours after induction, as it is based on the Gal4/UAS system. It therefore requires time for the cells to transcribe the UAS construct transgene and afterwards translate it into a functional protein that must additionally be post-translationally processed before it can begin functioning. The effects of protein overexpression by the Gal80^{ts}/UAS system can thus only be observed in the intermediate or longer term and in fixed cells, because this process on the tissue level will be gradual and dependent on each cell's metabolism. By contrast, the LAMA system dispenses with this time lag by trapping already synthesized and processed protein, so that when the release from the hook is induced by TMP addition, the protein can immediately begin exerting its function. The release of the reporter from the LAMA hook is synchronized in all cells through the addition of TMP and is observable within minutes in live imaging as well as fixed cells. This allows for the study of immediate or short-term effects of protein overexpression on the cells and tissues.

I was able to demonstrate this advantage by using the LAMA system to study the effect of Rab7 overexpression on Wnt tissue distribution and cellular localization. I identified Rab7 as one of the Rab GTPases whose perturbation induced a Wnt secretion phenotype and chose to overexpress wildtype Rab7 with the Mito-LAMA-hook to study the dynamics of the phenotype. I could show that the changes in Wnt distribution and localization are induced within 60 minutes of the release of overexpressed Rab7 from the Mito-hook (Figure 35).

In addition, the Gal80^{ts}/UAS system allows only for the control of protein overexpression, whereas the LAMA system can be used with endogenously expressed proteins as well. The Gal80^{ts}/UAS system is a variation on the Gal4/UAS system and therefore, after induction, it

will overexpress proteins in similar levels to the Gal4-driven overexpression without temporal control. This is a problem in such cases where strong overexpression is toxic for the cells and tissues, as is the case I observed with UAS-Wg construct overexpressed with commonly used wing disc drivers like hh-Gal4. Lower levels of overexpression can be achieved by placing the gene under the direct control of a select promoter within the transgenic construct; unfortunately, this expression cannot be controlled temporally with the activity of $Gal80^{ts}$. The LAMA system, however, would allow for this, as it would sequester the protein expressed from such a transgenic construct its release is induced by TMP addition.

After establishing and testing the LAMA system in *Drosophila melanogaster*, I was able to show that it can be used to induce knockdown phenotypes through the continual endogenous protein trapping, to reconstitute an overexpression phenotype blocked by protein sequestration after protein release, and finally, to study protein dynamics after such a synchronous release. My assessment is therefore that, while there are some limitations that still need to be overcome, the LAMA system is a valuable tool for the *Drosophila* community.

4.3 The role of Rab7 in Wnt secretion

The main biological question that I chose to explore in my thesis was the role that Rab GTPases play in Wnt secretion. Wnt proteins must be synthesized and secreted from Wnt-producing cells in order to exert their function. In this process, they pass through the cellular secretory and endosomal pathways. As Rab GTPases are the main trafficking regulators within the cell, it is to be expected that they are also involved with directing Wnt secretion. Indeed, Rab1 [Ching et al., 2008], Rab4 [Linnemannstöns et al., 2020], Rab5 [Belenkaya et al., 2008], Rab8 [Das et al., 2015] and Rab11 [Koles et al., 2009] have been shown to play important roles in this process in various contexts (more detailed summary is found in Introduction Section 2.2 'The role of Rabs in Wnt secretion'). However, there are twenty-six Rab GTPases in *Drosophila*, and no systematic studies have been done yet to determine which of these may be required for Wnt secretion in *Drosophila* wing imaginal discs.

Of the twenty-six Rab GTPases in fruit flies, eight are ubiquitously expressed and indispensable for development and cellular functioning (Rab 1, 2, 5, 6, 7, 8, 11, and 35). Their homozygous null mutants are lethal before the adult fruit fly stage. The remaining eighteen Rabs, however, are surprisingly all homozygous null mutant viable. I therefore collaborated with the Robin Hiesinger Laboratory from the Free University of Berlin, who generated the Rab null mutant collection, to characterize these lines [Kohrs et al., 2021].

After studying the adult wings of the viable null mutants, only Rab23 null mutant showed a consistent wing planar cell polarity (PCP) phenotype, with several wing hairs developing from individual cells and growing towards the wing margin rather than in a distal orientation (Figure 30A-E). One of the non-canonical Wnt pathways regulates PCP formation (the Wnt/PCP pathway), and both Frizzled 1 (Fz1) and Dishevelled (Dsh) proteins belong to the core group of PCP genes [Seifert & Mlodzik, 2007]. The phenotype therefore initially appeared to have a potential connection to Wnt signaling. Two arguments against this hypothesis arose from

literature, however. The first was the evidence that the Fz/PCP phenotype in *Drosophila* wing is not dependent on secreted Wnts [Ewen-Campen et al., 2020; Yu et al., 2020]. The second was a prior study on the Rab23 PCP phenotype [Pataki et al., 2010], which found that Rab23 does not affect the subcellular distribution of either Fz or Dsh, and is instead more likely to be connected to two other PCP gene groups, the In (*inturned*) group and the Mwh (*multiple wing hairs*) group, which work in parallel with the Fz/PCP pathway.

The Rab23 PCP phenotype was also studied in the context of Rab protein redundancy [Dunst et al, 2015]. Rab23 and Rab35 both localize at the cell cortex, and Rab35 depletion causes only occasional mild changes to wing hair morphology. The study found that the combined knockdown of Rab23 and Rab35 does not enhance the PCP phenotype, but instead causes the formation of ectopic crossveins. Interestingly, I was also able to observe a wing vein phenotype, namely the shortening of the same crossvein affected by the double knockdown of Rab23 and Rab35. As Dpp signaling is required for crossvein formation [Antson et al., 2022], this result may point towards Rab23 playing a role in Dpp signaling, rather than Wnt signaling.

Nevertheless, the results published by Dunst and colleagues illustrate the functional redundancy which can be found in the Rab protein family. Given that the second screen I conducted, on the effect of Rab perturbation on Wg expression in the wing imaginal discs, revealed surprisingly few potential candidates (Figure 31A), one of the possibilities may be that some of the Rabs whose perturbation did not show a Wg phenotype may be compensated for by the activity of another Rab to whom they are functionally redundant. Double perturbations would in this case be required to confirm the hypothesis.

The other possibility may be that only the ubiquitous Rabs, which have been connected to general secretory routes, are required for Wg secretion in the *Drosophila* wing disc, rather than any of the non-ubiquitous Rabs. This hypothesis is strengthened by the findings published in two studies, that five to eleven of the eighteen non-ubiquitous *Drosophila* Rabs are not expressed in the wing imaginal disc cells. Rab 3, 26, 27, 32 and X4 were shown not to be present in this tissue by both GFP overexpression under the control of selected Rab promoters [Chan et al., 2011], and also by YFP-endogenous tagging of the Rabs themselves [Dunst et al., 2015]. There is more question when it comes to Rab 9, 14, 19, 30, X1 and X6, which were found to be present in the wing imaginal discs in one study but not in the other. Moreover, thirteen out of eighteen *Drosophila* Rabs are either neuron-specific or neuron-enriched [Chan et al., 2011; Jin et al., 2012, summary in Figure 31A]. Taken together, these studies make it likely that Wg protein does not require any Rab GTPases uniquely specialized for its secretion in this tissue, and is instead trafficked by the Rabs responsible for the trafficking between the secretory route organelles in general.

Indeed, three of the eight ubiquitous Rabs were positive candidates of the screen, namely Rab1, Rab5 and Rab7 (Figure 31B-D). Rab 1 serves to traffic proteins between the ER and the Golgi; Rab5 is required for endocytosis and early endosome formation; and Rab7 is the key

player in late endosomal trafficking and degradation routes. Of the three, I further characterized the Rab7 phenotype, as neither overexpression nor the knockdown of Rab7 induced cell lethality the way that Rab1 and Rab5 perturbations did, allowing me to study the effects of the perturbation not just on wing disc cells, but also the organ's development into adult wing. Furthermore, unlike Rab1 and Rab5, Rab7 has previously not been directly associated with Wg secretion.

Intriguingly, the overexpression of Rab7-WT and the knockdown of Rab7 by RNAi both induced a similar Wg accumulation phenotype in the wing discs (Figure 32). While this seems counterintuitive, a prior publication has shown that the knockdown of Rab7 as well as overexpression of Rab7-DN cause the formation of enlarged late endosomal structures, likely due to impaired lysosome formation and accumulation of degradation-targeted cargo [Girard et al., 2014; Bucci et al., 2000]. Overexpression of Rab7-WT or Rab7-CA similarly causes the enlargement of late endosomal structures due to the increase in vesicle fusion [Bucci et al., 2000; Entchev et al., 2000]. It is therefore possible that Wg accumulates in the endosomal pathway in both cases, causing the phenotype similarity.

I observed the Wg accumulation phenotype in both Wg-secreting cells at the dorsoventral boundary and the pouch rings, as well as in the Wg-receiving cells in the remainder of the wing disc pouch (Figure 33). While Wg passes through the endosomal pathway in both cell types, the purpose of it differs. In the secreting cells, the transport of Wg through the endosomal network is tied to its translocation from the apical to the basal side of the polarized epithelial cells [Linnemannstöns et al., 2020], as well as secretion on exosomes [Gross et al., 2012]. In Wg-receiving cells, once bound to its receptor proteins Arrow (homolog to human Lrp5/6) and Fz2, Wg is internalized and passes through the endosomal network in order to be degraded by the lysosome [Marois et al., 2006]. Rab7 perturbation therefore likely causes similar effects in separate cellular processes: in secreting cells, it affects Wg transcytosis and potentially its basal secretion; in receiving cells, by contrast, it affects Wg degradation.

I additionally found that Wg strongly accumulates on the basal side of the wing discs, especially in Wg-secreting cells (Figure 34). Wg is known to be secreted from both apical and basal sides of the wing disc cells in processes that are separately governed. The exocyst complex is required for apical secretion [Chaudhary & Boutros, 2019]. Basal secretion requires the re-internalization of Wg and transcytosis from the apical side. While the mechanism is not fully understood, individual players such as the E3 ubiquitin ligase Godzilla [Yamazaki et al., 2016] and the kinesin motor Klp98A [Witte et al., 2020] have been implicated in this process. Klp98A was directly associated with the late endosomes, as its knockdown resulted in the accumulation of Rab7 on the apical side of the wing disc in the same region where Rab5-positive early endosomes are located [Witte et al., 2020]. Rab7 might therefore likewise play a role in transcytosis, which could explain the accumulation of Wg on the basal side of the cells upon Rab7 overexpression.

However, if this is the case, it nonetheless does not affect how much Wg is secreted from either side of the wing disc cells, as surface Wg staining revealed that the levels of Wg secretion from both the apical and the basal side remained unchanged upon Rab7 overexpression (Figure 38). This finding can be contrasted with the perturbation of the exocyst complex, whose knockdown resulted in the downregulation of Wg secretion on the apical side and the accumulation of Wg on the basal side of the cells [Chaudhary & Boutros, 2019], or the knockdown of Godzilla, which induces an increase of apical secretion of Wg protein that in wildtype cells is secreted basally [Yamazaki et al., 2016].

The change in wing size was the only downstream Wnt signaling phenotype present (Figure 37), and none of the three Wnt pathway target genes I studied – Fz3, Sens and Dll – showed any change in expression patterns (Figure 36). The Wnt pathway is involved with the tissue growth of the wing imaginal disc; however, it is far from the only process involved. Hedgehog, Dpp, Wnt and Hippo pathways are involved in a complex network of crosstalk, which is not yet fully understood, to coordinate wing disc growth [Gou et al., 2020]. Beyond that, wing growth is also affected by external signals such as temperature, mechanical forces, nutrient levels and hormones. Given this, as well as the central position that Rab7 holds in the late endosomal pathway regulation, including early-to-late endosome transition [Langemeyer et al., 2020] as well as lysosome formation [Bucci et al., 2000], it cannot be assumed that the enlarged size of the wings induced by Rab7 overexpression is due to Wg accumulation alone.

In fact, Rab7 perturbation has been shown to affect Dpp signaling range instead, with the expression of the Dpp pathway target gene *spalt major* (*salm*) being reduced upon Rab7-CA overexpression [Entchev et al., 2000]. Such overexpression in the posterior wing disc compartment likewise led to the compression of the anteroposterior axis in the posterior half of the adult wing. The authors postulated that the regulation mechanism for Dpp signaling is likely to be the degradation of the Dpp morphogen in Dpp-receiving cells. This is contrasted with my observations that Wnt pathway target gene expression is not affected upon Rab7-WT overexpression, nor was there any Wnt phenotype present in the adult wing, such as notches or dysregulation of bristle formation. Therefore, unlike in the Dpp signaling pathway, Rab7 overexpression in Wg-receiving cells does not affect Wnt signaling range attenuation, findings which match similar observations with regards to the degradation of Fz2 and Arrow [Rives et al., 2006]. This study found that the accumulation of internalized Wnt ligand and receptors in the receiving cells upon the knockdown of Hrs, a protein involved with the invagination of late endosomal membrane [Lloyd et al., 2002], did not affect the expression of Wnt signaling target genes, concluding that Wg degradation in Wnt-receiving cells is not the main method of signal attenuation in wing imaginal discs.

While Wg is targeted for lysosomal degradation in the receiving cells [Marois et al., 2006], no publication shows that this is similarly the case in Wg-secreting cells, which should not be surprising given that the purpose of these cells is to release Wg into the extracellular space in order to facilitate signaling. Nevertheless, I found Wg colocalizing with both LAMP1 (Figure

39) and Arl8 (Figure 40) in both secreting and receiving cells upon Rab7 overexpression. The LAMP1 protein has been used primarily as a lysosomal marker, though more recent evaluations have suggested that it is also present in significant quantities on other endosome species as well [Shearer & Peterson, 2019]. The colocalization with Arl8 was therefore more interesting, as Arl8 is required on the lysosomes for the recruitment of the HOPS complex [Khatter et al., 2015], which in turn facilitates the late endosome/lysosome fusion through recruitment to the late endosome by Rab7 effector RILP [Li et al., 2014]. These results combined indicate that Wg is being targeted to the lysosome in both cell types and not just receiving cells.

I observed fewer and smaller basally located Wg puncta upon Arl8 depletion in Wg-secreting cells overexpressing Rab7 than upon sole Rab7 overexpression (Figure 41). Additionally, these cells showed significant LAMP1 accumulation in comparison to cells only overexpressing Rab7 or in which only Arl8 was knocked down (Supplemental Figure S11). Arl8 knockout in wing disc cell clones has previously been found to induce mild accumulation of LAMP1 and Rab7 [Rosa-Ferreira et al., 2018]. This study also noted that Rab7- and LAMP1-positive endosomes were enlarged upon Arl8 knockdown, which corresponds to my own observations in both Rab7 overexpressing cells as well as those with combined Rab7 overexpression and Arl8 knock-down. Given that Arl8 downregulation interferes with the degradation pathway through the disruption of endosome/lysosome fusion [Boda et al., 2019], it is intriguing that Wg accumulation phenotype is ameliorated by it, rather than enhanced.

Taken together, I was able to show that Rab7 perturbation induces Wg accumulation within both Wg-secreting and Wg-receiving cells, as well as its accumulation on the basal side of the polarized epithelial wing disc cells. I found that the accumulated Wg is found in Rab7-positive endosomes and Arl8-positive lysosomes; however, this accumulation in the degradative pathway does not disrupt Wg secretion from either the apical or the basal side of the cells, and furthermore does not disrupt Wg downstream signaling, either.

Given all of this, as well as that the process of transcytosis uses the endosomal pathway through the cells [Witte et al, 2020], it is likely that Rab7 is involved with Wg transcytosis from the apical to the basal side to some extent. If Wg shuttling is therefore disrupted due to the malfunctioning of the late endosomes as a result of Rab7 perturbation, the protein is likely accumulating in these compartments in excess of what is standard in wildtype cells. Directing this excess into the degradation pathway instead of secreting it may be a way to regulate intracellular Wg protein levels in Wg-secreting cells and prevent excess secretion from taking place. My attempts to overexpress Wg with the Gal4/UAS system, even using the wg-Gal4 driver to limit the overexpression only to Wg-secreting cells, were always lethal. This may indicate that too much Wg is more detrimental to the organism than too little, given that downregulation of Wg causes phenotypes in adults such as the wing notches, but is not lethal even when driven by a very strong and broadly expressed driver like hh-Gal4.

Thus, I postulate the existence of a mechanism that can control the secretion levels of Wg regardless of the accumulation of Wg within the secreting cells. My hypothesis would be that such a mechanism might rely on the degradation of any excess Wg that is produced by the secreting cells. Disrupting Rab7 function could be causing accumulation of Wg in late endosomal compartments over time, such that after the secretion equilibrium is reestablished following Rab7 perturbation effects, any excess Wg still remaining in the pathway is instead directed into the degradation route. A similar mechanism called crinophagy has been described for specialized secretory cells such as the *Drosophila* salivary gland cells [Csizmadia et al., 2018]. During crinophagy, secretory vesicles which are not released by exocytosis are instead fused directly to lysosomes for degradation [Szenci et al., 2023], a process which has been associated with the regulation of secretion from the secretory cells. It is therefore possible that cells which are not specialized for secretion but still secrete ligands such as the Wnt-secreting cells in the wing imaginal discs may have similar mechanisms in place. Further study is required to determine if this is the case.

4.4 Conclusion and outlook

Wnt secretion

Wnt protein secretion is crucial for the proper functioning of the Wnt signaling pathway. Though the initial synthesis and processing steps are straightforward, the release and trafficking of Wnts between the secreting and receiving cells is a far more complex matter, including a variety of trafficking modes which have been discovered so far. This multiplicity leaves open the matter of regulation that Rab GTPases would be able to fill, as they are responsible for all intracellular trafficking in the cell. In my thesis, I studied the involvement of the Rab protein family in Wnt secretion in the *Drosophila melanogaster* wing imaginal disc. I was able to determine that in these epithelial cells, no Rabs exist which are specialized for Wg secretion, as those Rabs whose perturbation affected Wg distribution are Rabs involved with general trafficking steps in the cell. The study of Rab7 in this context revealed that Wg can accumulate in the late endosomes and lysosomes without disrupting its secretion from the cells.

My results suggest a regulatory method in the cell which enables the maintenance of secretion in spite of the accumulation of Wg in the endosomal pathway. Further study would be required to elucidate whether this is indeed the case. A suitable approach would be the manipulation of Wg secretion and the general degradation pathway. Wg localization upon mildly upregulated protein production would provide insight into whether the secreting cells use the degradation pathway for the regulation of secretion. This would likely require more efficient titration of Wg overexpression than is possible with the currently available fly lines. However, an approach as was applied by Port and colleagues to titrate Cas9 by inserting an upstream ORFs of various lengths to the UAS-Cas9 transgenic construct [Port et al., 2020] could be used with a UAS-Wg construct instead to solve this problem.

Additionally, preventing the upregulated Wg from entering the degradation pathway would provide further insight into the tolerance that the tissue has for Wg expression. One additional foreseeable issue with this approach would be that disruption of the general degradation pathway would have negative effects on the cell homeostasis and induce toxicity phenotypes, which may be difficult to separate from the effects on Wg secretion. If this proved too toxic for the wing imaginal disc cells, attempting it in another *Drosophila* tissue or cell culture would be a workaround. Another approach could be the blocking of Wg secretion in the endosomal pathway and observation on whether the accumulated Wg is being directed instead to the degradation route. Knockdown of Ykt6 would block Wg secretion after endocytosis [Linnemannstöns et al., 2020], while the blocking of Wg secretion at the late endosome/MVB stage could be achieved by the use of extracellular vesicle inhibitors [Catalano & O'Driscoll, 2020].

Lastly, further study into any potential Rabs specialized for Wnt secretion would likely prove more successful in neuronal tissue, as thirteen out of twenty-six *Drosophila* Rabs are either expressed exclusively or predominantly in neurons [Kiral et al., 2018]. Wnt activity has previously been connected to neuronal maturation and synaptogenesis as well [Rosso & Inestrosa, 2013], making this a viable avenue of investigation.

Drosophila *tool development*

The general toolbox shared by scientists within a given field is crucial for research, as it provides a framework on which to design studies and experiments. Development of tools and techniques contributes to this process by enabling more advanced research of ongoing topics, novel studies which were not previously possible with existing tools, and the reevaluation of already gained knowledge that may have been incomplete due to technical limitations. As part of the thesis, I generated novel endogenously tagged Wg and Evi fly lines. In the process, I identified locations within the Evi sequence where the insertion of a fluorescent protein does not affect the protein's function. This discovery was not only useful for my own work, but is of material contribution to Wnt research performed with other model organisms such as the human cell lines, where Evi tagging has so far resulted in reduction of protein activity or disruption in its trafficking pathway, according to attempts by my colleagues in the laboratory. I also showed the importance of fluorophore selection with respect to secreted proteins, as different fluorescent proteins may not be actively fluorescent in all cellular contexts. Furthermore, I adapted the LAMA system from cell culture, a protein trap-and-release technique which had previously never been implemented in the *Drosophila melanogaster*. It can be used for the sequestration of endogenous proteins at specific organelle membranes in order to induce loss-of-function phenotypes, as well as for the study of protein dynamics through the acute release of sequestered proteins during live imaging.

The question of precise parameters of the fluorescent protein properties leading to different fluorophore activities upon tagging remains open. This is especially important with regards to the tagging the proteins passing through the secretory and endosomal pathways, which

encounter a range of pH values within the organelle lumens. One way to determine the effect of pH value on tagged secreted proteins like Wg and Evi would be to affect the pH of different secretory and endosomal pathway organelles and study the behavior of a protein tagged with different fluorescent proteins (such as the Wg:EGFP and Wg:mScarlet) passing through the organelles. Lysosome acidification, for instance, can be disrupted with bifalomycin A_1, which inhibits the lysosomal proton pump V-ATPase [Mauvezin & Neufeld, 2015]. Another approach would be to test a range of fluorescent proteins with higher or lower pKa values, such as mTurquoise2 (3.1 pKa) and EYFP (6.9 pKa) in comparison to EGFP (6 pKa) and mScarlet (5.4 pKa), and compare them to one another in order to determine the one best suited for different experimental approaches.

It would also be interesting to determine whether this effect is a general phenomenon irrespective of the tagged protein and cellular context. If the problem in visualizing secreted proteins is the pH value of the organelle, tagging a cytoplasmic or transmembrane protein and observing the fluorophore behavior in this case would likely shed more light on the matter. Lastly, when working within organ systems, the context plays an important role; thus, a viable strategy would also be testing whether this phenomenon is observed in different *Drosophila* organs expressing Wg or in different model organisms such as hydra or in human cells.

Additionally, moving towards other methods for protein visualization in live imaging would be beneficial if this effect of tagging with fluorescent proteins impedes the experimental design. Such a case could be, for instance, the requirement of a red fluorophore for the visualization of intracellular Wg movement, as Wg:mScarlet proved far less suitable for such imaging analysis than Wg:EGFP. Alternative protein visualization tools would be chemical tags such as HaloTag or Snap and Clip tags. They require tissue incubation with their respective chemical dyes, but still enable *ex vivo* live imaging of wing imaginal discs. Their advantage over fluorescent proteins would also be the ability to use cell permeable or impermeable dyes to visualize various fractions of Wg more reliably than the fluorescent tags, and using dyes that react with the tags at differing pH values.

The limitations of the LAMA system equally raise further avenues of optimization. The most important question is the reporter release inability in the ER. A useful tool for testing whether this is a problem of the ER membrane permeability to TMP would be fluorescently-labelled TMP, which could shed light on how much TMP colocalizes with the ER-LAMA-hook [Phetsang et al., 2016]. There are as yet no functional NADPH/NADP+ sensors for the ER [Gansemer & Rutkowski, 2022], though induction of NADPH production in the ER through genetic manipulation of the hexose-6-phosphate dehydrogenase (H6PD) [Atanasov et al., 2004] in tandem with TMP may at least show whether NADPH levels are the limiting step in this context. Improvement on this point may lie with the generation of a mutated DHFR which does not require NADPH binding. Testing other reporters which transit through the ER lumen would be another strategy, if the problem is with the reporter rather than the hook. It would

also be worthwhile to generate and test additional hooks for the lumen of other organelles to determine the precise spatial limitations of the LAMA system. If the LAMA reporter release is not functional within organelles which possess insufficient NADPH levels, it can nonetheless serve as a general method of protein trapping for the purposes of protein downregulation.

LAMAs as initially published are designed for reversible binding [Farrants et al., 2020], which is another advantage over the RUSH system. Establishing the functionality of this system feature and subsequent optimization in the context of *Drosophila* tissues would be of great benefit, as it would allow for greater control of the system, especially in cases when the trapping of reporter protein being studied could lead to strong loss-of-function phenotypes, or the goal is to study the effect of rapid protein level changes and protein degradation is deemed too slow.

In summary, the LAMA system could potentially prove to be a versatile and very useful tool for the *Drosophila* field of research, though further refinement is needed to achieve its full potential.

5 Materials and Methods

5.1 Methods

5.1.1 Cloning

Cloning was used to generate all plasmids required for endogenous tagging by CRISPR/Cas9, as well as for transgenic insertion of UAS constructs. The plasmid backbone was either amplified by PCR or was prepared by linearizing a circular plasmid using restriction digestion. The inserts were amplified by PCR from existing plasmids carrying the inserts required or from genomic *Drosophila* DNA.

Plasmid restriction digestion

In case when a linearized pre-existing plasmid was used as the backbone for plasmid cloning, 1µg of plasmid was incubated with 1µL of the selected restriction digestion enzyme in 2µL of appropriate digestion buffer and remainder volume up to 20µL with distilled deionized water (ddH_2O) in case of digestion with only one enzyme, or with 1µL of each of a pair of enzymes in case of two enzyme digestion, with the buffer chosen to be best suited for both enzymes. If the plasmid was digested with only one enzyme, the reaction was incubated at 37°C for 45min, after which 1µL of alkaline phosphatase CIP was added to dephosphorylate the cut ends and prevent re-ligation and the reaction was incubated for an additional 15min at 37°C. In case two enzymes were used for digestion, the reaction was incubated at 37°C for 60min and no alkaline phosphatase was used, as the two cut sites were different and couldn't re-ligate to one another. After the incubation, the sample was run on a 1% agarose gel in 1xTAE buffer and containing 0,01% SYBR Safe for DNA visualization under UV light. The correctly digested backbone was then gel purified using the QIAquick Gel Extraction Kit (Qiagen) according to manufacturer's instructions and eluted in 20µL ddH_2O.

PCR

PCR was used for the synthesis of the insert, as well as for cloning in which the backbone was PCR amplified from an existing plasmid. PCR amplification primers for the inserts were designed with a minimum of 15nt overhang overlapping the plasmid backbone, with the annealing temperature of the primer section without the overhang in the range of 60-63°C. PCR was performed in 50µL reactions by mixing 25µL of the Q5 High-Fidelity 2X Master Mix (NEB), 2,5µL forward and reverse primers each, 1,5µL DNA template diluted to 50-100ng/µL range, and 18,5µL ddH_2O. Prior to the PCR cycles, the reaction was incubated for 30sec at 98°C for the initial melting of the DNA template. 35 PCR cycles were run consisting of 10sec at 98°C, 30sec at 60-63°C depending on the primer annealing temperature, and 30sec/1kb length at 72°C, with a 5min final elongation at 72°C after the PCR cycles. The PCR product was run on a 1% agarose gel after PCR, gel purified using the QIAquick Gel Extraction Kit (Qiagen) according to manufacturer's instructions and eluted in 20µL ddH_2O.

In-Fusion cloning and bacterial transformation

In-Fusion cloning (Takara Inc.) was used to ligate the insert and the vector. 2µL of the 5x In-Fusion HD Enzyme Premix were mixed with 100ng vector and up to 100ng insert in at least a 2:1 molar ratio with the vector. ddH_2O was used to set up the reaction to 10µL, and the mix was then incubated at 50°C for 30min, after which it was placed on ice. 2µL of the In-Fusion reaction were added to 50µL of Stellar Competent *E.coli* bacteria, which were thawed on ice for at least 20min prior to the reaction addition. The mix was allowed to sit on ice for 20min, after which the bacteria were heat shocked by placing them at 42°C for 45sec, before returning them for 2min on ice. 500µL of SOC (Super Optimal Growth) medium was added to the bacteria and they were allowed to recover from the heat shock for 30min at 37°C with shaking at 600rpm. Afterwards, 150µL of the bacteria were plated onto LB agar plates with 1:1000 dilution of Carbenicillin and incubated over night at 37°C. Individual colonies were picked the next day and used to inoculate 5mL of Carbenicillin-containing LB medium, which was followed by overnight incubation at 37°C. Plasmids were isolated from the liquid culture the next day using the QIAprep Spin Miniprep kit (Qiagen) according to the manufacturer's instructions. The isolated plasmids were sent for Sanger sequencing to confirm the correct ligation of the vector and the insert.

Cloning for tagging using CRISPR/Cas9

A set of two plasmids – a donor plasmid and a gRNA plasmid – were cloned per insertion site for CRISPR/Cas9 endogenous tagging. For the Wg:mScarlet tagging, the gRNA plasmid (pFP411) and the plasmids used for the donor plasmid backbone (pFP450) and the mScarlet insert (pFP889) were generously provided by Fillip Port, as the insertion site in the *wg* locus was the same for the mScarlet as for the EGFP tag [Port et al., 2014]. The backbone and insert were both PCR amplified.

For the Evi tagging, the donor plasmids were generated in a three-step cloning process, used to sequentially insert the 5' (for Sites 1, 2, 3, 4 and 6) or the 3' (for Site 5) homology arm, the fluorescent protein sequence, and the 3' (for Sites 1, 2, 3, 4, and 6) or the 5' (for Site 5) homology arm. Type IIS restriction enzymes – BbsI for Sites 1, 2, 3, 5, and 6; Esp3I (isoschisomer of BsmBI) for Site 4 – were used to open the plasmid in the second and third step without leaving a restriction digestion site between the individual inserts. The restriction enzyme sequence was added to the vector through the primers for the first homology arm inserts. For the 5' and 3' homology arms, the inserts were synthesized by PCR amplification from the *Drosophila* genomic DNA. The genomic DNA was obtained by collecting five w^{1118} flies and homogenizing them through mechanical force in the Squishing buffer containing 1:50 Proteinase K. The sample was then incubated for 30min at 37°C, followed by 2 min at 95°C and was stored at -20°C when not needed. For the mScarlet and EGFP, the inserts were obtained by PCR amplification from plasmids pFP889 (mScarlet) and pFP030 (EGFP), provided by Fillip Port. pBluescript SK (+) plasmid was used for the backbone of the donor plasmid, and was linearized by restriction digestion using the Type IIP restriction digestion enzymes XhoI and HindIII.

For the Evi tagging gRNA plasmids, an sgRNA as close as possible to the insertion site was identified based on the NGG PAM sequence. The plasmid pCFD5 was used for the backbone and the cloning was performed according to the protocol generated by the CRISPRFlyDesign project [Port & Bullock, 2016]. The pCFD5 plasmid was digested with BbsI and gel purified. The gRNA insert was generated by oligonucleotide annealing. 1µL of the top and 1µL of the bottom oligo (100µM stock) for each gRNA were mixed with 0,5µL T4 kinase (NEB), 1µL of 10xT4 ligation buffer and 6,5µL ddH_2O, and incubated at 37°C for 30min, followed by 5min at 95°C and a gradual reduction in temperature to 20°C at 5°C/min rate. The insert and the linearized backbone were then ligated using T4 DNA ligase (NEB), such that 1µL of annealed oligos in a 1:200 dilution was incubated with 60ng digested pCFD5 plasmid, 1,5µL 10x T4 ligation buffer and 1µL T4 DNA ligase, with the total volume reaction of 15µL filled by addition of ddH_2O. The reaction was allowed to stand for 30min at room temperature before transformation into Stellar competent bacteria.

Cloning for UAS-LAMA-hook plasmids

For the transgenic insertion of UAS constructs, pCFD6 plasmid was used as the backbone, as it contains the *miniwhite* marker, as well as the 10xUAS sequence, the wg 5'UTR and the p10 3'UTR. The backbone was PCR amplified from the pCFD6 plasmid. When necessary, multiple 50µL reactions were set up in parallel to obtain enough PCR-amplified backbone. In this case, the reactions were pooled together during the gel purification step. The inserts for the Mito-LAMA-hook were PCR amplified from NTOM001 and NTOM004, generously provided by Helen Farrants for the project [Farrants et al., 2020], as they already contained the TOM20 transmembrane region sequence and the LAMA hook sequence. The hook inserts for the ER-LAMA-hook were similarly PCR amplified from NTOM001 and NTOM004, with the KDEL sequence added through a primer. The ER signaling sequence preceding the hook was obtained with a gBlock gene fragment (IDT) and cloned subsequently into the plasmid already containing the hook by digestion of both the plasmid lacking the signaling sequence and the signaling sequence gBlock with the XbaI enzyme and ligated using T4 DNA ligase (NEB) as described in the previous section.

5.1.2 *Drosophila* fly line generation

Fly line generation methods

CRISPR/Cas9 homology-directed repair [Port et al., 2014] was used for the insertion of fluorescent tag sequences into the genomic loci of Wg and Evi proteins. For each selected insertion site, a donor plasmid was generated such that the tag sequence was flanked on both the 5' and the 3' side with 1000bp homology arms corresponding to the genomic sequence upstream and downstream of the insertion site respectively (Figure 42A). Additionally, a gRNA plasmid was generated for each insertion site with the sgRNA cutting as close as possible to the insertion site. The donor plasmid/gRNA plasmid pairs were injected concurrently into fly embryos of *nos-Cas9* flies, expressing the Cas9 in the germline (Figure 42B), such that the double-stranded cutting of the genomic DNA and homology-directed repair using the donor plasmid as the template would occur in the germline cells and allow for the progeny of the

injected flies to carry the insertion in all cells. Progeny were therefore the ones selected for the insertion by genotyping and stable fly line stocks were made by crossing to balancer flies to preserve the insertion.

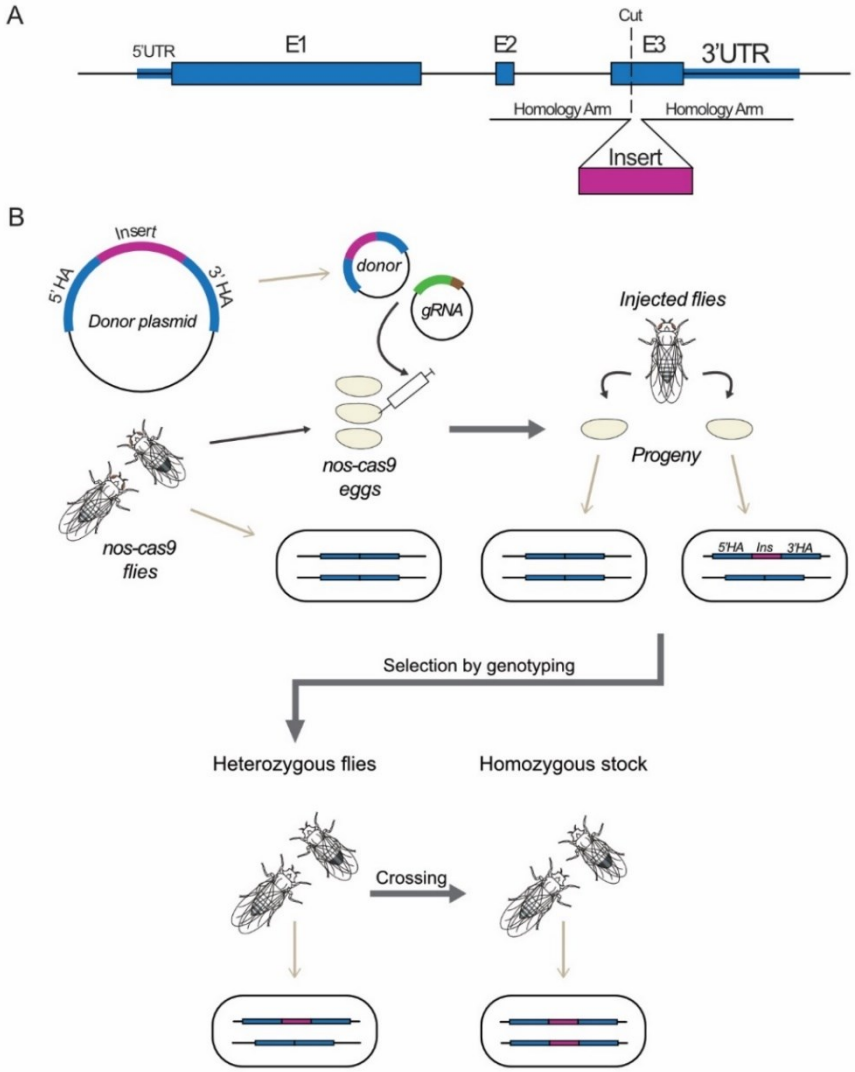

Figure 42: General strategy for endogenous protein tagging using CRISPR/Cas9 homology-directed repair system

A Schematic representation of the alignment of the donor DNA carrying the insertion sequence with the endogenous locus of the protein to be tagged. Homology arms extend for ca. 1000bp directly from the insertion site. The insert (magenta) is flanked by flexible linker regions of ca. 20aa.

B Schematic representation of the generation of fly stocks expressing endogenously tagged proteins. *nos-Cas9* fly embryos are injected with donor plasmid containing the insert flanked by homology arms, as well as plasmid containing the sgRNA sequence. The injected flies are crossed and the collected F1 generation is reared to adulthood. Genotyping is performed on the progeny to identify individuals with the insertion, and their F2 generation progeny are used for the establishment of stable stock lines.

Insertion of the transgenic UAS constructs was achieved by using a germline-specific ϕC31 integrase [Bischof et al., 2007]. The method relies on the integrase recognizing the attP and attB sites and recombining them into the attL and attR sites, in the process integrating anything flanked by the attB sites into the genomic locus of the attP site. The UAS construct plasmids were injected into flies expressing the integrase under the *vasa* promoter and additionally carrying single attP sequences at predetermined safe landing sites. These were attP40 site for insertion on the 2nd chromosome and attP3B for insertion on the 3rd chromosome. The UAS construct plasmids injected into the eggs of these flies in turn carried a single attB sequence, which was required for the integrase to insert the full length of the plasmid into the genome. In addition, the UAS construct plasmids carried a mini-white marker, which allowed for the selection of flies with successful transgenic integration through the eye color in flies with *white* background.

Fly injections

In order to inject the plasmids required for genome manipulation, adult flies aged 3-4 days of the selected fly line were collected into an injection cage and kept on apple juice/agar plates with yeast paste at room temperature overnight. On the day of injection, their egg laying was synchronized through the exchange of old for fresh plates at 30min intervals for 2hr prior to injection. During the injection process, eggs were collected at 30min intervals and dechorionated by incubation in 10% bleach solution for 3min. After washing under a water stream to remove the degraded chorion until the eggs began sticking to one another, the eggs were aligned in a column with their caudal side facing the same direction and affixed to a glass cover slip coated with liquid glue. The eggs were covered by oil to prevent drying out and the injection samples consisting of plasmids at 250ng/µL concentration in ddH_2O were injected into the caudal egg section. The eggs were incubated in a high-humidity chamber at 18^{o}C until hatching.

Surviving larvae were collected after hatching and transferred to the standard fly food, after which they were reared at 25^{o}C until adulthood. The surviving adult flies were individually crossed to single or double balancer flies, with two balancer flies to one injected fly, and the progeny were allowed to reach adulthood. In the case where genotyping was required to identify genome changes, from each cross, five F1 females were collected for genotyping by PCR. The PCR primers were designed to bind within the insert sequence, so that a positive band would be present on the agarose gel only if the insert was present in the genomic DNA, which was prepared as described in the section 'Cloning for tagging using CRISPR/Cas9' above. From the crosses where positive instances of insertion were identified, individual F1 males were crossed to female balancer flies. After ensuring that the female balancer flies were fertilized, the F1 males used in the crosses were genotyped by PCR to determine which of them carried the tag insertion. The F2 progeny of these crosses were used to establish balanced stable stocks and the insertion was verified in these stocks by amplifying by PCR the sequence beginning and ending outside of the homology arms region and Sanger sequencing the amplicons to determine if any unexpected mutations were present. If necessary, any homozygous progeny from these crosses was isolated in order to create homozygous fly stocks of the generated fly lines.

In the case of UAS construct transgenic insertion, the flies carrying the insertion in F1 generation were identified by their yellow or orange eyes due to the mini-white marker found on the UAS construct plasmid. These flies were crossed to balancer flies and the correct insertion was tested by crossing the resulting stock to a Gal4 line.

5.1.3 *Drosophila* husbandry and fly crossing

Fly stocks were maintained on standard cornmeal food at 18^{o}C in a 12h/12h light/dark cycle. Virgin female flies were collected for all fly crosses (younger than 16hr when reared at 18^{o}C and 10hrs when reared at 25^{o}C). The fly crosses were kept at 25^{o}C in all cases where Gal4 driver lines were used. In cases where $Gal80^{ts}$ driver lines were used, the crosses were kept

at 18°C and transferred to 29°C for the experimentally determined length of time before being returned to 18°C.

For the imaging of fly wings, adult flies of the correct genotype were placed in 1:1 glycerol/ethanol mixture for several hours until fully perfused. Afterwards, the wings were separated from the fly abdomen at the joint and mounted onto a microscope slide in glycerol/ethanol. The wings were imaged with the Cell Observer microscope (Zeiss).

5.1.4 Immunohistochemistry and fluorescence imaging

Larval wing imaginal discs and salivary glands were analyzed by immunohistochemistry and fluorescence imaging of endogenous or overexpressed tagged proteins. Larvae were dissected in late third instar wandering stage, on average 5 days after fly crossing. For wing disc staining, the caudal section of the larva was removed and the cranial section was inverted to expose the organs, after which the fatty tissue, salivary glands and the intestinal tract were removed, while the imaginal discs and brain were left on the carcass. For salivary glands, the brain and salivary glands were extracted from the larval body by gentle tugging on the mouth hooks, which were left intact for the subsequent steps.

Fixed imaging

For fixed imaging including the immunohistochemical assay as well as imaging of fluorescently tagged proteins, the carcasses were fixed after dissection for 30min in 4% paraformaldehyde diluted in PBS from 16% stock solution at room temperature. In case where the wing discs were fixed in methanol, the carcasses were incubated for 1hr in ice-cold 100% methanol instead of PFA.

If the experimental setup required immunohistochemistry, the carcasses were washed in PBST (PBS with 0.3% Triton-100X) three times for 5min each and incubated for 30min in PBST containing 2% heat inactivated normal goat serum (HINGS) for blocking. The primary antibody solution was prepared to a predetermined concentration in PBS with 2% HINGS. The carcasses were incubated over night at 4°C in the primary antibody solution, after which they were washed in PBST three times for 10min each. The secondary antibody solution was prepared with 1:800 dilution of the corresponding secondary antibody and 1:2000 dilution of Hoechst dye for DNA visualization. The carcasses were incubated in the secondary antibody solution for either 2hr at room temperature or overnight at 4°C. Following a final wash cycle in PBST three times for 10min each, the sample wing discs or salivary glands were removed from the carcasses and mounted onto poly-lysin coated cover slips in PBS. The samples were finally mounted in VectaShield medium and the coverslips were sealed to the microscopy slides with nail polish at the edges. Fixed samples were imaged on Leica SP5 and Leica SP8 laser scanning electron microscopes.

The surface antibody staining was performed as previously published [Strigini & Cohen, 2000]. The carcasses were incubated in a 1:30 dilution of the α-Wg antibody (4D4; DSHB) in PBS on ice for 1hr after dissection. They were subsequently washed once with PBS and fixed with 4%

PFA for 30min at room temperature. The later steps were performed similarly to regular immunofluorescent staining.

If the experimental setup did not require any immunohistochemistry, the carcasses were washed in PBS twice for 5 minutes and incubated with 1:2000 Hoechst dye dilution in PBS for 15min, after which they were washed in PBS twice for 5min and mounted in VectaShield. For the SNAP-tag visualization, samples were incubated in SNAP-Cell 647-SiR dye (NEB) in a 1:200 dilution in Schneider's medium for 15min followed by three times 5min washing in Schneider's medium if the staining was done before fixation, or in PBS with similar timing if the staining was done after fixation. For MitoTracker staining, samples were incubated in MitoTracker Red CMXRos (Invitrogen) in 1:5000 dilution in Schneider's medium for 15min followed by three times 5 min washing in Schneider's medium before fixation.

For the LAMA experiments, shaking incubation with trimethoprim (TMP) dissolved in DMSO (stock concentration 200mM) and diluted to the chosen concentration in Schneider's medium was performed after dissection but before fixation for the correct time. Carcasses were rinsed in PBS once before fixation and the SNAP tag dying was performed after fixation.

Live imaging

For live imaging, late stage third instar larvae were dissected as described in the previous section. If SNAP-tag or mitochondrial visualization was required, SNAP-tag dye and MitoTracker staining respectively, diluted in live imaging medium, were performed on carcasses with living organs still attached. After washing, the carcasses were transferred from the imaging medium to PBS and the wing discs and salivary glands were removed from them and mounted onto poly-lysin coated 8-well chambered imaging slides. After mounting, PBS was exchanged for live imaging medium and the samples were taken directly for imaging.

For the LAMA experiments, individual wing discs were mounted in separate wells prior to imaging. Samples were positioned at the microscope and the imaging settings were adjusted. Afterwards, the correct amount of TMP dissolved in DMSO (200mM) was gently pipetted into the well so as to achieve the correct concentration (100µM or 1mM). Imaging was started directly afterwards and was not interrupted until the end. Two to three wing discs were imaged per session, and the length of wing disc *ex vivo* culturing per session did not exceed 3h. Live imaging was performed either on the Leica SP8 laser scanning confocal microscope, or on the Nikon Ti-Crest spinning disc confocal microscope at the Nikon Imaging Center in Heidelberg.

5.1.5 Surface protein biotinylation assay

Surface protein biotinylation assay relies on using the cell impermeable biotinylation agent EZ-Link Sulfo-NHS-SS-Biotin (ThermoFisher) to label only the proteins found on the surface of the wing imaginal discs. The labelled proteins are subsequently isolated by incubation with streptavidin agarose beads and analyzed by Western blot analysis.

Surface protein biotinylation

35 to 50 larvae per sample were dissected and the wing discs separated from the carcass in parallel for all samples. The *ex vivo* wing discs were incubated in a 1mg/ml solution of Sulfo-NHS-SS-Biotin in ice-cold PBS for 20min on ice. After this, the biotin was quenched by incubation of the wing discs for 25min in ice-cold PBS with 100mM glycine. Discs were washed in ice-cold PBS and transferred to the lysis buffer (1µL buffer per wing disc), after which they were broken down with mechanical force and sonicated to ensure separation of the cells. This was followed by additional 30min incubation in the lysis buffer on ice to ensure the cells fully lysed. The samples were centrifuged at max speed for 15 min at 4°C and the supernatant was transferred to a new Eppendorf tube. 40µL were taken from the supernatant for the total lysate samples, and the supernatant was afterwards incubated with 30µL streptavidin agarose bead slurry at 4°C with rotation overnight to isolate the biotinylated proteins. The next day, the samples were centrifuged for 3min at 3000g and the supernatant was removed and saved for the flowthrough samples. The beads were washed in lysis buffer five times with 3min centrifugation at 3000g between each step to pellet the beads. Finally, the bound biotinylated protein was eluted by the addition of 60µL 2xLaemmli Sample buffer and the boiling of the pulldown samples for 5min at 95°C before storage at -20°C.

SDS-PAGE and Western Blotting

The concentration of the total lysate, pulldown and flowthrough was measured using the Pierce BCA protein assay (Thermo Scientific) according to manufacturer's instructions, and equal protein amounts were used for SDS polyacrylamide gel electrophoresis (SDS-PAGE), with the final loading volume of each sample being 40µL. The samples were loaded on the Bolt 4-12% Bis-Tris Plus Gel in MOPS buffer and were separated by size by running the electric current through the gel for 15min at 80V, followed by 45min at 180V until the loading dye ran out of the gel bottom. The proteins were afterwards transferred onto a nitrocellulose membrane by wet blotting in the NuPage transfer buffer with 10% methanol for 90min at 20V. The successful transfer onto the membrane was confirmed by Ponceau Red staining of the membrane.

The membrane was washed in TBST and the Western blot signal enhancer (Pierce) kit was used according to manufacturer's instructions prior to any antibody incubation in order to ensure a stronger signal and the preservation of proteins bound to the membrane. Following this, the membrane was blocked in 5% skim milk in TBST for 30min, after which the membrane was incubated in primary antibody solution in TBST at 4°C overnight with rotation. The next day, the membrane was washed three times for 10min in TBST and incubated with the secondary antibody solution in TBST for 2hr at room temperature. The membrane was subsequently washed in TBST three times for 10min and incubated with the Immobilon Western Chemiluminescent HRP substrate (Merck Millipore) to visualize the signal. In case the signal was too weak even with development time longer than 10min, the membrane was incubated with the SuperSignal West Femto Maximum Sensitivity Substrate (Thermo Scientific) in order to enhance the signal. The membrane was imaged using Amersham

Hyperfilm ECL in the COMPACT 2 X-Ray Film Processor. After developing the signal, the membrane was stripped using the Restore Western Blot Stripping Buffer (Thermo Scientific) so as to allow for the development using another antibody from the same animal species.

5.1.6 Computational analyses

Evi protein sequences of different species were obtained from the NCBI database (National Center for Biotechnology Information) and were aligned using Clustal Omega (EMBL-EBI). The degree of conservation and the alignment were visualized using Jalview.

Image analysis was performed using Fiji. Kymograph visualization was generated using the Live Kymographer plugin. Particle tracking analysis was performed by using the MTrack2 plugin. Wing size measurements were obtained by free tracing the wing border and measuring the encircled surface area. Plot profiling was achieved by rotating the images into correct position and drawing a rectangular area of interest for which the intensity profile was plotted. Wg spread measurements were achieved by rotating the wing discs and drawing one-cell-wide areas of interest dorsally and ventrally from the dorsoventral boundary, as well as in the middle of the wing disc for background measurement. The average intensity was measured for each area of interest and the background value was subtracted from the value (Figure 43). Processed images were saved in TIFF or PNG format and the figures were made using Affinity Designer 2.0 software (Serif).

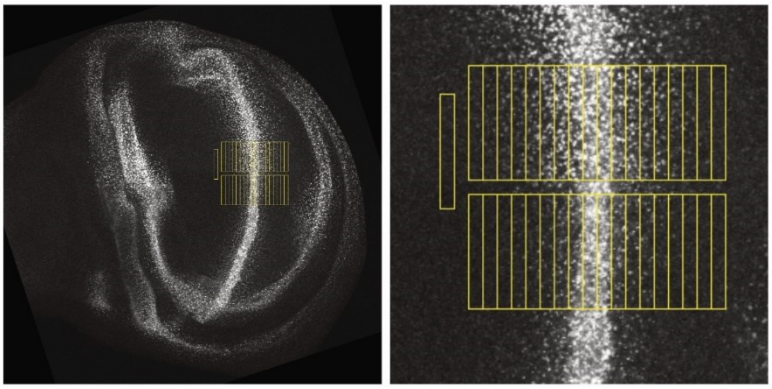

Figure 43: Wg spread measurement
One-cell-wide areas of interest are drawn and average intensity for each is measured. Background is subtracted and the values are plotted. Wing discs must be rotated in order to draw the areas of interest.

5.2 Materials

5.2.1 Plasmids and primers for tagging and sequencing

Table 1: List of plasmids used for and generated by cloning

Plasmid	Plasmid content	Source	Purpose
pFP450	pBlueSK(+) wg-GFP HR donor	Fillip Port	PCR amplification
pFP889	pBlue_Scar_Sens_Donor	Fillip Port	PCR amplification
pFP411	gRNA plasmid for wg:tag	Fillip Port	CRISPR/Cas9 tagging
pBluescript SK (+)	GenBank: X52325.1	AddGene	XhoI, HindIII
pBP02	Wg-mScarlet-HR donor	Generated plasmid	CRISPR/Cas9 tagging
pFP030	mEGFP MS2 SV40	Fillip Port	PCR amplification
pCFD5	For Evi tagging gRNA plasmids	Fillip Port	PCR amplification

Plasmid	Plasmid content	Source	Purpose
pBP04	Evi-mScarlet-1 donor	Generated plasmid	CRISPR/Cas9 tagging
pBP05	Evi-mScarlet-2 donor	Generated plasmid	CRISPR/Cas9 tagging
pBP06	Evi-mScarlet-3 donor	Generated plasmid	CRISPR/Cas9 tagging
pBP07	Evi-mScarlet-4 donor	Generated plasmid	CRISPR/Cas9 tagging
pBP08	Evi-mScarlet-5 donor	Generated plasmid	CRISPR/Cas9 tagging
pBP09	Evi-mScarlet-6 donor	Generated plasmid	CRISPR/Cas9 tagging
pBP10	gRNA plasmid for Evi-Site1	Generated plasmid	CRISPR/Cas9 tagging
pBP11	gRNA plasmid for Evi-Site2	Generated plasmid	CRISPR/Cas9 tagging
pBP12	gRNA plasmid for Evi-Site3	Generated plasmid	CRISPR/Cas9 tagging
pBP13	gRNA plasmid for Evi-Site4	Generated plasmid	CRISPR/Cas9 tagging
pBP14	gRNA plasmid for Evi-Site5	Generated plasmid	CRISPR/Cas9 tagging
pBP15	gRNA plasmid for Evi-Site6	Generated plasmid	CRISPR/Cas9 tagging
pBP27	Evi-EGFP-5 donor	Generated plasmid	CRISPR/Cas9 tagging
pCFD6	For UAS-LAMA-hook plasmids	Fillip Port	PCR amplification
NTOM001	TOM20-LAMA_F98-hook	Helen Farrants	PCR amplification
NTOM004	TOM29-LAMA_G97-hook	Helen Farrants	PCR amplification
pBP28	UAS-Mito_TOM20-LAMA-hook	Generated plasmid	Transgenic insertion
pBP29	UAS-ER_KDEL-LAMA-hook	Generated plasmid	Transgenic insertion

Table 2: List of primers used for cloning

Primer (pair) name	Forward primer sequence Reverse primer sequence	Purpose
pFP450 Backbone	ATCGCCTCGAAGCCAAAGGGC AGATCTGGGTGCACGAACCGAG	Backbone amplification from pFP450 for wg-mScarlet tagging
pFP450 mScarlet	AAGGGCGCCTCGGTTCGTGCACCCAGATC TATGGTTAGTAAGGGCGAAGCTG AACCGAGGCGCCCTTTGGCTTCGAGGCGA TCTTATACAGTTCATCCATTCCGCC	mScarlet amplification for wg-mScarlet tagging from pFP889 with pFP450 backbone overhangs
Wg genotyping	AGAGTGTGTGTGCCGTCGAACAG GGCTTCCGCATTTGGTGCGTGACG	Primers for genotyping Wg:tag within the HR regions
Wg HR genotyping	GAAGCGGCCAAGCAATGGATGAGG TCGCTGGGTCCATGTACATGATGGG	Primers for genotyping Wg:tag from outside the HR regions
Evi-Site1-5HR	GGCGAATTGGGTACCGGGCCCCCCCTCGA GTCAGCAACTGCCGCACACGCTAA ACTAGTGGATCCCCCGGGCTGCAGGAATT CGAAGACCAGTACAGCAGGAAACTGGTGT CATTCTGG	5’ homology arm for Evi:tag-1 insertion site, including BbsI restriction digestion sequence, for amplification from *Drosophila* genomic DNA

Primer (pair) name	Forward primer sequence Reverse primer sequence	Purpose
Evi-Site1-3HR	TCGAAGCCAAAGGGCGCCTCGGTTCGTGCATCACGCGGTGCAGGAGCCTGCAT ATCCCCCGGGCTGCAGGAATTCGAAGACCAAAGTCATGGCCACCTTAGCGCCCAG	3' homology arm for Evi:tag-1 insertion site, for amplification from *Drosophila* genomic DNA
Evi-Site2-5HR	GGCGAATTGGGTACCGGGCCCCCCCTCGAGCTTCCGCTTTACACTAGATTACGCAGCT ACTAGTGGATCCCCCGGGCTGCAGGAATTCGAAGACCAAGAAGTGACACAATCCAGGTAGCGAT	5' homology arm for Evi:tag-2 insertion site, including BbsI restriction digestion sequence, for amplification from *Drosophila* genomic DNA
Evi-Site2-3HR	TCGAAGCCAAAGGGCGCCTCGGTTCGTGCACATGTGGGTCCCACAGAAACGCTGTA ATCCCCCGGGCTGCAGGAATTCGAAGACCAAACAAGGGTGTCCCGCAAAACTAATT	3' homology arm for Evi:tag-2 insertion site for amplification from *Drosophila* genomic DNA
Evi-Site3-5HR	GGCGAATTGGGTACCGGGCCCCCCCTCGAGCAGCGCAGGGCAGTAAACCAGTGA ACTAGTGGATCCCCCGGGCTGCAGGAATTCGAAGACCAATGCACTCGCCTCCAGAACCATATC	5' homology arm for Evi:tag-3 insertion site, including BbsI restriction digestion sequence, for amplification from *Drosophila* genomic DNA
Evi-Site3-3HR	TCGAAGCCAAAGGGCGCCTCGGTTCGTGCACTGCTGCAACGATCCCCCGCCCT ATCCCCCGGGCTGCAGGAATTCGAAGACCACGCGGTATTATTTCAGTGGAGCTTCTGG	3' homology arm for Evi:tag-3 insertion site for amplification from *Drosophila* genomic DNA
Evi-Site4-5HR	GGCGAATTGGGTACCGGGCCCCCCCTCGAGTGTCACCGTGCTGGGATCGCTGT ACTAGTGGATCCCCCGGGCTGCAGGAATTCCGTCTCCCGACTTGTTCGGAGCATCCTGAATGAGC	5' homology arm for Evi:tag-4 insertion site, including Esp3I restriction digestion sequence, for amplification from *Drosophila* genomic DNA
Evi-Site4-3HR	TCGAAGCCAAAGGGCGCCTCGGTTCGTGCAACCATTCGCTCGCGTTACTGGAAAC ATCCCCCGGGCTGCAGGAATTCGAAGACCACCTCGGCCATTTGGCCCATAATGAA	3' homology arm for Evi:tag-4 insertion site for amplification from *Drosophila* genomic DNA

Primer (pair) name	Forward primer sequence Reverse primer sequence	Purpose
Evi-Site5-5HR	GGCGAATTGGGTACCGGGCCCCCCCTCGAGGAAGACCAAATGTGGCAATTCAGCCAACTTCCGC ACTAGTGGATCCCCCGGGCTGCAGGAATTCCTACCGCACTCCTCAAAGGATCATATGGT	5' homology arm for Evi:tag-5 insertion site for amplification from *Drosophila* genomic DNA
Evi-Site5-3HR	GGGTACCGGGCCCCCCCTCGAGGAAGACCAACCATTCGCTCGCGTTACTGGAAACAT AACCGAGGCGCCCTTTGGCTTCGAGGCGATGTCGTTCCAGTCCCACTGGCCCTC	3' homology arm for Evi:tag-5 insertion site, including BbsI restriction digestion sequence, for amplification from *Drosophila* genomic DNA
Evi-Site6-5HR	GGCGAATTGGGTACCGGGCCCCCCCTCGAGGCCGGAGTTTCGGCAGCCATTTATT ACTAGTGGATCCCCCGGGCTGCAGGAATTCGAAGACCACATTGTCGGCCATTGCTTGTGACTGG	5' homology arm for Evi:tag-6 insertion site, including BbsI restriction digestion sequence, for amplification from *Drosophila* genomic DNA
Evi-Site6-3HR	TCGAAGCCAAAGGGCGCCTCGGTTCGTGCACACCACAGTGACGAGACCACACAGTCG ATCCCCCGGGCTGCAGGAATTCGAAGACCAGGCTGGAGCTCGGAGCTCATCTGC	3' homology arm for Evi:tag-6 insertion site for amplification from *Drosophila* genomic DNA
Evi-Site1-Scarlet (Fw)	CGCCAGAATGACACCAGTTTCCTGCTGTACATCGCCTCGAAGCCAAAGGCAGGAAGCGTTCGTGCACCCAGATCTAT	Combined with Evi-Scarlet-BbsI (Rv) for Scarlet insert from pBP02 into BlueScript(+) with Site1-5HR after BbsI digestion
Evi-Site2-Scarlet (Fw)	GAGCATCGCTACCTGGATTGTGTCACTTCTATCGCCTCGAAGCCAAAGGGC	Combined with pFP450 mScarlet (Rv) for Scarlet insert from pBP02 into BlueScript(+) with Site2-5HR after BbsI digestion
Evi-Site3-Scarlet (Fw)	ATCATGATATGGTTCTGGAGGCGAGTGCATATCGCCTCGAAGCCAAAGGGCGCCTCGGTTCGTGCACCCAGATCTAT	Combined with pFP450 mScarlet (Rv) for Scarlet insert from pBP02 into BlueScript(+) with Site3-5HR after BbsI digestion
Evi-Site6-Scarlet (Fw)	GCGCCCAGTCACAAGCAATGGCCGACAATGATCGCCTCGAAGCCAAAGGGC	Combined with pFP450 mScarlet (Rv) for Scarlet insert from pBP02 into BlueScript(+) with Site6-5HR after BbsI digestion

Primer (pair) name	Forward primer sequence Reverse primer sequence	Purpose
Evi-Scarlet-BbsI (Rv)	ATCCCCCGGGCTGCAGGAATTCGAAGACC ATGCACGAACCGAGGCGCCCTTTGGCTTC GAGGCGATCTTATACA	Reverse primer for Scarlet insert for Sites 1, 2, 3 and 6
Evi-Site4-Scarlet	ATGCTCATTCAGGATGCTCCGAACAAGTCG ATCGCCTCGAAGCCAAAGGGCGCCTCGGT TCGTGCACCCAGATCTAT	Scarlet insert from pBP02 for Evi-Site4, including BsmBI restriction digestion sequence
	GATCCCCCGGGCTGCAGGAATTCCGTCTCC TGCACGAACCGAGGCGCCCTTTGGCTTCG AGGCGATCTTATACAG	
Evi-Site5-Scarlet	GGGTACCGGGCCCCCCCTCGAGGAAGACC AATCGCCTCGAAGCCAAAGGGC	Scarlet insert from pBP02 for Evi-Site5, after insertion of Site5 3' homology arm
	GAAGGCGGAAGTTGGCTGAATTGCCACAT TTGCACGAACCGAGGCGCCCT	
gRNA Evi-Site1	TGCAAGTTTCCTGCTGTACTCACG	Top and bottom oligos for insertion of Evi-Site1 sgRNA into pCFD5 vector
	AAACCGTGAGTACAGCAGGAAACT	
gRNA Evi-Site2	TGCAGGATTGTGTCACTTCTCATG	Top and bottom oligos for insertion of Evi-Site2 sgRNA into pCFD5 vector
	AAACCATGAGAAGTGACACAATCC	
gRNA Evi-Site3	TGCAGCATCATGATATGGTTCTGG	Top and bottom oligos for insertion of Evi-Site3 sgRNA into pCFD5 vector
	AAACCCAGAACCATATCATGATGC	
gRNA Evi-Site4	TGCATTTCCAGTAACGCGAGCGAA	Top and bottom oligos for insertion of Evi-Site4 sgRNA into pCFD5 vector
	AAACTTCGCTCGCGTTACTGGAAA	
gRNA Evi-Site5	TGCAGTGGGACTGGAACGACAATG	Top and bottom oligos for insertion of Evi-Site5 sgRNA into pCFD5 vector
	AAACCATTGTCGTTCCAGTCCCAC	
gRNA Evi-Site6	TGCATCGTCACTGTGGTGCATTGT	Top and bottom oligos for insertion of Evi-Site6 sgRNA into pCFD5 vector
	AAACACAATGCACCACAGTGACGA	
Scarlet genotyping	AGGTACACATGGAGGGTTCG	Primers for amplification within the mScarlet sequence
	ACCTACCACCATCTTTGAGCC	
EGFP genotyping	ATGGTGAGCAAGGGCGAGGA	Primers for amplification within the EGFP sequence
	CTTGTACAGCTCGTCCATGCCG	
Evi-Site1 HR genotyping	GCCATTGAGTGCTCTTTTGCCTCGA	Primers for genotyping Evi:tag-1 from outside the HR regions
	CATCGGCTGATGTGAATAAATTTGGAACT	

Primer (pair) name	Forward primer sequence Reverse primer sequence	Purpose
Evi-Site5 HR genotyping	TCTGGCTGGTCTTCGCCGGTGAA ATCTGCTGCTCAATGTGGCCACG	Primers for genotyping Evi:tag-5 from outside the HR regions
pCFD6 backbone	TCTAGAGGATCTTTGTGAAGGAACCTTACTTCT ACAAATATATATTGTATCGTAAATTTGGCTGTTTCGATAG	Backbone amplification for LAMA-hooks from pCFD6 plasmid
Mito-LAMA-hook	AATTTACGATACAATATATATTTGTATGGTGGGCCGCAACAGC CTTCACAAAGATCCTCTAGAGCTGCTCACGGTCACCTGGG	TOM20-SNAP-VHH_E-cpDHFR-VHH_E insert amplification from NTOM001 and NTOM004 into pCFD6 vector
LAMA-KDEL-pCFD6	AATTTACGATACAATATATATTTGTATGTCTAGAGATAAAGACTGCGAAATGAAACGCACTA CTTCACAAAGATCCTCTAGATCACAGTTCATCTTTACCACCGCTGCTCACGGTCACCTGGG	SNAP-VHH_E-cpDHFR-VHH_E-KDEL insert amplification from NTOM001 and NTOM004 into pCFD6 vector; KDEL added on reverse primer
LAMA-KDEL-Signal sequence gBlock	ACGATACAATATATATTTGTATGTCTAGAGATGTATGCGTCCGTCTTGCCCTGTGGCTCCTCTGGGGACTCCTCCTGCACCAGGGCCAGAGCCTCAGCCATAGTCACAGTGAGAAGGCGACAGGAACCAGCTCGGGCGCCTCTAGAGATAAAGACTGCGAAATGAA	ER signaling sequence from human STIM1 protein. XbaI digestion sites flanking the sequence for cloning into pCFD6 with LAMA-KDEL after XbaI digestion

5.2.2 Chemicals, kits and buffers

Table 3: Enzymes and associated buffers

Cloning enzymes and buffers	Supplier and reference	Buffer compatibility
BbsI-HF	NEB; R3539	CutSmart Buffer
Esp3I-FD	Thermo Scientific; FD0454	FastDigest Buffer
XhoI	NEB; R0146	CutSmart Buffer
BamHI-HF	NEB; R3136	CutSmart Buffer
XbaI	NEB; R014	CutSmart Buffer
CutSmart Buffer (10x)	NEB	
FastDigest Buffer (10x)	Thermo Scientific	
T4 DNA ligase	NEB M0202	T4 DNA ligase buffer
T4 polynucleotide kinase	NEB M0201	T4 DNA ligase buffer
T4 DNA ligase buffer (10x)	NEB B0202	

Cloning enzymes and buffers	Supplier and reference	Buffer compatibility
Proteinase K	Thermo Scientific, EO0491	
cOmplete Mini, EDTA-free Protease Inhibitor Cocktail	Roche 11836170001	

Table 4: Chemicals and consumables used in the project

Chemicals and Consumables	Reference	Supplier
Agarose NEEO Ultra-Quality	2267.4	Carl Roth
Amersham Hyperfilm ECL	GE28-9068	Sigma
Amersham Protran Western blotting membrane (nitrocellulose)	GE10600002	Sigma
Bicine	sc-216087A	Santa Cruz Biotechnology
Biotin	B4639	Sigma
BIS-Tris	sc-216088A	Santa Cruz Biotechnology
Bleach (Sodium hypochlorite solution)	1.05614	Sigma Aldrich
Carbenicillin disodium salt	A1491,0010	Th.Geyer
DMSO (dimethyl sulfoxide)	276855	Sigma Aldrich
EDTA, Tetrasodium Tetrayhdrate Salt	A5097,0500	AppliChem
Egg white from chicken	E0500	Sigma
Ethanol, ≥99.9%, EMSURE	1.00983.2511	Supelco
Oil 10S (fly injection oil)	24627.188	VWR Chemicals
Formaldehyde, 16%, Methanol-free	28906	Pierce
Glycerol	G5516	Sigma-Aldrich
Glycine	G7126	Sigma-Aldrich
Heptane	32287	Sigma-Aldrich
Methanol, ≥99.9%, EMSURE	1.06009.2511	Supelco
MOPS	A1076,0250	AppliChem
Nipagin (methyl 4-hydroxybenzoate)	1067575000	Sigma-Aldrich
Normal Goat Serum	5425S	Cell Signaling
NP-40 Surfact-Amps™ Detergent Solution	85124	Thermo Fisher
NuPAGE Novex 4-12% Bis-Tris Protein Gel	NP0323BOX	Life Technologies
Poly-L-lysine hydrobromide	P1524	Sigma
Schneider's Insect Medium	S0146	Sigma
SOC medium	15544034	Life Technologies
Sodium Dodecyl Sulfate (SDS)	75746	Sigma
Stellar Competent Cells	ID: 636766	Takara Bio
SYBR Safe DNA Gel Stain	S33102	Life Technologies
Trimethoprim (TMP)	T7883	Sigma
Tris-Base	4855.2	Carl Roth

Chemicals and Consumables	Reference	Supplier
Triton X-100	T8787	Sigma
VectaShield Mounting Medium	VEC-H-1000	Biozol Diagnostica

Table 5: Kits used in the project

Kit	Reference	Supplier
BCA Protein-Assay Kit	23227	Pierce
Immobilon Western Chemiluminescent HRP substrate	WBKLS0100	Merck Millipore
In-Fusion HD Cloning Kit	639650	Takara Bio
MinElute PCR Purification Kit	28004	QIAGEN
QIAprep Spin Miniprep Kit	27104	QIAGEN
QIAquick Gel Extraction Kit	28706	QIAGEN
Restore Western Blot Stripping Buffer	21059	Thermo Scientific
SuperSignal West Femto Maximum Sensitivity Substrate	34094	Thermo Scientific
Western Blot Signal Enhancer	21050	Pierce

Table 6: Buffer recipes

Buffer	Purpose	Composition
Apple juice-agar plates (egg-laying plates)	*Drosophila* egg injections	2,25g agar, 75mL dH_2O; 25mL apple juice, 2,5g dextrose, 0,15g nipagin
Biotin-deficient fly food	RUSH System	20g powdered egg white in 20mL ddH2O added to 230mL normal fly food
LB agar medium	Bacterial culturing for cloning	1L LB liquid medium, 15g Agar; 1:1000 antibiotics added before use
LB liquid medium	Bacterial culturing for cloning	1% Tryptone, 1% NaCl, 0.5% yeast extract in ddH_2O, pH 7.0; 1:1000 antibiotics added before use
Live Imaging Medium	Drosophila organ live imaging	Whole fly extract 500ul, pen/strep 100ul, insulin 100ul, juvenile hormone 1330ul, hidroxy-ecdysone 830ul, rest 7140ul, TMP 323uL and schneider's medium 6817ul
Lysis buffer	Wing disc lysis for surface protein biotinylation assay	PBS, 2% NP-40, 0.2% SDS, proteinase inhibitors

Buffer	Purpose	Composition
MOPS buffer (20x)	SDS-PAGE running buffer	1M MOPS, 1M Tris-Base, 20mM EDTA, 69.3mM SDS in ddH_20
Normal fly food	Fly husbandry	30L H2O, 240g Agar, 660g sugar beet syrup, 2.4kg malt, 2.4kg corn flour, 300g soja flour, 540g beer yeast, 72g nipagin, 500ml 37% propionic acid, 500ml 3% phosphoric acid
NuPage transfer buffer (20x)	Western blot transfer buffer	500mM Bicine, 500mM Bis-Tris, 20mM EDTA; 10% Methanol added right before use
PBS (1x)	Immunofluorescence	Sigma P4417 – 1 tablet (137mM NaCL, 2.7mM KCl, 10mM Na2HPO4, pH 7.4) in 200mL ddH2O
PBST (0.3%)	Immunofluorescence	0.3% Triton X-100 in PBS (1x)
Squishing buffer	*Drosophila* DNA extraction	10 mM Tris-Cl pH 8.2, 1 mM EDTA, 25 mM NaCl. 200 ug/ml Proteinase K added fresh immediately before DNA extraction.
TAE buffer (50x)	Gel electrophoresis	50mM EDTA, 2M Tris, 1M acetic acid
TBST buffer (10x)	Western blot staining	1.37M NaCL, 200mM Tris-HCl, pH 7.6, 1% Tween-20

5.2.3 Fly lines

Table 7: Fly lines used in the project

Fly line name	Genotype	Source
w^{1118}/wildtype	w^{1118};;	Lab collection
Vasa-int; attP40	*y w M(eGFP, vas-int, dmRFP)ZH-2A; P{CaryP}attP40*	Lab collection
VK00033	*y w M(eGFP, vas-int, dmRFP)ZH-2A;; PBac{y[+]-attP-3B}VK00033*	Lab collection
If 2nd chr balancer	;If/CyO;	Lab collection
Sp 2nd chr balancer	y w Flp;wg^{sp}/CyO;	Lab collection

Fly line name	Genotype	Source
3rd chr balancer	;;Sb/TM6B	Lab collection
Double balancer	;If/CyO;Sb/TM6B	Lab collection
nos-cas9	y[1] M{w[+mC]=nanos-Cas9.P}ZH-2A w[*]	BDSC 54591
hh-gal4	;If/CyO; P{Gal4}hh-Gal4/TM6B	Lab collection
hh-gal4, UAS-u^{M}-Cas9	P{ry[+t7.2]=hsFLP}12, y[1] w[*]; P{y[+t7.7] w[+mC]=UAS-uMCas9}attP40; P{Gal4}hh-Gal4/TM6B	VDRC 340019
en-Gal4	; P{Gal4}en-Gal4/CyO;	Lab collection
nub-Gal4	;nubbin-Gal4;	Lab collection
sgs3-Gal4	w; P{w[+mC]=Sgs3-GAL4.PD}TP1	BDSC 6870
ptc-Gal80^{ts}	;ptc-Gal4 tub-Gal80^{ts}; Sb/TM6B	Lab collection
vvl-Gal4	w; P{y[+t7.7] w[+mC]=GMR17C08-GAL4}attP2	BDSC 48761
wg-Gal4	;wg-Gal4/CyO-GFP;	Lab collection
Wg:EGFP	y w Flp; wg:egfp;	Port et al., 2014
Wg:mScarlet	y w Flp; wg:mscarlet;	Generated stock
Evi:EGFP-5	w;;evi:egfp-5	Generated stock
Evi:mScarlet-1	w;;evi:mscarlet-1	Generated stock
Evi:mScarlet-5	w;;evi:mscarlet-5	Generated stock
Wg:EGFP; Evi:mScarlet	w; wg:egfp; evi:mscarlet	Generated stock
Wg:EGFP; hh-Gal4 Evi:mScarlet	w; wg:egfp; P{Gal4}hh-Gal4 UAS-u^{M}-Cas9 evi:mscarlet/TM6B	Generated stock
Wg:EGFP Dll:Tom; hh-Gal4	w; wg:egfp dll:tomato; P{Gal4}hh-Gal4 UAS-u^{M}-Cas9/TM6B	Michaela Holzem
Fz3-RFP	w[*]; P{w[+mC]=fz3-RFP.O}3	BDSC 92358
hh-Gal4 Fz3-RFP	;If/CyO; hh-Gal4 Fz3-RFP/TM6B	Generated stock
Wg gRNA	y w;P{U6:3-gRNA-wg.FP411};	Port et al., 2015
Evi gRNA	y w; P{U6:3-gRNA-wg.FP854};	Port et al., 2015
Wg RNAi	;P{KK108857}VIE-260B;	VDRC 104579KK
Evi RNAi	;P{KK101700}VIE-260B;	VDRC 103812KK
Evi^{2} FRT80	;;evi^{2} FRT80/TM3	Lab collection
FRT80B	;;ubi-gfp FRT80B	Lab collection
RUSH-Rab7	w*; UAS-SBP-YFP-Rab7@VK00002/CyO;	WellGenetics Inc
RUSH-RabX1	w*; UAS-SBP-YFP-RabX1@VK00002/CyO;	WellGenetics Inc
Golgi-RUSH-hook	w*/y1 w* P{nos-phiC31\int.NLS}X; L1/+; UAS-Streptavidin-Golgin84@VK00033/TM6B	WellGenetics Inc
RUSH-Rab7; Golgi-RUSH-hook	w*; UAS-SBP-YFP-Rab7/CyO; UAS-Streptavidin-Golgin84/TM6B	Generated stock

Fly line name	Genotype	Source
ER-RUSH-hook (Ii)	w*/y1 w* P{nos-phiC31\int.NLS}X; L1/+; UAS-Streptavidin-Ii@VK00033/TM6B	WellGenetics Inc
RUSH-RabX1; ER-RUSH-hook	w*; UAS-SBP-YFP-RabX1/CyO; UAS-Streptavidin-Ii/TM6B	Generated stock
Golgi-LAMA-hook	w*/y1 w* M{vas-int.Dm}ZH-2A; UAS-VHHEnhancerG97-cpDHFR-VHHE-Golgin84@VK00033/TM6B	WellGenetics Inc
RUSH-Rab7; Golgi-LAMA-hook	w*; UAS-SBP-YFP-Rab7/CyO; UAS-VHHEnhancerG97-cpDHFR-VHHE-Golgin84/TM6B	Generated stock
Mito-LAMA-hook	w*; If/CyO; UAS-TOM20-VHHEnhancerG97-cpDHFR-VHHE@VK00033/TM6B	Generated stock
RUSH-Rab7; Mito-LAMA-hook	w*; UAS-SBP-YFP-Rab7/CyO; UAS-TOM20-VHHEnhancerG97-cpDHFR-VHHE/TM6B	Generated stock
en-Gal4; Mito-LAMA-hook	w*; en-Gal4/CyO; UAS-TOM20-VHHEnhancerG97-cpDHFR-VHHE/TM6B	Generated stock
ER-LAMA-hook (III)	w*; If/CyO; UAS-SS-VHHEnhancerG97-cpDHFR-KDEL@VK00033/TM6B	Generated stock
ER-LAMA-hook (II)	w*; UAS-SS-VHHEnhancerG97-cpDHFR-KDEL@attP40/CyO; Sb/TM6B	Generated stock
Wg:EGFP; ER-LAMA-hook	w*; wg:egfp: UAS-SS-VHHEnhancerG97-cpDHFR-KDEL/TM6B	Generated stock
ER-LAMA-hook; Evi:EGFP	w*; UAS-SS-VHHEnhancerG97-cpDHFR-KDEL/CyO; evi:egfp	Generated stock
Sgg:GFP	y[1] Mi{PT-GFSTF.1}sgg[MI11971-GFSTF.1] w[*]/FM7c	BDSC 66770
Rab1 WT	y[1] w[*]; P{w[+mC]=UAST-YFP.Rab1}Mes2[01]	BDSC 24104
Rab1 CA	y[1] P{w[+mC]=UASp-YFP.Rab1.Q70L}CG3638[12c] w[*]	BDSC 23234
Rab1 DN	y[1] w[*]; P{w[+mC]=UAST-YFP.Rab1.S25N}01	BDSC 9757
Rab1 RNAi	y[1] sc[*] v[1] sev[21]; P{y[+t7.7] v[+t1.8]=TRiP.HMS01148}attP2	BDSC 34670
Rab1 KO	w[1118]; PBac{w[+mC]=RB}Rab1[e01287]/TM6B, Tb[1]	BDSC 17936
Rab2 WT	y[1] w[*]; P{w[+mC]=UAST-YFP.Rab2}l(3)neo38[02]/TM3, Sb[1]	BDSC 23246
Rab2 CA	y[1] w[*]; P{w[+mC]=UASp-YFP.Rab2.Q65L}02	BDSC 9760
Rab2 DN	y[1] w[*]; P{w[+mC]=UAST-YFP.Rab2.S20N}hlk[01]/CyO	BDSC 9759

Fly line name	Genotype	Source
Rab2 RNAi	y[1] sc[*] v[1] sev[21]; P{y[+t7.7] v[+t1.8]=TRiP.HMS01271}attP2	BDSC 34922
Rab2 KO	;TI{GAL4}Rab2$^{Gal4\text{-}KO}$;	Kohrs et al., 2021
Rab3 WT	y[1] w[*]; P{w[+mC]=UASp-YFP.Rab3}lolal[02]	BDSC 9762
Rab3 CA	y[1] w[*]; P{w[+mC]=UASp-YFP.Rab3.Q80L}11	BDSC 9764
Rab3 DN	y[1] w[*]; P{w[+mC]=UASp-YFP.Rab3.T35N}04L	BDSC 9766
Rab3 RNAi	y[1] sc[*] v[1] sev[21]; P{y[+t7.7] v[+t1.8]=TRiP.HMS01131}attP2	BDSC 34655
Rab3 KO	w[*]; Rab3[rup]	BDSC 78045
Rab4 WT	y[1] w[*]; P{w[+mC]=UASp-YFP.Rab4}Sap-r[32]	BDSC 9767
Rab4 CA	y[1] w[*]; P{w[+mC]=UASp-YFP.Rab4.Q67L}fz2[28]	BDSC 9770
Rab4 DN	y[1] w[*]; P{w[+mC]=UASp-YFP.Rab4.S22N}37	BDSC 9768
Rab4 RNAi	y[1] sc[*] v[1] sev[21]; P{y[+t7.7] v[+t1.8]=TRiP.HMS01100}attP2	BDSC 33757
Rab4 KO	;TI{GAL4}Rab4$^{Gal4\text{-}KO}$;	Kohrs et al., 2021
Rab5 WT	y[1] w[*]; P{w[+mC]=UASp-YFP.Rab5}02	BDSC 24616
Rab5 CA	y[1] w[*]; P{w[+mC]=UASp-YFP.Rab5.Q88L}Reph[24]	BDSC 9774
Rab5 DN	y[1] w[*]; P{w[+mC]=UASp-YFP.Rab5.S43N}01	BDSC 9771
Rab5 RNAi	y[1] sc[*] v[1] sev[21]; P{y[+t7.7] v[+t1.8]=TRiP.HMS00147}attP2	BDSC 34832
Rab5 KO	w; Rab5^{2} P{neoFRT}40A/CyO	Wucherpfennig et al., 2003
Rab6 WT	y[1] w[*]; P{w[+mC]=UAST-YFP.Rab6}Ip6k[01]/CyO	BDSC 23251
Rab6 CA	y[1] w[*]; P{w[+mC]=UASp-YFP.Rab6.Q71L}05	BDSC 9776
Rab6 DN	y[1] w[*]; P{w[+mC]=UAST-YFP.Rab6.T26N}01	BDSC 23249
Rab6 RNAi	y[1] sc[*] v[1] sev[21]; P{y[+t7.7] v[+t1.8]=TRiP.HMS01486}attP2	BDSC 35744
Rab6 KO	w[*]; Rab6[D23D]/CyO; ry[506]	BDSC 5821
Rab7 WT	w[*]; P{w[+mC]=UAS-Rab7.GFP}3	BDSC 42706
Rab7 CA	y[1] w[*]; P{w[+mC]=UASp-YFP.Rab7.Q67L}19	BDSC 24103
Rab7 DN	y[1] w[*]; P{w[+mC]=UASp-YFP.Rab7.T22N}06	BDSC 9778
Rab7 RNAi	y[1] v[1]; P{y[+t7.7] v[+t1.8]=TRiP.JF02377}attP2	BDSC 27051
Rab7 KO	;Sp/CyO; P{neoFRT}82B, Rab7Gal4-KO /TM3	Cherry et al., 2013
Rab8 WT	y[1] w[*]; P{w[+mC]=UASp-YFP.Rab8}45	BDSC 9782
Rab8 CA	y[1] w[*]; P{w[+mC]=UASp-YFP.Rab8.Q67L}05	BDSC 9781

Fly line name	Genotype	Source
Rab8 DN	y[1] w[*]; P{w[+mC]=UASp-YFP.Rab8.T22N}12	BDSC 9780
Rab8 RNAi	y[1] sc[*] v[1] sev[21]; P{y[+t7.7] v[+t1.8]=TRiP.HMS01363}attP2	BDSC 34373
Rab8 KO	Rab8[1] red[1] e[4]/TM6B, Sb[1] Tb[1] ca[1]	BDSC 26173
Rab9 WT	y[1] w[*]; P{w[+mC]=UASp-YFP.Rab9}22	BDSC 9784
Rab9 CA	w[*]; P{w[+mC]=UASp-YFP.Rab9.Q71L}20	BDSC 9785
Rab9 DN	y[1] w[*]; P{w[+mC]=UASp-YFP.Rab9.S26N}04	BDSC 23642
Rab9 RNAi	y[1] sc[*] v[1] sev[21]; P{y[+t7.7] v[+t1.8]=TRiP.HMS02635}attP40	BDSC 42942
Rab9 KO	;TI{TI}Rab9^{CRISPR};	Kohrs et al., 2021
Rab10 WT	y[1] w[*]; P{w[+mC]=UASp-YFP.Rab10}21	BDSC 9789
Rab10 CA	y[1] w[*]; P{w[+mC]=UASp-YFP.Rab10.Q68L}27a	BDSC 9787
Rab10 DN	y[1] w[*]; P{w[+mC]=UASp-YFP.Rab10.T23N}15	BDSC 9788
Rab10 RNAi	y[1] v[1]; P{y[+t7.7] v[+t1.8]=TRiP.JF02058}attP2	BDSC 26289
Rab10 KO	TI{TI}Rab10^{CRISPR}/FM7;;	Kohrs et al., 2021
Rab11 WT	y[1] w[*]; P{w[+mC]=UASp-YFP.Rab11}sra[32]/TM3, Sb[1]	BDSC 9790
Rab11 CA	y[1] w[*]; P{w[+mC]=UASp-YFP.Rab11.Q70L}CG13895[31]	BDSC 9791
Rab11 DN	y[1] w[*]; P{w[+mC]=UASp-YFP.Rab11.S25N}35	BDSC 9792
Rab11 RNAi	y[1] v[1]; P{y[+t7.7] v[+t1.8]=TRiP.JF02812}attP2	BDSC 27730
	w[*]; P{w[+mC]=EP}Rab11[EP3017]/TM6B, Tb[1]	BDSC 42708
Rab14 WT	y[1] w[*]; P{w[+mC]=UASp-YFP.Rab14}CG9967[5L]	BDSC 9793
Rab14 CA	y[1] w[*]; P{w[+mC]=UASp-YFP.Rab14.Q94L}Sos[02]	BDSC 9795
Rab14 DN	y[1] w[*]; P{w[+mC]=UASp-YFP.Rab14.S49N}Cse1[01] mdy[01]/CyO	BDSC 23263
Rab14 RNAi	y[1] sc[*] v[1] sev[21]; P{y[+t7.7] v[+t1.8]=TRiP.HMS01130}attP2	BDSC 34654
Rab14 KO	;TI{TI}Rab14^{CRISPR};	Kohrs et al., 2021
Rab18 WT	y[1] w[*]; P{w[+mC]=UAST-YFP.Rab18}CG9775[01]	BDSC 9796
Rab18 CA	y[1] w[*]; P{w[+mC]=UASp-YFP.Rab18.A64L}Ptp99A[02]	BDSC 9797
Rab18 DN	y[1] w[*]; P{w[+mC]=UAST-YFP.Rab18.S19N}03	BDSC 23238
Rab18 RNAi	y[1] sc[*] v[1] sev[21]; P{y[+t7.7] v[+t1.8]=TRiP.HMS01214}attP2	BDSC 34734
Rab18 KO	TI{TI}Rab18^{CRISPR};;	Kohrs et al., 2021

Fly line name	Genotype	Source
Rab19 WT	y[1] w[*]; P{w[+mC]=UAST-YFP.Rab19}Hr39[02]	BDSC 24150
Rab19 CA	y[1] w[*]; P{w[+mC]=UASp-YFP.Rab19.Q80L}06	BDSC 9800
Rab19 DN	y[1] w[*]; P{w[+mC]=UAST-YFP.Rab19.T35N}04/TM3, Sb[1]	BDSC 9799
Rab19 RNAi	y[1] sc[*] v[1] sev[21]; P{y[+t7.7] v[+t1.8]=TRiP.HMS00592}attP2	BDSC 34607
Rab19 KO	;;TI{GAL4}Rab19$^{Gal4\text{-}KO}$	Kohrs et al., 2021
Rab21 WT	y[1] w[*]; P{w[+mC]=UAST-YFP.Rab21}smog[04]	BDSC 23242
Rab21 CA	y[1] w[*] P{w[+mC]=UASp-YFP.Rab21.Q73L}rg[09] CG15465[09]	BDSC 9801
Rab21 DN	y[1] w[*]; P{w[+mC]=UAST-YFP.Rab21.T27N}03	BDSC 23241
Rab21 RNAi	y[1] v[1]; P{y[+t7.7] v[+t1.8]=TRiP.JF03338}attP2	BDSC 29403
Rab21 KO	TI{TI}Rab21^{CRISPR};;	Kohrs et al., 2021
Rab23 WT	y[1] w[*]; P{w[+mC]=UASp-YFP.Rab23}01	BDSC 9802
Rab23 CA	y[1] w[*]; P{w[+mC]=UASp-YFP.Rab23.Q96L}04	BDSC 9806
Rab23 DN	y[1] w[*]; P{w[+mC]=UASp-YFP.Rab23.S51N}01	BDSC 9804
Rab23 RNAi	y[1] sc[*] v[1] sev[21]; P{y[+t7.7] v[+t1.8]=TRiP.HMC04039}attP40	BDSC 55352
Rab23 KO	;;TI{TI}Rab23^{CRISPR}	Kohrs et al., 2021
Rab26 WT	y[1] w[*]; P{w[+mC]=UAST-YFP.Rab26}Lmpt[01]	BDSC 23244
Rab26 CA	y[1] w[*]; P{w[+mC]=UAST-YFP.Rab26.Q250L}01	BDSC 23243
Rab26 DN	y[1] w[*]; P{w[+mC]=UAST-YFP.Rab26.T204N}tou[02]	BDSC 9807
Rab26 RNAi	y[1] v[1]; P{y[+t7.7] v[+t1.8]=TRiP.JF01684}attP2	BDSC 31177
Rab26 KO	;;TI{TI}Rab26^{CRISPR}	Kohrs et al., 2021
Rab27 WT	y[1] w[*]; P{w[+mC]=UASp-YFP.Rab27}14	BDSC 24769
Rab27 CA	y[1] w[*]; P{w[+mC]=UASp-YFP.Rab27.Q74L}07	BDSC 9811
Rab27 DN	y[1] w[*]; P{w[+mC]=UASp-YFP.Rab27.T25N}nsl1[02]	BDSC 23267
Rab27 RNAi	y[1] sc[*] v[1] sev[21]; P{y[+t7.7] v[+t1.8]=TRiP.HMS01523}attP2	BDSC 35774
Rab27 KO	TI{GAL4}Rab27$^{Gal4\text{-}KO}$;;	Chan et al., 2011
Rab30 WT	y[1] w[*]; P{w[+mC]=UASp-YFP.Rab30}Cdk4[10]	BDSC 9812
Rab30 CA	y[1] w[*]; P{w[+mC]=UASp-YFP.Rab30.Q66L}11	BDSC 9814
Rab30 DN	y[1] w[*]; P{w[+mC]=UASp-YFP.Rab30.T21N}wdb[07]	BDSC 9813
Rab30 RNAi	y[1] v[1]; P{y[+t7.7] v[+t1.8]=TRiP.JF01593}attP2	BDSC 31120
Rab30 KO	;TI{GAL4}Rab30$^{Gal4\text{-}KO}$/CyO;	Kohrs et al., 2021

Fly line name	Genotype	Source
Rab32 WT	y[1] w[*]; P{w[+mC]=UASp-YFP.Rab32}RhoGDI[11]	BDSC 9815
Rab32 CA	y[1] w[*]; P{w[+mC]=UASp-YFP.Rab32.Q79L}sprt[08]	BDSC 9816
Rab32 DN	y[1] w[*]; P{w[+mC]=UASp-YFP.Rab32.T33N}Eb1[04]	BDSC 23281
Rab32 RNAi	y[1] v[1]; P{y[+t7.7] v[+t1.8]=TRiP.HMS01870}attP40/CyO	BDSC 38956
Rab32 KO	;Rab32[ltd-1]/CyO;	BDSC 338
Rab35 WT	y[1] w[*]; P{w[+mC]=UASp-YFP.Rab35}15	BDSC 9821
Rab35 CA	y[1] w[*]; P{w[+mC]=UASp-YFP.Rab35.Q67L}11	BDSC 9818
Rab35 DN	y[1] w[*]; P{w[+mC]=UAST-YFP.Rab35.S22N}01	BDSC 9819
Rab35 RNAi	y[1] sc[*] v[1] sev[21]; P{y[+t7.7] v[+t1.8]=TRiP.HMS06057}attP40	BDSC 80457
Rab35 KO	TI{TI}Rab35^{CRISPR}/FM7;;	Kohrs et al., 2021
Rab39 WT	y[1] w[*]; P{w[+mC]=UASp-YFP.Rab39}13	BDSC 9825
Rab39 CA	y[1] w[*] P{w[+mC]=UASp-YFP.Rab39.Q69L}02	BDSC 9822
Rab39 DN	y[1] w[*]; P{w[+mC]=UAST-YFP.Rab39.S23N}Ir76b[05]	BDSC 9824
Rab39 RNAi	y[1] v[1]; P{y[+t7.7] v[+t1.8]=TRiP.JF01973}attP2	BDSC 25953
Rab39 KO	TI{TI}Rab39^{CRISPR};;	Kohrs et al., 2021
Rab40 WT	y[1] w[*]; P{w[+mC]=UAST-YFP.Rab40}05	BDSC 23248
Rab40 CA	y[1] w[*]; P{w[+mC]=UASp-YFP.Rab40.Q75L}RhoGEF3[13]	BDSC 9827
Rab40 DN	y[1] w[*]; P{w[+mC]=UAST-YFP.Rab40.H25N}DIP-epsilon[04]	BDSC 9829
Rab40 RNAi	y[1] v[1]; P{y[+t7.7] v[+t1.8]=TRiP.HMS06073}attP40	BDSC 80472
Rab40 KO	TI{TI}Rab40^{CRISPR};;	Kohrs et al., 2021
RabX1 WT	y[1] w[*]; P{w[+mC]=UASp-YFP.RabX1}12	BDSC 9840
RabX1 CA	y[1] w[*]; P{w[+mC]=UASp-YFP.RabX1.Q66L}02	BDSC 9837
RabX1 DN	y[1] w[*]; P{w[+mC]=UAST-YFP.RabX1.T19N}Pabp2[01]/SM5	BDSC 9838
RabX1 RNAi	y[1] v[1]; P{y[+t7.7] v[+t1.8]=TRiP.JF02868}attP2	BDSC 28033
RabX1 KO	;TI{GAL4}RabX1$^{Gal4\text{-}KO}$/CyO;	Kohrs et al., 2021
RabX4 WT	y[1] w[*]; P{w[+mC]=UASp-YFP.RabX4}how[19]	BDSC 9851
RabX4 CA	y[1] w[*]; P{w[+mC]=UASp-YFP.RabX4.Q67L}hry[13a]/TM3, Sb[1]	BDSC 9848
RabX4 DN	y[1] w[*]; P{w[+mC]=UAST-YFP.RabX4.T40N}03	BDSC 9850

Fly line name	Genotype	Source
RabX4 RNAi	y[1] sc[*] v[1] sev[21]; P{y[+t7.7] v[+t1.8]=TRiP.HMS02787}attP40	BDSC 44070
RabX4 KO	;;TI{TI}RabX4^{CRISPR}/TM6B	Kohrs et al., 2021
RabX6 WT	y[1] w[*]; P{w[+mC]=UASp-YFP.RabX6}03	BDSC 23278
RabX6 CA	y[1] w[*]; P{w[+mC]=UASp-YFP.RabX6.M69L}Baldspot[27]	BDSC 23646
RabX6 DN	y[1] w[*]; P{w[+mC]=UAST-YFP.RabX6.S22N}02	BDSC 9856
RaBX6 RNAi	y[1] v[1]; P{y[+t7.7] v[+t1.8]=TRiP.JF02050}attP2	BDSC 26281
RabX6 KO	;;TI{GAL4}RabX6$^{Gal4-KO}$	Kohrs et al., 2021
Arl8 RNAi	w[1118]; P{GD10612}v26085	VDRC 26085GD
EEA1 RNAi	w[1118]; P{GD13947}v24114	VDRC 24114GD
Arl8 RNAi; Rab7-WT	Arl8 RNAi/CyO; UAS-Rab7-GFP/TM6B	Generated stock
EEA1 RNAi; Rab7-WT	EEA1 RNAi/CyO; UAS-Rab7-GFP/TM6B	Generated stock

5.2.4 Antibodies and dyes

Table 8: Primary antibodies used in the project

Antibody	Supplier and reference	Dilution, host (purpose)
α-Wg (concentrate)	DSHB 4D4	1:300 mouse (IF) 1:30 mouse (IF, Surface staining) 1:50 mouse (WB)
α-Sens	Gross et al., 2012	1:300 guinea pig (IF)
α-Evi	Port et al., 2008	1:800 rabbit (IF)
α-FasII (concentrate)	DSHB 1D4 anti-Fasciclin II	1:66 mouse (WB)
α-Tub	Cell Signaling Technology #2144	1:2000 (WB)
α-Streptavidin	Novus Biologicals S8E4 (NB120-10023)	1:100 mouse (IF)
α-Rab5	Abcam ab31261	1:500 rabbit (IF)
α-LAMP1	Abcam ab30687	1:100 rabbit (IF)
α-Arl8	DSHB Arl8	1:200 rabbit (IF)
α-Atg8	Sigma-Aldrich ZRB1585	1:50 rabbit (IF)

Table 9: Secondary antibodies and dyes used in the project

Antibody	Supplier and Reference	Dilution, host (purpose)
α-mouse Alexa Fluor 488	Invitrogen A21202	1:800 donkey (IF)
α-mouse Alexa Fluor 594	Invitrogen A21201	1:800 chicken (IF)

α-mouse Alexa Fluor 647	Invitrogen A21463	1:800 chicken (IF)
α-mouse HRP	Jackson ImmunoResearch AB_10015289	1:5000 goat (WB)
α-guinea pig Alexa Fluor 633	Invitrogen A21105	1:800 goat (IF)
α-rabbit Alexa Fluor 488	Invitrogen A11008	1:800 goat (IF)
α-rabbit Alexa Fluor 594	Invitrogen A11012	1:800 goat (IF)
α-rabbit Alexa Fluor 647	Invitrogen A21245	1:800 goat (IF)
α-rabbit HRP	Jackson ImmunoResearch AB_2313567	1:5000 goat (WB)
Hoechst 33342	Invitrogen H1399	1:2000 (IF)
SNAP-Cell 647-SiR	New England Biolabs S9102S	1:200 (IF)
MitoTracker Red CMXRos	Invitrogen M7512	1:2000 (IF)

6 References

6.1 Literature

1. **Aberle, H., Bauer, A., Stappert, J., Kispert, A., Kemler, R.,** 1997. beta-catenin is a target for the ubiquitin-proteasome pathway. EMBO J 16, 3797–3804. https://doi.org/10.1093/emboj/16.13.3797
2. **Abrams, E.W., Cheng, Y.L., Andrew, D.J.,** 2013. Drosophila KDEL Receptor Function in the Embryonic Salivary Gland and Epidermis. PLoS One 8, e77618. https://doi.org/10.1371/journal.pone.0077618
3. **Aebi, M.,** 2013. N-linked protein glycosylation in the ER. Biochimica et Biophysica Acta (BBA) - Molecular Cell Research, Functional and structural diversity of the endoplasmic reticulum 1833, 2430–2437. https://doi.org/10.1016/j.bbamcr.2013.04.001
4. **Alberts, B., Johnson. A., Lewis, J., Morgan, D., Raff, M., Roberts, K., Walter, P.,** 2014. Molecular Biology of the Cell, 6th edition
5. **Aldaz, S., Escudero, L.M.,** 2010. Imaginal discs. Current Biology 20, R429–R431. https://doi.org/10.1016/j.cub.2010.03.010
6. **Andrew, D.J., Henderson, K.D., Seshaiah, P.,** 2000. Salivary gland development in Drosophila melanogaster. Mechanisms of Development 92, 5–17. https://doi.org/10.1016/S0925-4773(99)00321-4
7. **Antson, H., Tõnissoo, T., Shimmi, O.,** 2022. The developing wing crossvein of Drosophila melanogaster: a fascinating model for signaling and morphogenesis. Fly (Austin) 16, 118–127. https://doi.org/10.1080/19336934.2022.2040316
8. **Atanasov, A.G., Nashev, L.G., Schweizer, R.A.S., Frick, C., Odermatt, A.,** 2004. Hexose-6-phosphate dehydrogenase determines the reaction direction of 11β-hydroxysteroid dehydrogenase type 1 as an oxoreductase. FEBS Letters 571, 129–133. https://doi.org/10.1016/j.febslet.2004.06.065
9. **Babst, M.,** 2011. MVB Vesicle Formation: ESCRT-Dependent, ESCRT-Independent and Everything in Between. Curr Opin Cell Biol 23, 452–457. https://doi.org/10.1016/j.ceb.2011.04.008
10. **Baeg, G.-H., Lin, X., Khare, N., Baumgartner, S., Perrimon, N.,** 2001. Heparan sulfate proteoglycans are critical for the organization of the extracellular distribution of Wingless. Development 128, 87–94. https://doi.org/10.1242/dev.128.1.87
11. **Bainbridge, S.P., Bownes, M.,** 1981. Staging the metamorphosis of Drosophila melanogaster. Development 66, 57–80. https://doi.org/10.1242/dev.66.1.57
12. **Bänziger, C., Soldini, D., Schütt, C., Zipperlen, P., Hausmann, G., Basler, K.,** 2006. Wntless, a Conserved Membrane Protein Dedicated to the Secretion of Wnt Proteins from Signaling Cells. Cell 125, 509–522. https://doi.org/10.1016/j.cell.2006.02.049
13. **Barlowe, C., Orci, L., Yeung, T., Hosobuchi, M., Hamamoto, S., Salama, N., Rexach, M.F., Ravazzola, M., Amherdt, M., Schekman, R.,** 1994. COPII: A membrane coat formed by Sec proteins that drive vesicle budding from the endoplasmic reticulum. Cell 77, 895–907. https://doi.org/10.1016/0092-8674(94)90138-4
14. **Bartscherer, K., Pelte, N., Ingelfinger, D., Boutros, M.,** 2006. Secretion of Wnt Ligands Requires Evi, a Conserved Transmembrane Protein. Cell 125, 523–533. https://doi.org/10.1016/j.cell.2006.04.009
15. **Beck, R., Ravet, M., Wieland, F.T., Cassel, D.,** 2009. The COPI system: Molecular mechanisms and function. FEBS Letters 583, 2701–2709. https://doi.org/10.1016/j.febslet.2009.07.032
16. **Behnia, R., Munro, S.,** 2005. Organelle identity and the signposts for membrane traffic. Nature 438, 597–604. https://doi.org/10.1038/nature04397
17. **Behrens, J., von Kries, J.P., Kühl, M., Bruhn, L., Wedlich, D., Grosschedl, R., Birchmeier, W.,** 1996. Functional interaction of β-catenin with the transcription factor LEF-1. Nature 382, 638–642. https://doi.org/10.1038/382638a0
18. **Beira, J.V., Paro, R.,** 2016. The legacy of Drosophila imaginal discs. Chromosoma 125, 573–592. https://doi.org/10.1007/s00412-016-0595-4
19. **Belenkaya, T.Y., Wu, Y., Tang, X., Zhou, B., Cheng, L., Sharma, Y.V., Yan, D., Selva, E.M., Lin, X.,** 2008. The Retromer Complex Influences Wnt Secretion by Recycling Wntless from Endosomes to the Trans-Golgi Network. Developmental Cell 14, 120–131. https://doi.org/10.1016/j.devcel.2007.12.003
20. **Bellec, K., Gicquel, I., Le Borgne, R.,** 2018. Stratum recruits Rab8 at Golgi exit sites to regulate the basolateral sorting of Notch and Sanpodo. Development 145, dev163469. https://doi.org/10.1242/dev.163469

21. **Bhanot, P., Brink, M., Samos, C.H., Hsieh, J.-C., Wang, Y., Macke, J.P., Andrew, D., Nathans, J., Nusse, R.,** 1996. A new member of the frizzled family from Drosophila functions as a Wingless receptor. Nature 382, 225–230. https://doi.org/10.1038/382225a0
22. **Bi, G.-Q., Morris, R.L., Liao, G., Alderton, J.M., Scholey, J.M., Steinhardt, R.A.,** 1997. Kinesin- and Myosin-driven Steps of Vesicle Recruitment for Ca2+-regulated Exocytosis. J Cell Biol 138, 999–1008.
23. **Bindels, D.S., Haarbosch, L., van Weeren, L., Postma, M., Wiese, K.E., Mastop, M., Aumonier, S., Gotthard, G., Royant, A., Hink, M.A., Gadella, T.W.J.,** 2017. mScarlet: a bright monomeric red fluorescent protein for cellular imaging. Nat Methods 14, 53–56. https://doi.org/10.1038/nmeth.4074
24. **Bischof, J., Maeda, R.K., Hediger, M., Karch, F., Basler, K.,** 2007. An optimized transgenesis system for Drosophila using germ-line-specific ϕC31 integrases. Proceedings of the National Academy of Sciences 104, 3312–3317. https://doi.org/10.1073/pnas.0611511104
25. **Boda, A., Lőrincz, P., Takáts, S., Csizmadia, T., Tóth, S., Kovács, A.L., Juhász, G.,** 2019. Drosophila Arl8 is a general positive regulator of lysosomal fusion events. Biochimica et Biophysica Acta (BBA) - Molecular Cell Research 1866, 533–544. https://doi.org/10.1016/j.bbamcr.2018.12.011
26. **Boncompain, G., Divoux, S., Gareil, N., de Forges, H., Lescure, A., Latreche, L., Mercanti, V., Jollivet, F., Raposo, G., Perez, F.,** 2012. Synchronization of secretory protein traffic in populations of cells. Nat Methods 9, 493–498. https://doi.org/10.1038/nmeth.1928
27. **Boutros, M., Paricio, N., Strutt, D.I., Mlodzik, M.,** 1998. Dishevelled Activates JNK and Discriminates between JNK Pathways in Planar Polarity and wingless Signaling. Cell 94, 109–118. https://doi.org/10.1016/S0092-8674(00)81226-X
28. **Brand, A.H., Perrimon, N., 1993.** Targeted gene expression as a means of altering cell fates and generating dominant phenotypes. Development 118, 401–415. https://doi.org/10.1242/dev.118.2.401
29. **Brunt, L., Greicius, G., Rogers, S., Evans, B.D., Virshup, D.M., Wedgwood, K.C.A., Scholpp, S.,** 2021. Vangl2 promotes the formation of long cytonemes to enable distant Wnt/β-catenin signaling. Nat Commun 12, 2058. https://doi.org/10.1038/s41467-021-22393-9
30. **Bucci, C., Parton, R.G., Mather, I.H., Stunnenberg, H., Simons, K., Hoflack, B., Zerial, M.,** 1992. The small GTPase rab5 functions as a regulatory factor in the early endocytic pathway. Cell 70, 715–728. https://doi.org/10.1016/0092-8674(92)90306-W
31. **Bucci, C., Thomsen, P., Nicoziani, P., McCarthy, J., van Deurs, B.,** 2000. Rab7: A Key to Lysosome Biogenesis. Mol Biol Cell 11, 467–480.
32. **Buechling, T., Boutros, M.,** 2011. Chapter two - Wnt Signaling: Signaling at and Above the Receptor Level, in: Birchmeier, C. (Ed.), Current Topics in Developmental Biology, Growth Factors in Development. Academic Press, pp. 21–53. https://doi.org/10.1016/B978-0-12-385975-4.00008-5
33. **Buechling, T., Chaudhary, V., Spirohn, K., Weiss, M., Boutros, M.,** 2011. p24 proteins are required for secretion of Wnt ligands. EMBO Rep 12, 1265–1272. https://doi.org/10.1038/embor.2011.212
34. **Bulleid, N.J.,** 2012. Disulfide Bond Formation in the Mammalian Endoplasmic Reticulum. Cold Spring Harb Perspect Biol 4, a013219. https://doi.org/10.1101/cshperspect.a013219
35. **Cai, H., Reinisch, K., Ferro-Novick, S.,** 2007. Coats, Tethers, Rabs, and SNAREs Work Together to Mediate the Intracellular Destination of a Transport Vesicle. Developmental Cell 12, 671–682. https://doi.org/10.1016/j.devcel.2007.04.005
36. **Callejo, A., Bilioni, A., Mollica, E., Gorfinkiel, N., Andrés, G., Ibáñez, C., Torroja, C., Doglio, L., Sierra, J., Guerrero, I.,** 2011. Dispatched mediates Hedgehog basolateral release to form the long-range morphogenetic gradient in the Drosophila wing disk epithelium. Proceedings of the National Academy of Sciences 108, 12591–12598. https://doi.org/10.1073/pnas.1106881108
37. **Carroll, K.S., Hanna, J., Simon, I., Krise, J., Barbero, P., Pfeffer, S.R.,** 2001. Role of Rab9 GTPase in Facilitating Receptor Recruitment by TIP47. Science 292, 1373–1376. https://doi.org/10.1126/science.1056791
38. **Catalano, M., O'Driscoll, L.,** 2020. Inhibiting extracellular vesicles formation and release: a review of EV inhibitors. J Extracell Vesicles 9, 1703244. https://doi.org/10.1080/20013078.2019.1703244
39. **Carvalho, J.R., Fortunato, I.C., Fonseca, C.G., Pezzarossa, A., Barbacena, P., Dominguez-Cejudo, M.A., Vasconcelos, F.F., Santos, N.C., Carvalho, F.A., Franco, C.A.,** 2019. Non-canonical Wnt signaling regulates junctional mechanocoupling during angiogenic collective cell migration. eLife 8, e45853. https://doi.org/10.7554/eLife.45853
40. **Cavallo, R.A., Cox, R.T., Moline, M.M., Roose, J., Polevoy, G.A., Clevers, H., Peifer, M., Bejsovec, A.,** 1998. Drosophila Tcf and Groucho interact to repress Wingless signalling activity. Nature 395, 604–608. https://doi.org/10.1038/26982

41. **Chalfie, M., Tu, Y., Euskirchen, G., Ward, W. W. & Prasher, D. C.,** 1994. Green Fluorescent Protein as a Marker for Gene Expression. *Science* **263**, 802–805
42. **Chan, C.-C., Scoggin, S., Wang, D., Cherry, S., Dembo, T., Greenberg, B., Jin, E.J., Kuey, C., Lopez, A., Mehta, S.Q., Perkins, T.J., Brankatschk, M., Rothenfluh, A., Buszczak, M., Hiesinger, P.R.,** 2011. Systematic Discovery of Rab GTPases with Synaptic Functions in Drosophila. Current Biology 21, 1704–1715. https://doi.org/10.1016/j.cub.2011.08.058
43. **Chaudhary, V., Boutros, M.,** 2019. Exocyst-mediated apical Wg secretion activates signaling in the Drosophila wing epithelium. PLOS Genetics 15, e1008351. https://doi.org/10.1371/journal.pgen.1008351
44. **Chavrier, P., Parton, R.G., Hauri, H.P., Simons, K., Zerial, M.,** 1990. Localization of low molecular weight GTP binding proteins to exocytic and endocytic compartments. Cell 62, 317–329. https://doi.org/10.1016/0092-8674(90)90369-P
45. **Cherry, S., Jin, E.J., Özel, M.N., Lu, Z., Agi, E., Wang, D., Jung, W.-H., Epstein, D., Meinertzhagen, I.A., Chan, C.-C., Hiesinger, P.R.,** 2013. Charcot-Marie-Tooth 2B mutations in rab7 cause dosage-dependent neurodegeneration due to partial loss of function. eLife 2, e01064. https://doi.org/10.7554/eLife.01064
46. **Ching, W., Hang, H.C., Nusse, R.,** 2008. Lipid-independent Secretion of a Drosophila Wnt Protein. J Biol Chem 283, 17092–17098. https://doi.org/10.1074/jbc.M802059200
47. **Christianson, H.C., Belting, M.,** 2014. Heparan sulfate proteoglycan as a cell-surface endocytosis receptor. Matrix Biology, Proteoglycan Biology 35, 51–55. https://doi.org/10.1016/j.matbio.2013.10.004
48. **Christianson, H.C., Svensson, K.J., van Kuppevelt, T.H., Li, J.-P., Belting, M.,** 2013. Cancer cell exosomes depend on cell-surface heparan sulfate proteoglycans for their internalization and functional activity. Proceedings of the National Academy of Sciences 110, 17380–17385. https://doi.org/10.1073/pnas.1304266110
49. **Christis, C., Lubsen, N.H., Braakman, I.,** 2008. Protein folding includes oligomerization – examples from the endoplasmic reticulum and cytosol. The FEBS Journal 275, 4700–4727. https://doi.org/10.1111/j.1742-4658.2008.06590.x
50. **Chu, M.L.-H., Ahn, V.E., Choi, H.-J., Daniels, D.L., Nusse, R., Weis, W.I.,** 2013. Structural studies of Wnts and identification of an LRP6 binding site. Structure 21, 1235–1242. https://doi.org/10.1016/j.str.2013.05.006
51. **Cong, L., Ran, F.A., Cox, D., Lin, S., Barretto, R., Habib, N., Hsu, P.D., Wu, X., Jiang, W., Marraffini, L.A., Zhang, F.,** 2013. Multiplex Genome Engineering Using CRISPR/Cas Systems. Science 339, 819–823. https://doi.org/10.1126/science.1231143
52. **Coombs, G.S., Yu, J., Canning, C.A., Veltri, C.A., Covey, T.M., Cheong, J.K., Utomo, V., Banerjee, N., Zhang, Z.H., Jadulco, R.C., Concepcion, G.P., Bugni, T.S., Harper, M.K., Mihalek, I., Jones, C.M., Ireland, C.M., Virshup, D.M.,** 2010. WLS-dependent secretion of WNT3A requires Ser209 acylation and vacuolar acidification. Journal of Cell Science 123, 3357–3367. https://doi.org/10.1242/jcs.072132
53. **Costantini, L.M., Baloban, M., Markwardt, M.L., Rizzo, M.A., Guo, F., Verkhusha, V.V., Snapp, E.L.,** 2015. A palette of fluorescent proteins optimized for diverse cellular environments. Nat Commun 6, 7670. https://doi.org/10.1038/ncomms8670
54. **Costantini, L.M., Snapp, E.L.,** 2013. Fluorescent Proteins in Cellular Organelles: Serious Pitfalls and Some Solutions. DNA Cell Biol 32, 622–627. https://doi.org/10.1089/dna.2013.2172
55. **Croce, J.C., McClay, D.R.,** 2008. Evolution of the Wnt Pathways. Methods Mol Biol 469, 3–18. https://doi.org/10.1007/978-1-60327-469-2_1
56. **D'Arcangelo, J.G., Crissman, J., Pagant, S., Copic, A., Latham, C.F., Snapp, E.L., Miller, E.A.,** 2015. Traffic of p24 proteins and COPII coat composition mutually influence membrane scaffolding. Curr Biol 25, 1296–1305. https://doi.org/10.1016/j.cub.2015.03.029
57. **Dahmann, C.,** 2008. Drosophila: Methods and Protocols, 2nd edition
58. **Daniels, D.L., Weis, W.I.,** 2005. Beta-catenin directly displaces Groucho/TLE repressors from Tcf/Lef in Wnt-mediated transcription activation. Nat Struct Mol Biol 12, 364–371. https://doi.org/10.1038/nsmb912
59. **Das, S., Yu, S., Sakamori, R., Vedula, P., Feng, Q., Flores, J., Hoffman, A., Fu, J., Stypulkowski, E., Rodriguez, A., Dobrowolski, R., Harada, A., Hsu, W., Bonder, E.M., Verzi, M.P., Gao, N.,** 2015. Rab8a vesicles regulate Wnt ligand delivery and Paneth cell maturation at the intestinal stem cell niche. Development 142, 2147–2162. https://doi.org/10.1242/dev.121046
60. **Davidson, G., Wu, W., Shen, J., Bilic, J., Fenger, U., Stannek, P., Glinka, A., Niehrs, C.,** 2005. Casein kinase 1 γ couples Wnt receptor activation to cytoplasmic signal transduction. Nature 438, 867–872. https://doi.org/10.1038/nature04170

61. **De Luca, M., Bucci, C.,** 2014. A new V-ATPase regulatory mechanism mediated by the Rab interacting lysosomal protein (RILP). Commun Integr Biol 7, e971572. https://doi.org/10.4161/cib.29616
62. **Denecke, J., De Rycke, R., Botterman, J.,** 1992. Plant and mammalian sorting signals for protein retention in the endoplasmic reticulum contain a conserved epitope. EMBO J 11, 2345–2355.
63. **Di Paolo, G., De Camilli, P.,** 2006. Phosphoinositides in cell regulation and membrane dynamics. Nature 443, 651–657. https://doi.org/10.1038/nature05185
64. **Diaz de la Loza, M.C., Thompson, B.J.,** 2017. Forces shaping the Drosophila wing. Mechanisms of Development, Roles of physical forces in development 144, 23–32. https://doi.org/10.1016/j.mod.2016.10.003
65. **Dickson, L.J., Liu, S., Storrie, B.,** 2020. Rab6 is required for rapid, cisternal-specific, intra-Golgi cargo transport. Sci Rep 10, 16604. https://doi.org/10.1038/s41598-020-73276-w
66. **Ducharme, N.A., Williams, J.A., Oztan, A., Apodaca, G., Lapierre, L.A., Goldenring, J.R.,** 2007. Rab11-FIP2 regulates differentiable steps in transcytosis. American Journal of Physiology-Cell Physiology 293, C1059–C1072. https://doi.org/10.1152/ajpcell.00078.2007
67. **Dunst, S., Kazimiers, T., von Zadow, F., Jambor, H., Sagner, A., Brankatschk, B., Mahmoud, A., Spannl, S., Tomancak, P., Eaton, S., Brankatschk, M.,** 2015. Endogenously Tagged Rab Proteins: A Resource to Study Membrane Trafficking in Drosophila. Developmental Cell 33, 351–365. https://doi.org/10.1016/j.devcel.2015.03.022
68. **Echard, A., Jollivet, F., Martinez, O., Lacapère, J.-J., Rousselet, A., Janoueix-Lerosey, I., Goud, B.,** 1998. Interaction of a Golgi-Associated Kinesin-Like Protein with Rab6. Science 279, 580–585. https://doi.org/10.1126/science.279.5350.580
69. **Elkin, S.R., Lakoduk, A.M., Schmid, S.L.,** 2016. Endocytic pathways and endosomal trafficking: a primer. Wien Med Wochenschr 166, 196–204. https://doi.org/10.1007/s10354-016-0432-7
70. **Ellgaard, L., McCaul, N., Chatsisvili, A., Braakman, I.,** 2016. Co- and Post-Translational Protein Folding in the ER. Traffic 17, 615–638. https://doi.org/10.1111/tra.12392
71. **Entchev, E.V., Schwabedissen, A., González-Gaitán, M.,** 2000. Gradient Formation of the TGF-β Homolog Dpp. Cell 103, 981–992. **https://doi.org/10.1016/S0092-8674(00)00200-2**
72. **Eskelinen, E.-L., Tanaka, Y., Saftig, P.,** 2003. At the acidic edge: emerging functions for lysosomal membrane proteins. Trends in Cell Biology 13, 137–145. https://doi.org/10.1016/S0962-8924(03)00005-9
73. **Ewen-Campen, B., Comyn, T., Vogt, E., Perrimon, N.,** 2020. No Evidence that Wnt Ligands Are Required for Planar Cell Polarity in Drosophila. Cell Reports 32, 108121. https://doi.org/10.1016/j.celrep.2020.108121
74. **Fanto, M., Weber, U., Strutt, D.I., Mlodzik, M.,** 2000. Nuclear signaling by Rac and Rho GTPases is required in the establishment of epithelial planar polarity in the Drosophila eye. Current Biology 10, 979-S1. https://doi.org/10.1016/S0960-9822(00)00645-X
75. **Farkaš, R., Beňová-Liszeková, D., Mentelová, L., Mahmood, S., Ďatková, Z., Beňo, M., Pečeňová, L., Raška, O., Šmigová, J., Chase, B.A., Raška, I., Mechler, B.M.,** 2015. Vacuole dynamics in the salivary glands of Drosophila melanogaster during prepupal development. Development, Growth & Differentiation 57, 74–96. https://doi.org/10.1111/dgd.12193
76. **Farkas, R., Mechler, B.M.,** 2000. The timing of Drosophila salivary gland apoptosis displays an l(2)gl-dose response. Cell Death Differ 7, 89–101. https://doi.org/10.1038/sj.cdd.4400621
77. **Farrants, H., Tarnawski, M., Müller, T.G., Otsuka, S., Hiblot, J., Koch, B., Kueblbeck, M., Kräusslich, H.-G., Ellenberg, J., Johnsson, K.,** 2020. Chemogenetic Control of Nanobodies. Nat Methods 17, 279–282. https://doi.org/10.1038/s41592-020-0746-7
78. **Ford, C., Parchure, A., von Blume, J., Burd, C.G.,** 2021. Cargo sorting at the trans-Golgi network at a glance. Journal of Cell Science 134, jcs259110. https://doi.org/10.1242/jcs.259110
79. **Francis, C.R., Kincross, H., Kushner, E.J.,** 2022. Rab35 governs apicobasal polarity through regulation of actin dynamics during sprouting angiogenesis. Nat Commun 13, 5276. https://doi.org/10.1038/s41467-022-32853-5
80. **Gansemer, E.R., Rutkowski, D.T.,** 2022. Pathways Linking Nicotinamide Adenine Dinucleotide Phosphate Production to Endoplasmic Reticulum Protein Oxidation and Stress. Frontiers in Molecular Biosciences 9.
81. **Gasnereau, I., Herr, P., Chia, P.Z.C., Basler, K., Gleeson, P.A.,** 2011. Identification of an Endocytosis Motif in an Intracellular Loop of Wntless Protein, Essential for Its Recycling and the Control of Wnt Protein Signaling. J Biol Chem 286, 43324–43333. https://doi.org/10.1074/jbc.M111.307231
82. **Girard, E., Chmiest, D., Fournier, N., Johannes, L., Paul, J.-L., Vedie, B., Lamaze, C.,** 2014. Rab7 Is Functionally Required for Selective Cargo Sorting at the Early Endosome. Traffic 15, 309–326. https://doi.org/10.1111/tra.12143

83. **Glaeser, K., Urban, M., Fenech, E., Voloshanenko, O., Kranz, D., Lari, F., Christianson, J.C., Boutros, M.,** 2018. ERAD-dependent control of the Wnt secretory factor Evi. The EMBO Journal 37, e97311. https://doi.org/10.15252/embj.201797311
84. **Glashauser, J., Camelo, C., Hollmann, M., Backer, W., Jacobs, T., Sanchez, J.I., Schleutker, R., Förster, D., Berns, N., Riechmann, V., Luschnig, S.,** 2023. Acute manipulation and real-time visualization of membrane trafficking and exocytosis in Drosophila. Developmental Cell 58, 709-723.e7. https://doi.org/10.1016/j.devcel.2023.03.006
85. **Golic, M.M., Rong, Y.S., Petersen, R.B., Lindquist, S.L., Golic, K.G.,** 1997. FLP-mediated DNA mobilization to specific target sites in Drosophila chromosomes. Nucleic Acids Res 25, 3665–3671.
86. **Goodenough, D.A., Paul, D.L.,** 2009. Gap Junctions. Cold Spring Harb Perspect Biol 1, a002576. https://doi.org/10.1101/cshperspect.a002576
87. **Gou, J., Stotsky, J.A., Othmer, H.G.,** 2020. Growth control in the Drosophila wing disk. WIREs Systems Biology and Medicine 12, e1478. https://doi.org/10.1002/wsbm.1478
88. **Graab, P., Bock, C., Weiss, K., Hirth, A., Koller, N., Braner, M., Jung, J., Loehr, F., Tampé, R., Behrends, C., Abele, R.,** 2019. Lysosomal targeting of the ABC transporter TAPL is determined by membrane-localized charged residues. Journal of Biological Chemistry 294, 7308–7323. https://doi.org/10.1074/jbc.RA118.007071
89. **Gratz, S.J., Cummings, A.M., Nguyen, J.N., Hamm, D.C., Donohue, L.K., Harrison, M.M., Wildonger, J., O'Connor-Giles, K.M.,** 2013. Genome Engineering of Drosophila with the CRISPR RNA-Guided Cas9 Nuclease. Genetics 194, 1029–1035. https://doi.org/10.1534/genetics.113.152710
90. **Gratz, S.J., Ukken, F.P., Rubinstein, C.D., Thiede, G., Donohue, L.K., Cummings, A.M., O'Connor-Giles, K.M.,** 2014. Highly Specific and Efficient CRISPR/Cas9-Catalyzed Homology-Directed Repair in Drosophila. Genetics 196, 961–971. https://doi.org/10.1534/genetics.113.160713
91. **Gross, J.C., Chaudhary, V., Bartscherer, K., Boutros, M.,** 2012. Active Wnt proteins are secreted on exosomes. Nat Cell Biol 14, 1036–1045. https://doi.org/10.1038/ncb2574
92. **Gruenberg, J.,** 2001. The endocytic pathway: a mosaic of domains. Nat Rev Mol Cell Biol 2, 721–730. https://doi.org/10.1038/35096054
93. **Guerra, F., Bucci, C.,** 2016. Multiple Roles of the Small GTPase Rab7. Cells 5, 34. https://doi.org/10.3390/cells5030034
94. **Hales, C.M., Vaerman, J.-P., Goldenring, J.R.,** 2002. Rab11 Family Interacting Protein 2 Associates with Myosin Vb and Regulates Plasma Membrane Recycling*. Journal of Biological Chemistry 277, 50415–50421. https://doi.org/10.1074/jbc.M209270200
95. **Hales, K.G., Korey, C.A., Larracuente, A.M., Roberts, D.M.,** 2015. Genetics on the Fly: A Primer on the Drosophila Model System. Genetics 201, 815–842. https://doi.org/10.1534/genetics.115.183392
96. **Han, J., Pluhackova, K., Böckmann, R.A.,** 2017. The Multifaceted Role of SNARE Proteins in Membrane Fusion. Frontiers in Physiology 8.
97. **Hanke, T., Szawlowski, P., Randall, R.E.,** 1992. Construction of solid matrix-antibody-antigen complexes containing simian immunodeficiency virus p27 using tag-specific monoclonal antibody and tag-linked antigen. Journal of General Virology 73, 653–660. https://doi.org/10.1099/0022-1317-73-3-653
98. **Harterink, M., Port, F., Lorenowicz, M.J., McGough, I.J., Silhankova, M., Betist, M.C., van Weering, J.R.T., van Heesbeen, R.G.H.P., Middelkoop, T.C., Basler, K., Cullen, P.J., Korswagen, H.C.,** 2011. A SNX3-dependent Retromer pathway mediates retrograde transport of the Wnt sorting receptor Wntless and is required for Wnt secretion. Nat Cell Biol 13, 914–923. https://doi.org/10.1038/ncb2281
99. **Haupts, U., Maiti, S., Schwille, P., Webb, W.W.,** 1998. Dynamics of fluorescence fluctuations in green fluorescent protein observed by fluorescence correlation spectroscopy. Proceedings of the National Academy of Sciences 95, 13573–13578. https://doi.org/10.1073/pnas.95.23.13573
100. **Hayat, R., Manzoor, M., Hussain, A.,** 2022. Wnt signaling pathway: A comprehensive review. Cell Biology International 46, 863–877. https://doi.org/10.1002/cbin.11797
101. **Heider, M.R., Munson, M.,** 2012. Exorcising the Exocyst Complex. Traffic 13, 898–907. https://doi.org/10.1111/j.1600-0854.2012.01353.x
102. **Hiller-Sturmhöfel, S., Bartke, A.,** 1998. The Endocrine System. Alcohol Health Res World 22, 153–164.
103. **Hochuli, E., Bannwarth, W., Döbeli, H., Gentz, R., Stüber, D.,** 1988. Genetic Approach to Facilitate Purification of Recombinant Proteins with a Novel Metal Chelate Adsorbent. Nat Biotechnol 6, 1321–1325. https://doi.org/10.1038/nbt1188-1321
104. **Holstein, T.W.,** 2012. The Evolution of the Wnt Pathway. Cold Spring Harb Perspect Biol 4, a007922. https://doi.org/10.1101/cshperspect.a007922

105. **Homma, Y., Hiragi, S., Fukuda, M.,** 2021. Rab family of small GTPases: an updated view on their regulation and functions. The FEBS Journal 288, 36–55. https://doi.org/10.1111/febs.15453
106. **Hu, Y.-B., Yan, C., Mu, L., Mi, Y.-L., Zhao, H., Hu, H., Li, X.-L., Tao, D.-D., Wu, Y.-Q., Gong, J.-P., Qin, J.-C.,** 2019. Exosomal Wnt-induced dedifferentiation of colorectal cancer cells contributes to chemotherapy resistance. Oncogene 38, 1951–1965. https://doi.org/10.1038/s41388-018-0557-9
107. **Huang, H., Kornberg, T.B.,** 2015. Myoblast cytonemes mediate Wg signaling from the wing imaginal disc and Delta-Notch signaling to the air sac primordium. eLife 4, e06114. https://doi.org/10.7554/eLife.06114
108. **Ikeda, S., Kishida, S., Yamamoto, H., Murai, H., Koyama, S., Kikuchi, A.,** 1998. Axin, a negative regulator of the Wnt signaling pathway, forms a complex with GSK-3beta and beta-catenin and promotes GSK-3beta-dependent phosphorylation of beta-catenin. EMBO J 17, 1371–1384. https://doi.org/10.1093/emboj/17.5.1371
109. **Ishitani, T., Ninomiya-Tsuji, J., Nagai, S., Nishita, M., Meneghini, M., Barker, N., Waterman, M., Bowerman, B., Clevers, H., Shibuya, H., Matsumoto, K.,** 1999. The TAK1–NLK–MAPK-related pathway antagonizes signalling between β-catenin and transcription factor TCF. Nature 399, 798–802. https://doi.org/10.1038/21674
110. **Jafar-Nejad, H., Tien, A.-C., Acar, M., Bellen, H.J.,** 2006. Senseless and Daughterless confer neuronal identity to epithelial cells in the Drosophila wing margin. Development 133, 1683–1692. https://doi.org/10.1242/dev.02338
111. **Janda, C.Y., Waghray, D., Levin, A.M., Thomas, C., Garcia, K.C.,** 2012. Structural basis of Wnt recognition by Frizzled. Science 337, 59–64. https://doi.org/10.1126/science.1222879
112. **Jean, S., Kiger, A.A.,** 2012. Coordination between RAB GTPase and phosphoinositide regulation and functions. Nat Rev Mol Cell Biol 13, 463–470. https://doi.org/10.1038/nrm3379
113. **Jefferies, K.C., Cipriano, D.J., Forgac, M.,** 2008. Function, structure and regulation of the vacuolar (H+)-ATPases. Arch Biochem Biophys 476, 33–42. https://doi.org/10.1016/j.abb.2008.03.025
114. **Jin, E.J., Chan, C.-C., Agi, E., Cherry, S., Hanacik, E., Buszczak, M., Hiesinger, P.R.,** 2012. Similarities of Drosophila rab GTPases Based on Expression Profiling: Completion and Analysis of the rab-Gal4 Kit. PLOS ONE 7, e40912. https://doi.org/10.1371/journal.pone.0040912
115. **Jinek, M., Chylinski, K., Fonfara, I., Hauer, M., Doudna, J.A., Charpentier, E.,** 2012. A Programmable Dual-RNA–Guided DNA Endonuclease in Adaptive Bacterial Immunity. Science 337, 816–821. https://doi.org/10.1126/science.1225829
116. **Jordens, I., Fernandez-Borja, M., Marsman, M., Dusseljee, S., Janssen, L., Calafat, J., Janssen, H., Wubbolts, R., Neefjes, J.,** 2001. The Rab7 effector protein RILP controls lysosomal transport by inducing the recruitment of dynein-dynactin motors. Current Biology 11, 1680–1685. https://doi.org/10.1016/S0960-9822(01)00531-0
117. **Jovic, M., Sharma, M., Rahajeng, J., Caplan, S.,** 2010. The early endosome: a busy sorting station for proteins at the crossroads. Histol Histopathol 25, 99–112.
118. **Kaiser, K., Gyllborg, D., Procházka, J., Salašová, A., Kompaníková, P., Molina, F.L., Laguna-Goya, R., Radaszkiewicz, T., Harnoš, J., Procházková, M., Potěšil, D., Barker, R.A., Casado, Á.G., Zdráhal, Z., Sedláček, R., Arenas, E., Villaescusa, J.C., Bryja, V.,** 2019. WNT5A is transported via lipoprotein particles in the cerebrospinal fluid to regulate hindbrain morphogenesis. Nat Commun 10, 1498. https://doi.org/10.1038/s41467-019-09298-4
119. **Kaksonen, M., Roux, A.,** 2018. Mechanisms of clathrin-mediated endocytosis. Nat Rev Mol Cell Biol 19, 313–326. https://doi.org/10.1038/nrm.2017.132
120. **Katanaev, V.L., Ponzielli, R., Sémériva, M., Tomlinson, A.,** 2005. Trimeric G Protein-Dependent Frizzled Signaling in Drosophila. Cell 120, 111–122. https://doi.org/10.1016/j.cell.2004.11.014
121. **Katayama, H., Yamamoto, A., Mizushima, N., Yoshimori, T., Miyawaki, A.,** 2008. GFP-like Proteins Stably Accumulate in Lysosomes. Cell Structure and Function 33, 1–12. https://doi.org/10.1247/csf.07011
122. **Keppler, A., Gendreizig, S., Gronemeyer, T., Pick, H., Vogel, H., Johnsson, K.,** 2003. A general method for the covalent labeling of fusion proteins with small molecules in vivo. Nat Biotechnol 21, 86–89. https://doi.org/10.1038/nbt765
123. **Khatter, D., Raina, V.B., Dwivedi, D., Sindhwani, A., Bahl, S., Sharma, M.,** 2015. The small GTPase Arl8b regulates assembly of the mammalian HOPS complex on lysosomes. Journal of Cell Science 128, 1746–1761. https://doi.org/10.1242/jcs.162651
124. **Kiral, F.R., Kohrs, F.E., Jin, E.J., Hiesinger, P.R.,** 2018. Rab GTPases and Membrane Trafficking in Neurodegeneration. Current Biology 28, R471–R486. https://doi.org/10.1016/j.cub.2018.02.010

125. **Kirchhausen, T., Owen, D., Harrison, S.C.,** 2014. Molecular Structure, Function, and Dynamics of Clathrin-Mediated Membrane Traffic. Cold Spring Harb Perspect Biol 6, a016725. https://doi.org/10.1101/cshperspect.a016725
126. **Kirkpatrick, C.A., Selleck, S.B.,** 2007. Heparan sulfate proteoglycans at a glance. Journal of Cell Science 120, 1829–1832. https://doi.org/10.1242/jcs.03432
127. **Klöpper, T.H., Kienle, N., Fasshauer, D., Munro, S.,** 2012. Untangling the evolution of Rab G proteins: implications of a comprehensive genomic analysis. BMC Biology 10, 71. https://doi.org/10.1186/1741-7007-10-71
128. **Kohrs, F.E., Daumann, I.-M., Pavlović, B., Jin, E.J., Kiral, F.R., Lin, S.-C., Port, F., Wolfenberg, H., Mathejczyk, T.F., Linneweber, G.A., Chan, C.-C., Boutros, M., Hiesinger, P.R.,** 2021. Systematic functional analysis of rab GTPases reveals limits of neuronal robustness to environmental challenges in flies. eLife 10, e59594. https://doi.org/10.7554/eLife.59594
129. **Koles, K., Nunnari, J., Korkut, C., Barria, R., Brewer, C., Li, Y., Leszyk, J., Zhang, B., Budnik, V.,** 2012. Mechanism of Evenness Interrupted (Evi)-Exosome Release at Synaptic Boutons*. Journal of Biological Chemistry 287, 16820–16834. https://doi.org/10.1074/jbc.M112.342667
130. **Korkut, C., Ataman, B., Ramachandran, P., Ashley, J., Barria, R., Gherbesi, N., Budnik, V.,** 2009. Trans-Synaptic Transmission of Vesicular Wnt Signals through Evi/Wntless. Cell 139, 393–404. https://doi.org/10.1016/j.cell.2009.07.051
131. **Kouranti, I., Sachse, M., Arouche, N., Goud, B., Echard, A.,** 2006. Rab35 Regulates an Endocytic Recycling Pathway Essential for the Terminal Steps of Cytokinesis. Current Biology 16, 1719–1725. https://doi.org/10.1016/j.cub.2006.07.020
132. **Kremers, G.-J., Gilbert, S.G., Cranfill, P.J., Davidson, M.W., Piston, D.W.,** 2011. Fluorescent proteins at a glance. Journal of Cell Science 124, 157–160. https://doi.org/10.1242/jcs.072744
133. **Kühl, M., Sheldahl, L.C., Malbon, C.C., Moon, R.T.,** 2000. Ca2+/Calmodulin-dependent Protein Kinase II Is Stimulated by Wnt and Frizzled Homologs and Promotes Ventral Cell Fates in Xenopus*. Journal of Biological Chemistry 275, 12701–12711. https://doi.org/10.1074/jbc.275.17.12701
134. **Kurokawa, K., Nakano, A.,** 2019. The ER exit sites are specialized ER zones for the transport of cargo proteins from the ER to the Golgi apparatus. The Journal of Biochemistry 165, 109–114. https://doi.org/10.1093/jb/mvy080
135. **Lafourcade, C., Sobo, K., Kieffer-Jaquinod, S., Garin, J., van der Goot, F.G.,** 2008. Regulation of the V-ATPase along the Endocytic Pathway Occurs through Reversible Subunit Association and Membrane Localization. PLoS One 3, e2758. https://doi.org/10.1371/journal.pone.0002758
136. **Landenberger, A., Kabil, H., Harshman, L.G., Zempleni, J.,** 2004. Biotin deficiency decreases life span and fertility but increases stress resistance in Drosophila melanogaster. The Journal of Nutritional Biochemistry 15, 591–600. https://doi.org/10.1016/j.jnutbio.2004.04.006
137. **Langemeyer, L., Borchers, A.-C., Herrmann, E., Füllbrunn, N., Han, Y., Perz, A., Auffarth, K., Kümmel, D., Ungermann, C.,** 2020. A conserved and regulated mechanism drives endosomal Rab transition. eLife 9, e56090. https://doi.org/10.7554/eLife.56090
138. **Le Gall, S., Neuhof, A., Rapoport, T.,** 2004. The Endoplasmic Reticulum Membrane Is Permeable to Small Molecules. MBoC 15, 447–455. https://doi.org/10.1091/mbc.e03-05-0325
139. **Lee, M.-T., Mishra, A., Lambright, D.G.,** 2009. Structural mechanisms for regulation of membrane traffic by Rab GTPases. Traffic 10, 1377–1389. https://doi.org/10.1111/j.1600-0854.2009.00942.x
140. **Lee, Y.-K., Lee, J.-A.,** 2016. Role of the mammalian ATG8/LC3 family in autophagy: differential and compensatory roles in the spatiotemporal regulation of autophagy. BMB Reports 49, 424. https://doi.org/10.5483/BMBRep.2016.49.8.081
141. **Lemus, L., Goder, V.,** 2014. Regulation of Endoplasmic Reticulum-Associated Protein Degradation (ERAD) by Ubiquitin. Cells 3, 824–847. https://doi.org/10.3390/cells3030824
142. **Li, G., Marlin, M.C.,** 2015. Rab Family of GTPases, in: Li, G. (Ed.), Rab GTPases: Methods and Protocols, Methods in Molecular Biology. Springer, New York, NY, pp. 1–15. https://doi.org/10.1007/978-1-4939-2569-8_1
143. **Li, X., DiFiglia, M.,** 2012. The recycling endosome and its role in neurological disorders. Progress in Neurobiology, The Neurotoxicity of Mutant Proteins 97, 127–141. https://doi.org/10.1016/j.pneurobio.2011.10.002
144. **Li, X., Wu, Y., Shen, C., Belenkaya, T.Y., Ray, L., Lin, X.,** 2015. Drosophila p24 and Sec22 regulate Wingless trafficking in the early secretory pathway. Biochemical and Biophysical Research Communications 463, 483–489. https://doi.org/10.1016/j.bbrc.2015.04.151

145. **Lin, X., Yang, T., Wang, S., Wang, Z., Yun, Y., Sun, L., Zhou, Y., Xu, X., Akazawa, C., Hong, W., Wang, T.,** 2014. RILP interacts with HOPS complex via VPS41 subunit to regulate endocytic trafficking. Sci Rep 4, 7282. https://doi.org/10.1038/srep07282
146. **Linnemannstöns, K., Witte, L., Karuna M, P., Kittel, J.C., Danieli, A., Müller, D., Nitsch, L., Honemann-Capito, M., Grawe, F., Wodarz, A., Gross, J.C.,** 2020. Ykt6-dependent endosomal recycling is required for Wnt secretion in the Drosophila wing epithelium. Development 147, dev185421. https://doi.org/10.1242/dev.185421
147. **Lippincott-Schwartz, J., Snapp, E.L., Phair, R.D.,** 2018. The Development and Enhancement of FRAP as a Key Tool for Investigating Protein Dynamics. Biophys J 115, 1146–1155. https://doi.org/10.1016/j.bpj.2018.08.007
148. **Liu, W., Sato, A., Khadka, D., Bharti, R., Diaz, H., Runnels, L.W., Habas, R.,** 2008. Mechanism of activation of the Formin protein Daam1. Proc Natl Acad Sci U S A 105, 210–215. https://doi.org/10.1073/pnas.0707277105
149. **Lloyd, T.E., Atkinson, R., Wu, M.N., Zhou, Y., Pennetta, G., Bellen, H.J.,** 2002. Hrs Regulates Endosome Membrane Invagination and Tyrosine Kinase Receptor Signaling in Drosophila. Cell 108, 261–269. https://doi.org/10.1016/S0092-8674(02)00611-6
150. **Logan, C.Y., Nusse, R.,** 2004. The Wnt signaling pathway in development and disease. Annu. Rev. Cell Dev. Biol. 20, 781–810. https://doi.org/10.1146/annurev.cellbio.20.010403.113126
151. **Lőrincz, P., Tóth, S., Benkő, P., Lakatos, Z., Boda, A., Glatz, G., Zobel, M., Bisi, S., Hegedűs, K., Takáts, S., Scita, G., Juhász, G.,** 2017. Rab2 promotes autophagic and endocytic lysosomal degradation. J Cell Biol 216, 1937–1947. https://doi.org/10.1083/jcb.201611027
152. **Los, G.V., Encell, L.P., McDougall, M.G., Hartzell, D.D., Karassina, N., Zimprich, C., Wood, M.G., Learish, R., Ohana, R.F., Urh, M., Simpson, D., Mendez, J., Zimmerman, K., Otto, P., Vidugiris, G., Zhu, J., Darzins, A., Klaubert, D.H., Bulleit, R.F., Wood, K.V.,** 2008. HaloTag: A Novel Protein Labeling Technology for Cell Imaging and Protein Analysis. ACS Chem. Biol. 3, 373–382. https://doi.org/10.1021/cb800025k
153. **MacDonald, B.T., Hien, A., Zhang, X., Iranloye, O., Virshup, D.M., Waterman, M.L., He, X.,** 2014. Disulfide Bond Requirements for Active Wnt Ligands. J Biol Chem 289, 18122–18136. https://doi.org/10.1074/jbc.M114.575027
154. **Marois, E., Mahmoud, A., Eaton, S.,** 2006. The endocytic pathway and formation of the Wingless morphogen gradient. Development 133, 307–317. https://doi.org/10.1242/dev.02197
155. **Matanis, T., Akhmanova, A., Wulf, P., Del Nery, E., Weide, T., Stepanova, T., Galjart, N., Grosveld, F., Goud, B., De Zeeuw, C.I., Barnekow, A., Hoogenraad, C.C.,** 2002. Bicaudal-D regulates COPI-independent Golgi–ER transport by recruiting the dynein–dynactin motor complex. Nat Cell Biol 4, 986–992. https://doi.org/10.1038/ncb891
156. **Mattes, B., Dang, Y., Greicius, G., Kaufmann, L.T., Prunsche, B., Rosenbauer, J., Stegmaier, J., Mikut, R., Özbek, S., Nienhaus, G.U., Schug, A., Virshup, D.M., Scholpp, S.,** 2018. Wnt/PCP controls spreading of Wnt/β-catenin signals by cytonemes in vertebrates. eLife 7, e36953. https://doi.org/10.7554/eLife.36953
157. **Mauvezin, C., Neufeld, T.P.,** 2015. Bafilomycin A1 disrupts autophagic flux by inhibiting both V-ATPase-dependent acidification and Ca-P60A/SERCA-dependent autophagosome-lysosome fusion. Autophagy 11, 1437–1438. https://doi.org/10.1080/15548627.2015.1066957
158. **McBride, H.M., Rybin, V., Murphy, C., Giner, A., Teasdale, R., Zerial, M.,** 1999. Oligomeric Complexes Link Rab5 Effectors with NSF and Drive Membrane Fusion via Interactions between EEA1 and Syntaxin 13. Cell 98, 377–386. https://doi.org/10.1016/S0092-8674(00)81966-2
159. **McGough, I.J., Vecchia, L., Bishop, B., Malinauskas, T., Beckett, K., Joshi, D., O'Reilly, N., Siebold, C., Jones, E.Y., Vincent, J.-P.,** 2020. Glypicans shield the Wnt lipid moiety to enable signalling at a distance. Nature 585, 85–90. https://doi.org/10.1038/s41586-020-2498-z
160. **McGuire, S.E., Le, P.T., Osborn, A.J., Matsumoto, K., Davis, R.L.,** 2003. Spatiotemporal Rescue of Memory Dysfunction in Drosophila. Science 302, 1765–1768. https://doi.org/10.1126/science.1089035
161. **McLauchlan, H., Newell, J., Morrice, N., Osborne, A., West, M., Smythe, E.,** 1998. A novel role for Rab5–GDI in ligand sequestration into clathrin-coated pits. Current Biology 8, 34–45. https://doi.org/10.1016/S0960-9822(98)70018-1
162. **Mehta, S., Hingole, S., Chaudhary, V.,** 2021. The Emerging Mechanisms of Wnt Secretion and Signaling in Development. Frontiers in Cell and Developmental Biology 9.
163. **Mellman, I., Nelson, W.J.,** 2008. Coordinated protein sorting, targeting and distribution in polarized cells. Nat Rev Mol Cell Biol 9, 833–845. https://doi.org/10.1038/nrm2525

164. **Mihara, E., Hirai, H., Yamamoto, H., Tamura-Kawakami, K., Matano, M., Kikuchi, A., Sato, T., Takagi, J.,** 2016. Active and water-soluble form of lipidated Wnt protein is maintained by a serum glycoprotein afamin/α-albumin. eLife 5, e11621. https://doi.org/10.7554/eLife.11621
165. **Mii, Y., Takada, S.,** 2020. Heparan Sulfate Proteoglycan Clustering in Wnt Signaling and Dispersal. Frontiers in Cell and Developmental Biology 8.
166. **Mikels, A.J., Nusse, R.,** 2006. Purified Wnt5a Protein Activates or Inhibits β-Catenin–TCF Signaling Depending on Receptor Context. PLoS Biol 4, e115. https://doi.org/10.1371/journal.pbio.0040115
167. **Miller, D.E., Cook, K.R., Hawley, R.S.,** 2019. The joy of balancers. PLOS Genetics 15, e1008421. https://doi.org/10.1371/journal.pgen.1008421
168. **Mirzoyan, Z., Sollazzo, M., Allocca, M., Valenza, A.M., Grifoni, D., Bellosta, P.,** 2019. Drosophila melanogaster: A Model Organism to Study Cancer. Frontiers in Genetics 10.
169. **Mojica, F.J.M., Díez-Villaseñor, C., García-Martínez, J., Soria, E.,** 2005. Intervening Sequences of Regularly Spaced Prokaryotic Repeats Derive from Foreign Genetic Elements. J Mol Evol 60, 174–182. https://doi.org/10.1007/s00239-004-0046-3
170. **Morgan, T.H.,** 1910. Sex Limited Inheritance in *Drosophila*. Science 32, 120–122. https://doi.org/10.1126/science.32.812.120
171. **Moti, N., Yu, J., Boncompain, G., Perez, F., Virshup, D.M.,** 2019. Wnt traffic from endoplasmic reticulum to filopodia. PLoS One 14, e0212711. https://doi.org/10.1371/journal.pone.0212711
172. **Muller, H.J.,** 1928. The Production of Mutations by X-Rays. Proc Natl Acad Sci U S A 14, 714–726.
173. **Mulligan, K.A., Fuerer, C., Ching, W., Fish, M., Willert, K., Nusse, R.,** 2012. Secreted Wingless-interacting molecule (Swim) promotes long-range signaling by maintaining Wingless solubility. Proceedings of the National Academy of Sciences 109, 370–377. https://doi.org/10.1073/pnas.1119197109
174. **Naschberger, A., Orry, A., Lechner, S., Bowler, M.W., Nurizzo, D., Novokmet, M., Keller, M.A., Oemer, G., Seppi, D., Haslbeck, M., Pansi, K., Dieplinger, H., Rupp, B.,** 2017. Structural Evidence for a Role of the Multi-functional Human Glycoprotein Afamin in Wnt Transport. Structure 25, 1907-1915.e5. https://doi.org/10.1016/j.str.2017.10.006
175. **Neumann, C.J., Cohen, S.M.,** 1997. Long-range action of Wingless organizes the dorsal-ventral axis of the Drosophila wing. Development 124, 871–880. https://doi.org/10.1242/dev.124.4.871
176. **Neumann, S., Coudreuse, D.Y.M., Van Der Westhuyzen, D.R., Eckhardt, E.R.M., Korswagen, H.C., Schmitz, G., Sprong, H.,** 2009. Mammalian Wnt3a is Released on Lipoprotein Particles. Traffic 10, 334–343. https://doi.org/10.1111/j.1600-0854.2008.00872.x
177. **Ng, L.F., Kaur, P., Bunnag, N., Suresh, J., Sung, I.C.H., Tan, Q.H., Gruber, J., Tolwinski, N.S.,** 2019. WNT Signaling in Disease. Cells 8, 826. https://doi.org/10.3390/cells8080826
178. **Nusse, R., Clevers, H.,** 2017. Wnt/β-Catenin Signaling, Disease, and Emerging Therapeutic Modalities. Cell 169, 985–999. https://doi.org/10.1016/j.cell.2017.05.016
179. **Nusse, R., Varmus, H.E.,** 1982. Many tumors induced by the mouse mammary tumor virus contain a provirus integrated in the same region of the host genome. Cell 31, 99–109. https://doi.org/10.1016/0092-8674(82)90409-3
180. **Nygaard, R., Yu, J., Kim, J., Ross, D.R., Parisi, G., Clarke, O.B., Virshup, D.M., Mancia, F.,** 2021. Structural Basis of WLS/Evi-Mediated Wnt Transport and Secretion. Cell 184, 194-206.e14. https://doi.org/10.1016/j.cell.2020.11.038
181. **Ozawa, M., Baribault, H., Kemler, R.,** 1989. The cytoplasmic domain of the cell adhesion molecule uvomorulin associates with three independent proteins structurally related in different species. The EMBO Journal 8, 1711–1717. https://doi.org/10.1002/j.1460-2075.1989.tb03563.x
182. **Pankiv, S., Alemu, E.A., Brech, A., Bruun, J.-A., Lamark, T., Øvervatn, A., Bjørkøy, G., Johansen, T.,** 2010. FYCO1 is a Rab7 effector that binds to LC3 and PI3P to mediate microtubule plus end–directed vesicle transport. J Cell Biol 188, 253–269. https://doi.org/10.1083/jcb.200907015
183. **Parker, J., Struhl, G.,** 2020. Control of Drosophila wing size by morphogen range and hormonal gating. Proceedings of the National Academy of Sciences 117, 31935–31944. https://doi.org/10.1073/pnas.2018196117
184. **Paroutis, P., Touret, N., Grinstein, S.,** 2004. The pH of the Secretory Pathway: Measurement, Determinants, and Regulation. Physiology 19, 207–215. https://doi.org/10.1152/physiol.00005.2004
185. **Pataki, C., Matusek, T., Kurucz, É., Andó, I., Jenny, A., Mihály, J.,** 2010. Drosophila Rab23 Is Involved in the Regulation of the Number and Planar Polarization of the Adult Cuticular Hairs. Genetics 184, 1051–1065. https://doi.org/10.1534/genetics.109.112060
186. **Patterson, G.H., Knobel, S.M., Sharif, W.D., Kain, S.R., Piston, D.W.,** 1997. Use of the green fluorescent protein and its mutants in quantitative fluorescence microscopy. Biophys J 73, 2782–2790.

187. **Petersen, C.P., Reddien, P.W.,** 2009. Wnt Signaling and the Polarity of the Primary Body Axis. Cell 139, 1056–1068. https://doi.org/10.1016/j.cell.2009.11.035
188. **Pfeffer, S.R.,** 2017. Rab GTPases: master regulators that establish the secretory and endocytic pathways. MBoC 28, 712–715. https://doi.org/10.1091/mbc.e16-10-0737
189. **Phetsang, W., Pelingon, R., Butler, M.S., Pitt, M.E., Kaeslin, G., Cooper, M.A., Blaskovich, M.A.T.,** 2016. Fluorescent Trimethoprim Conjugate Probes To Assess Drug Accumulation in Wild Type and Mutant Escherichia coli. ACS Infect. Dis. 2, 688–701. https://doi.org/10.1021/acsinfecdis.6b00080
190. **Piccirella, S., Czegle, I., Lizák, B., Margittai, É., Senesi, S., Papp, E., Csala, M., Fulceri, R., Csermely, P., Mandl, J., Benedetti, A., Bánhegyi, G.,** 2006. Uncoupled Redox Systems in the Lumen of the Endoplasmic Reticulum: pyridine nucleotides stay reduced in an oxidative environment. Journal of Biological Chemistry 281, 4671–4677. https://doi.org/10.1074/jbc.M509406200
191. **Piper, R.C., Katzmann, D.J.,** 2007. Biogenesis and Function of Multivesicular Bodies. Annu Rev Cell Dev Biol 23, 519–547. https://doi.org/10.1146/annurev.cellbio.23.090506.123319
192. **Port, F., Bullock, S.L.,** 2016. Augmenting CRISPR applications in Drosophila with tRNA-flanked Cas9 and Cpf1 sgRNAs. Nat Methods 13, 852–854. https://doi.org/10.1038/nmeth.3972
193. **Port, F., Chen, H.-M., Lee, T., Bullock, S.L.,** 2014. Optimized CRISPR/Cas tools for efficient germline and somatic genome engineering in Drosophila. Proceedings of the National Academy of Sciences 111, E2967–E2976. https://doi.org/10.1073/pnas.1405500111
194. **Port, F., Hausmann, G., Basler, K.,** 2011. A genome-wide RNA interference screen uncovers two p24 proteins as regulators of Wingless secretion. EMBO Rep 12, 1144–1152. https://doi.org/10.1038/embor.2011.165
195. **Port, F., Kuster, M., Herr, P., Furger, E., Bänziger, C., Hausmann, G., Basler, K.,** 2008. Wingless secretion promotes and requires retromer-dependent cycling of Wntless. Nat Cell Biol 10, 178–185. https://doi.org/10.1038/ncb1687
196. **Port, F., Muschalik, N., Bullock, S.L.,** 2015. Systematic Evaluation of Drosophila CRISPR Tools Reveals Safe and Robust Alternatives to Autonomous Gene Drives in Basic Research. G3 Genes|Genomes|Genetics 5, 1493–1502. https://doi.org/10.1534/g3.115.019083
197. **Port, F., Strein, C., Stricker, M., Rauscher, B., Heigwer, F., Zhou, J., Beyersdörffer, C., Frei, J., Hess, A., Kern, K., Lange, L., Langner, N., Malamud, R., Pavlović, B., Rädecke, K., Schmitt, L., Voos, L., Valentini, E., Boutros, M.,** 2020. A large-scale resource for tissue-specific CRISPR mutagenesis in Drosophila. eLife 9, e53865. https://doi.org/10.7554/eLife.53865
198. **Poteryaev, D., Datta, S., Ackema, K., Zerial, M., Spang, A.,** 2010. Identification of the Switch in Early-to-Late Endosome Transition. Cell 141, 497–508. https://doi.org/10.1016/j.cell.2010.03.011
199. **Pradhan-Sundd, T., Verheyen, E.M.,** 2014. The role of Bro1- domain-containing protein Myopic in endosomal trafficking of Wnt/Wingless. Developmental Biology 392, 93–107. https://doi.org/10.1016/j.ydbio.2014.04.019
200. **Rattner, A., Hsieh, J.-C., Smallwood, P.M., Gilbert, D.J., Copeland, N.G., Jenkins, N.A., Nathans, J.,** 1997. A family of secreted proteins contains homology to the cysteine-rich ligand-binding domain of frizzled receptors. Proc Natl Acad Sci U S A 94, 2859–2863.
201. **Rieder, L.E., Larschan, E.N.,** 2014. Wisdom from the fly. Trends in Genetics 30, 479–481. https://doi.org/10.1016/j.tig.2014.08.003
202. **Rives, A.F., Rochlin, K.M., Wehrli, M., Schwartz, S.L., DiNardo, S.,** 2006. Endocytic trafficking of Wingless and its receptors, Arrow and DFrizzled-2, in the Drosophila wing. Dev Biol 293, 268–283. https://doi.org/10.1016/j.ydbio.2006.02.006
203. **Rodriguez, E.A., Campbell, R.E., Lin, J.Y., Lin, M.Z., Miyawaki, A., Palmer, A.E., Shu, X., Zhang, J., Tsien, R.Y.,** 2017. The growing and glowing toolbox of fluorescent and photoactive proteins. Trends Biochem Sci 42, 111–129. https://doi.org/10.1016/j.tibs.2016.09.010
204. **Rogina, B., Wolverton, T., Bross, T.G., Chen, K., Müller, H.-G., Carey, J.R.,** 2007. Distinct Biological Epochs in the Reproductive Life of Female Drosophila melanogaster. Mech Ageing Dev 128, 477–485. https://doi.org/10.1016/j.mad.2007.06.004
205. **Rojas, R., van Vlijmen, T., Mardones, G.A., Prabhu, Y., Rojas, A.L., Mohammed, S., Heck, A.J.R., Raposo, G., van der Sluijs, P., Bonifacino, J.S.,** 2008. Regulation of retromer recruitment to endosomes by sequential action of Rab5 and Rab7. J Cell Biol 183, 513–526. https://doi.org/10.1083/jcb.200804048
206. **Rosa-Ferreira, C., Sweeney, S.T., Munro, S.,** 2018. The small G protein Arl8 contributes to lysosomal function and long-range axonal transport in Drosophila. Biol Open 7, bio035964. https://doi.org/10.1242/bio.035964

207. **Ross, S.H., Cantrell, D.A.,** 2018. Signaling and Function of Interleukin-2 in T Lymphocytes. Annu Rev Immunol 36, 411–433. https://doi.org/10.1146/annurev-immunol-042617-053352
208. **Rosso, S., Inestrosa, N.C.,** 2013. WNT signaling in neuronal maturation and synaptogenesis. Frontiers in Cellular Neuroscience 7.
209. **Rothman, J.E., Schmid, S.L.,** 1986. Enzymatic recycling of clathrin from coated vesicles. Cell 46, 5–9. https://doi.org/10.1016/0092-8674(86)90852-4
210. **Routledge, D., Scholpp, S.,** 2019. Mechanisms of intercellular Wnt transport. Development 146, dev176073. https://doi.org/10.1242/dev.176073
211. **Sato, K., Nakano, A.,** 2005. Dissection of COPII subunit-cargo assembly and disassembly kinetics during Sar1p-GTP hydrolysis. Nat Struct Mol Biol 12, 167–174. https://doi.org/10.1038/nsmb893
212. **Satoh, A., Tokunaga, F., Kawamura, S., Ozaki, K.,** 1997. In situ inhibition of vesicle transport and protein processing in the dominant negative Rab1 mutant of Drosophila. Journal of Cell Science 110, 2943–2953. https://doi.org/10.1242/jcs.110.23.2943
213. **Satoh, T., Nakamura, Y., Satoh, A.K.,** 2016. Rab6 functions in polarized transport in Drosophila photoreceptors. Fly (Austin) 10, 123–127. https://doi.org/10.1080/19336934.2016.1182273
214. **Schmid, S.L., Frolov, V.A.,** 2011. Dynamin: Functional Design of a Membrane Fission Catalyst. Annual Review of Cell and Developmental Biology 27, 79–105. https://doi.org/10.1146/annurev-cellbio-100109-104016
215. **Schmitt, H.D., Wagner, P., Pfaff, E., Gallwitz, D.,** 1986. The ras-related YPT1 gene product in yeast: a GTP-binding protein that might be involved in microtubule organization. Cell 47, 401–412. https://doi.org/10.1016/0092-8674(86)90597-0
216. **Seaman, M.N.J.,** 2012. The retromer complex – endosomal protein recycling and beyond. J Cell Sci 125, 4693–4702. https://doi.org/10.1242/jcs.103440
217. **Seifert, J.R.K., Mlodzik, M.,** 2007. Frizzled/PCP signalling: a conserved mechanism regulating cell polarity and directed motility. Nat Rev Genet 8, 126–138. https://doi.org/10.1038/nrg2042
218. **Semerdjieva, S., Shortt, B., Maxwell, E., Singh, S., Fonarev, P., Hansen, J., Schiavo, G., Grant, B.D., Smythe, E.,** 2008. Coordinated regulation of AP2 uncoating from clathrin-coated vesicles by rab5 and hRME-6. J Cell Biol 183, 499–511. https://doi.org/10.1083/jcb.200806016
219. **Shaner, N.C., Patterson, G.H., Davidson, M.W.,** 2007. Advances in fluorescent protein technology. Journal of Cell Science 120, 4247–4260. https://doi.org/10.1242/jcs.005801
220. **Shearer, L.J., Petersen, N.O.,** 2019. Distribution and Co-localization of endosome markers in cells. Heliyon 5, e02375. https://doi.org/10.1016/j.heliyon.2019.e02375
221. **Sheff, D.R., Daro, E.A., Hull, M., Mellman, I.,** 1999. The Receptor Recycling Pathway Contains Two Distinct Populations of Early Endosomes with Different Sorting Functions. J Cell Biol 145, 123–139.
222. **Sheldahl, L.C., Park, M., Malbon, C.C., Moon, R.T.,** 1999. Protein kinase C is differentially stimulated by Wnt and Frizzled homologs in aG-protein-dependent manner. Current Biology 9, 695-S1. https://doi.org/10.1016/S0960-9822(99)80310-8
223. **Sheldahl, L.C., Slusarski, D.C., Pandur, P., Miller, J.R., Kühl, M., Moon, R.T.,** 2003. Dishevelled activates Ca2+ flux, PKC, and CamKII in vertebrate embryos. J Cell Biol 161, 769–777. https://doi.org/10.1083/jcb.200211094
224. **Shimomura, O., Johnson, F.H., Saiga, Y.,** 1962. Extraction, Purification and Properties of Aequorin, a Bioluminescent Protein from the Luminous Hydromedusan, Aequorea. Journal of Cellular and Comparative Physiology 59, 223–239. https://doi.org/10.1002/jcp.1030590302
225. **Simonsen, A., Gaullier, J.-M., D'Arrigo, A., Stenmark, H.,** 1999. The Rab5 Effector EEA1 Interacts Directly with Syntaxin-6*. Journal of Biological Chemistry 274, 28857–28860. https://doi.org/10.1074/jbc.274.41.28857
226. **Simonsen, A., Lippe, R., Christoforidis, S., Gaullier, J.-M., Brech, A., Callaghan, J., Toh, B.-H., Murphy, C., Zerial, M., Stenmark, H.,** 1998. EEA1 links PI(3)K function to Rab5 regulation of endosome fusion. Nature 394, 494–498. https://doi.org/10.1038/28879
227. **Sivasankaran, R., Calleja, M., Morata, G., Basler, K.,** 2000. The Wingless target gene Dfz3 encodes a new member of the Drosophila Frizzled family. Mechanisms of Development 91, 427–431. https://doi.org/10.1016/S0925-4773(99)00313-5
228. **Slusarski, D.C., Corces, V.G., Moon, R.T.,** 1997. Interaction of Wnt and a Frizzled homologue triggers G-protein-linked phosphatidylinositol signalling. Nature 390, 410–413. https://doi.org/10.1038/37138
229. **Smith, E.M., Hoi, J.T., Eissenberg, J.C., Shoemaker, J.D., Neckameyer, W.S., Ilvarsonn, A.M., Harshman, L.G., Schlegel, V.L., Zempleni, J.,** 2007. Feeding Drosophila a Biotin-Deficient Diet for Multiple Generations

Increases Stress Resistance and Lifespan and Alters Gene Expression and Histone Biotinylation Patterns. The Journal of Nutrition 137, 2006–2012. https://doi.org/10.1093/jn/137.9.2006

230. **Smolich, B.D., McMahon, J.A., McMahon, A.P., Papkoff, J.,** 1993. Wnt family proteins are secreted and associated with the cell surface. Mol Biol Cell 4, 1267–1275.
231. **Söllner, T., Whiteheart, S.W., Brunner, M., Erdjument-Bromage, H., Geromanos, S., Tempst, P., Rothman, J.E.,** 1993. SNAP receptors implicated in vesicle targeting and fusion. Nature 362, 318–324. https://doi.org/10.1038/362318a0
232. **Stamos, J.L., Weis, W.I.,** 2013. The β-Catenin Destruction Complex. Cold Spring Harb Perspect Biol 5, a007898. https://doi.org/10.1101/cshperspect.a007898
233. **Stanganello, E., Hagemann, A.I.H., Mattes, B., Sinner, C., Meyen, D., Weber, S., Schug, A., Raz, E., Scholpp, S.,** 2015. Filopodia-based Wnt transport during vertebrate tissue patterning. Nat Commun 6, 5846. https://doi.org/10.1038/ncomms6846
234. **Stanganello, E., Scholpp, S.,** 2016. Role of cytonemes in Wnt transport. J Cell Sci 129, 665–672. https://doi.org/10.1242/jcs.182469
235. **Stenmark, H.,** 2009. Rab GTPases as coordinators of vesicle traffic. Nat Rev Mol Cell Biol 10, 513–525. https://doi.org/10.1038/nrm2728
236. **Stenmark, H., Olkkonen, V.M., 2001**. The Rab GTPase family. Genome Biol 2, reviews3007.1-reviews3007.7.
237. **Strassburger, K., Lorbeer, F.K., Lutz, M., Graf, F., Boutros, M., Teleman, A.A.,** 2017. Oxygenation and adenosine deaminase support growth and proliferation of ex vivo cultured Drosophila wing imaginal discs. Development 144, 2529–2538. https://doi.org/10.1242/dev.147538
238. **Strigini, M., Cohen, S.M.,** 2000. Wingless gradient formation in the Drosophila wing. Current Biology 10, 293–300. https://doi.org/10.1016/S0960-9822(00)00378-X
239. **Südhof, T.C., Malenka, R.C.,** 2008. Understanding Synapses: Past, Present, and Future. Neuron 60, 469–476. https://doi.org/10.1016/j.neuron.2008.10.011
240. **Sun, J., Yu, S., Zhang, X., Capac, C., Aligbe, O., Daudelin, T., Bonder, E.M., Gao, N.,** 2017. A Wntless–SEC12 complex on the ER membrane regulates early Wnt secretory vesicle assembly and mature ligand export. J Cell Sci 130, 2159–2171. https://doi.org/10.1242/jcs.200634
241. **Swarup, S., Verheyen, E.M.,** 2012. Wnt/Wingless Signaling in Drosophila. Cold Spring Harb Perspect Biol 4, a007930. https://doi.org/10.1101/cshperspect.a007930
242. **Takada, R., Satomi, Y., Kurata, T., Ueno, N., Norioka, S., Kondoh, H., Takao, T., Takada, S.,** 2006. Monounsaturated Fatty Acid Modification of Wnt Protein: Its Role in Wnt Secretion. Developmental Cell 11, 791–801. https://doi.org/10.1016/j.devcel.2006.10.003
243. **Takahashi, S., Kubo, K., Waguri, S., Yabashi, A., Shin, H.-W., Katoh, Y., Nakayama, K.,** 2012. Rab11 regulates exocytosis of recycling vesicles at the plasma membrane. Journal of Cell Science 125, 4049–4057. https://doi.org/10.1242/jcs.102913
244. **Tamai, K., Semenov, M., Kato, Y., Spokony, R., Liu, C., Katsuyama, Y., Hess, F., Saint-Jeannet, J.-P., He, X.,** 2000. LDL-receptor-related proteins in Wnt signal transduction. Nature 407, 530–535. https://doi.org/10.1038/35035117
245. **Tang, X., Wu, Y., Belenkaya, T.Y., Huang, Q., Ray, L., Qu, J., Lin, X.,** 2012. Roles of N-glycosylation and lipidation in Wg secretion and signaling. Dev Biol 364, 32–41. https://doi.org/10.1016/j.ydbio.2012.01.009
246. **Tassew, N.G., Charish, J., Shabanzadeh, A.P., Luga, V., Harada, H., Farhani, N., D'Onofrio, P., Choi, B., Ellabban, A., Nickerson, P.E.B., Wallace, V.A., Koeberle, P.D., Wrana, J.L., Monnier, P.P.,** 2017. Exosomes Mediate Mobilization of Autocrine Wnt10b to Promote Axonal Regeneration in the Injured CNS. Cell Reports 20, 99–111. https://doi.org/10.1016/j.celrep.2017.06.009
247. **Tauriello, D.V.F., Jordens, I., Kirchner, K., Slootstra, J.W., Kruitwagen, T., Bouwman, B.A.M., Noutsou, M., Rüdiger, S.G.D., Schwamborn, K., Schambony, A., Maurice, M.M.,** 2012. Wnt/β-catenin signaling requires interaction of the Dishevelled DEP domain and C terminus with a discontinuous motif in Frizzled. Proc Natl Acad Sci U S A 109, E812-820. https://doi.org/10.1073/pnas.1114802109
248. **Tennessen, J.M., Thummel, C.S.,** 2011. Coordinating Growth and Review Maturation — Insights from Drosophila. Curr Biol 21, R750–R757. https://doi.org/10.1016/j.cub.2011.06.033
249. **Tisdale, E.J., Jackson, M.R.,** 1998. Rab2 Protein Enhances Coatomer Recruitment to Pre-Golgi Intermediates*. Journal of Biological Chemistry 273, 17269–17277. https://doi.org/10.1074/jbc.273.27.17269
250. **Trajkovic, K., Hsu, C., Chiantia, S., Rajendran, L., Wenzel, D., Wieland, F., Schwille, P., Brügger, B., Simons, M.,** 2008. Ceramide Triggers Budding of Exosome Vesicles into Multivesicular Endosomes. Science 319, 1244–1247. https://doi.org/10.1126/science.1153124

251. **Tsao, C.-K., Ku, H.-Y., Lee, Y.-M., Huang, Y.-F., Sun, Y.H.,** 2016. Long Term Ex Vivo Culture and Live Imaging of Drosophila Larval Imaginal Discs. PLOS ONE 11, e0163744. https://doi.org/10.1371/journal.pone.0163744
252. **Ugur, B., Chen, K., Bellen, H.J.,** 2016. Drosophila tools and assays for the study of human diseases. Disease Models & Mechanisms 9, 235–244. https://doi.org/10.1242/dmm.023762
253. **Üren, A., Reichsman, F., Anest, V., Taylor, W.G., Muraiso, K., Bottaro, D.P., Cumberledge, S., Rubin, J.S.,** 2000. Secreted Frizzled-related Protein-1 Binds Directly to Wingless and Is a Biphasic Modulator of Wnt Signaling*. Journal of Biological Chemistry 275, 4374–4382. https://doi.org/10.1074/jbc.275.6.4374
254. **Valenta, T., Hausmann, G., Basler, K.,** 2012. The many faces and functions of β-catenin. EMBO J 31, 2714–2736. https://doi.org/10.1038/emboj.2012.150
255. **Van der Beek, J., Jonker, C., van der Welle, R., Liv, N., Klumperman, J.,** 2019. CORVET, CHEVI and HOPS – multisubunit tethers of the endo-lysosomal system in health and disease. Journal of Cell Science 132, jcs189134. https://doi.org/10.1242/jcs.189134
256. **Vanlandingham, P.A., Ceresa, B.P.,** 2009. Rab7 Regulates Late Endocytic Trafficking Downstream of Multivesicular Body Biogenesis and Cargo Sequestration. J Biol Chem 284, 12110–12124. https://doi.org/10.1074/jbc.M809277200
257. **Viotti, C.,** 2016. ER to Golgi-Dependent Protein Secretion: The Conventional Pathway, in: Pompa, A., De Marchis, F. (Eds.), Unconventional Protein Secretion: Methods and Protocols, Methods in Molecular Biology. Springer, New York, NY, pp. 3–29. https://doi.org/10.1007/978-1-4939-3804-9_1
258. **Walter, P., Johnson, A.E.,** 1994. Signal Sequence Recognition and Protein Targeting to the Endoplasmic Reticulum Membrane. Annu Rev Cell Biol 10, 87-119. https://doi.org/10.1146/annurev.cb.10.110194.000511
259. **Watson, E.T., Pauers, M.M., Seibert, M.J., Vevea, J.D., Chapman, E.R.,** 2023. Synaptic vesicle proteins are selectively delivered to axons in mammalian neurons. eLife 12, e82568. https://doi.org/10.7554/eLife.82568
260. **White, J.J., Mazzeu, J.F., Coban-Akdemir, Z., Bayram, Y., Bahrambeigi, V., Hoischen, A., Bon, B.W.M. van, Gezdirici, A., Gulec, E.Y., Ramond, F., Touraine, R., Thevenon, J., Shinawi, M., Beaver, E., Heeley, J., Hoover-Fong, J., Durmaz, C.D., Karabulut, H.G., Marzioglu-Ozdemir, E., Cayir, A., Duz, M.B., Seven, M., Price, S., Ferreira, B.M., Vianna-Morgante, A.M., Ellard, S., Parrish, A., Stals, K., Flores-Daboub, J., Jhangiani, S.N., Gibbs, R.A., Genomics, B.-H.C. for M., Brunner, H.G., Sutton, V.R., Lupski, J.R., Carvalho, C.M.B.,** 2018. WNT Signaling Perturbations Underlie the Genetic Heterogeneity of Robinow Syndrome. American Journal of Human Genetics 102, 27. https://doi.org/10.1016/j.ajhg.2017.10.002
261. **Willert, K., Brown, J.D., Danenberg, E., Duncan, A.W., Weissman, I.L., Reya, T., Yates, J.R., Nusse, R.,** 2003. Wnt proteins are lipid-modified and can act as stem cell growth factors. Nature 423, 448–452. https://doi.org/10.1038/nature01611
262. **Willert, K., Nusse, R.,** 2012. Wnt Proteins. Cold Spring Harb Perspect Biol 4, a007864. https://doi.org/10.1101/cshperspect.a007864
263. **Witte, L., Linnemannstöns, K., Honemann-Capito, M., Gross, J.C.,** 2021. Visualization and Quantitation of Wg trafficking in the Drosophila Wing Imaginal Epithelium. Bio Protoc 11, e4040. https://doi.org/10.21769/BioProtoc.4040
264. **Witte, L., Linnemannstöns, K., Schmidt, K., Honemann-Capito, M., Grawe, F., Wodarz, A., Gross, J.C.,** 2020. The kinesin motor Klp98A mediates apical to basal Wg transport. Development 147, dev186833. https://doi.org/10.1242/dev.186833
265. **Wolf, L.M., Lambert, A.M., Haenlin, J., Boutros, M.,** 2021. EVI/WLS function is regulated by ubiquitylation and is linked to ER-associated degradation by ERLIN2. J Cell Sci 134, jcs257790. https://doi.org/10.1242/jcs.257790
266. **Woodman, P.G., Futter, C.E.,** 2008. Multivesicular bodies: co-ordinated progression to maturity. Curr Opin Cell Biol 20, 408–414. https://doi.org/10.1016/j.ceb.2008.04.001
267. **Wucherpfennig, T., Wilsch-Bräuninger, M., González-Gaitán, M.,** 2003. Role of Drosophila Rab5 during endosomal trafficking at the synapse and evoked neurotransmitter release. Journal of Cell Biology 161, 609–624. https://doi.org/10.1083/jcb.200211087
268. **Xavier, C.P., Melikova, M., Chuman, Y., Üren, A., Baljinnyam, B., Rubin, J.S.,** 2014. Secreted Frizzled-related protein potentiation versus inhibition of Wnt3a/β-catenin signaling. Cellular Signalling 26, 94–101. https://doi.org/10.1016/j.cellsig.2013.09.016

269. **Yamamoto, H., Awada, C., Hanaki, H., Sakane, H., Tsujimoto, I., Takahashi, Y., Takao, T., Kikuchi, A.,** 2013. The apical and basolateral secretion of Wnt11 and Wnt3a in polarized epithelial cells is regulated by different mechanisms. Journal of Cell Science 126, 2931–2943. https://doi.org/10.1242/jcs.126052
270. **Yamazaki, Y., Palmer, L., Alexandre, C., Kakugawa, S., Beckett, K., Gaugue, I., Palmer, R.H., Vincent, J.-P.,** 2016. Godzilla-dependent transcytosis promotes Wingless signalling in Drosophila wing imaginal discs. Nat Cell Biol 18, 451–457. https://doi.org/10.1038/ncb3325
271. **Yang, C., Wang, X.,** 2021. Lysosome biogenesis: Regulation and functions. J Cell Biol 220, e202102001. https://doi.org/10.1083/jcb.202102001
272. **Yang, Y., Mlodzik, M.,** 2015. Wnt-Frizzled/Planar Cell Polarity Signaling: Cellular Orientation by Facing the Wind (Wnt). Annu Rev Cell Dev Biol 31, 623–646. https://doi.org/10.1146/annurev-cellbio-100814-125315
273. **Yu, J., Chia, J., Canning, C.A., Jones, C.M., Bard, F.A., Virshup, D.M.,** 2014. WLS Retrograde Transport to the Endoplasmic Reticulum during Wnt Secretion. Developmental Cell 29, 277–291. https://doi.org/10.1016/j.devcel.2014.03.016
274. **Yu, J.J.S., Maugarny-Calès, A., Pelletier, S., Alexandre, C., Bellaiche, Y., Vincent, J.-P., McGough, I.J.,** 2020. Frizzled-Dependent Planar Cell Polarity without Secreted Wnt Ligands. Dev Cell 54, 583-592.e5. https://doi.org/10.1016/j.devcel.2020.08.004
275. **Yu, L., McPhee, C.K., Zheng, L., Mardones, G.A., Rong, Y., Peng, J., Mi, N., Zhao, Y., Liu, Z., Wan, F., Hailey, D.W., Oorschot, V., Klumperman, J., Baehrecke, E.H., Lenardo, M.J.,** 2010. Termination of autophagy and reformation of lysosomes regulated by mTOR. Nature 465, 942–946. https://doi.org/10.1038/nature09076
276. **Yuan, W., Song, C.,** 2020. The Emerging Role of Rab5 in Membrane Receptor Trafficking and Signaling Pathways. Biochem Res Int 2020, 4186308. https://doi.org/10.1155/2020/4186308
277. **Zecca, M., Basler, K., Struhl, G.,** 1996. Direct and Long-Range Action of a Wingless Morphogen Gradient. Cell 87, 833–844. https://doi.org/10.1016/S0092-8674(00)81991-1
278. **Zhang, C., Scholpp, S.,** 2019. Cytonemes in development. Current Opinion in Genetics & Development, Developmental mechanisms, patterning and evolution 57, 25–30. https://doi.org/10.1016/j.gde.2019.06.005
279. **Zhang, J., Schulze, K.L., Hiesinger, P.R., Suyama, K., Wang, S., Fish, M., Acar, M., Hoskins, R.A., Bellen, H.J., Scott, M.P.,** 2007. Thirty-One Flavors of Drosophila Rab Proteins. Genetics 176, 1307–1322. https://doi.org/10.1534/genetics.106.066761

6.2 List of Figures

Figure 1: Wnt secretion and trafficking 8
Figure 2: Wnt signaling pathways 12
Figure 3: The Rab cycle 14
Figure 4: Drosophila melanogaster wing imaginal disc and salivary glands 20
Figure 5: The Gal4/UAS and Gal80^{ts}/UAS systems 21
Figure 6: CRISPR HDR tagging system 22
Figure 7: The RUSH and LAMA systems 24
Figure 8: Potential endogenous tag insertion sites identified in Evi based on protein sequence conservation 29
Figure 9: Wg and Evi endogenously tagged with mScarlet and EGFP show the same expression pattern in the wing imaginal disc as wildtype proteins 31
Figure 10: Endogenously tagged Wg and Evi do not cause any aberrant adult fly wing phenotypes 32
Figure 11: Wg:mScarlet accumulates in secreting cells upon induction of Evi clones and Evi:mScarlet-5 is no longer stabilized in cells with Wg knockdown 33
Figure 12: Wg:EGFP and Wg:mScarlet are expressed in the same pattern in the wing imaginal disc, but intracellular localization differs 35
Figure 13: Wg:mScarlet resembles the surface staining of Wg, but methanol fixation reveals a previously weakly detectable intracellular Wg:mScarlet fraction in secreting cells 36
Figure 14: Surface protein biotinylation shows that Wg:mScarlet is secreted in similar amounts as Wg:EGFP and wildtype Wg 37
Figure 15: Live imaging of wing imaginal discs facilitates tracking of Wg:EGFP through the wing disc cells and enables particle tracking analysis 39
Figure 16: Live imaging of Wg:mScarlet reveals diverse dynamics of puncta depending on the fluorescence localization within the wing imaginal disc 40
Figure 17: Live imaging and tracking of Wg:EGFP and Evi:mScarlet over time reveals that Wg and Evi colocalize most of the time, but not always 41
Figure 18: The RUSH system components Golgi-RUSH-hook and RUSH-Rab7 induce mild apoptosis when co-expressed in wing imaginal discs 43
Figure 19: Overexpression of Golgi-RUSH-hook alone or together with RUSH-Rab7 in flies fed on biotin-deficient fly food (BDF) causes massive morphological deformities and apoptosis in the tissue 44
Figure 20: RUSH system expressed in the salivary glands using Golgi-hook and RUSH-Rab7 causes morphological changes to the Golgi, but functions well when reared on biotin-deficient fly food and can be released with biotin incubation 46
Figure 21: Co-expression of the RUSH-Rab7 together with the Golgi-LAMA-hook in wing imaginal discs causes severe apoptosis and morphological defects 48
Figure 22: Golgi-LAMA-hook causes toxicity within 36h of expression, whereas the Mito-LAMA-hook is well tolerated by the wing imaginal disc cells 49
Figure 23: The LAMA system using the Golgi-LAMA-hook is not toxic to salivary gland cells and the addition of TMP can reduce the localization of RUSH-Rab7 to the hook 50
Figure 24: The Mito-LAMA-hook correctly localizes to the mitochondria in salivary gland cells and the addition of TMP can reduce the localization of RUSH-Rab7 to the hook and the mitochondria 51

Figure 25: Live imaging of the LAMA system using RUSH-Rab7 and Mito-LAMA-hook demonstrates the changes in the distribution of the LAMA system components within the wing imaginal disc tissue after addition of TMP 53
Figure 26: Expression of the ER-LAMA-hook in wing discs endogenously tagged for Wg:EGFP or Evi:EGFP caused a strong accumulation of Wg:EGFP and a mild accumulation of Evi:EGFP in the cells 55
Figure 27: Sequestration of the Wg:EGFP in ER-LAMA-hook expressing cells causes a significant reduction in Wg:EGFP secretion as well as reduction in Wnt pathway target gene expression 56
Figure 28: TMP incubation for 2 hours does not induce the secretion of Wg:EGFP from the ER-LAMA-hook expressing cells 57
Figure 29: Mito-LAMA-hook can successfully sequester endogenous Sgg:EGFP present in the cytoplasm, which is released upon addition of TMP 58
Figure 30: Characterization of adult wings of 18 non-ubiquitous homozygous viable Rab null mutants 60
Figure 31: Genetic screening of Rab GTPase perturbation revealed Rab7 overexpression caused changes in Wg secretion 62
Figure 32: Rab7-WT overexpression and Rab7 knockdown by RNAi cause more Wg accumulation in the cells close to the dorsoventral boundary 64
Figure 33: Rab7-WT expression in both secreting and receiving cells induces Wg accumulation in large Rab7-positive puncta 65
Figure 34: Rab7-WT over-expression caused a strong accumulation in Wg puncta on the basal side of the discs 66
Figure 35: Trapping RUSH-Rab7 with the Mito-LAMA-hook almost fully rescues the Wg phenotype, which begins reconstituting within 30 minutes of TMP incubation 67
Figure 36: Overexpression of Rab7-WT does not affect the expression of downstream Wnt signaling targets Sens, Fz3 and Dll 69
Figure 37: Overexpression of Rab7-WT does not affect the shape of adult wings, though it does have an effect on wing size 69
Figure 38: Overexpression of Rab7-WT does not affect Wg secretion at the dorsoventral boundary 71
Figure 39: Colocalization of Wg and LAMP1 with Rab7 overexpressed in wing imaginal disc cells 72
Figure 40: Colocalization of Wg and Arl8 with Rab7 overexpressed in wing imaginal disc cells 73
Figure 41: Knockdown of Arl8 in wing discs expressing Rab7-WT in Wg-secreting cells ameliorates the Wg basal translocation phenotype 75
Figure 42: General strategy for endogenous protein tagging using CRISPR/Cas9 homology-directed repair system 100
Figure 43: Wg spread measurement 1005

Figure S1: Chromosomal distribution analysis in the F2 offspring shows similar chromosomal distribution of the wg:tag gene as the unaltered wt gene 139
Figure S2: Wg:EGFP more closely matches the antibody staining of Wg than Wg:mScarlet does 139
Figure S3: Evi:EGFP and Evi:mScarlet differ in the localization of their fluorescence in the wing imaginal disc cells 140

Figure S4: Co-expression of Ii ER-RUSH-hook and RUSH-RabX1 in flies fed on normal food or biotin-deficient fly food (BDF) 141
Figure S5: Secretion of Wg:EGFP from the ER-LAMA-hook expressing cells was not induced when the hook was only expressed for 24h before 1h TMP incubation or if flies were fed on TMP-containing food 142
Figure S6: Overexpression of Rab14-WT, Rab21-WT and Rab26-CA induces cell toxicity in wing imaginal discs 143
Figure S7: Overexpression of CA and DN forms of Rab7 shows no changes in Wg localization and distribution 143
Figure S8: Quantifications of Wg spread induced by the release of the LAMA system using Mito-LAMA-hook and RUSH-Rab7 144
Figure S9: Colocalization of Wg and Rab5 with Rab7 overexpressed in wing imaginal disc cells 145
Figure S10: Colocalization of Wg and Atg8 with Rab7 overexpressed in wing imaginal disc cells 146
Figure S11: Colocalization of Wg and LAMP1 with Rab7 overexpressed in wing imaginal disc cells with additional Arl8 knockdown 147

6.3 List of Tables

Table 1: List of plasmids used for and generated by cloning 105
Table 2: List of primers used for cloning 106
Table 3: Enzymes and associated buffers 110
Table 4: Chemicals and consumables used in the project 111
Table 5: Kits used in the project 112
Table 6: Buffer recipes 112
Table 7: Fly lines used in the project 113
Table 8: Primary antibodies used in the project 120
Table 9: Secondary antibodies and dyes used in the project 120

7 Appendix

7.1 Supplemental Figures

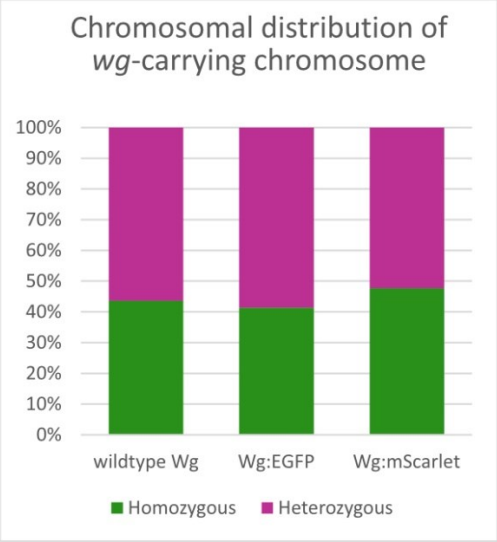

Figure S1: Chromosomal distribution analysis in the F2 offspring shows similar chromosomal distribution of the wg:tag gene as the unaltered wt gene
Percentage distribution of F2 flies heterozygous for *wg/wg^{sp}* and homozygous for *wg/wg* after crossing of F1 heterozygous *wg/wg^{sp}* flies. n=1164-1343 flies

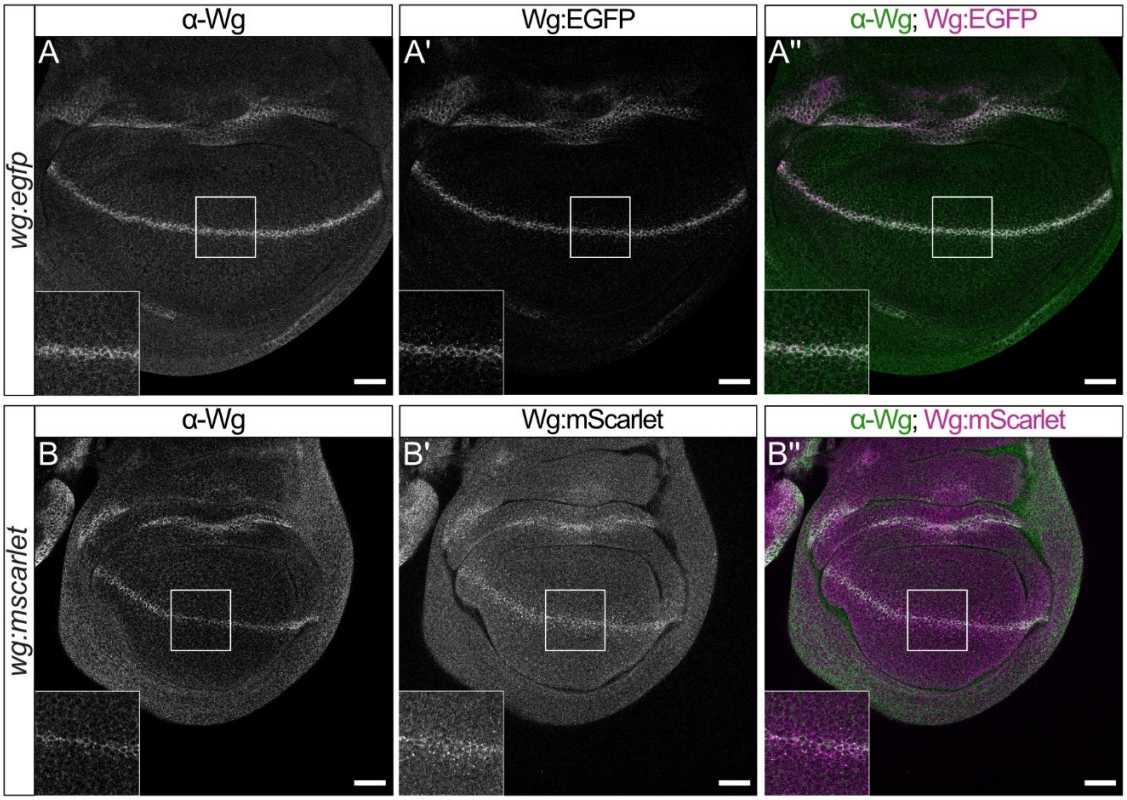

Figure S2: Wg:EGFP more closely matches the antibody staining of Wg than Wg:mScarlet does
A Representative image of immunofluorescence with anti-Wg antibody of Wg:EGFP expressing wing disc
B Representative image of immunofluorescence with anti-Wg antibody of Wg:mScarlet expressing wing disc
Scale bar = 50µm

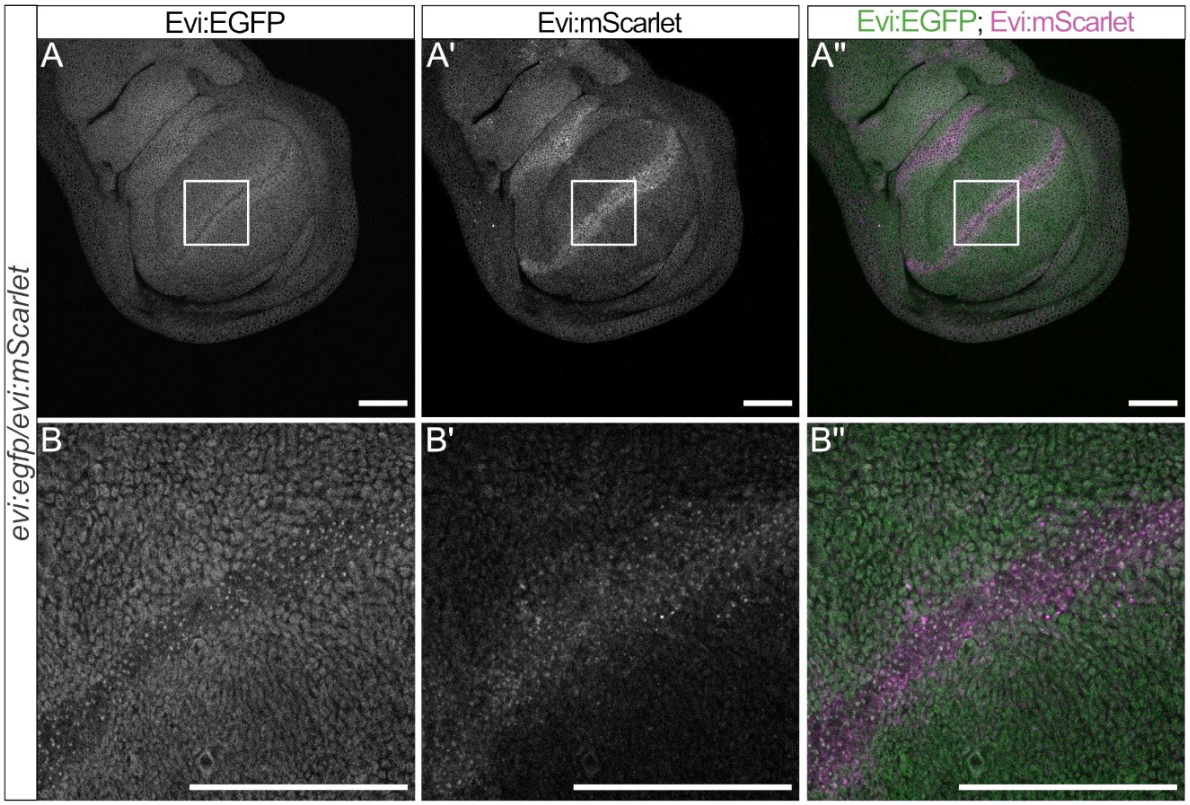

Supplemental Figure S3: Evi:EGFP and Evi:mScarlet differ in the localization of their fluorescence in the wing imaginal disc cells

A Representative images of a wing imaginal disc of the fly heterozygous for Evi:EGFP and Evi:mScarlet.

B Magnification of the dorsoventral boundary showing the difference in localization between Evi:EGFP and Evi:mScarlet fluorescence.

Scale bar = 50µm

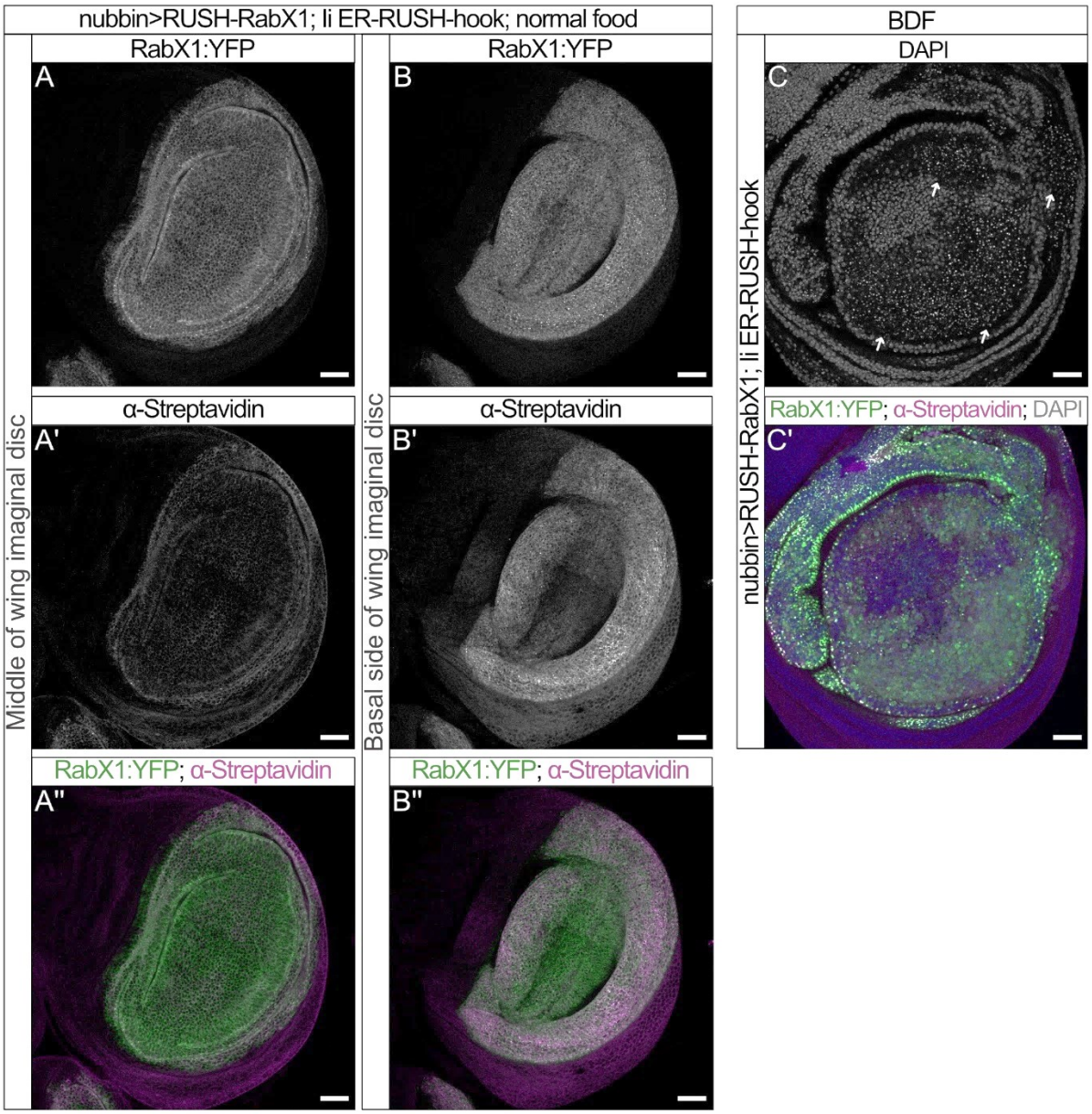

Supplemental Figure S4: Co-expression of Ii ER-RUSH-hook and RUSH-RabX1 in flies fed on normal food or biotin-deficient fly food (BDF)

A-B Representative image of a wing disc co-expressing Ii ER-RUSH-hook and RUSH-RabX1 under the nub-Gal4 driver in flies fed on normal food. Two different sections – the middle (A) and the basal side (B) of the disc are shown to demonstrate colocalization levels between the two RUSH system components.

C Representative image of a wing disc co-expressing Ii ER-RUSH-hook and RUSH-RabX1 under the nub-Gal4 driver in flies fed on BDF. Arrows indicate morphological deformities and apoptotic cell extrusion debris.

Scale bar = 50µm

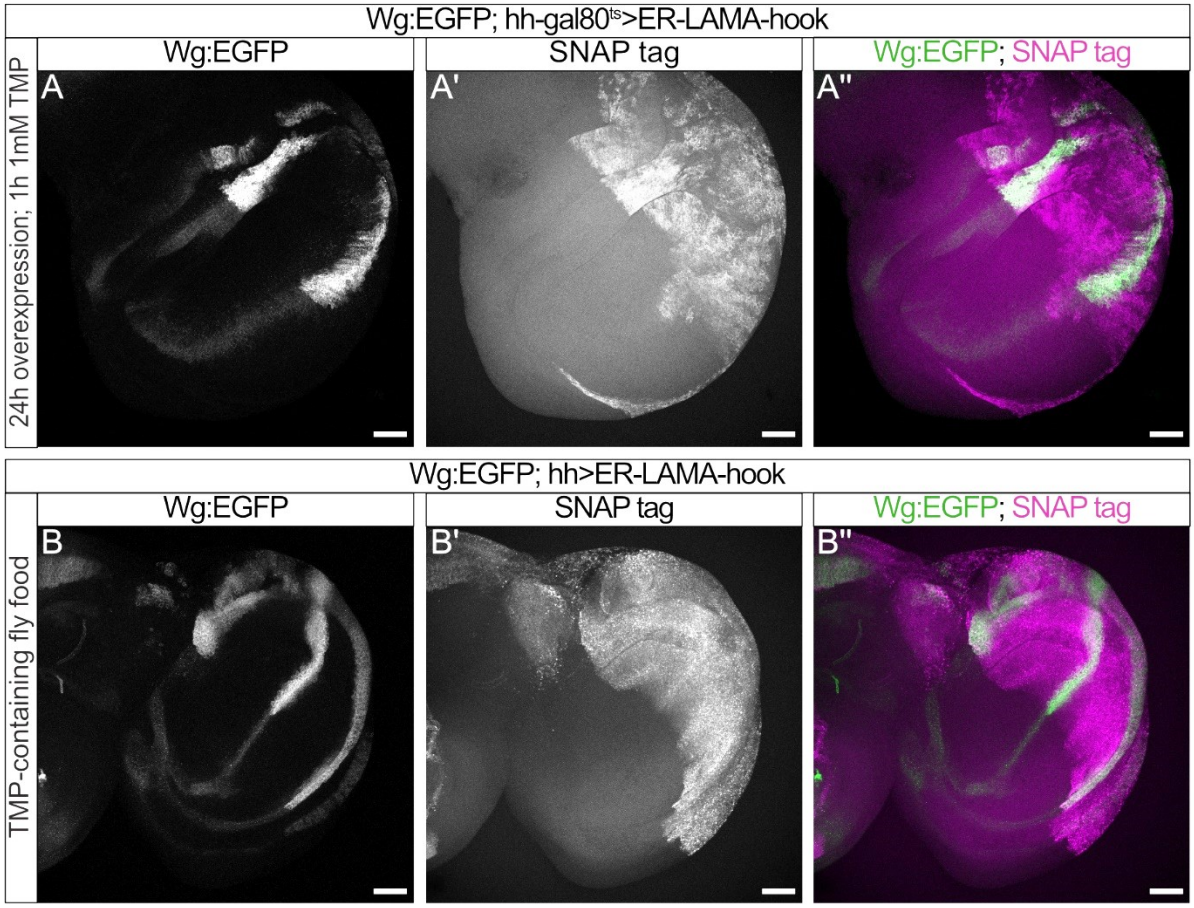

Supplemental Figure S5: Secretion of Wg:EGFP from the ER-LAMA-hook expressing cells was not induced when the hook was only expressed for 24h before 1h TMP incubation or if flies were fed on TMP-containing food

A Representative image of Wg:EGFP expressing wing discs overexpressing ER-LAMA-hook for 24h using the hh-Gal80^{ts} driver. It was incubated for 1h with TMP-containing medium.

B Representative image of Wg:EGFP expressing wing discs overexpressing ER-LAMA-hook under the hh-Gal4 driver. Flies were fed on TMP-containing fly food.

Scale bar = 50µm

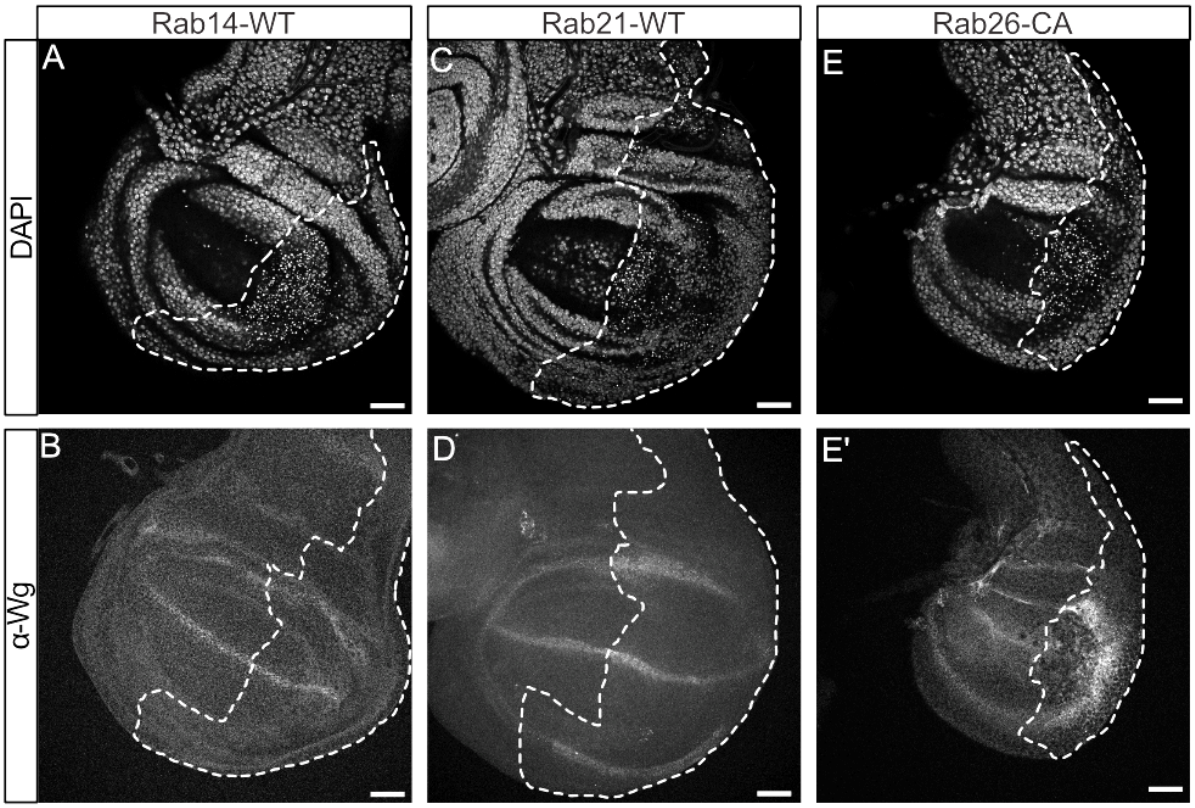

Supplemental Figure S6: Overexpression of Rab14-WT, Rab21-WT and Rab26-CA induces cell toxicity in wing imaginal discs
A-B Representative images of basal side (A) or middle (B) of wing disc overexpressing Rab14-WT under the hh-Gal4 driver.
C-D Representative images of basal side (A) or maximum intensity projection (B) of wing disc overexpressing Rab21-WT under the hh-Gal4 driver.
E Representative images of basal side of wing disc overexpressing Rab26-CA under the hh-Gal4 driver.
All discs show basal cell extrusion of apoptotic cells due to cell toxicity. Scale bar = 50µm

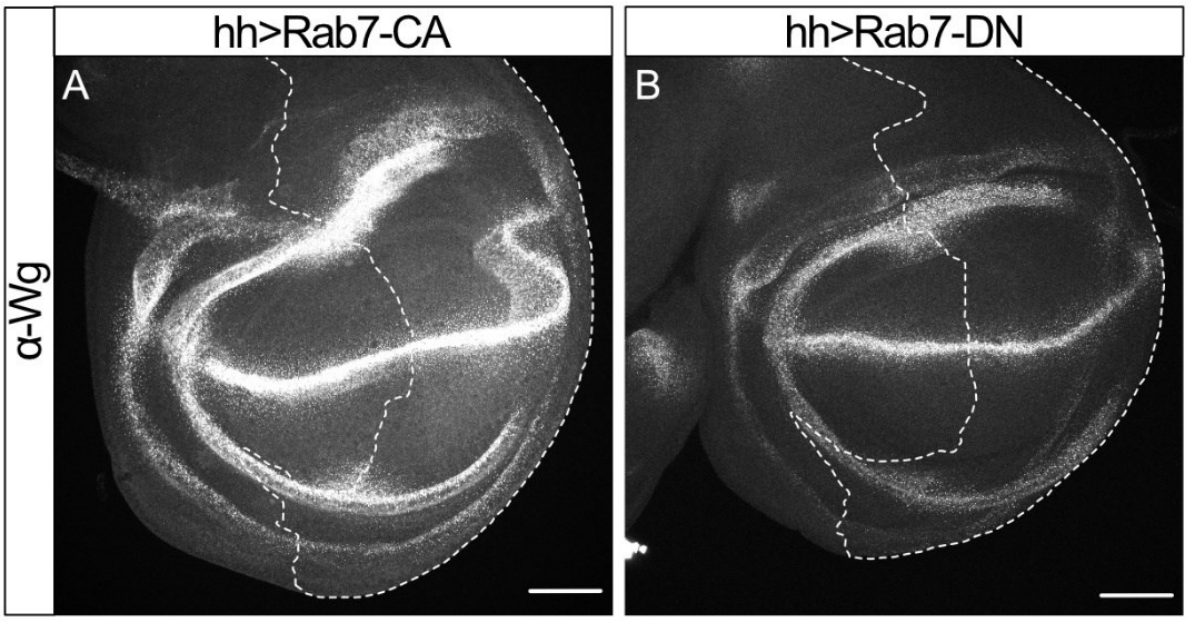

Supplemental Figure S7: Overexpression of CA and DN forms of Rab7 shows no changes in Wg localization and distribution
A Representative image of wing disc overexpressing Rab7-CA under the hh-Gal4 driver and stained with α-Wg antibody.
B Representative image of wing disc overexpressing Rab7-DN under the hh-Gal4 driver and stained with α-Wg antibody.
All images are maximum intensity projections. Scale bar = 50µm

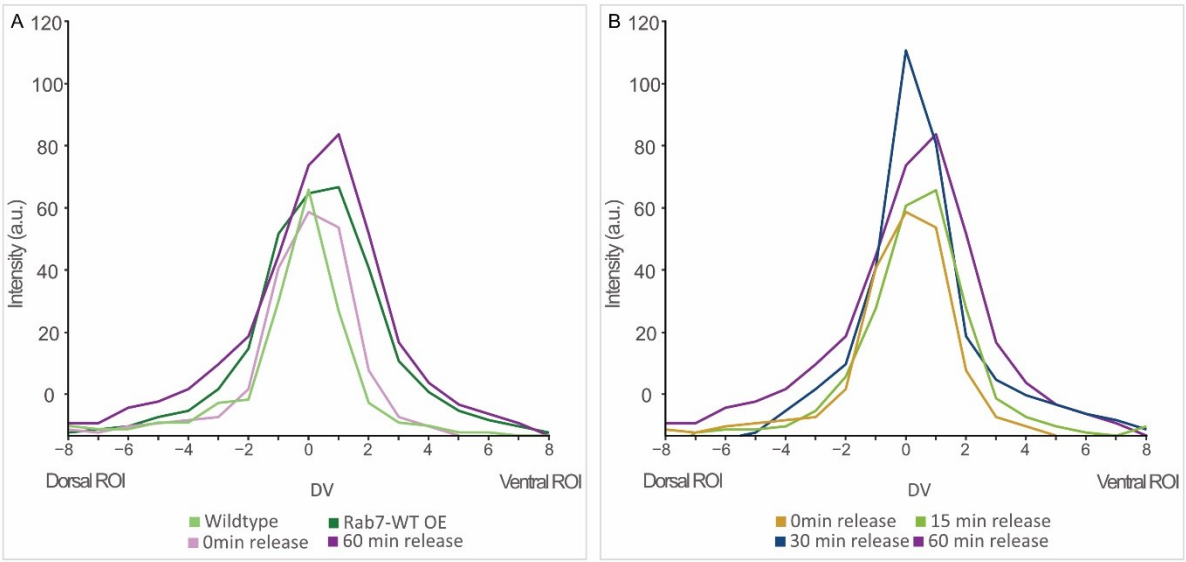

Supplemental Figure S8: Quantifications of Wg spread induced by the release of the LAMA system using Mito-LAMA-hook and RUSH-Rab7

A Graph showing Wg spread in wing disc depicted in Figure 35A expressing only RUSH-Rab7 quantified in the unperturbed (light green, wildtype) and perturbed (dark green, Rab7-WT overexpression) halves of the disc, as well as in wing discs shown in Figure 35B and 35E expressing the LAMA system before release (light magenta, 0min release) and 60 min after release (dark magenta). This graph is the fusion of the two graphs depicted in Figure 35F-G.

B Graph showing Wg spread in wing discs shown in Figure 35B-E overexpressing the LAMA system. Shown are quantifications of wing discs before release (yellow, 0min release), 15 min (green), 30min (blue) and 60 min (magenta) after release. The gradual increase in Wg presence further away from the dorsoventral boundary (DV) is visible in this graph.

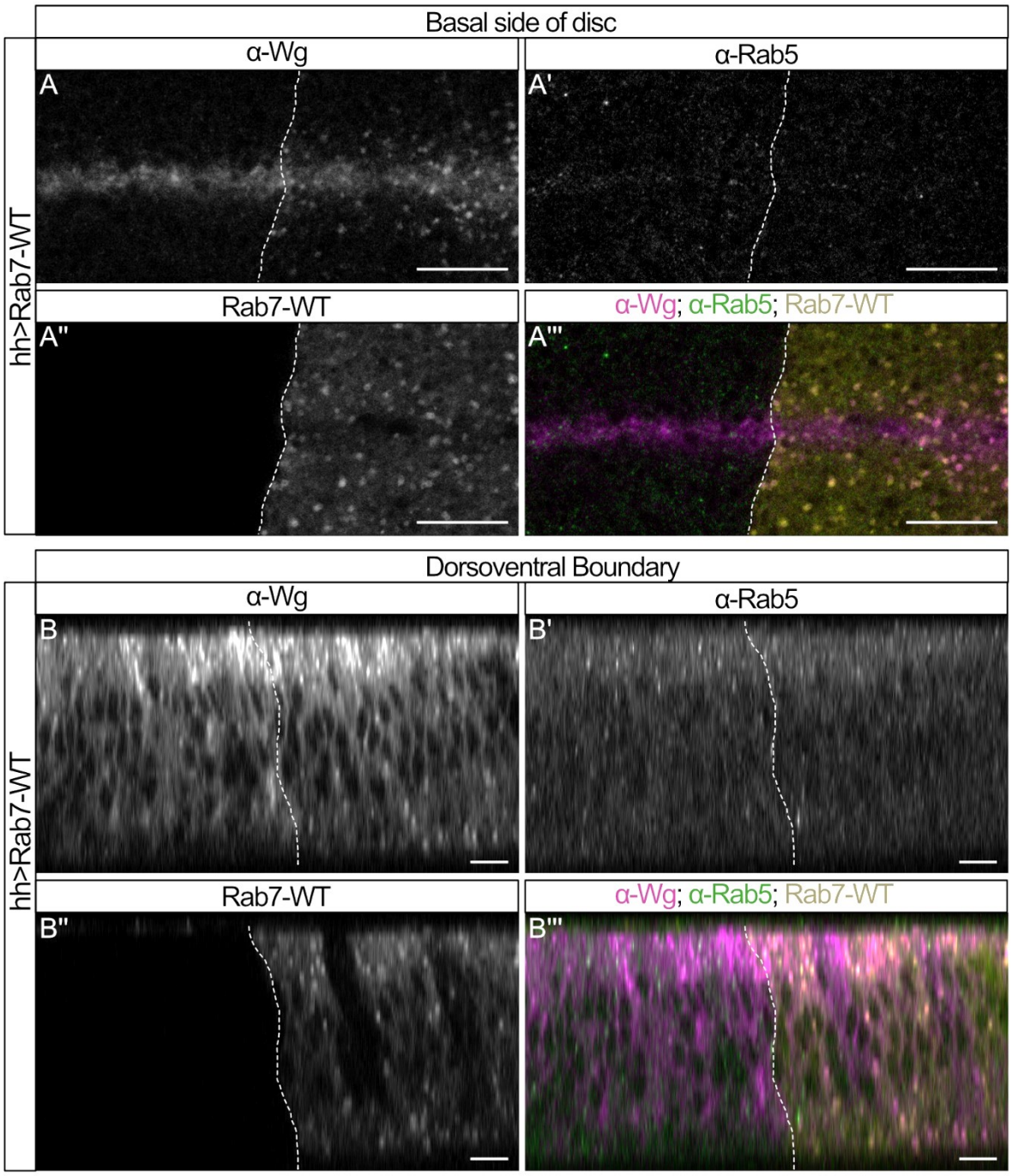

Supplemental Figure S9: Colocalization of Wg and Rab5 with Rab7 overexpressed in wing imaginal disc cells

A Representative image of the basal side of dorsoventral boundary of wing discs expressing Rab7-WT under control of hh-Gal4 driver, stained with Wg and Rab5 antibodies.

B Representative image of the lateral view through the Wg-secreting dorsoventral boundary cells of wing discs expressing Rab7-WT under control of hh-Gal4 driver, stained with Wg and Rab5 antibodies.

Scale bar=10 µm.

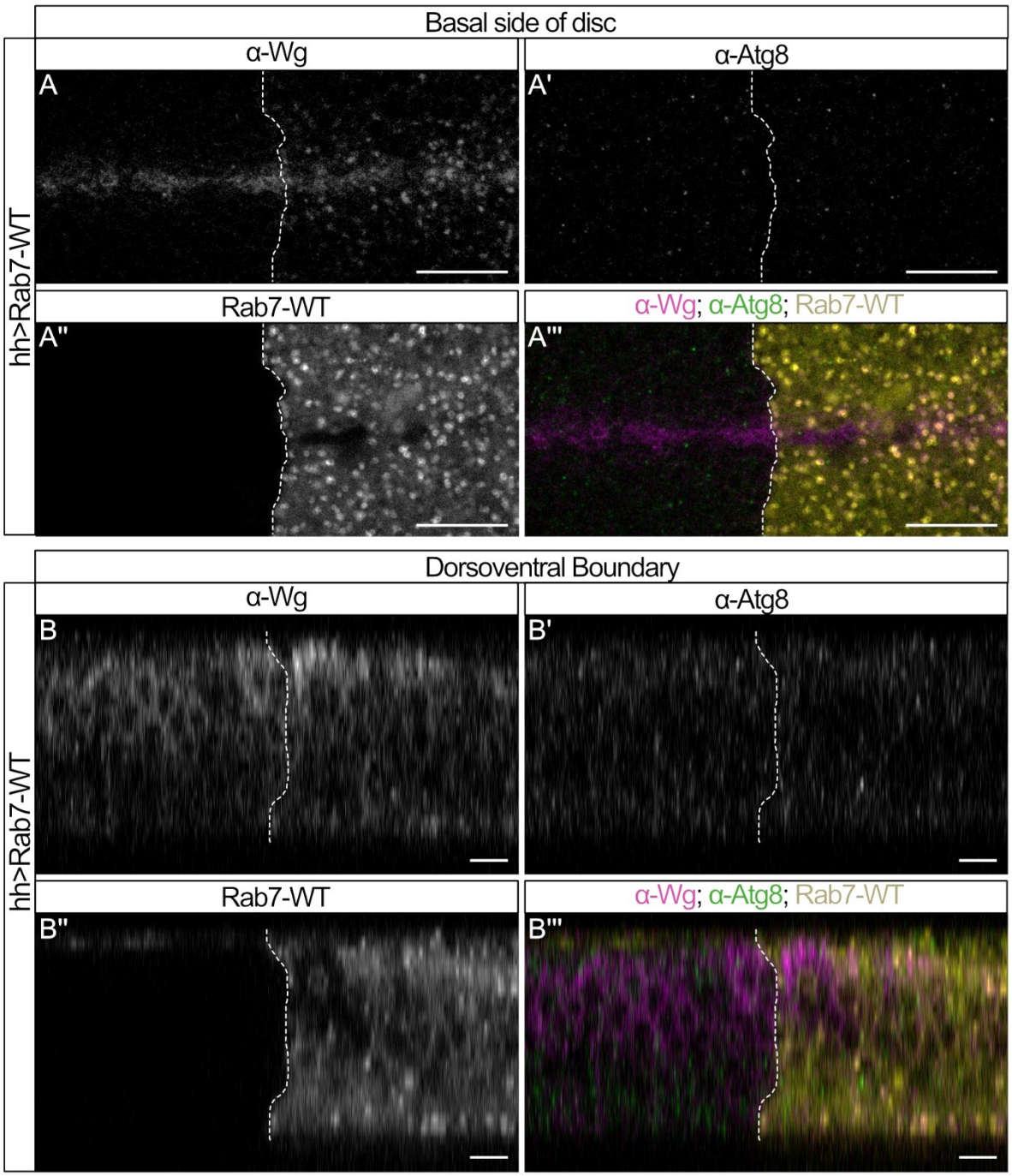

Supplemental Figure S10: Colocalization of Wg and Atg8 with Rab7 overexpressed in wing imaginal disc cells

A Representative image of the basal side of dorsoventral boundary of wing discs expressing Rab7-WT under control of hh-Gal4 driver, stained with Wg and Atg8 antibodies.

B Representative image of the lateral view through the Wg-secreting dorsoventral boundary cells of wing discs expressing Rab7-WT under control of hh-Gal4 driver, stained with Wg and Atg8 antibodies.

Scale bar=10 µm.

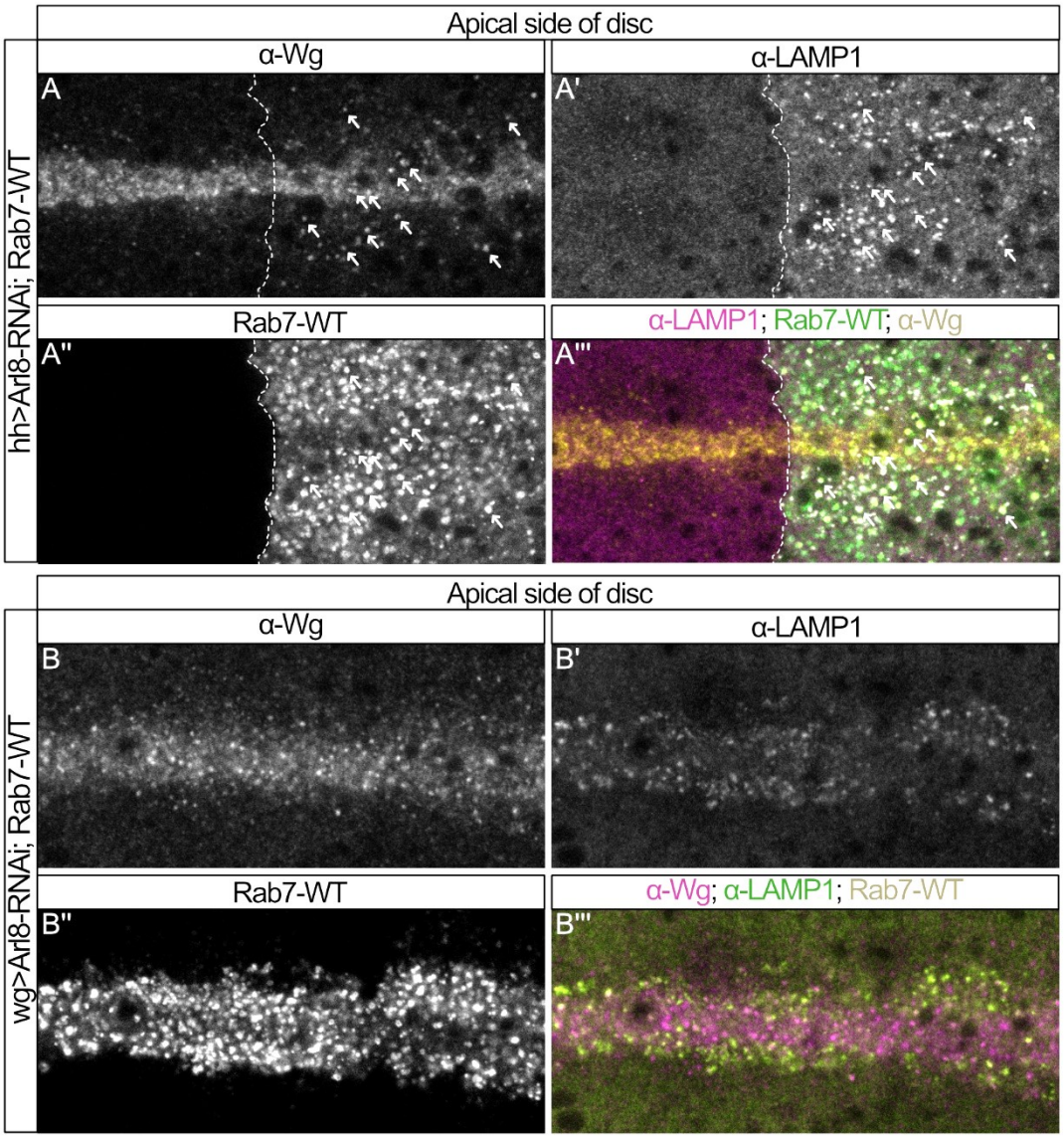

Supplemental Figure S11: Colocalization of Wg and LAMP1 with Rab7 overexpressed in wing imaginal disc cells with additional Arl8 knockdown

A Representative image of the basal side of dorsoventral boundary of wing discs expressing Rab7-WT and Arl8 RNAi under control of hh-Gal4 driver, stained with Wg and LAMP1 antibodies.

B Representative image of the lateral view through the Wg-secreting dorsoventral boundary cells of wing discs expressing Rab7-WT and Arl8 RNAi under control of hh-Gal4 driver, stained with Wg and LAMP1 antibodies.

Scale bar=10 µm.

7.2 Scientific publications, presentations and supervision

Publications

Jin, Y., Patel, P.H., Kohlmaier, A., Pavlovic, B., Zhang, C., Edgar, B.A., 2017. Intestinal Stem Cell Pool Regulation in Drosophila. Stem Cell Reports 8, 1479–1487. https://doi.org/10.1016/j.stemcr.2017.04.002

Patel, P.H., Pénalva, C., Kardorff, M., Roca, M., Pavlović, B., Thiel, A., Teleman, A.A., Edgar, B.A., 2019. Damage sensing by a Nox-Ask1-MKK3-p38 signaling pathway mediates regeneration in the adult Drosophila midgut. Nat Commun 10, 4365. https://doi.org/10.1038/s41467-019-12336-w

Port, F., Strein, C., Stricker, M., Rauscher, B., Heigwer, F., Zhou, J., Beyersdörffer, C., Frei, J., Hess, A., Kern, K., Lange, L., Langner, N., Malamud, R., Pavlović, B., Rädecke, K., Schmitt, L., Voos, L., Valentini, E., Boutros, M., 2020. A large-scale resource for tissue-specific CRISPR mutagenesis in Drosophila. eLife 9, e53865. https://doi.org/10.7554/eLife.53865

Kohrs, F.E., Daumann, I.-M., Pavlovic, B., Jin, E.J., Kiral, F.R., Lin, S.-C., Port, F., Wolfenberg, H., Mathejczyk, T.F., Linneweber, G.A., Chan, C.-C., Boutros, M., Hiesinger, P.R., 2021. Systematic functional analysis of rab GTPases reveals limits of neuronal robustness to environmental challenges in flies. eLife 10, e59594. https://doi.org/10.7554/eLife.59594

Poster presentations

SFB/TRR186 Annual Meeting, 2017, Heidelberg, Germany

Acute control of intracellular trafficking through Rab GTPases in living tissues in *D. melanogaster*, Kohrs F, Pavlovic B, Kiral F, Port P, Hiesinger R, Boutros M

SFB/TRR 186 – International Symposium, 2018, Heidelberg, Germany

Using the RUSH system to study intracellular trafficking through Rab GTPases in living tissues in *Drosophila*, Behnke L, Kohrs F, Pavlovic B, Kiral F, Hiesinger R, Boutros

Functional characterization of Rab GTPases and the generation of endogenously tagged Wnt proteins fly lines, Kohrs F, Pavlovic B, Dauman I, Wolfenberg H, Port F, Hiesinger R, Boutros M

SFPB 1324 Retreat, 2018, Heidelberg, Germany

Fluorescent tagging of Wg and Evi/Wls proteins in *Drosophila melanogaster*, Pavlovic B, Port F, Boutros M

European Wnt Meeting, 2018, Heidelberg, Germany

Fluorescent tagging of Wg and Evi/Wls proteins in *Drosophila melanogaster*, Pavlovic B, Port F, Boutros M

SFPB 1324 Retreat, 2019, Heidelberg, Germany

Mechanisms of Wnt secretion – Evi and Wg interactions, Pavlovic B, Holzem M, Port F, Boutros M

2nd Wnt Signaling Gordon Research Conference (GRC), 2019, Mount Snow, USA

Dissection of Wnt secretion in vivo through the use of endogenously tagged *Drosophila* Wg and Evi/Wls proteins, Pavlovic B, Port F, Boutros M

26th European Drosophila Research Conference, 2019, Lausanne, Switzerland

Dissection of Wnt secretion in vivo through the use of endogenously tagged *Drosophila* Wg and Evi/Wls proteins, Pavlovic B, Port F, Boutros M

SFB/TRR186 Annual Meeting, 2021, Heidelberg, Germany

Acute control of intracellular trafficking through Rab GTPases in living tissues in *D. melanogaster*, Kohrs F, Pavlovic B, Hiesinger R, Boutros M

SFB/TRR186 Annual Meeting, 2022, Heidelberg, Germany

Acute control of intracellular trafficking through Rab GTPases in living tissues in *D. melanogaster*, Kohrs F, Pavlovic B, Hiesinger R, Boutros M

Oral presentations

2nd Wnt Signaling Gordon Research Seminar (GRC), 2019, Mount Snow, USA

Endogenous tagging of *Drosophila* Wg and Evi/Wls proteins, Pavlovic B

SFB/TRR 186 Annual PhD and PostDoc meeting, 2019, Heidelberg, Germany

CRISPR methods in Drosophila Research, Pavlovic B

SFB/TRR 186 Annual PhD and PostDoc meeting, 2021, Online, Germany

A Bit on Method: Switching the Switches on 3D Scale, Pavlovic B

SFB/TRR 186 Annual PhD and PostDoc meeting, 2022, Berlin, Germany

Studying Wnt secretion in Drosophila tissue, live, Pavlovic B

Student supervision

Elisa Facen, Master student, 8-week lab rotation 2018-2019

Vivien Bertelmann, BOGY praktikum, 2022

7.3 Acknowledgements

This is for all the people who directly and indirectly contributed to the completion of this thesis: *thank you all from the bottom of my heart*. I wouldn't have made it here without you. The inclusive – but not exhaustive – list of these people is below; all my regards, also, to those I've forgotten to list.

Michael Boutros, my direct supervisor, who gave me the opportunity to do the research in his lab, and who supported and advised me in growing as a scientist and provided me with the tools and resources I needed to achieve this feat.

Walter Nickel and Ingrid Lohmann, for being on my thesis advisory committee and for providing me with their advice to get the work completed; Walter Nickel, Ingrid Lohmann and Kai Johnsson, for agreeing to be my thesis defense committee (even if the defense ended up being at 5pm in the afternoon).

Fillip Port, firstly and foremostly, for teaching me so much about the technical wonders of *Drosophila* genetic manipulation, for always being there and finding time to look over my data with me and for giving brilliant suggestions and advice, without which this work wouldn't have gotten nearly as far as it has. Michaela Holzem and Siamak Redhai, furthermore, who sat with me and racked their brains on how best to wrangle uncooperative project threads into a coherent whole. To all three – your scientific knowledge and passion bolstered me when I was stumbling.

Michaela Holzem and Dominique Kranz, for all the time and effort they expended on getting my disappointing first thesis draft into quite some semblance of shape, for all the patience they offered without a single complaint at a stressful, exhausting time in my life. It was the support I needed to get things finished.

Robin Hiesinger and Friederike Kohrs, who've been my collaborators on our shared A02 project for the SFB/TRR186, and who've been instrumental in my development of the RUSH and LAMA systems especially. Friederike and the other PhD students and PostDocs of the consortium, for the fun yearly gatherings and science exchanges, whether here in Heidelberg or there in Berlin.

Ulrike Engel and the Nikon Imaging Center, for all her advice and teaching when it came to live imaging of *Drosophila* tissue; Damir Krunić, for the great help in cobbling together a particle tracking analysis macro, where I was a total noob.

All of my fellow B110 lab members past and present, with whom I've shared my progress through lab meetings, afternoon coffee discussions, and random hallway conversations. Giulia Ambrosi, Oksana Voloshanenako, Alena Ivanova, Lucie Wolf, Florian Heigwer, Maja

Funk, Cornelia Redel, Nadine Winkel, Kim Boonekamp, and Pradhipa Karuna are just some among many, but all helped this thesis become what it is.

Shivohum Bahuguna, for all the scientific and not so scientific debates and discussions, for the home-cooked Indian food and the fly flipping and taking care of each other's projects when one of us had to travel hundreds of kilometers away to our first homes. We international drosophilists have to stick together, after all.

Antonia Schubert, not just for the science sharing and office laughter, but for asking me "How are you doing?" on a random Saturday noon in November 2021, when I was at my lowest and closest to quitting. It was the cry I needed to have in order to get through the irrational fears and the imposter syndrome that had found its way into my otherwise logical brain.

Dajana Tanasić, my fellow Bosnian drosophilist whom I only met here in the far-off Germany when we actually grew up two streets over from one another, and whose area of scientific focus happened to so closely relate to mine that we could go into the nitty-gritty of our projects in Serbian (even if a few English phrases snuck in here and there), for all the theater and opera outings, for the lunches and dinners, and for all the traveling together, to conferences and home. Ženo moja, tvoj i moj susret je bilo stvarno sudbina.

Bobana Vučanović, for her great help all the way from a random café in Banja Luka in making the introductory figure graphics, even though cellular secretion and the endosomal pathway are as far from her profession as art and programming are from mine. Ne bih nikuda došla sa tim figurama bez tebe.

And of course, my family and friends, who may not have been able to help with any science directly, but whose love and support have made me who I am today and have seen me through the most difficult times in my life.

My mother and sister, Milena Pavlović and Ksenija Pavić, who felt my joy when things were going their best and my pain when things were going their worst, who've always had the time the patience and the support for my constant chattering, my tears and my laughter in equal measure, and whom I love beyond compare. My father, Zoran Pavlović, who never doubted me and what I could achieve, who always told me to grab for more, who taught me how to get up when I stumbled and to never give up, and in whose image I find I have been made. My aunt, Vanda Havranek, whose laughter has always been able to brighten up my day, and whose support has meant the world. Mami, tati, schwe, tetka, volim vas sve puno, puno!

My brother in all but blood, Robert Tomić, who knows me as well as anyone in the world, and with whom I never have to censure myself or even be careful what I say, because nothing either of us say will ever weaken our bond. Robi, tvoja odbrana je sledeća.

My fanfic best friend, Nour Moukarzel, whose joy and excitement about our shared fandoms and our mutual writing is the bright part of any week, month or year, regardless of how much

time either of us may have for it, and whose listening ear has helped me work through the frustrations of everyday and not-so-everyday life. Thank you for always being there when I needed you.

My closest friends here in Germany, Henriette Hesselmann and Alexej Kapis, who came into my life through an advert for a room in the WG, but who stayed for the cats and video games and hair dying and TV shows and sewing and fantasy books and crepes and warm tea. Als ich eine Umarmung brauchte, wart ihr beide immer da und dafür hab ich euch lieb.

And finally, my cat Lily, the other living being in my home, whose tractor purring, ridiculous sleeping poses and loud meowing make sure I am never lonely and my phone memory is always full.

7.4 Erklärung zur wissenschaftlichen Praxis

GESAMTFAKULTÄT FÜR MATHEMATIK; INGENIEUR- UND NATURWISSENSCHAFTEN

Eidesstattliche Versicherung gemäß § 8 der Promotionsordnung der Gesamtfakultät für Mathematik, Ingenieur- und Naturwissenschaften der Universität Heidelberg.

1. Bei der eingereichten Dissertation mit dem Titel
Investigating the role of Rab GTPases in Wnt secretion in *Drosophila melanogaster*
handelt es sich um meine eigenständig erbrachte Leistung.

2. Ich habe nur die angegebenen Quellen und Hilfsmittel benutzt und mich keiner unzulässigen Hilfe Dritter bedient. Insbesondere habe ich wörtlich oder sinngemäß aus anderen Werken übernommene Inhalte als solche kenntlich gemacht.

3. Die Arbeit oder Teile davon habe ich bislang nicht an einer Hochschule des In- oder Auslands als Bestandteil einer Prüfungs- oder Qualifikationsleistung vorgelegt.

4. Die Richtigkeit der vorstehenden Erklärungen bestätige ich.

5. Die Bedeutung der eidesstattlichen Versicherung und die strafrechtlichen Folgen einer unrichtigen oder unvollständigen eidesstattlichen Versicherung sind mir bekannt. Ich versichere an Eides statt, dass ich nach bestem Wissen die reine Wahrheit erklärt und nichts verschwiegen habe.

Heidelberg, den 17. Juli 2023 ……..……

Bojana Pavlović, M.Sc.